Charles University in Prague

Faculty of Science

Ph.D. study program: Biochemistry

Mgr. Anna Kádková

Functional and structural study of thermally activated TRP ion channels: The role of evolutionarily conserved motifs in the TRPA1 modulation

Studium funkce a struktury teplotně aktivovaných TRP iontových kanálů: Role evolučně konzervovaných motivů v modulaci TRPA1

Doctoral Thesis

Supervisor: RNDr. Viktorie Vlachová, DrSc.

Prague 2016

Declaration

I declare that I have worked on this thesis under the guidance of my supervisor and that all sources of the previous knowledge are properly cited. No part of this work was used and will not be used for obtaining any other academic degree than Ph.D. from Charles University in Prague.

In Prague, 26th July 2016

Mgr. Anna Kádková

Declaration of authorship

I declare that Anna Kádková contributed significantly to the experiments and to all 4 scientific publications contained in this doctoral thesis. She performed most of the experiments, substantially contributed to their planning, and took a significant part in the primary data interpretation and their preparation for the publication.

In Prague, 26th July 2016

RNDr. Viktorie Vlachová, DrSc.

Acknowledgements

First, I would like to express my gratitude to my supervisor Viktorie Vlachová for her patience, support, advice and encouragement. Thanks to her I could work independently, attend international scientific meetings and gain professional experience in our partner laboratory in the UK. Joining her group was one of the best decisions I have ever made.

I also thank my colleagues Lucie Zímová, who taught me the patch clamp technique and helped me much when I started in the lab, and Lenka Vyklická, who was always ready to give me advice on anything I needed. I really appreciate all members of the Department of Cellular Neurophysiology, namely Ivan Dittert and Jan Krůšek for their willingness to solve technical problems with me and our excellent lab technician Magdaléna Kuntošová for her constant support.

I am really grateful for the opportunity to work with our undergraduate students Jana Vašková and Viktor Synytsya. I would like to emphasize our inspiring discussions and pleasant collaboration.

Last but not least I would like to thank my parents for their patience and support during my university studies and my beloved husband, with whom I can share my enthusiasm for science.

ABSTRAKT

Ankyrinový receptor TRPA1 je iontový kanál exprimovaný převážně na primárních aferentních senzorických neuronech, kde působí jako polymodální senzor pro bolestivé a dráždivé podněty. Kromě chemických látek (např. isothiokyanáty, skořicový aldehyd a jeho deriváty, akrolein, menthol) může být aktivován chladem, depolarizací membránového potenciálu nebo vápenatými ionty z intracelulární strany.

Iontový kanál TRPA1 je homotetramerem podjednotek, jež jsou topologicky uspořádány do transmembránové oblasti a cytoplazmaticky orientovaných N- a C-konců. Transmembránová oblast je tvořena šesti alfa-helixy propojenými intra- a extracelulárními kličkami. N-konec receptoru se vyznačuje přítomností 16 až 17 ankyrinových repetic (AR), zatímco C-konec je výrazně kratší a má převážně helikální strukturu. Přesná struktura TRPA1 byla částečně rozřešena roku 2015 pomocí kryo-elektronové mikroskopie, avšak funkční úloha jednotlivých oblastí v polymodální aktivaci receptoru není prozatím plně objasněna.

Předkládaná disertační práce se zabývá úlohou mezidruhově konzervovaných strukturních a sekvenčních motivů v cytoplazmatických koncích a v S4-S5 oblasti TRPA1 v napěťové a chemické citlivosti receptoru. Pomocí homologního modelování, molekulárně-dynamických simulací, bodové mutageneze a elektrofyziologických technik bylo popsáno možné vazebné místo pro vápenaté ionty, jež jsou nejdůležitějšími fyziologickými modulátory TRPA1. Dále byla navržena hypotéza, pomocí níž byla vysvětlena molekulární podstata dědičného onemocnění "familiálního epizodického bolestivého syndromu", které je způsobeno bodovou mutací N855S v S4-S5 oblasti receptoru. Nejnovější studie, jež je součástí této práce, byla zaměřena na objasnění funkční úlohy T/SPLH motivů v ankyrinových repeticích AR2, AR6, AR11-13 na aminovém konci v modulaci TRPA1 receptoru.

Klíčová slova: Ankyrinový receptor (TRPA), C-konec, N-konec, S4-S5 oblast, strukturně-funkční vztah, vápenaté ionty, napěťově závislé vrátkování, bodová mutace.

ABSTRACT

Ankyrin receptor TRPA1 is an ion channel widely expressed on primary afferent sensory neurons, where it acts as a polymodal sensor of nociceptive stimuli. Apart from pungent chemicals (e. g. isothiocyanates, cinnamaldehyde and its derivatives, acrolein, menthol), it could be activated by cold temperatures, depolarizing voltages or intracellular calcium ions.

TRPA1 channel is a homotetramer in which each subunit consists of cytoplasmic N and C termini and a transmembrane region. The transmembrane part is organized into six alpha-helices connected by intra- and extracellular loops. The N terminus comprises a tandem set of 16 to 17 ankyrin repeats (AR), while the C terminus has a substantially shorter, dominantly helical structure. In 2015, a partial cryo-EM structure of TRPA1 was resolved; however, the functional roles of the individual regions of the receptor have not yet been fully understood.

This doctoral thesis is concerned to elucidate the role of highly conserved sequence and structural motifs within the cytoplasmic termini and the S4-S5 region of TRPA1 in voltage- and chemical sensitivity of the receptor. The probable binding site for calcium ions that are the most important physiological modulators of TRPA1 was described by using homology modeling, molecular-dynamics simulations, site-directed mutagenesis and electrophysiological techniques. Next, the molecular mechanism of a heritable disorder called “familial episodic pain syndrome”, which is caused by a point mutation within the S4-S5 region, has been proposed. The latest study was focused on the functional role of T/SPLH motifs within the N-terminal ankyrin repeats AR2, AR6 and AR11-13 in the TRPA1 modulation.

Key words: Ankyrin receptor (TRPA), C terminus, N terminus, S4-S5 region, structure-function relationship, calcium ions, voltage-dependent gating, point mutation.

Contents

List of abbreviations

AA	amino acid
AC	adenylate cyclase
AITC	allyl isothiocyanate
AR	ankyrin repeat
ARD	ankyrin repeat domain
ATP	adenosine triphosphate
CA	cinnamaldehyde
cAMP	cyclic adenosine monophosphate
Ca_v	voltage-gated calcium channel
Cdk5	cyclin-dependent kinase 5
cDNA	complementary DNA
CGRP	calcitonin gene-related peptide
CK2	casein kinase 2
CNS	central nervous system
cryo-EM	cryo-electron microscopy
DAG	diacylglycerol
dTRPA1	*Drosophila melanogaster* TRPA1 receptor
EGTA	ethylene glycol tetraacetic acid
EM	electron microscopy
ER	endoplasmic reticulum
GFP	green fluorescent protein
GPCRs	G-protein coupled receptors
H1 – H6	predicted α-helices within the C terminus of TRPA1
HEDTA	(2-hydroxyethyl)ethylenediaminetriacetic acid
HEK293T	human embryonic kidney cells 293T
hTRPA1	human TRPA1 receptor
IP_3	inositol triphosphate
IP6	inositol hexakisphosphate
Kv	voltage-gated potassium channel
MD	molecular dynamics
mTRPA1	mouse TRPA1 receptor
PAR_2	protease-activated receptor 2

PIP_2	phosphatidylinositol-4,5-bisphosphate
PKA	protein kinase A
PKC	protein kinase C
PLC	phospholipase C
RNS	reactive nitrogen species
ROS	reactive oxygen species
S1 – S6	transmembrane helices 1 to 6 of the TRPA1 subunit
SEM	standard error of mean
T_{50}	time to decay to the half maximum of inhibition
THC	Δ^9-tetrahydrocannabinol
TRP	transient receptor potential
TRPA1	TRP ankyrin receptor subtype 1
Trpa1	gene for TRPA1 protein
Trpa1$^{-/-}$	knock-out gene for TRPA1 protein
TRPC	TRP canonical receptor
TRPM	TRP melastatin receptor
TRPML	TRP mucolipin receptor
TRPN	TRP no mechanoreceptor potential C
TRPP	TRP polycystin receptor
TRPV	TRP vanilloid receptor
WT	wild-type
15d – PGJ_2	15-deoxy-Δ-12,14-Prostaglandin J_2

1. Introduction

Transient Receptor Potential (TRP) channels represent a relatively ancient family of cation channels that have been found in many eukaryotic organisms except for plants[1]. They are expressed in both excitable and non-excitable tissues where they play key roles in sensory signal transduction (such as nociception, chemical and temperature sensation or taste transduction) and homeostatic functions (e. g. Ca^{2+} and Mg^{2+} reabsorption or osmoregulation). In particular, the thermosensitive TRP channels have been intensively studied for their polymodal activation in nociceptive pathways since 1997, when the first member, the vanilloid receptor TRPV1, was identified[2].

Mammalian TRPs are encoded by 28 genes and classified into six subfamilies according to their sequence homology: canonical (TRPC), vanilloid (TRPV), polycystin (TRPP), melastatin (TRPM), ankyrin (TRPA) and mucolipin (TRPML)[3,4]. In spite of little sequence homology among subfamilies, TRP channels exhibit a similar membrane topology, which is characterized by tetrameric organization of receptor subunits. Each subunit contains six transmembrane helices (S1 - S6) with a pore-forming loop between S5 and S6 and cytoplasmically located N and C termini[5].

The TRPA1 receptor is the only member of mammalian ankyrin subfamily. This non-selective cation channel was first cloned from human fibroblasts in 1999[6], however, its role in nociception was first described in 2003[7]. Since then, a large amount of chemical activators and inhibitors of TRPA1 have been identified and synthetized for its potential role in inflammatory and neuropathic pain. In addition, mutations within the *Trpa1* gene cause heritable pain disorders such as familial episodic pain syndrome[8] and paradoxical heat sensation in neuropathic patients[9]. Despite more than a decade of intensive research on TRPA1, the molecular mechanisms of channel gating remain largely unknown. This thesis focuses on the functional and structural role of the TRPA1 cytoplasmic termini and the S4-S5 linker in agonist- and voltage-induced gating, and calcium-dependent modulation.

2. Literature review

2.1. Physiological role of temperature-sensitive TRP channels

The ability to detect harmful and irritating stimuli is essential for the survival of all living organisms. Therefore, various mechanisms for recognizing harmless stimuli from the life threatening have evolved. The processes of transduction and transmission of painful signals are called *nociception*. In animals, the nociceptors in primary afferent sensory neurons specifically respond to noxious stimuli by converting them to electrical signals, which are transferred to the central nervous system to produce pain. Myelinated Aδ-fibers and unmyelinated C-fibers are the two main nociceptors, which have cell bodies in the trigeminal, dorsal root and nodose ganglia and terminate as free nerve endings in peripheral tissues such as skin[10]. Apart from the detection of painful stimuli, these fibers are involved in mechanical and thermal detection. The chemical, thermal or mechanical signals are transduced into action potentials by specialized receptors that are expressed in the free nerve endings. Transient Receptor Potential (TRP) channels have been identified as one of the groups of key molecular transducers of thermal and painful stimuli.

In humans, twenty seven TRP channels are expressed in diverse types of cells and tissues. Among them, eleven were described as temperature-sensitive: vanilloid receptors TRPV1 – TRPV4, melastatin receptors TRPM2, TRPM3, TRPM4, TRPM5 and TRPM8, TRPA1 and TRPC5[11–13]. These so called "thermoTRPs" display distinct thermal thresholds. TRPV3 and TRPV4 are sensitive to moderate temperatures (25 – 35 °C)[14–16] while the capsaicin receptor TRPV1 to noxious hot temperatures above 43 °C[2,17]. The thermal threshold for the activation of the TRPV2 channel, which is structurally similar to TRPV1, is even above 52 °C[18]. Melastatin receptors TRPM2 – TRPM5 were described as heat sensors[12,19,20] whereas TRPM8 and TRPC5 are known to be activated by cold. The temperature threshold for TRPC5 activation is between 37 and 25 °C[21] while TRPM8 receptor is activated by cooling agents such as menthol and icilin and noxious cold temperatures below 25 °C[22–24] (Fig. 1, p. 12).

The TRPA1 protein was cloned as one of the last members of the TRP channel family in 2003[7], which implies that the ankyrin family is still not as properly described as the other TRP families. As yet, it cannot be unambiguously decided if TRPA1 is a cold or a

heat-activated channel because the temperature sensitivity of TRPA1 seems to depend strongly on experimental conditions and to be species-specific.

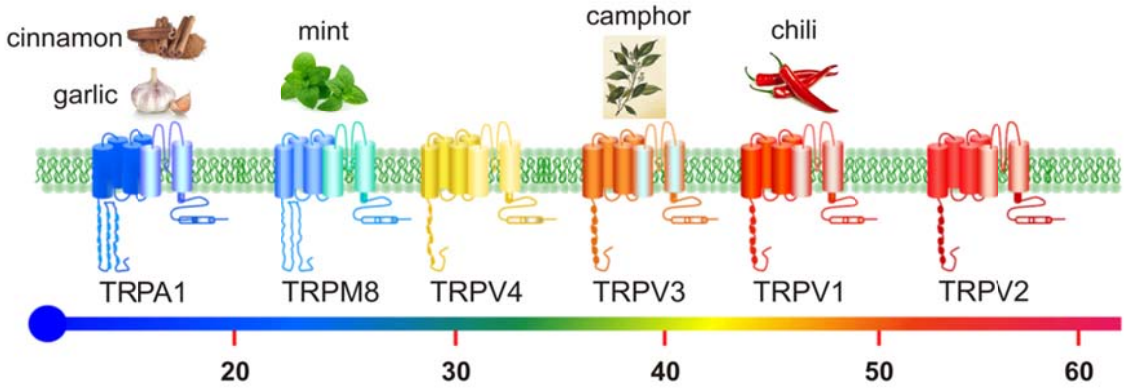

Figure 1. Schematic representation of six mammalian thermoTRP channels. Each subunit consists of six transmembrane helices (S1-S6) and large cytoplasmic N and C termini. ThermoTRPs display distinct thermal thresholds from very hot (TRPV2) to cold temperatures (TRPA1). Each thermoTRP is also activated by specific natural compounds and synthetic substances, which are known to induce the relevant thermal and pain sensations in mammals. Adopted from [13].

2.2. Physiological role of TRP Ankyrin 1 channel and inter-species differences

Mammalian Transient Receptor Potential Ankyrin 1, originally called ANKTM1, is predominantly expressed in free nerve endings in a subset of TRPV1-positive neurons[25] where it acts as a polymodal sensor of diverse physical and chemical stimuli of extracellular or intracellular origin. This only member of the mammalian ankyrin subfamily is a unique protein among TRP channels in that it contains a large number of ankyrin repeats (ARs) within its cytoplasmic N terminus. The TRPA1 channel cDNA was first cloned from mouse trigeminal ganglia in 2003[7]. Also, the role of mouse TRPA1 as a cold sensor in neuronal culture and in heterologous expression system (Chinese hamster ovary cells) was proposed for the first time. Since then, this important property of TRPA1 has been further studied by several scientific groups; however, their observations were not as unambiguous as would be expected.

Two independent lines of knockout mice were generated in 2006[26,27]. The animals were created using similar genetic schemes; however, the resulting phenotypes were different. The first group reported that TRPA1-null mice displayed normal cold sensitivity but

decreased sensitivity to pungent chemicals[26]. The second group described rapidly decreased paw lifting in *TRPA1*$^{-/-}$ mice exposed to 0 °C- cold plate suggesting the involvement of TRPA1 in cold sensation[27]. Other groups either confirmed direct cold activation of rodent TRPA1 in vivo and/ or in vitro[28–30] or disputed it[31–33]. The human orthologue has been shown to be activated by cold in artificial liposomes[34], however, its cold sensitivity was not unambiguously confirmed in heterologous expression system[35–38]. The reason for differences between the results obtained by various groups could be caused by using different experimental conditions, such as expression system, composition of experimental solutions, cooling system etc.

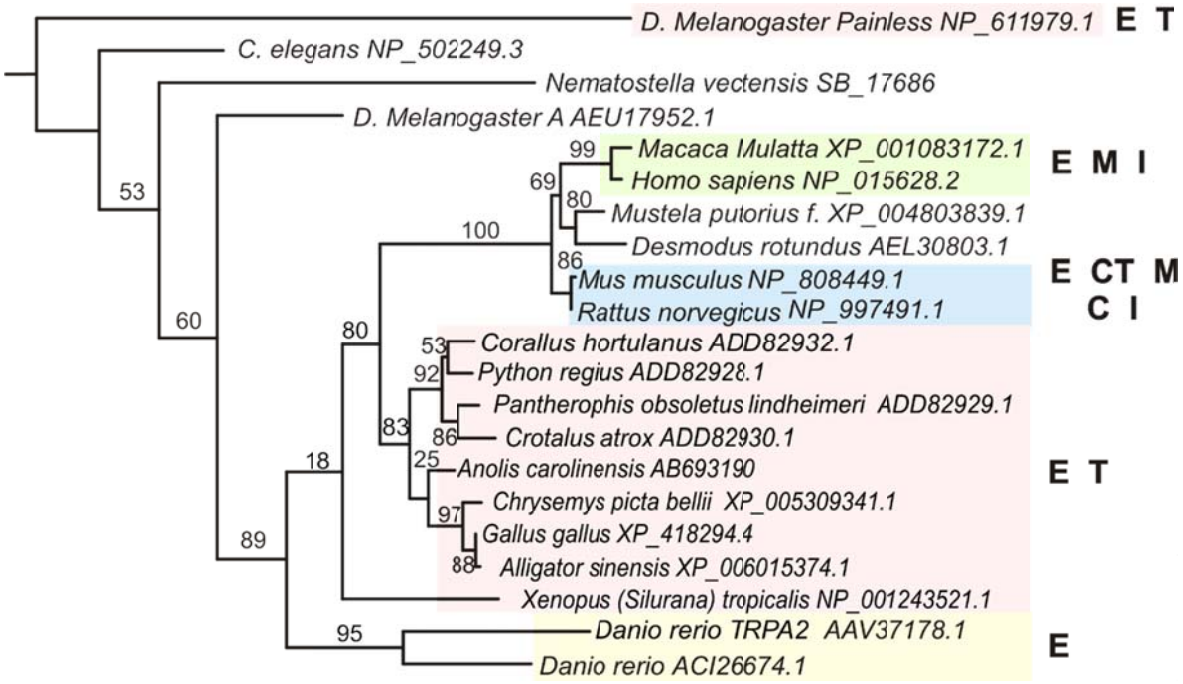

Figure 2. The phylogenic tree of the TRP ankyrin subfamily. Bootstrap, by which the degree of the statistical support for the branching is expressed, is given in percent. Phylogram was constructed by phylogeny.fr server, PhyML method, sequence ordering by ProbCons method for transmembrane parts of TRPA proteins. Identification codes of the individual orthologues correspond to primary sequences from NCBI (National Center for Biotechnology Information) database. On the right, various activation stimuli characterized for the orthologues are indicated – electrophiles (E), temperature (T), cold (CT), menthol (M), caffein (C), inflammatory mediators (I).

Unlike the rodent or human orthologues, some isoforms of the TRPA1 channel in vertebrates can be activated by hot temperatures instead of cold (such as frog, lizard[39], non-pit bearing snake[40] and bird[41] orthologues). Moreover, TRPA1 orthologues from pit bearing snakes act as heat as well as infrared radiation sensors[40]. In lower animals, some

isoforms of TRPA1 can also be activated by heat. *Drosophila melanogaster* orthologue (dTRPA1) functions as a thermotaxis and temperature preference control in both larvae[42] and adult flies[43]. Mosquitos TRPA1 receptors were evolved to sense warm-blooded animals[44]. Surprisingly, both isoforms of zebrafish TRPA1 do not exhibit temperature activation at all[45]. In spite of the fact that different TRPA1 orthologues do not exhibit the same temperature sensitivity, all of them can be activated by pungent chemical compounds. This probably means that the primary evolutionary role of TRPA1 was the detection of harmful substances and its sensitivity to temperature stimuli evolved later as a consequence of selective pressure (Fig. 2, p. 13).

2.3. Inflammatory pain and sensitization of TRPA1 by signaling pathways

As has been mentioned before, nociceptive pain is primarily a physiological protective mechanism. After a tissue damage caused by an injury, a burn, an infection, or a tumor, peripheral sensory system is stimulated. As a secondary effect, an inflammatory reaction follows to protect the organisms against further damage. Inflammatory mediators such as bradykinin, prostaglandins or glutamate are depleted to activate neuronal and non-neuronal cells on site of damage. Several components of this inflammatory soup activate a subset of primary afferent sensory neurons expressing ion channels including TRPA1, which release pro-inflammatory neuropeptides, calcitonin gene-related peptide (CGRP) or substance P. These neuropeptides enhance the immune cell activation and recruitment, and promote a hypersensitivity to thermal, chemical and mechanical stimuli[46,47].

The TRPA1 channel is regarded as a key regulator of neuropeptide release and neurogenic inflammation. Despite a direct activation of TRPA1 by some endogenous inflammatory neuropeptides (such as cyclopentenone prostaglandins), the receptor can also be activated indirectly by an increased concentration of intracellular Ca^{2+} provoked by the interaction of inflammatory mediator bradykinin with one of the G protein-coupled receptors (GPCR) called B_2 receptor. Stimulation of B_2 receptor initiates the phospholipase C (PLC) pathway: PLC breaks down phosphatidylinositol bisphosphate (PIP_2) into diacylglycerol (DAG) and inositol triphosphate (IP_3). Diacylglycerol either activates protein kinase C (PKC) or it can be converted into polyunsaturated fatty acids, such as arachidonic acid, by DAG lipase. Inositol triphosphate, in turn, induces depletion of calcium ions from the intracellular stores in endoplasmic reticulum (ER)[29,48,49]. Calcium

ions released from the ER sensitize the TRPV1 receptor and the influx of extracellular calcium ions together with Ca^{2+} depleted from intracellular stores open TRPA1[31,50]. Similarly, the phosphorylation of TRPV1 by PKC leads to a resembling effect (Fig. 3).

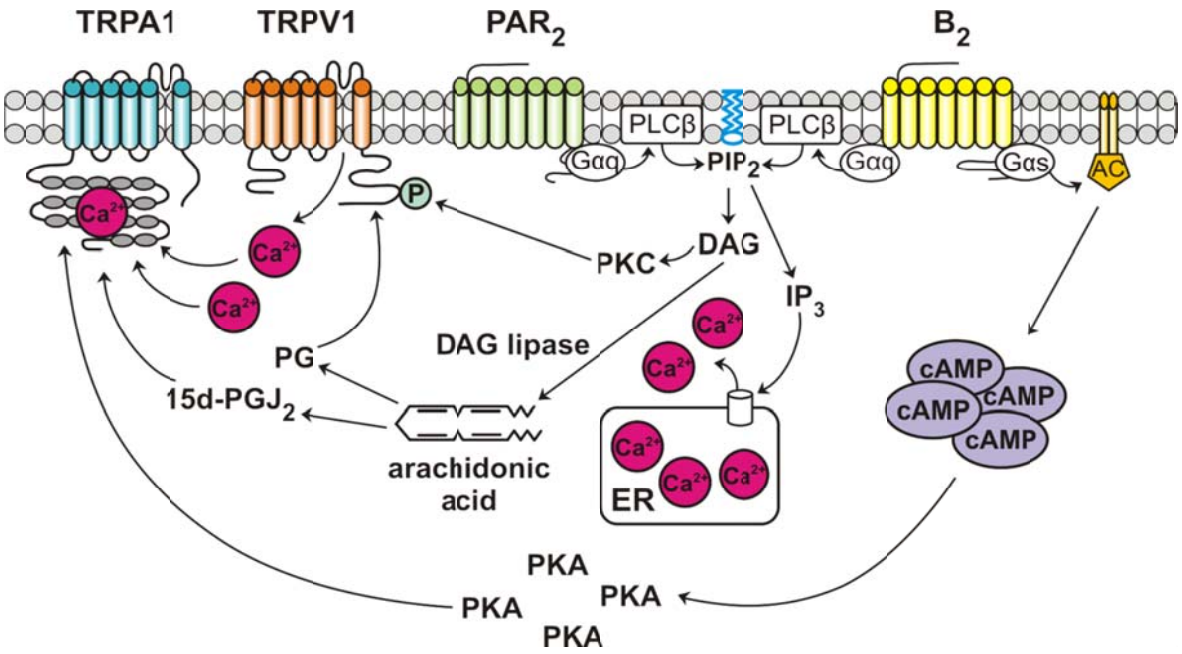

Figure 3. Intracellular mechanisms of TRPA1 sensitization. The binding of an agonist to bradykinin receptor 2 (B_2) or protease-activated receptor 2 (PAR_2) triggers phospholipase Cβ (PLCβ) through Gαq protein coupled mechanism. PLCβ cleaves phosphatidylinositol-4,5-bisphosphate (PIP_2) in diacylglycerol (DAG) and inositol triphosphate (IP_3). Ca^{2+} release from the endoplasmic reticulum (ER) induced by IP_3 directly sensitizes the TRPA1 receptor. The activation of protein kinase C (PKC) by diacylglycerol phosphorylates TRPV1 and sensitizes this receptor to an agonist, promoting Ca^{2+} influx. The unsaturated arachidonic acid is yielded from DAG by DAG lipase. The product of metabolism of the arachidonic acid, 15-deoxy-$\Delta^{12,14}$-prostaglandin J2 (15d-PGJ_2), directly activates TRPA1. The other prostaglandins (PG) yielded from arachidonic acid also sensitize TRPV1. The B_2 receptor stimulates the Gαs protein that activates the synthesis of cyclic adenosine monophosphate (cAMP) by adenylate cyclase (AC). The activation of protein kinase A (PKA) by cAMP sensitizes TRPA1. Adopted and adjusted from [49].

In addition, after binding of bradykinin, B_2 receptor stimulates another subunit, Gαs, which activates adenylate cyclase to produce cyclic adenosine monophosphate (cAMP). cAMP activates protein kinase A (PKA) that directly sensitizes TRPA1[51] (see the scheme in Fig. 3).

The TRPA1 sensitization by another GPCR, protease-activated receptor 2 (PAR_2), shares a similar mechanism to the indirect activation by bradykinin. After a cleavage of

PAR_2 by proteases within its extracellular N terminus, the receptor stimulates its Gαq subunit, which activates PLC pathway[52] (Fig. 3, p. 15).

2.4. Heritable disorders of pain sensation: The role of TRPA1

Generally, TRP channels are associated with physiological and pathophysiological pain. However, the molecular mechanisms of cold or heat hyperalgesia, allodynia or paradoxical temperature sensation have not yet been fully understood.

Inherited neurological disorders caused by mutations in various ion channels are associated with diverse pathological pain states. In case of TRPA1, two heritable pain disorders (also called *channelopathies*) caused by point mutations in the *Trpa1* gene have been described.

The first pain-associated channelopathy that was identified in one Colombian family (South America) by Kremeyer et al. in 2010 is called familial episodic pain syndrome[8]. This rare autosomal-dominant syndrome is characterized by episodes of intense upper body pain usually triggered by fasting, fatigue or cold temperatures. Outside the episodes, no altered pain sensitivity was reported. After a genome-wide linkage scan, the mutation of asparagine 855 to serine (N855S) located in the linker between the fourth and fifth transmembrane helices (S4-S5 linker) of TRPA1 was identified.

Heterologously expressed N855S mutant was characterized by using whole-cell electrophysiology. The mutant exhibited 4-fold increase in inward current than wild-type channel (WT) while the outward currents remained unchanged. This result is consistent with the observed pain syndrome.

Another variant of TRPA1 channel E179K is associated with paradoxical perception of cold stimuli in neuropathic pain patients[9]. Functional *in vitro* analysis confirmed that E179K mutant is not activated by cold although it is widely expressed in both cold- or heat-treated cells. The loss of cold sensitivity of TRPA1 with a lysine at position 179 was explained as a disturbance in ability to form oligomers.

2.5. Structure of the TRPA1 channel

The TRPA1 channel, similarly as the other TRP channels, shares a resembling membrane topology as the voltage-gated potassium (Kv) channels. Molecular structure of a subunit of the human TRPA1 receptor is formed by 1,119 amino acid (AA) residues, and consists of the cytoplasmically oriented amino- and carboxy-termini and six transmembrane helices. The TRPA1 ion channel is usually formed by a symmetric homotetrameric organization of these subunits in plasma membrane. However, heterotetrameric forms of TRPA1 with TRPV1 channels have also been described *in vitro* and *in vivo*[53,54].

The three-dimensional structure of any of the TRP channels has not been resolved for a long time because the crystallization of the transmembrane parts of membrane proteins still remains a rather difficult task. In 2011, the first structural information about the mouse TRPA1 was obtained by single-particle electron microscopy (EM)[55]. The resolution was not very high, only about 16 Å. However, the proportions of the individual parts of the channel protein have been predicted by using primary sequence analysis. According to these results, TRPA1 is a homotetrameric structure. The 3D density map revealed a transmembrane and a cytoplasmic region, which is organized in a compact structure reminding "a hanging basket" and, unlike the other TRP proteins, forms a central cavity. The transmembrane part is formed by 22% of amino acids, the N terminus by 64% and the C terminus by 14% of amino acids. The resolution, however, was not sufficient for determining the molecular interactions between the individual residues (Fig. 4A, p. 18).

Most recently, a structure of the human TRPA1 at a 4.2 Å resolution has been published[56]. The authors used an originally developed method of reconstruction of single-particle electron cryo-microscopy (cryo-EM) data similarly as two years earlier when they resolved a near-atomic structure of the related protein TRPV1[57,58]. Unlike the TRPV1 structure, the structure of TRPA1 was obtained only for a closed state of the channel. Due to the presence of highly flexible regions, the high-resolution structure of the TRPA1 includes the region from Lys446 to Thr1078, which represents about 50% of the protein (Fig. 4B, 4C and 4D, p. 18). However, thanks to the new structure, many previous observations on TRPA1 can be explained in a structural context and may contribute to understanding of molecular activation mechanisms of TRPA1.

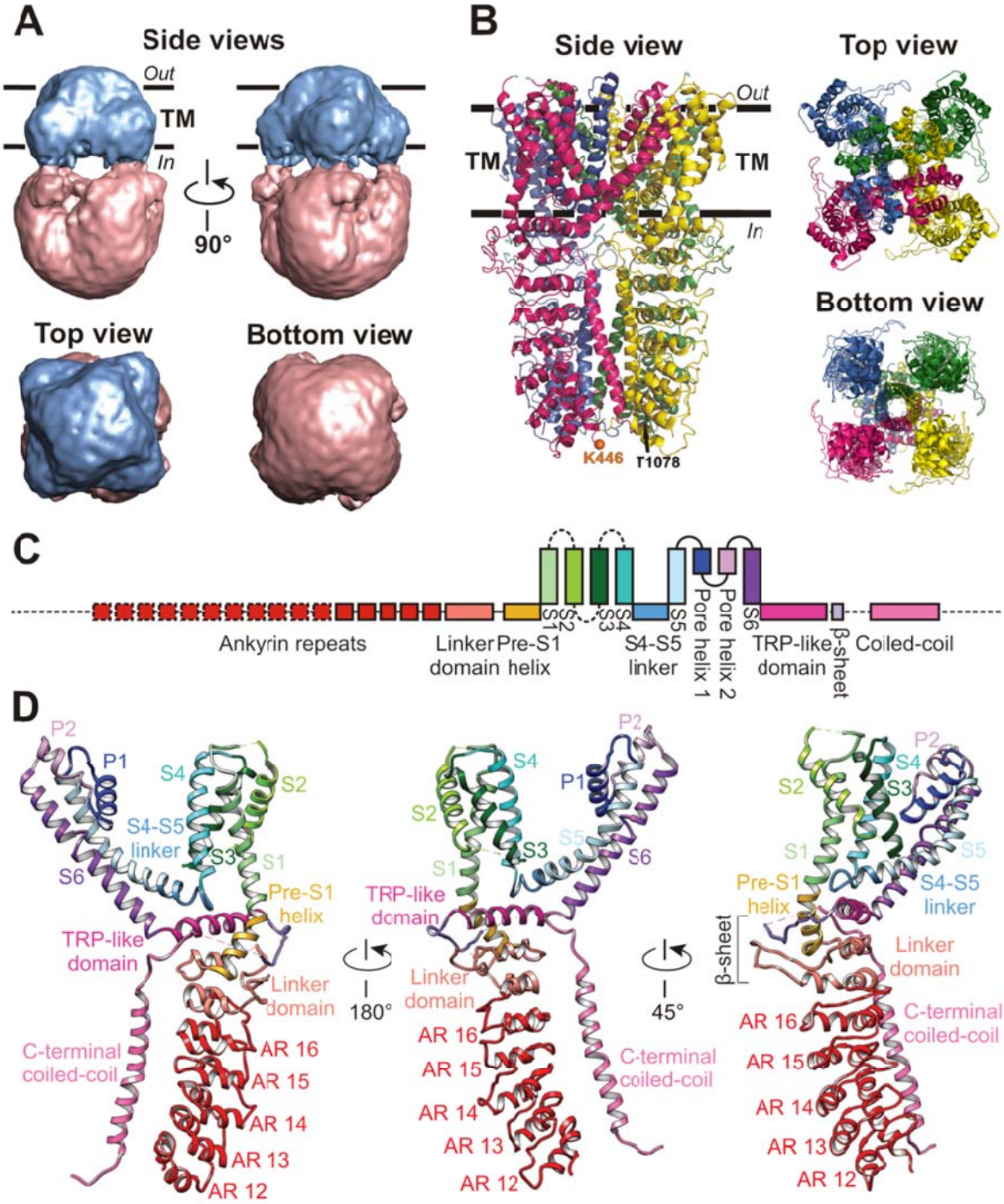

Figure 4. Structure of TRPA1. ***(A)*** Three dimensional reconstruction of electron microscopy structure of mouse TRPA1. Transmembrane part is indicated in blue, cytoplasmic part in pink. Side, top and bottom views are shown. Adopted from [55]. ***(B)*** Ribbon diagram of atomic model of human TRPA1 for residues K446 – R1078 with each subunit colored. Side, top and bottom views are shown. ***(C)*** Linear diagram depicting major structural domains color-coded to match ribbon diagrams below. Dashed lines and boxes denote regions for which density was insufficient to resolve detailed structure (sequence before AR12, loop containing Cys 665, S1–S2, S2–S3 and S3–S4 linkers, connection between third β-strand and coiled-coil, C terminus subsequent to coiled-coil), or where specific residues could not be definitively assigned (portion of the linker before and after the coiled-coil). ***(D)*** Ribbon diagrams depicting three views of the TRPA1 subunit. (B, C, and D) adopted from [56].

2.5.1. Transmembrane region of TRPA1

The transmembrane domain is the most conserved region among TRP channel proteins. Each subunit of TRPA1 consists of six transmembrane helices (S1-S6) that are connected with extra- and intracellular loops while the helices S5 and S6 together with the S5-S6 loop comprise the central pore of the ion channel. The detailed structure of the linkers between S1-S2, S2-S3 and S3-S4 has not yet been resolved but the S4-S5 linker is formed by a single α-helix. The tetrameric architecture of the TRPA1 transmembrane domain is similar to TRPV1 and, in general, voltage-gated channels: transmembrane helices S1-S4 form a "bundle" and this so-called *sensor domain* is in contact with S5 and S6 helices of the neighboring subunit, which forms a domain-swapping structure[57,59–61] (Fig. 5A, p. 20).

The outer pore domain of TRPA1 contains two pore helices unlike the TRPV1 channel with a single pore helix[56,57]. The selectivity of TRPA1 for mono- and divalent cations is determined by a selectivity filter (AA sequence ^{914}GDI^{916}), which is located between the two pore helices[62]. According to the new structural model, the aspartate D915 forms the upper gate of TRPA1. The restriction point between two diagonally opposed D915 residues is 7 Å wide, which indicates that the upper gate is wide enough to accommodate partially dehydrated calcium ions[63]. The lower gate of TRPA1 is formed by two hydrophobic residues isoleucine I957 and valine V961 that are located at the lower part of the S6 helix (Fig. 5B, p. 20). The constriction between them (6 Å) is sufficient to block conduction of rehydrated cations[56].

The gating mechanisms of TRPA1 have been intensively studied, however, they have not yet been fully understood. Several mutagenesis studies have been performed to identify residues within the pore region, which could be involved in the channel gating. A non-polar residue leucine L906 within the first pore helix of mouse TRPA1 plays an important role in the voltage-dependent activation and inactivation[64]. Residues G958 and G962 located within the S6 helix in the vicinity of the lower gate of TRPA1 correspond to a bi-glycine motif G(X)$_3$G in voltage-gated calcium channels $Ca_v1.2$ and $Ca_v2.3$[65]. Mutations of these two glycines may narrow the pore size and affect the ion permeation properties of TRPA1. Also, proline P949 is structurally required for opening and closing of the channel[66].

Various studies based on homology modeling and molecular dynamics (MD) simulations have been performed to find out the gating mechanisms of TRP channels by comparison with Kv channels. The authors of the most recent one compared the

transmembrane regions of TRPV1 and Kv1.2/2.1 paddle chimera using structural-based alignment[61].

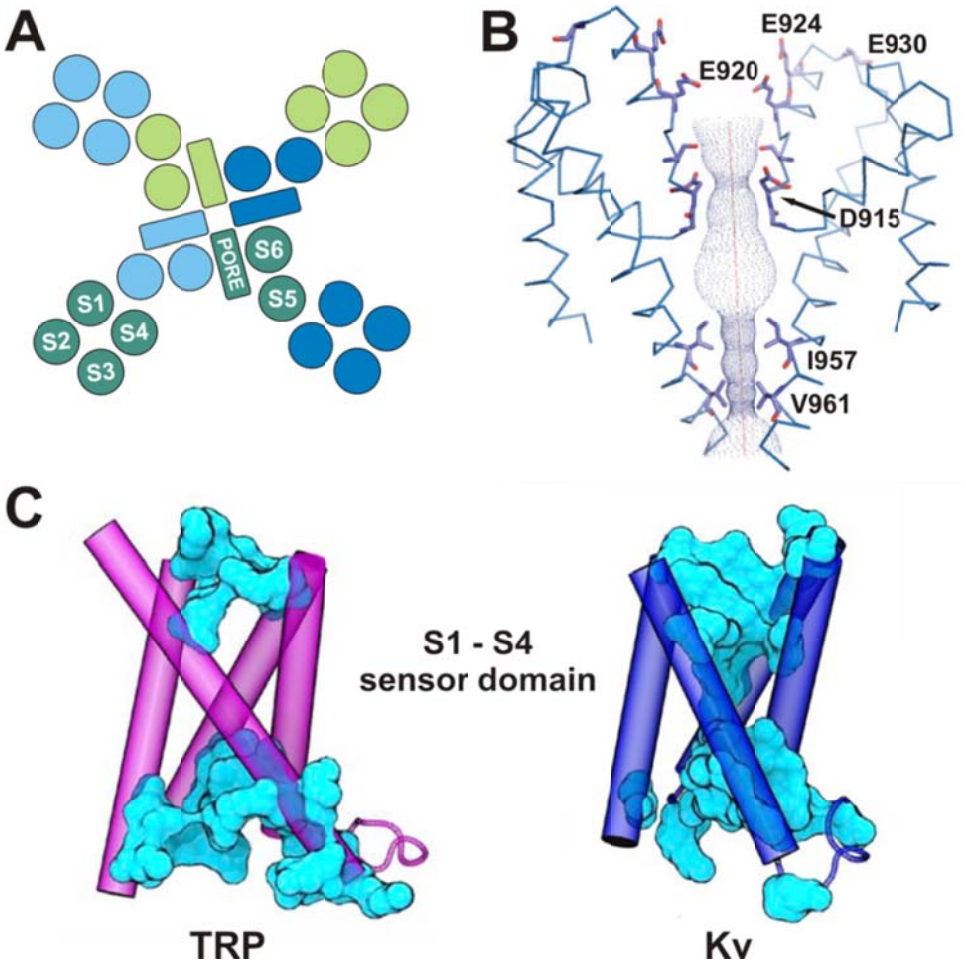

Figure 5. Transmembrane region of TRPA1. ***(A)*** Conserved architecture of tetrameric channels with six transmembrane segments. Four S5 helix - pore helix – S6 helix motifs form an ion conducting pore whereas helices S1-S4 from each subunit form a separate „sensor domain". ***(B)*** Wire-frame model of the TRPA1 channel pore. D915 between the first and second pore helices contributes to the upper restriction of the pore, I957 and V961 form the lower gate. Negatively charged residues E920, E924 and E930 in the second pore helix probably form a negatively charge conduit to attract cations and repel anions. Adopted from [56]. ***(C)*** Average polarity in the TRP- or Kv-sensor domains. Positions slightly more polar than serine are shown as a blue surface. Note the asymmetric solvation of the TRP sensor domain. Adopted from [61].

The TRPV1 channel has been chosen as a "typical TRP" because several structures of TRPV1 in a closed and two open states have been resolved and the sequence of its transmembrane domain predominantly corresponds to other TRPs. Despite the structural similarity with Kv channels, the TRP sensor domain (S1 – S4 helices) probably does not act as a canonical voltage sensor in any of TRP homologues because of asymmetric

solvation of the sensor. The lower vestibule of TRPV1 is splayed open and occupied by the polar face of the C-terminal TRP helix. The upper part of the vestibule, on the contrary, is densely packed with the aromatic and hydrophobic residues and rather unsolvated. The authors mean that the asymmetric solvation of the sensor domain is likely to be a conserved feature of TRP channels (Fig. 5C, p. 20). In addition, the S4 helix of TRPV1 contains only one positively charged residue corresponding with a weak voltage-sensitivity of TRPs.

On the other hand, the structural models suggest that the TRP pore helix is a highly dynamic structure, which could act as a fundamental gating feature of most TRPs. This idea is supported by the three structures of TRPV1 in different conformations where the pore helix shows a different location in each conformation. Another important gating element is the transmembrane helix S6, which seems to be flexible due to its distortion around a tyrosine residue in the middle of the helix. The distorted conformation of S6 is probably stabilized by an interaction with the bottom part of S5. During the channel opening, the aforementioned motion of the pore helix is probably translated into pore gating by enhancing the relative stability of S6 backbone hydrogen bond networks[58,61].

Importantly, the new structure of TRPA1 revealed an analogous distortion of its S6 indicating a similar gating mechanisms of both channels. In TRPA1, the antagonist binding site is located within the S5 helix in the vicinity of a helical distortion of S6, suggesting that the subtle conformational changes around the helical defect could promote a displacement of some of the pore-lining residues[56,61]. However, some differences between TRPV1 and TRPA1 channel gating could be expected because of the presence of two pore helices in the TRPA1 structure. Furthermore, the structure of TRPA1 in an open state with a bound agonist still has to be elucidated.

2.5.2. Amino terminus of TRPA1

The N-terminal part of TRPA1 constitutes more than a half of the protein size (720 of 1119 amino acids in a human orthologue). It is characterized by a prominent ankyrin repeat domain (ARD; residues 1-649) consisting of a tandem array of 16 or 17 ankyrin repeats (ARs) and a linker region connecting the ARD with the fist transmembrane segment[55,56,67]. The ankyrin repeat is a common structural motif, typically of 33 amino acid residues, which forms an anti-parallel helix-turn-helix structure followed by a β-hairpin loop. Five of seventeen ARs of human TRPA1 contain a tetrapeptide motif T/SPLH, which is highly

conserved among ankyrin proteins. In such a motif, proline initiates the first α-helix, whereas the pair of threonine and histidine forms intra- and inter-repeat bonds thus contributing to local conformational stability of the AR[68,69] (Fig. 6A). The neighboring ankyrin repeats tend to stack together and form elongated domains, which are important for protein-protein interactions[70,71]. Moreover, the ARs can serve as the binding sites for non-protein ligands[72].

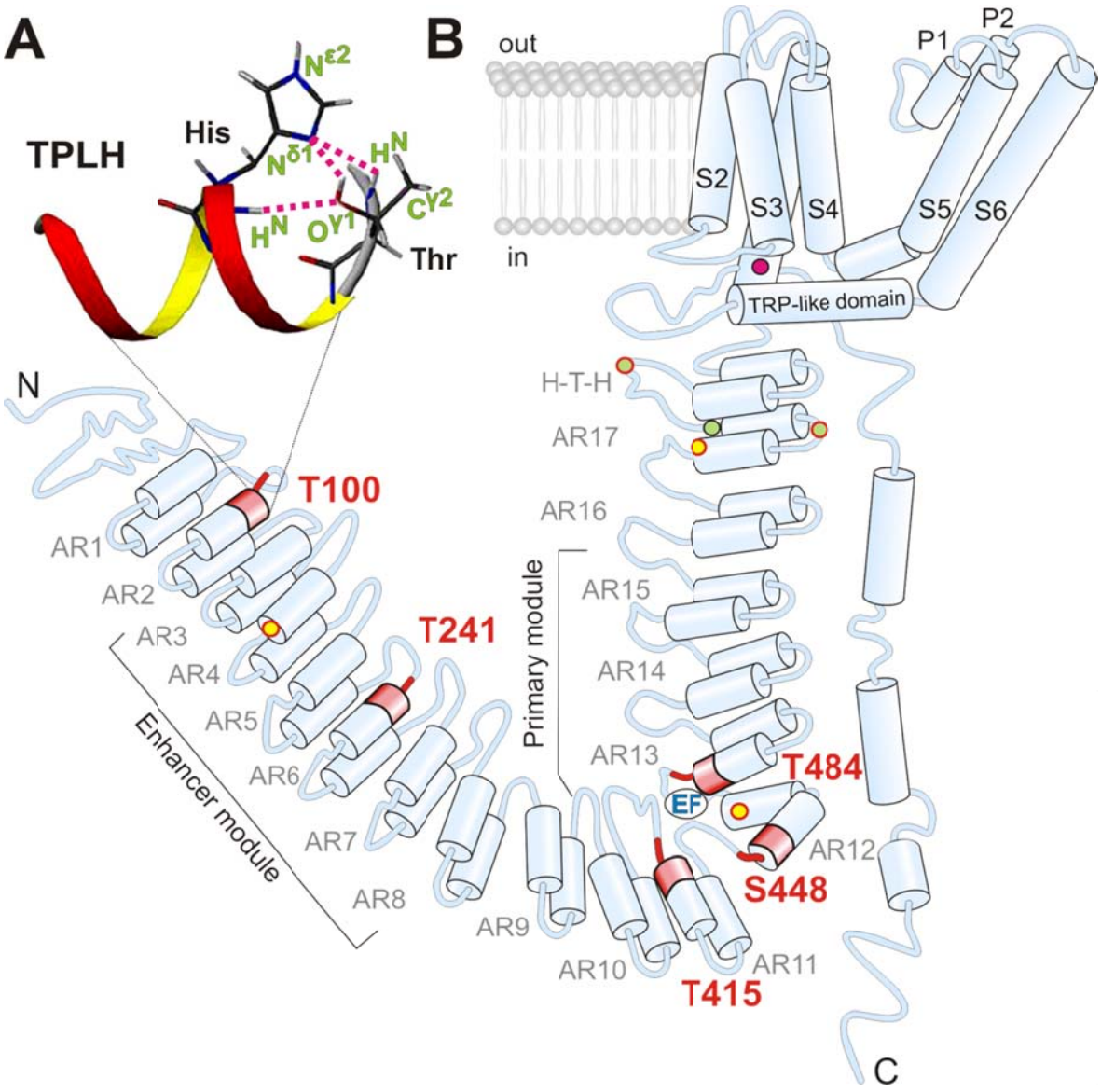

Figure 6: Topology of TRPA1. ***(A)*** Hydrogen bonds attributed to a TPLH motif (adopted from [68]). ***(B)*** Schematic of one hTRPA1 channel subunit. Conserved threonines and serine from T/SPLH tetrapeptide motifs are indicated in red, reactive cysteine residues (C621, C641 and C665) are represented by green circles, reactive lysine residue (K710) is depicted by a pink circle. Cysteine residues involved in forming disulphide bonds are represented by either yellow or green circles with a red edge. The EF-hand like domain is depicted as "EF".

Ankyrin repeat-containing proteins can be divided into two categories. The first one is characterized by a small set of four to seven ARs forming a structural domain. Among the TRP proteins, vanilloid receptors with five or six and canonical TRPs with four or five amino terminal ankyrin repeats fit into this group. Ankyrin and no mechanoreceptor potential C (TRPN) TRP channels, on the contrary, contain a high number of ARs (16 – 29). The TRPN channels are expressed in non-mammalian organisms and they are implicated in mechanosensation[73]. The ankyrin domain of TRPN channels consists of 29 ARs and it is predicted to have an elongated coil shape, which probably acts as a spring that directly senses mechanical stimuli[74]. Similarly, the TRPA1 protein in mammals is widely expressed in the hair cells of the inner ear, which makes it a candidate for the mechanosensitive channel responsible for transduction of acoustic stimuli into electrical signal[75]. However, this hypothesis was disproved by two independent studies where was shown that TRPA1 knock-out mice were not hearing-impaired[26,27]. Although TRPA1 does not act as a mechanotransducer in hearing, its role in mechanosensation was confirmed in mouse nerve-skin preparations[26].

The recent structural analysis of the human TRPA1 brought a new insight into the N-terminal ARD organization. The distal N terminus (AR1-AR11) has not been precisely resolved in the structure suggesting its flexibility, which could be mediated by AR10. The sequence of AR10 deviates from the consensus: two prolines probably disrupt the second helix and form a kink. On the contrary, the proximal N terminus (AR12-AR17 and the linker-region) has been described as a well-resolved convex “stem”. Secondary structure of the linker region consists of two helix-turn-helix motifs connected to each other by a putative β-strand and the second helix-turn-helix is connected to the pre-S1 helix. The structural model also indicates the side chain interactions of AR12 with the C-terminal coiled-coil domain as well as interaction of AR16 with the first helix-turn-helix[56] (see Fig. 7A and 7B, p. 26).

The N terminus has long been known to be an immediate detector and integrator of the TRPA1 activation stimuli. Initial mutagenesis studies proposed that membrane-permeable electrophilic molecules react with free sulfhydryl groups on specific cysteines and the primary amine of lysines (C621, C641, C665, K710 in human and C415, C422 and C622 in mouse), inducing conformational changes leading to channel opening[76,77] (Fig. 6B, p. 22). According to the structure of hTRPA1, the cysteines essential for binding electrophiles are solvent-accessible. However, even if the samples used for the structure

were exposed to allyl isothiocyanate, neither expected cysteine adducts, nor the channel opening were observed[56,67].

Alternatively, the cysteine residues can be involved in forming disulphide bonds. Four combinations of disulphide bonds in mouse TRPA1 have been identified by mass spectrometry: cysteine C666 with C622, C463 and C193, respectively, and C622 with C609. The authors hypothesized that the disulphide bonds may play a protective or regulatory role in the activation or desensitization mechanism of TRPA1[78] (Fig. 6B, p. 22).

The AR12 contains a sequence EF-hand-like motif (AA 468 – 480) which has been thought to regulate TRPA1 activity through binding the intracellular Ca^{2+} ions[31,50]. However, this hypothesis has been disputed because the Ca^{2+}-dependent activation mechanism is not much influenced by the mutations within the EF-hand-like motif while the deletion of this motif disturbs trafficking of TRPA1 to the plasma membrane[62,79].

A systematic study based on a series of chimeras between rattlesnake and human TRPA1 revealed that an AR cluster centred around AR11 acts as an important determinant of Ca^{2+}-dependent desensitization[37]. This work has also proposed two spatially distinct, independent and transferable N-terminal AR modules: the primary module (AR10-AR15) and the enhancer module (AR3-AR8). Each module is capable of conferring thermal or electrophilic sensitivity to the respective, otherwise insensitive orthologue (Fig. 6B, p. 22). In addition, AR6 is uniquely sensitive to changes in the coupling of temperature stimuli to the channel gate, and a single-point mutation S250N in AR6 induced heat- instead of cold-activation without changing the sensitivity to chemical agonists in mouse TRPA1[80].

Most recently, the N terminus of TRPA1 has been shown to be surprisingly dispensable for a functional channel[34]. After a deletion of the ARD (Δ1-688) of human TRPA1 and its reconstitution into a planar lipid bilayer, the channels remained functional and sensitive to electrophilic and non-electrophilic agonists and cold temperatures. Moreover, any accessory proteins or calcium ions do not seem to be required for the ARD-deleted channel activation. Thus, the functional role of the N terminus now appears to be less clear than previously assumed and may consist of forming multi-ligand binding sites, interacting with other proteins, including self-association with other non-contiguous structures of the TRPA1 channel homotetramer[71], the proper targeting of the protein into the plasma membrane[34,79], and, importantly, in the direct regulation of the channel's gating[34].

2.5.3. Carboxy terminus of TRPA1

The C terminus is the smallest part of TRPA1. Initially, six α-helical segments within the C terminus were predicted from primary sequence: two longer helices H1 (I964 – K989) and H4 (L1040 – K1071) and four shorter helices H2 (W993 – V998), H3 (L1016 – F1022), H5 (D1089 – Q1095) and H6 (W1103 – K1111)[81]. According to the new structural model, the proximal C terminus is divided into a TRP-like domain, a putative β-sheet and a long coiled-coil. The structure of the distal C terminus has not been resolved yet[56].

The TRP-like domain shows a structural similarity with an α-helical TRP domain containing a TRP box, which is a characteristic consensus sequence motif (EWKFAR) of many TRPs from vanilloid, canonical and melastatin families[82]. Similarly as a vanilloid TRP domain, the TRP-like domain of TRPA1 is running from S6 helix beneath the S4-S5 linker and interacting with the pre-S1 helix and the second helix-turn-helix (Fig. 7C, p. 26). Although the TRP box has never been predicted in ankyrin family[71], the helical TRP-like domain could play an important role in channel gating similarly as in TRPV1. This idea can be supported by a previous study, where the mutations of positively charged residues in the vicinity or within the TRP-like domain (namely R975, K988 and K989) affected voltage-dependent gating of TRPA1[81].

A newly discovered tetrameric coiled-coil domain is located below the central pore. Four α-helices (residues E1043 – Q1070) from each subunit of the TRPA1 tetramer interact together through the isoleucine and glutamine residues, which could have either a destabilizing (interaction of residues I1044 and Q1047) or a stabilizing effect (I1065 and Q1061) on the structure through intra-planar hydrogen bonds[56,83]. Unlike most coiled-coils, the residues on the exterior surface of TRPA1 coiled-coils are often hydrophobic or aromatic, which allows the interaction of the C-terminal coiled-coil with the aforementioned ankyrin repeats.

Some physiological studies have previously described the effects of inorganic polyphosphate on TRPA1 currents in excised membrane patches[62,84]. During the purification process, inositol hexakisphosphate (IP6) has been used to stabilize the TRPA1 structure. The negatively charged IP6 interacts with positively charged residues K1046 and K1050 from one coil and K1048 and K1052 from an adjacent coil. Furthermore, inositol hexakisphosphate helps to prevent the destabilizing effect of glutamine Q1047 through its coordination with neighboring K1046 and K1048[56]. As previously shown, mutations of the

positively charged residues that bind the IP6 mostly resulted in non-functional channels suggesting their importance for the stability of the channel[81].

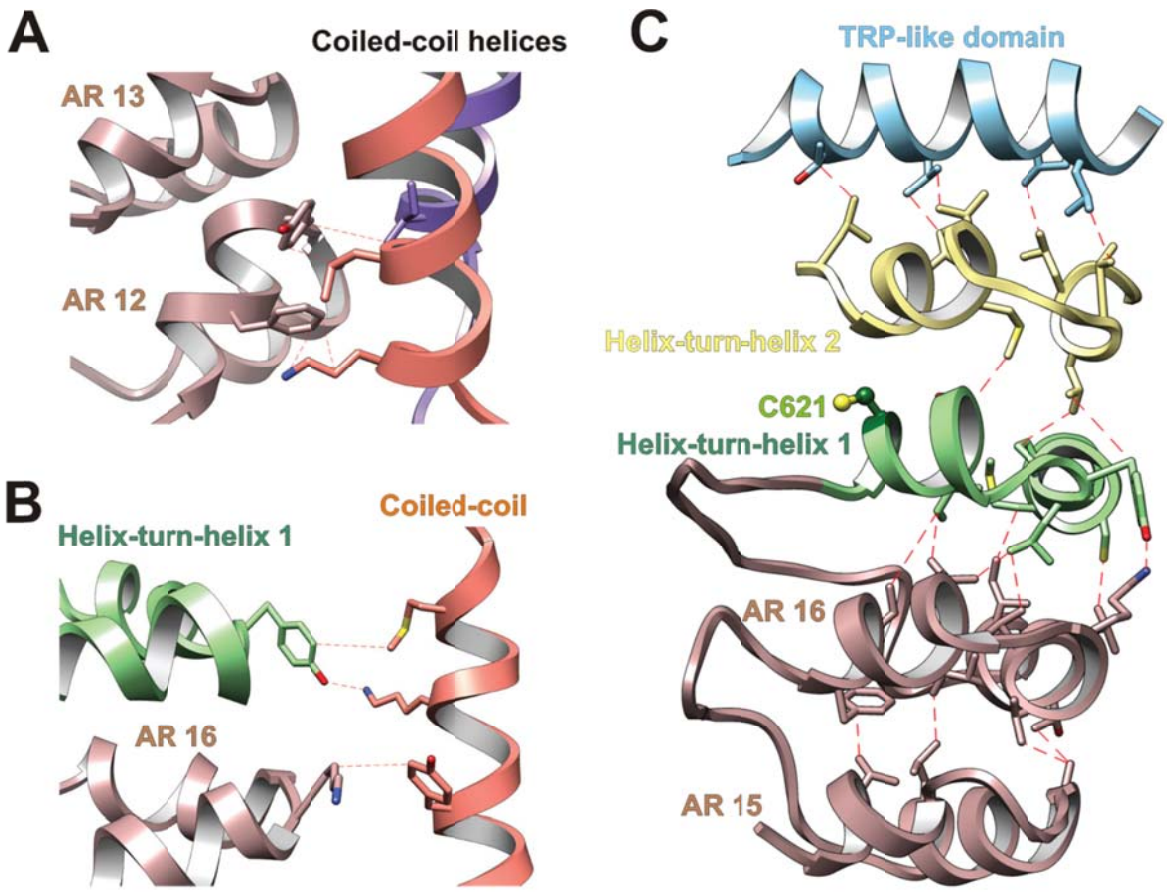

Figure 7. Interactions between N- and C-terminal structural motifs. ***(A and B)*** The ankyrin repeat domain (ARD) and the linker region make connections with the coiled-coil through a series of hydrophobic, polar and potentially π-cation interactions involving residues in AR12 and AR13 (A) as well as AR16 and the first helix-turn-helix of the linker region (B). ***(C)*** The interdigitated convex 'stem' region of the ARD consisting of AR12–AR16 (only AR15 and AR16 are shown; rose) couples to the allosteric TRP-like domain (blue) through interactions with two intervening helix-turn-helix motifs (green and yellow) of the linker region. AR15–AR16 stacking is stabilized through hydrophobic interactions. AR16 is also connected to the overlying first helix-turn-helix motif through hydrophobic and polar interactions. Adopted from [56].

2.6. Modulation of TRPA1 by post-translational modifications

TRPA1 is likely to be modulated by phosphorylation. As has been mentioned above, the function of the receptor can be modulated by polyphosphates and signaling cascades, whose components are protein kinases PKC and PKA[49]. Although the post-translational modifications of the TRPA1 protein have not been reported yet, the regulation of a channel expression and function can be expected because of a cross talk between TRPA1 and TRPV1 receptors[85].

In addition to phosphorylation by kinases PKC and PKA, the TRPV1 receptor has been reported to be phosphorylated by the cyclin-dependent kinase 5 (Cdk5). Cdk5 is predominantly expressed in neuronal tissues where it is involved in several cellular processes such as regulation of cytoarchitecture in the central nervous system, regulation of neuronal migration, axon guidance, synaptic structure and plasticity or membrane transport[86].

Cdk5 belongs to the large group of cyclin-dependent kinases, however, it is neither activated by cyclins, nor does it participate in the cell cycle progression. Instead, association of Cdk5 with p35 (or its splice variant p25) and/or p39 proteins is required for activation of the kinase[87–89]. As the p35 is a membrane-bound protein, physiological substrates of Cdk5 are likely to be transmembrane or membrane-associated proteins. The mice with deleted gene for Cdk5 and p35/p39 double knock-out mice have been shown to be embryonically lethal with neuronal migration defects, indicating that the kinase and its adaptor proteins are required for normal development[90–92].

Cdk5 is a protein-directed kinase that phosphorylates serine or threonine residues located immediately next to a proline residue. Its consensus motif is (S/T)PX(K/H/R), where X is any amino acid[93]. In TRPV1, two threonine and one serine residues correspond to this consensus where only threonine T407 is a target residue for Cdk5[94,95].

In TRPA1, serine 448 was predicted as a candidate residue for phosphorylation. A peptide containing S448 was shown to be phosphorylated by Cdk5 *in vitro*. However, fluorescence experiments in the living cells brought inconsistent results[96].

2.7. Chemical sensitivity of human TRPA1 channel

The TRPA1 receptor constitutes a target for various pungent and irritating chemical substances of endogenous and exogenous origin. As mentioned in section 2.3, endogenous inflammatory mediators such as bradykinin can activate the TRPA1 receptor to produce neurogenic inflammation and, therefore, hypersensitivity of the organism and pain[29]. The exogenous modulators of TRPA1 have the same effect on the receptor as endogenous compounds. The origin of the exogenous chemicals is either natural, or synthetic. Pungent compounds from cinnamon (cinnamaldehyde; CA), horseradish and wasabi (allyl isothiocyanate; AITC)[29,36] or garlic (allicin)[97] belong to the first aforementioned group whereas some synthetic drugs (general anesthetics isoflurane or propofol)[98,99] and acrolein, an irritant in tear gas and vehicle exhaust fumes[26], are only a few examples from the second group (Fig. 8A and 8B).

From chemical point of view, modulators of TRPA1 can be both electrophilic and non-electrophilic compounds. The electrophilic compounds bind covalently to TRPA1 while the non-polar ligands interact with TRPA1 by the mechanism ligand-receptor.

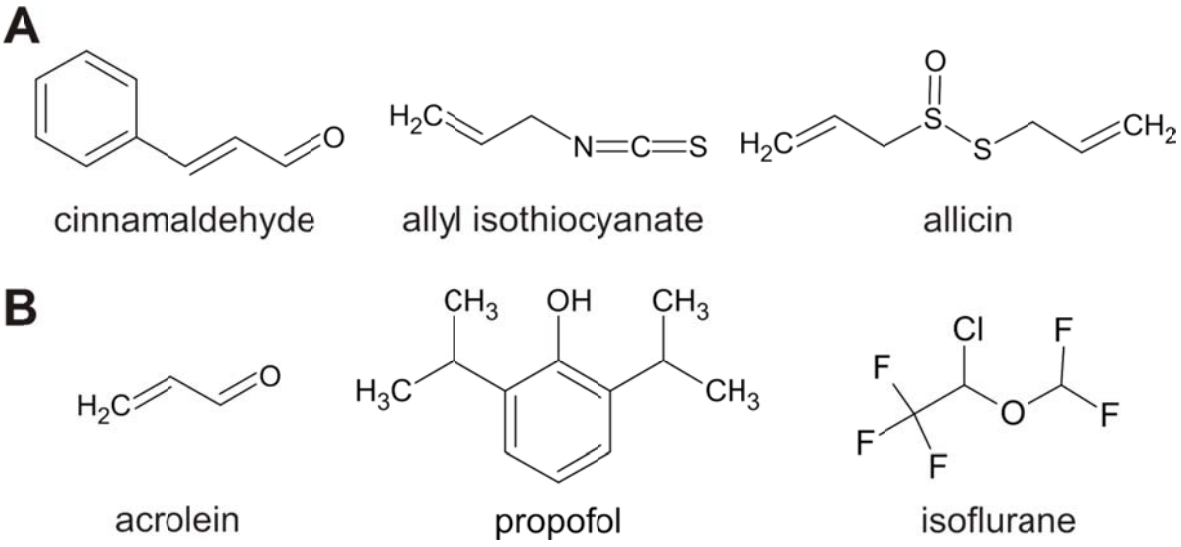

Figure 8. Examples of the TRPA1 agonists. ***(A)*** Natural exogenous compounds. ***(B)*** Synthetic exogenous compounds.

2.7.1. Activation of TRPA1 by electrophilic compounds

The variability of TRPA1 covalent agonists is enormous. Interestingly, except for exogenous and endogenous electrophilic pungent chemicals (CA, AITC, acrolein,

cyclopentenone prostaglandins), TRPA1 acts as a sensor for oxygen, reactive oxygen species (ROS) and reactive nitrogen species (RNS)[100–102].

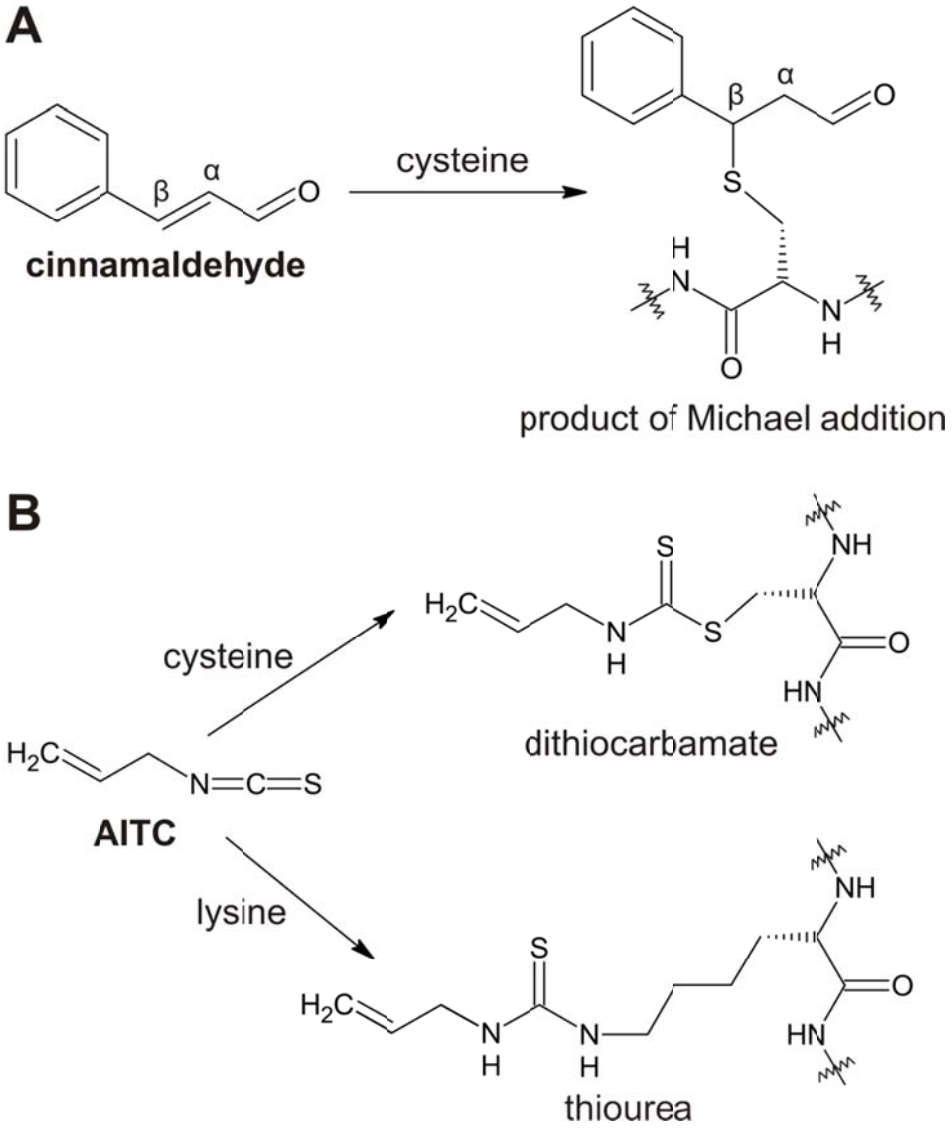

Figure 9. ***(A)*** Reaction of cinnamaldehyde with a cysteine residue of a protein. ***(B)*** Reaction of allyl isothiocyanate with a cysteine (top) or lysine (bottom) residue of a protein.

The mechanisms of covalent modification of nucleophilic cysteine or lysine residues C621, C641, C665, K710 in hTRPA1) within the N terminus have been well characterized. The reactions include nitrosylation (nitric oxide), sulfhydration (sulfane), forming of a disulphide bond (hydrogen peroxide) and alkylation[100]. The electrophiles alkylate TRPA by the mechanism known as the Michael addition. The unsaturated bond of α,β-unsaturated aldehydes such as acrolein, cinnamaldehyde or allyl isothiocyanate is attacked by

a nucleophilic mercapto-group of cysteine or an amino group of a lysine (Fig. 9A and 9B, p. 29)[76,77]. Surprisingly, electrophilic compounds require the presence of polyphosphates to activate TRPA1 in the inside-out patches while a non-electrophilic substance, Δ^9-tetrahydrocannabinol, does not, indicating the complexity of the TRPA1 channel gating[103].

2.7.2. Activation of TRPA1 by non-electrophilic compounds

The exact mechanism of non-covalent interaction with TRPA1 is much less understood, most likely in the manner of an interaction with a specific binding site. Until now, the only compound with a defined binding site is menthol, which binds between the fifth and sixth transmembrane helices (Fig. 10). Residues S876, T877 and G878 seem to be crucial for binding menthol as well as some non-covalent antagonists of TRPA1 (namely AP18 and AMG 5445)[104].

In addition, menthol shows a bimodal effect on TRPA1. This compound acts as and activator in submicromolar and low micromolar concentrations and has the inhibitory effect in higher concentrations[105]. Similar bimodal effects has also been described in other non-covalent activators of TRPA1 such as nicotine from tobacco and Δ^9-tetrahydrocannabinol (THC), a psychoactive drug from marijuana[106].

Similarly as cold and hot temperatures, some non-covalent TRPA1 modulators show a species-specific effect. Caffeine is an activator of mouse TRPA1 (mTRPA1) but an inhibitor of the human orthologue. A mutation of methionine M267 in mTRPA1 to proline, which is a cognate residue in hTRPA1 (P267), changes the activation effect of caffeine to the inhibition[107,108].

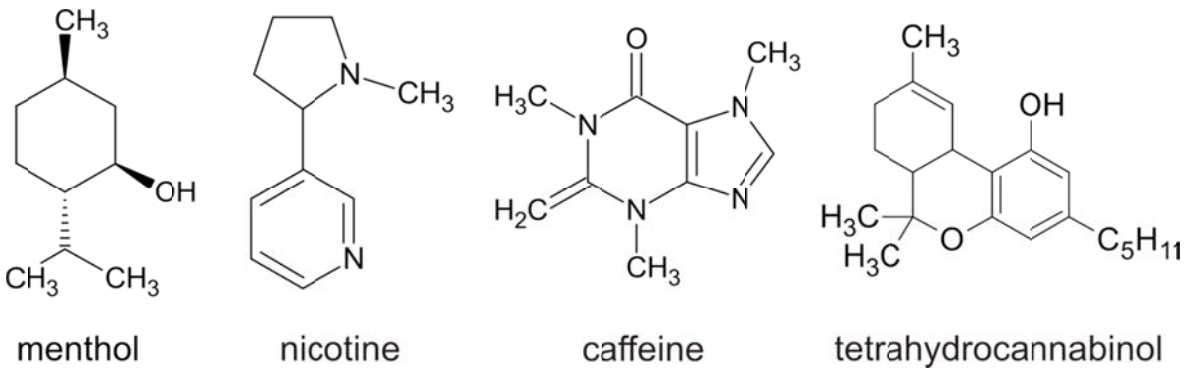

Figure 10. Examples of non-electrophilic agonists of TRPA1.

2.8. Modulation of TRPA1 by divalent cations

TRPA1 is a non-selective ion channel permeable for both mono- and divalent inorganic and small organic cations. The relative permeability of the human TRPA1 channel pore has been determined by using single channel recordings in the presence of an agonist AITC:

$$\mathbf{Ca^{2+}}\ (5.1) > \mathbf{Ba^{2+}}\ (3.5) > \mathbf{Mg^{2+}}\ (2.8) > \mathbf{NH_4^{+}}\ (1.5) > \mathbf{Na^{+}}\ (1.0) \geq \mathbf{K^{+}}\ (0.98) > \mathbf{Cs^{+}}\ (0.95)\ ^{109}$$

As shown above, the hTRPA1 channel is highly permeable to calcium ions. In addition, the Ca^{2+}-selectivity is controlled by a conserved aspartate residue (D915) within the selectivity filter of TRPA1[62]. Calcium ions are important physiological modulators of TRPA1; therefore the effects of Ca^{2+} have been intensively studied (for further information see section 2.8.1.).

On the contrary, the effects of other mono- and divalent ions on TRPA1 have been studied much less. Barium ions have been thought to play a similar role in the TRPA1 modulation as calcium ions because both elements belong to the second group in the periodic table. The authors of the study [62] showed that barium ions induced a robust potentiation followed by an inactivation of TRPA1 channels after a pre-application of cinnamaldehyde (CA). However, our results indicate that barium ions initially block TRPA1 and the blockage is followed by a potentiation and inactivation phases[110]. Magnesium ions, on the other hand, do not potentiate the TRPA1 responses induced by CA. Instead, the immediate desensitization has been observed after an application of extracellular Mg^{2+} [62].

Interestingly, the TRPA1 channel is modulated by zinc cations. Zinc is an essential heavy metal required for structure and function of over 300 proteins and its deficiency can lead to a variety of clinical manifestations. On the other hand, the overexposure to Zn^{2+} can lead to pain and inflammation. A thorough mutagenesis study identified N-terminal cysteine C614 and C-terminal cysteine C1021 and histidine H983 residues in mouse TRPA1 to be involved in Zn^{2+} binding. The TRPA1 sensitivity to zinc ions is high, as low nanomolar concentrations activate the channels and modulate their sensitivity[111]. In addition, even very low concentrations of Zn^{2+} augment TRPA1 responses induced by calcium ions about 3-fold than Ca^{2+} themselves[110]. The exact mechanism of this effect, however, remains unknown.

2.8.1. Activation and inactivation (desensitization) of TRPA1 by calcium ions

The importance of Ca^{2+} ions for the TRPA1 channel functioning was recognized together with the channel identification[7]. The intracellular Ca^{2+} from the endoplasmic reticulum or calcium ions passing through the channel pore from the extracellular space can influence the most important properties of the channel: conductance, ion selectivity and opening probability[79,103,112]. Moreover, the increase of the TRPA1 surface expression level, which can be induced by an agonist exposure, is not observed in Ca^{2+}-free solution suggesting the role of calcium ions in TRPA1 membrane trafficking[113].

TRPA1 is activated by intracellular Ca^{2+} ions in micromolar concentrations (EC_{50} = 905 ± 249 nM) and the activation mechanism does not depend on calmodulin or other Ca^{2+}-binding proteins[31,50]. The agonist- and voltage-induced TRPA1 currents are strongly amplified by the intracellular Ca^{2+}. The potentiation of TRPA1 currents is followed by an inactivation, which is almost complete and irreversible and both these processes can be accelerated by a higher concentration of Ca^{2+}. The potentiation and the inactivation (desensitization) are independent processes. The elevation of intracellular Ca^{2+} causes the TRPA1 potentiation whereas the extracellular Ca^{2+} are required for the inactivation[62]. However, the exact molecular mechanisms of these processes have not yet been fully understood.

The negatively charged residues within a loop between the N-terminal AR12 and AR13 have been thought to be a Ca^{2+}-binding site in TRPA1. However, the role of this so-called EF-hand in both Ca^{2+}-dependent potentiation and inactivation has been disputed by several studies as mentioned in section 2.5.2[62,79]. Thus, further studies are needed to find other calcium-binding sites within the TRPA1 protein.

2.9. Electrophysiological technique patch clamp as a tool for studying TRPA1 ion channels

The main functional assay used in this thesis was the patch clamp technique. *Patch clamp* is an electrophysiological technique, which allows the recording of electrical signals from living cells. Membrane currents are recorded while the membrane potential is kept constant (or it can be changed continually or in steps). Alternatively, the cell can be current-clamped while observing changes in membrane voltage. This technique was

developed by Erwin Neher and Bert Sakmann in late 1970s and early 1980s, who received the Nobel Prize in Physiology or Medicine in 1991 for this discovery.

A typical patch clamp setup consists of an inverted microscope with a fluorescence lamp, a micromanipulator, an antivibration table, a differential amplifier, an analog-to-digital converter and a computer (Fig. 11A, p. 34). The setup is usually placed in a Faraday cage to avoid the electrical noise.

Patch clamp recording uses two electrodes: a reference electrode placed in a bath solution around the cell and a recording electrode consisting of a silver electrode coated by a silver chloride layer placed in a glass micropipette filled with a conductive solution (Fig. 11B, p. 34). The diameter of the micropipette tip may vary though it is usually in a micrometer range. More often, the resistance of the micropipette tip is measured because it reflects the diameter of the tip. The tip of a micropipette can be heat polished to produce a smooth surface that assists in forming a high resistance seal with the cell membrane. To obtain this high resistance seal (also called "gigaseal"), the electrode is pressed against the cell membrane and suction is applied. The high resistance of the seal isolates electronically the currents measured across the membrane patch with little competing noise. According to the type of experiment, the micropipette can be filled with a solution matching the ionic composition of the bath solution or matching the cytoplasm (for whole-cell recording).

There are several variations of the patch clamp technique depending on the experimental task. The first one is called *cell-attached*: the tip of a micropipette is sealed onto a membrane to obtain a gigaseal. In this type of measurement, information about the current characteristics of one or several ion channels can be obtained. Next two variations are called "excised patch" techniques because a piece of membrane is excised (removed) from the cell. In the *inside-out* technique, the cytosolic surface of the membrane is exposed to the external media. The external surface of the plasma membrane is exposed to the bath solution in the *outside-out* variation. In the *whole cell* technique, more suction is applied to rupture the membrane patch, thus providing access from the interior of the pipette to the intracellular space of the cell. The whole cell configuration allows recording the currents from all ion channels of the entire cell (Fig. 11B, p. 34).

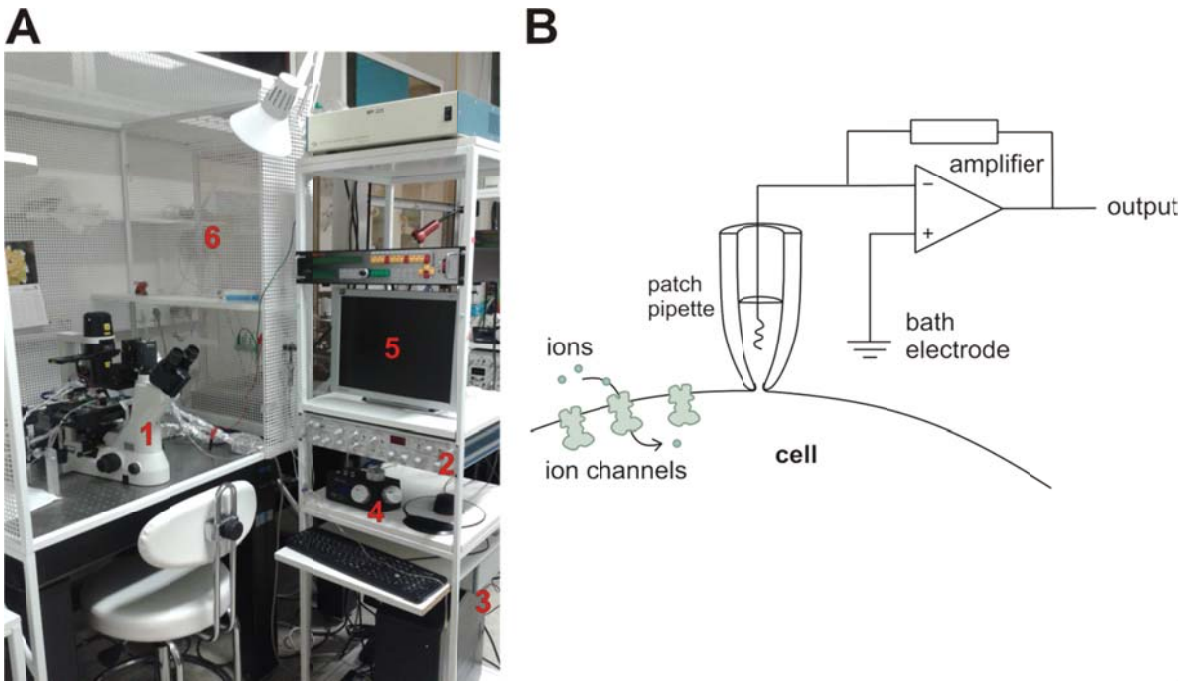

Figure 11. Patch clamp technique. ***(A)*** The setup for electrophysiological measurements consists of an inverted microscope (1), a differential amplifier (2), an analog-to-digital converter (3), a micromanipulator (4) and a computer (5). To avoid the electrical noise, a Farraday cage is used (6). ***(B)*** Schematic of whole-cell recording. Reference (bath) electrode is placed in a bath solution around the cell and a recording electrode consisting of a silver electrode placed in a glass micropipette filled with a conductive solution is used to record membrane currents.

3. Aims of the Thesis

- To elucidate the involvement of strictly conserved S/TPLH motifs within the N terminus of TRPA1 in voltage-, Ca^{2+}- and chemically-induced gating.

- To map the putative phosphorylation sites for cyclin-dependent kinase 5 (Cdk5) within the TRPA1 channel.

- To clarify the structural basis of the TRPA1 related channelopathy caused by a gain-of-function mutation N855S within the S4-S5 linker.

- To investigate the contribution of the acidic cluster in the distal C terminus of TRPA1 in Ca^{2+} - and voltage-dependent potentiation and/or inactivation of agonist-induced responses.

- To elucidate the function of the distal C terminus using truncated TRPA1 mutants.

4. Materials and methods

4.1. Chemicals and solutions

All of the chemicals were purchased from Sigma-Aldrich if not stated otherwise. All solutions were prepared using deionized water and sterilized.

The extracellular bath solutions contained: 150 mM NaCl and 10 mM HEPES, with an added 2 mM HEDTA for the **Ca^{2+}-free solution**, and 2 mM or 10 mM $CaCl_2$ for the **Ca^{2+}-containing solution**, adjusted to pH 7.3 with NaOH, 300 mOsm.

The *I-V* relationships were measured in the **control bath solution** containing 160 mM NaCl, 2.5 mM KCl, 1 mM $CaCl_2$, 2 mM $MgCl_2$, 10 mM HEPES, 10 mM glucose, adjusted to pH 7.3 and 320 mOsm.

The whole-cell pipette solution contained the **high buffer internal solution**: 145 mM CsCl, 5 mM EGTA, 3 mM $CaCl_2$, 10 mM HEPES, 2 mM MgATP, pH 7.3, adjusted with CsOH, 290 mOsm.

The pipette solution containing **100 µM free Ca^{2+}** was obtained by adding 10.24 mM Ca^{2+} and 10 mM EGTA to the internal solution.

Cinnamaldehyde and **allyl isothiocyanate** solution was prepared prior to use from a 0.1 M stock solution in dimethyl sulfoxide.

4.2. Cell cultures and transfection

Human embryonic kidney 293T (HEK293T) cells were cultured in Opti-MEM I media (Invitrogen) supplemented with 5% fetal bovine serum as described in[114].

Cells were transiently co-transfected with 400 ng of cDNA plasmid encoding wild-type (WT) or mutant human TRPA1 (wild type in the pCMV6-XL4 vector, OriGene) and with 200 ng of GFP plasmid (TaKaRa) per 1.6 mm dish using the magnet-assisted transfection (IBA GmbH.) technique.

In the experiments with Cdk5, the WT was co-expressed with Cdk5 and p25 (p35) in the cDNA ratio 250:250:125 (400:250:150). A 1:1 cDNA ratio was used for the co-expression of the WT with Cdk5, p25 or p35. The plasmids pcDNA3-Cdk5-GFP, pcDNA3.1-P25C-GFP and pCMV-P35 were obtained from the plasmid repository Addgene.

The cells were used 24–48 h after transfection. At least three independent transfections were used for each experimental group. The wild-type channel was regularly tested in the same batch as the mutants.

The mutants were generated by PCR using a QuikChange Site-Directed Mutagenesis Kit (Stratagene) and confirmed by DNA sequencing (GATC Biotech).

4.3. Electrophysiology

Whole-cell membrane currents were recorded by employing an Axopatch 200B amplifier and pCLAMP 10 software (Molecular Devices). Patch electrodes were pulled from a glass tube with a 1.65-mm outer diameter. The tip of the pipette was heat-polished, and its resistance was 3–5 MΩ. Series resistance was compensated by at least 70% in all recordings.

The experiments were performed at room temperature (23–25 °C). Only one recording was performed on any one coverslip of cells to ensure that recordings were made from cells not previously exposed to chemical stimuli. A system for rapid superfusion and heating of the cultured cells was used for drug application[115]. Capillary of the application system was placed at a distance of less than 100 μm from the surface of the examined cell.

4.4. Analysis of electrophysiological data

All of the electrophysiological data were analyzed using pCLAMP 10 (Molecular Devices), and curve fitting and statistical analyses were done in SigmaPlot 10 (Systat Software Inc.). Statistical significance was determined by Student's *t*-test or the analysis of variance, as appropriate. Differences were considered significant at $P < 0.05$ where not stated otherwise.

Voltage-induced activation

Conductance-voltage (*G*-*V*) relationships were obtained from steady-state whole cell currents measured at the end of voltage steps from -80 mV to +200 mV in increments of +20 mV (Fig. 12A), or from currents recorded by voltage ramp protocol in the presence of 100 µM cinnamaldehyde for 40 s.

Voltage-dependent gating parameters were estimated by fitting the conductance $G = I/(V-V_{rev})$ as a function of the test potential V to the Boltzmann equation:

$$G = \frac{\boldsymbol{Gmax} - \boldsymbol{Gmin}}{\mathbf{1} + \mathbf{exp} - \left(\frac{\boldsymbol{zF}}{\boldsymbol{RT}}\left(\boldsymbol{V} - \boldsymbol{V_{1/2}}\right)\right)} + \boldsymbol{G_{min}}$$

where z is the apparent number of gating charges, V_{50} is the half-activation voltage, G_{min} and G_{max} are the minimum and maximum whole cell conductance, V_{rev} is the reversal potential, F is the Faraday´s constant, R is the gas constant, and T is the thermodynamic temperature (Fig. 12B and 12C).

For statistical analysis of the voltage-independent component of gating (G_{min}/G_{max}) data, a logarithmic transformation was used to achieve a normal distribution. The data are presented as means ± S.E.M.

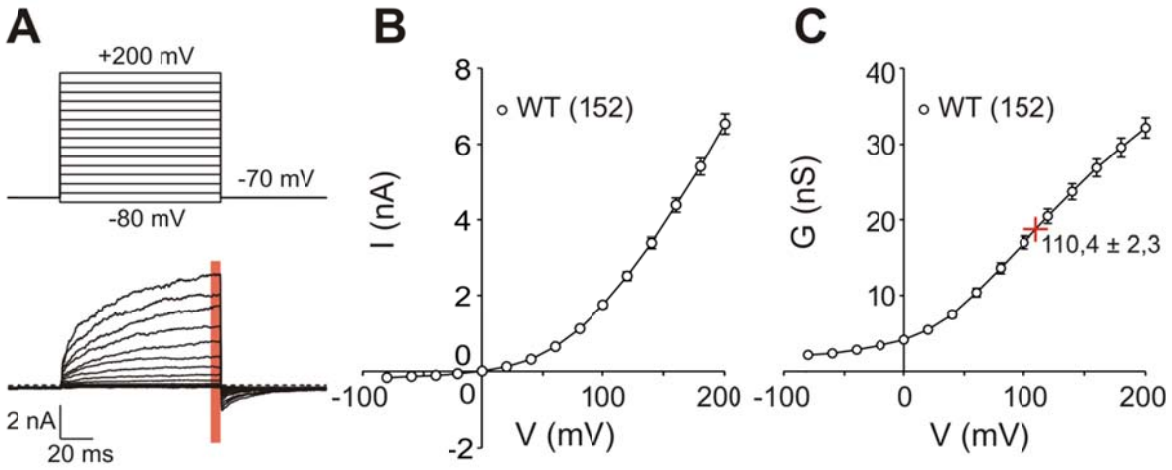

Figure 12. Voltage stimulation protocol. ***(A)*** Top: Scheme of voltage-step protocol recorded approximately 1 min after whole-cell formation. Bottom: Representative current trace of wild-type channel in response to voltage-step protocol in control extracellular solution. The maximal current amplitude is measured at the end of a pulse (depicted in red). ***(B)*** Average current-voltage relationship of TRPA1 (n = 152). ***(C)*** Average conductance-voltage relationship of TRPA1 (n = 152). The half-activation voltage (in mV) is depicted by a red cross.

Calcium- and agonist-induced activation

For exploring the effects of Ca^{2+} ions on hTRPA1 the protocol based on voltage ramps was used (Fig. 13A). In our experiments, voltage ramps are linear increases of the membrane potential from -80 to +80 mV repeated at the interval of 1 second[62]. The whole cell currents were measured in the absence of calcium ions for the first 10 seconds and then in the presence of agonist (100 µM cinnamaldehyde or 100 µM allyl isothiocyanate) for 40 seconds. Intracellular Ca^{2+} was buffered with 5 mM EGTA in the patch pipette to assess the effects of permeating calcium ions. The agonist is then washed out and extracellular solution containing 2 mM or 10 mM calcium ions was added.

Cinnamaldehyde (a partial agonist of TRPA1) evoked slowly and weakly developing currents that slightly relaxed upon washout. The application of calcium ions caused a strong increase of the activity of TRPA1 channels, which was followed by a slower inactivation phase, which was almost complete within about 1 min (Fig. 13B). The calcium induced potentiation was quantified as the fold increase in the amplitude after the addition of Ca^{2+} with respect to the preceding current level. The Ca^{2+}-dependent inactivation was characterized using a half-decay time, relative to peak (T_{50}).

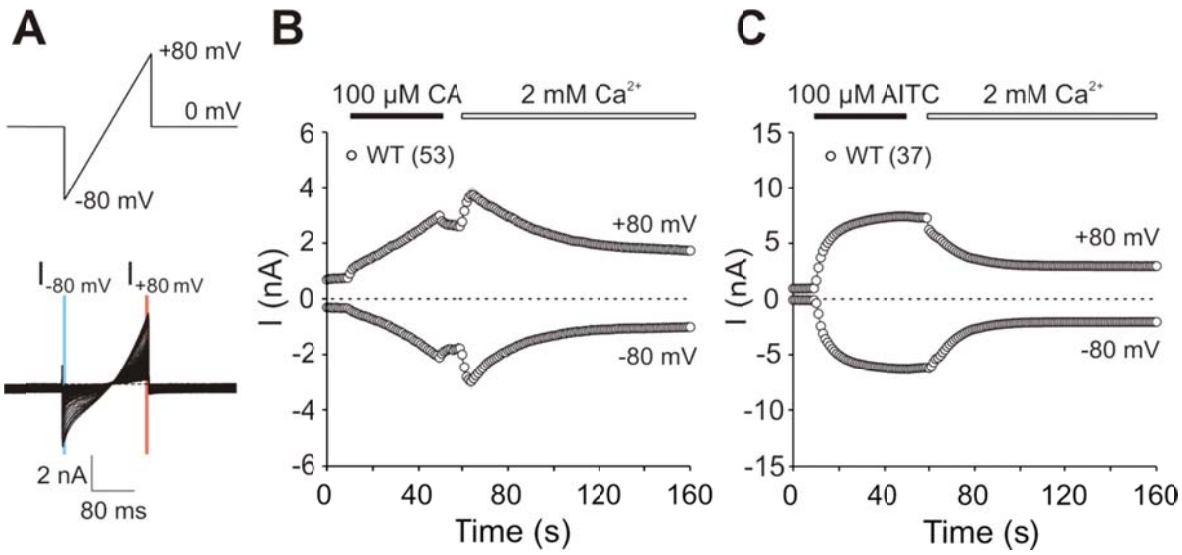

Figure 13. Chemical activation of TRPA1. ***(A)*** Top: The shape of stimulus voltage ramp that was applied every second to the tested cell. Bottom: Current responses of TRPA1 to the tested stimuli. For further analysis, current responses from +80 mV (in red) and -80 mV (in blue) were used. ***(B)*** Time course of average currents from wild-type measured at -80 mV and +80 mV (n = 53). The application time of 100 µM CA (partial agonist) and following addition of calcium is depicted above the graph. ***(C)*** Average currents at +80 mV and -80 mV from human TRPA1 channels upon activation of full agonist 100 µM AITC (n = 37). The data represents the means ± S.E. Note that AITC in this case activates channels close to saturation and addition of Ca^{2+} did not produced noticeable potentiation. Instead, the channels undergo inactivation, which is slow and only partial due to the covalent nature of AITC interaction with TRPA1.

Allyl isothiocyanate as a full agonist evoked a dramatic potentiation of the TRPA1 currents, which reached the saturation within the given 40 s (Fig. 13C, p. 39). The AITC induced activation was described by the mean time constant τ_{on}. The subsequent addition of Ca^{2+} to the bath solution induced only inactivation, characterized by percentage decline of the current at 160 s.

Changes in rectification ratio were plotted as a function of time, calculated as absolute value of current at +80 mV divided by current at -80 mV for each ramp from current-voltage relationships.

4.5. Biotinylation of cell surface proteins

The HEK293T cells were transfected with 1.5 μg of cDNA plasmid encoding wild-type or mutant C-terminally GFP-tagged human TRPA1 (in the pCMV6-AC-GFP vector; OriGene) with Lipofectamine 2000 and cultured in a 6-well plate.

At 48 h post-transfection, cells were washed with ice-cold phosphate buffered saline (PBS) buffer three times and incubated with 0.5 mg/ml EZ-link Sulfo-NHS-LC-biotin (Thermo Scientific) in PBS for 30 min at 4 °C. After quenching the reaction (50 mM glycine in PBS), the cells were homogenized and crude plasma membrane fraction was prepared as previously described[116].

The membrane fraction was incubated with streptavidin-agarose beads (Thermo Scientific) at room temperature with constant rotation for 2 hours, followed by four washes. The biotinylated protein fractions and the cell lysate fractions (1.5%) were separated using SDS/PAGE (7% SDS-polyacrylamide), followed by electroblotting onto PVDF membranes (polyvinylidene difluoride, Amersham, Germany).

Immunoblots were probed with a mouse anti-GFP (1:2000; OriGene) or a mouse anti-tubulin as a cytoplasmic marker (1:1500, Exbio) primary antibodies in TBS/Tween for 1 h at room temperature, and subsequently treated (1 h, room temperature) with horseradish peroxidase-conjugated goat anti-mouse IgG secondary antibody (1:20000, Thermo Scientific). Detection was done with a SuperSignal West Femto Maximum Sensitivity chemiluminiscent substrate (Thermo Scientific). Immunoblots were digitized and quantified with ImageJ 1.41v software (National Institutes of Health).

4.6. Homology modeling and molecular dynamics simulations

Structural hypotheses in Publication 1 were tested by mapping the residues onto the homology models of the N-terminal ankyrin repeat domain region made using the software Yasara (version 15.9.6)[117] in conjunction with the Swiss-Model and I-Tasser protein modeling servers[118–124].

Homology models and molecular dynamics simulations were performed by our collaborators Vlastimil Zíma and Ivan Barvík from the Faculty of Mathematics and Physics, Charles University in Prague. A precise description of the used methods is reported in Publications 2 and 3.

5. Results and Discussion

5.1. Effects of mutations within strictly conserved T/SPLH motifs on the TRPA1 stability

TRPA1 is unique among mammalian TRP channels in bearing an extensive cytoplasmic amino terminus (720 of 1119 amino acids) consisting of a tandem array of 17 ankyrin repeats (AR1-AR17), and a linker that connects ARD with the first transmembrane segment. The recently resolved high-resolution three-dimensional structure of the TRPA1 channel shows that AR12-AR16 is structurally integrated with the C-terminal tetrameric parallel coiled-coil, whereas the extended ankyrin repeats AR1-AR11 are suspended below the membrane and form a crescent-shaped structure.

The molecular architecture of an ankyrin repeat consists of about 33 amino acids, adopting a helix-turn-helix-extended loop secondary structure topology. Five of the ARs contain a strictly conserved T/SPLH tetrapeptide motif, a hallmark of the consensus ankyrin repeat sequence contributing substantially to local conformational stability. We hypothesized that the strict conservation within the evolutionary conserved T/SPLH motifs in AR2, AR6, AR11-AR13 across different species suggests that an especially precisely tuned stability of these N-terminal modules is essential for the proper functioning of the TRPA1 channel. Thus, we constructed mutants either within the T/SPLH motif or in the neighboring ankyrin repeat to either stabilize (by inserting the consensus motif GxTPLH into the neighboring AR) or destabilize (by mutation of threonine or serine to alanine or aspartate) the conformation of each of the T/SPLH-containing AR.

To characterize phenotypes of the individual mutants, we used whole-cell patch clamp recordings from transiently transfected HEK 293T cells and assessed their voltage-dependent activation properties using a voltage step protocol from -80 mV to +200 mV, in 20 mV increments. To test the chemical sensitivity of the mutants, we employed a protocol in which the membrane potential was ramped up each second from -80 mV to +80 mV (1 V/s) and 100 μM cinnamaldehyde (CA) or 100 μM allyl isothiocyanate (AITC) and 2 mM Ca^{2+} solution were applied.

Surprisingly, stabilization or destabilization of the T/SPLH consensus motifs resulted in very different phenotypes depending on location of the ankyrin repeat containing the motif within the N terminus. In addition, mutations within the T/SPLH motifs affect

different modalities of the TRPA1 channel gating depending on the specific location of the motif-containing ankyrin repeat.

Generally, the aspartate mutations of threonine residues in the TPLH motifs resulted in loss-of-function phenotypes whereas alanine mutations altered but did not abolish the channel´s functioning (Fig. 14A). The only exception was threonine T241 in AR6, whose both mutations remained functional, which suggests that strict TPLH conservation is not crucial for TRPA1 functioning. On the other hand, both alanine and aspartate mutations of serine S448 in the only SPLH motif within TRPA1 resulted in a loss-of-function phenotype, indicating that this strictly conserved serine is crucial either for conformational stability, function or expression.

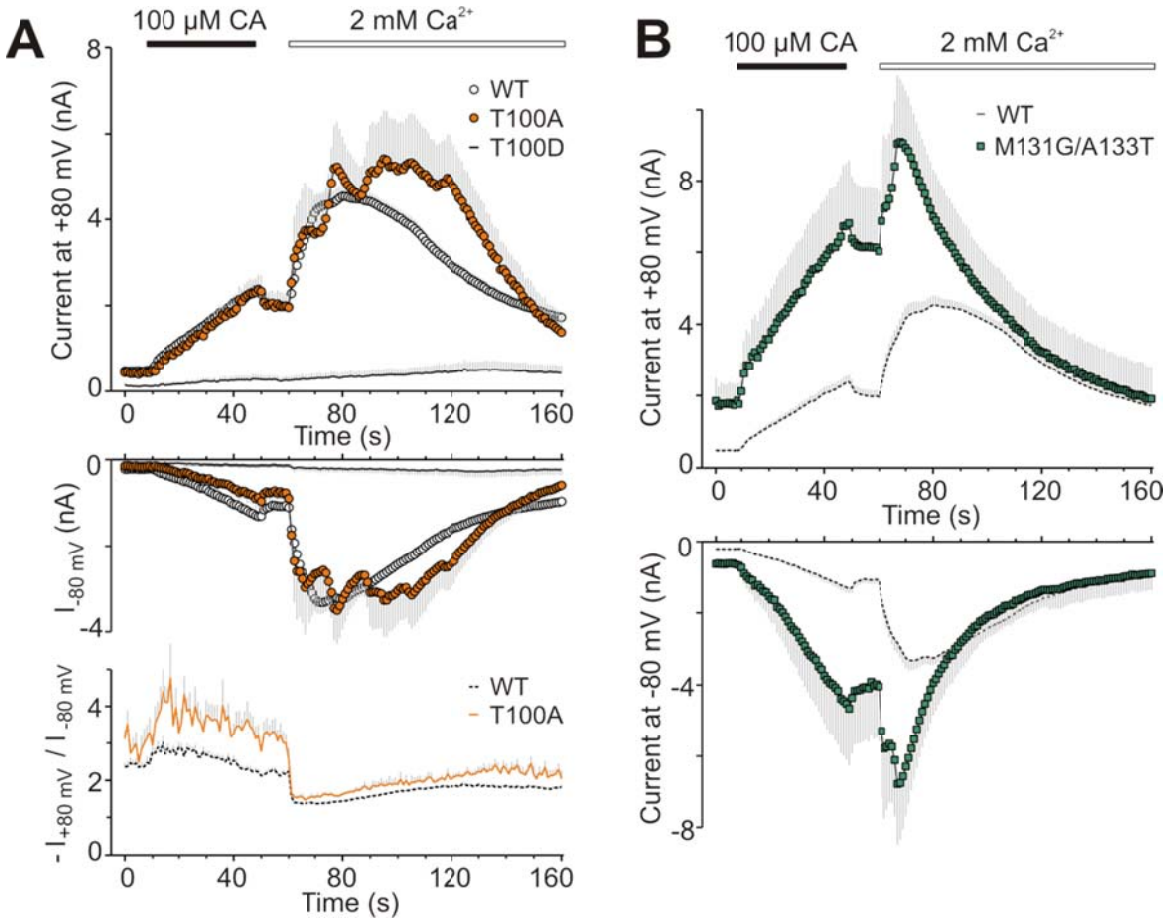

Figure 14. Mutations affecting the conformatial stability of the ankyrin repeat 2 and 3 affect voltage-dependent TRPA1 channel gating. ***(A and B)*** Time course of average whole-cell currents through wild-type and mutant hTRPA1 measured at +80 mV and -80 mV as marked. The application of 100 µM cinnamaldehyde (CA) and subsequent addition of 2 mM Ca^{2+} are indicated above. Below, average rectification of currents shown above.

The effect of the insertion of GxTPLH motifs into the neighboring ankyrin repeat was either stabilizing or destabilizing depending on the location within the N terminus as well as the mutations within T/SPLH motifs. Double mutation M131G/A133T in AR3 resulted in a gain of function phenotype, where the channel displayed significant voltage-independent gating at negative membrane potentials (G_{min} of 14 ± 1% of G_{max}; n = 7), suggesting that the energy required to activate the pore opening is reduced. In addition, the double mutant M131G/A133T channels displayed much larger responses to cinnamaldehyde at both negative and positive holding potentials, suggesting the previously proposed role of the cytoplasmic N-terminal ankyrin repeat-rich region in the regulation of TRPA1 and identify AR2 to be a domain contributing to voltage-dependent gating (Fig. 14B, p. 43). On the other hand, we did not observe any measurable currents through the N377T/F378P channels in response to either of the stimuli when we aimed to conform to the consensus signature by mutating a highly conserved ^{377}NFLH motif in AR10, which substantially deviates from the ankyrin repeat consensus and contributes to forming a sharp and flexible kink before repeat 12.

To further investigate the role of TPLH in AR6, in which both aspartate and alanine mutations of threonine 241 remained functional, we next constructed two additional mutants. The first, K239G, was anticipated to improve the ankyrin fold and allow for a more compact L shape of the repeat AR6. The second mutant, H244R, was designed to perturb AR6 by decreasing its mechanical stability[125]. Both the mutants yielded smaller currents in response to depolarizing voltages and also smaller maximal responses to chemical activators. This serious mutagenic impact was quite surprising in case of K239G mutation, which conforms to the consensus glycine two residues prior to the TPLH motif, most likely due to eliminating important interactions in the loop preceding AR6.

Recently, the study of [34] implicated the N-terminal ARD region as an important gating modifier that may regulate the channel's behavior in a voltage-dependent manner. Our results suggest that the ankyrin repeats AR2 and AR6, although sequentially distant from the transmembrane region, contribute to voltage-dependent gating. The recently resolved structure of TRPA1 provides a mechanistic explanation of how the proximal part of ARD can communicate with the channel gate: the information from the ARD can be transduced through the overlying helix-turn-helix motif of the linker region that forms a network of packed interactions with the TRP-like domain.

We used a similar approach to investigate why both aspartate and alanine mutations of serine 448 failed to induce any currents in response to depolarizing voltages as well as to

the full agonist AITC (Fig. 15B). We hypothesized that if S448 contributes substantially to ARD stability through intra- and inter-repeat hydrogen bonding, then the threonine at this position could improve ancillary interactions in its microenvironment by hydrophobic interactions associated with the threonine methyl group[68]. The second mutation introducing glycine at position K446 was anticipated to better stabilize the ankyrin fold by stabilizing its L-shaped conformation and further allowing for a better intrinsic stability of AR12 and the interfacial stability between neighboring ARs. Notably, both the mutations produced functional channels that exhibited greater currents in response to depolarizing voltage steps and a significant conductance at negative membrane potentials, indicating the presence of a strong voltage-independent component.

A remarkable finding was an apparent difference between the characteristic currents induced by cinnamaldehyde and AITC in S448T and K446G. The currents induced by 100 µM cinnamaldehyde were significantly greater and, upon the addition of Ca^{2+} to the bath solution, reached amplitudes that were ~1.4-fold and 1.7-fold the amplitude of the wild-type channels. In a striking contrast, the maximum currents induced by AITC were smaller than in the wild-type channels and exhibited only a slight calcium-dependent desensitization (to 72 ± 5 % and 84 ± 6 % of the maximal response; *n* = 6 and 10) (Fig. 15A and 15B).

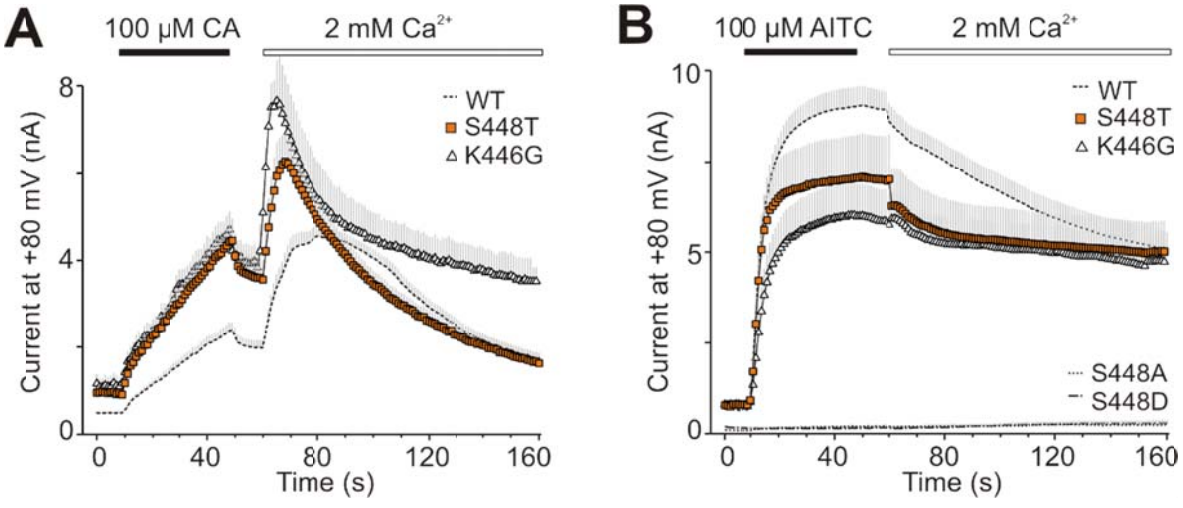

Figure 15. Strict conservations of the SPLH motif in AR12 is required for functional interactions. ***(A and B)*** Time course of average whole-cell currents through wild-type and mutant hTRPA1 measured at +80 mV. The application of 100 µM cinnamaldehyde (CA, in panel (A)) or 100 µM allyl isothiocyanate (AITC, in panel (B)) and subsequent addition of 2 mM Ca^{2+} are indicated above. Note that the S448T (n = 18) and K446G (n = 5) mutants exhibit greater currents in CA but not in the presence of AITC. Mutations S448A and S448D are AITC-insensitive (n = 9 and 9).

While serine is statistically three times less favored than threonine in T/SPLH tetrapeptides[68], the role of S448 in TRPA1 is likely to be specific and may be evolutionarily fine-tuned. As the expression level of the S448T mutant did not significantly differ from wild-type, we believe that the S448T mutation results in a gain-of-function by mainly impacting the transition between the closed and open state of the channel in a way that is independent of the putative voltage sensor.

Taken together, our data support the previous suggestion that calcium-dependent desensitization of AITC-induced responses is specified by an AR cluster centered around AR11[37]. Moreover, we show that subtle changes in AR12 stability affect the Ca^{2+}-dependent desensitization to varying degrees according to the mode of chemical activation, and increase the voltage-independent component of TRPA1 channel gating.

5.2. Conserved T/SPLH motifs as putative phosphorylation sites

Except for the role in the ankyrin repeat conformational stability, the T/SPLH motifs may represent potential phosphorylation sites, particularly for proline-directed Ser/Thr kinases. Among these, cyclin-dependent kinase 5 (Cdk5) is a neuron-specific kinase of great functional relevance, known to regulate nociceptive signaling via the N terminus of the related vanilloid receptor TRPV1.

Bioinformatics analysis of the primary sequence of human TRPA1, obtained by several prediction servers, predicted threonines T100, T241, T415, T484 and serine S448 to be consensus phosphorylation sites for Cdk5 at a high stringency level. However, our data suggest that the examined serine and threonine residues constituting the conserved T/SPLH motifs are not likely to be involved in the phosphorylation of TRPA1 because the phosphonull alanine mutations and phosphorylation mimicking aspartate mutations did not lead to opposite changes in the channel functioning. On the other hand, structural changes around these residues, such as the M131G/A133T double mutation, may affect phosphorylation at the contiguous sites. Therefore, we tested whether the co-expression of TRPA1 with Cdk5 and p35 protein, a Cdk5-specific activator, may modulate voltage-dependent channel activation.

The co-expression of p35 alone or with Cdk5 in HEK 293T cells significantly increased the cinnamaldehyde-evoked responses of hTRPA1 (Fig. 16A, p. 47). Thus, we

hypothesized that TRPA1 may be a substrate for the Cdk5/p35 complex and/or its interaction with p35 may stabilize the activated state of the channel.

Further sequence prediction analysis of the TRPA1 N terminus revealed other three putative phosphorylation sites for Cdk5, serine and threonine residues S344, S616 and T673. Therefore, we constructed alanine and aspartate additional mutants of these residues to obtain a complete picture of the role of the T/SP N-terminal motifs. Among the mutations, only S344D and T673D showed significant changes in TRPA1 channel´s activity. The S344D mutation failed to produce any appreciable currents indicating either a structural disturbance around AR9 or a failure of functional expression as a specific result of the phosphomimicking substitution. On the contrary, the T673D mutation resulted in channels whose responses to cinnamaldehyde were increased almost threefold compared with wild-type (from 2.4 ± 0.2 nA to 6.6 ± 1 nA at +80 mV; n = 70 and n = 8) (Fig. 16B). According to the newly resolved TRPA1 structure, threonine 673 is solvent-accessible and located in a flexible loop connecting the β-strands to the helix-turn-helix motif preceding the pre-S1 helix, indicating that it may represent a candidate target for Ser/Thr phosphorylation.

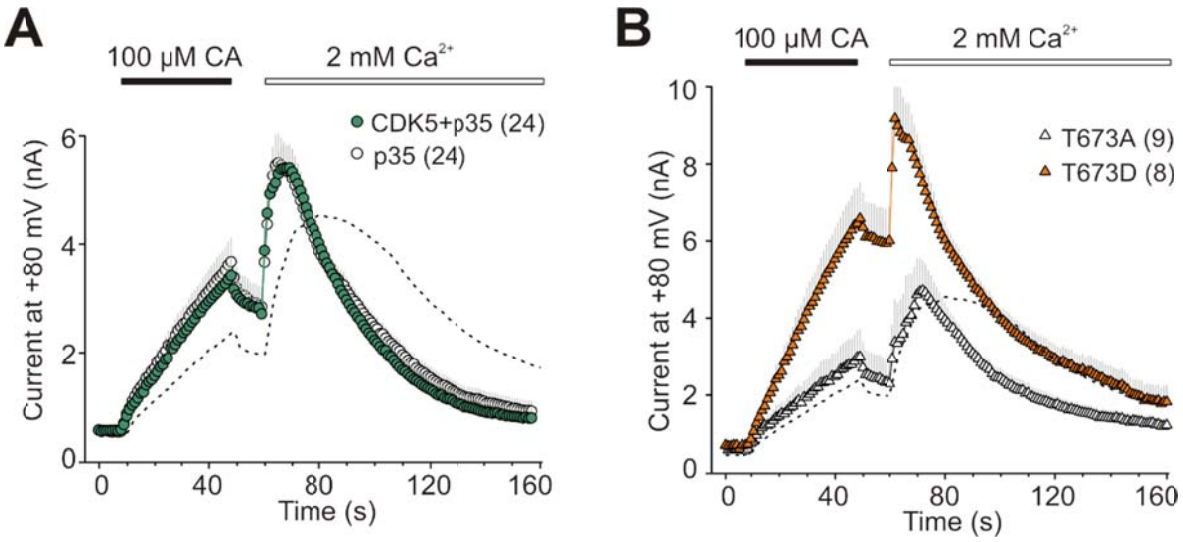

Figure 16. Conserved T/SPLH motifs as putative phosphorylation sites. ***(A)*** Time course of average whole-cell currents measured at +80 mV in wild-type (dashed line) and wild-type co-expressed with indicated proteins; *n* is indicated in brackets. The application of CA and subsequent addition of 2 mM Ca^{2+} are indicated above. ***(B)*** Time course of average whole-cell currents through wild-type and mutant hTRPA1 measured at +80 mV in wild-type and mutant channels; *n* is indicated in brackets. The application of 100 µM cinnamaldehyde (CA) and subsequent addition of 2 mM Ca^{2+} are indicated above. Note, the aspartate mutation of T673 resulted in a gain-of-function phenotype.

5.3. Structural basis of the heritable episodic pain syndrome

Our second study was motivated by the previous finding of a gain-of-function mutation N855S within the S4-S5 linker of hTRPA1, which underlies familial episodic pain syndrome. From electrophysiological point of view, the N855S mutation shifts activation toward more negative voltages and changes the channel´s gating through a Ca^{2+}-dependent mechanism, resulting in an increase in inward currents through the activated channels at normal resting membrane potentials. In our work, we applied homology modeling, molecular dynamics simulations and whole-cell electrophysiology to explore the structural basis of this channelopathy.

The initial homology model of the transmembrane part of hTRPA1 was based on the Kv1.2/2.1 crystal structure (pdb code 2R9R), further refinement of the model was based on the cryo-EM structure of TRPV1 (pdb code 3J5P), as the structure of TRPA1 had not yet been resolved in time our experiments had been performed.

The first model based on the Kv1.2/2.1 structure revealed an inter-subunit interaction between the polar glutamate residue E854 located in the S4-S5 linker in the immediate vicinity of N855, and lysine K868 in S5 transmembrane helix of an adjacent subunit of TRPA1 (Fig. 17A, p. 49). According to this finding, we hypothesized that the functional changes in the N855S mutant may originate, at least in part, from changes in inter-subunit interactions.

TRPA1 and Kv1.2/2.1 share very low sequence similarity (about 10%), therefore, the TRPV1 template structure was used to confirm the proximity of the residues E854 and K868. The primary sequences of the transmembrane parts of both TRP channels are, again, not very high (about 20%) but the sequence similarity of S4-S5 linkers reaches almost 50%. In TRPV1, R579 directly from S5 interacts directly with Q561 from the S4-S5 linker of the adjacent subunit. These residues are cognate to the R872 and N855 in TRPA1, which promotes a hypothesis that their interaction may underlie the gain-of-function effects observed in the N855S mutation. Therefore, another homology model was built, where only the S4-S5 linker of TRPV1 (Q560-R575) was replaced by the analogous sequence from TRPA1 (E854-K868). Inter-subunit salt bridges E854-K868 were not formed spontaneously during molecular dynamics (MD) simulations, yet results based on this model support the proximity and mutual orientation of the E854 and K868 residues.

We used whole-cell patch clamp recordings to investigate, whether the predicted inter-subunit interactions contribute to the TRPA1 channel functionality. We constructed charge-neutralizing (E854A, K868A) and charge-reversing (E854R, K868E) mutants of TRPA1 to test whether specific interactions between opposite charges are required for proper channel functioning. Furthermore, we constructed the charge-swapping double mutant E854R/K868E to test whether the double mutant might functionally rescue the channel. The voltage-dependent gating and chemical sensitivity of the individual mutants were measured by using the aforementioned protocols (see section 4.4).

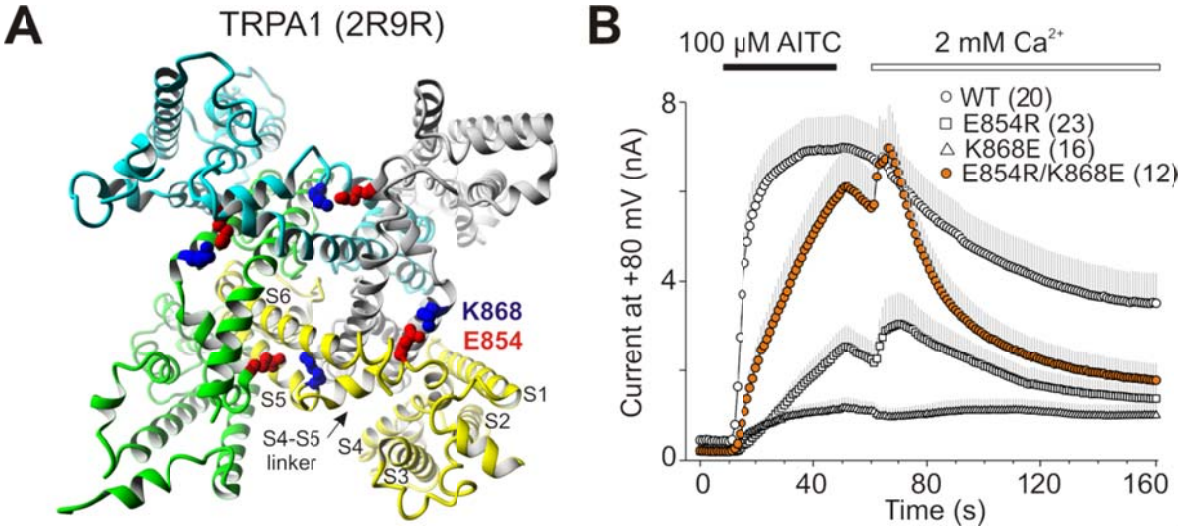

Figure 17. ***(A)*** Intracellular view of homology model of TRPA1 channel based on Kv1.2/2.1 paddle chimera with E854 and K868 residues indicated. ***(B)*** Time course of average whole-cell currents through wild-type and mutant hTRPA1 measured at +80 mV. The application of 100 µM allyl isothiocyanate (AITC) and subsequent addition of 2 mM Ca^{2+} are indicated above.

Our data indicate that substitutions at E854 and K868 result in channels with altered gating kinetics. Mutations at position K868 destabilized the closed, resting conformation of the channel and strongly reduced responses to all stimuli (depolarizing voltage, AITC). The E854A and E854R mutants expressed AITC-sensitive channels, however, their responses to depolarizing voltage steps were smaller in amplitude than wild type. The charge-swapping mutation E854R/K868E restored normal channel closure at hyperpolarizing voltages, although it did not rescue normal voltage dependency. However, the maximal amplitudes of AITC-induced responses of the double mutant were not significantly different from wild-type channels, although the onset of the E854R/K868E

currents was apparently slower (Fig. 17B, p. 49). The finding that the charge-swapping double mutation substantially rescues the functionality of TRPA1 supports the hypothesis that the spatial proximity of the two residues E854 and K868.

We further investigated whether introducing of an additional negative charge in the vicinity of E854 could affect the electrostatic attraction between the residues E854 and K868 and thus change the channel´s gating equilibrium. Therefore, we next measured currents from the R852E mutant and from the R852A mutant as a control. Mutation R852E resulted in a gain-of-function phenotype with increased basal activity and close-to-saturation responses to the partial agonist cinnamaldehyde (CA). Intriguingly, Ca^{2+} did not substantially potentiate the CA-induced responses and instead inactivated them faster than wild-type, suggesting an outstanding role for R852 in the Ca^{2+}-dependent modulation of TRPA1.

The original study, in which the N855S mutation has been identified as an origin of the heritable pain syndrome, described an altered Ca^{2+} sensitivity of this mutant[8]. Unlike the authors of this study, we identified the location of the asparagine N855 within the S4-S5 linker of TRPA1, which was confirmed by the newly resolved hTRPA1 structure. According to our data, the altered calcium sensitivity of the N855S mutant may arise from its vicinity to the residues E854 and K868 that are involved in allosteric coupling and voltage sensing. In addition, the exquisite changes in voltage-dependent gating of R852 mutants and the selective disruption of voltage-dependent gating in the charge-swap E854R/K868E indicate that these residues can be a part of a voltage-sensing domain of TRPA1.

5.4. C-terminal acidic cluster is involved in Ca^{2+}-induced modulation of hTRPA1

As has been thoroughly discussed in section 2.8.1., calcium ions belong to the most important physiological modulators of TRPA1. Therefore, our last project was focused on elucidating molecular mechanisms of Ca^{2+}-dependent potentiation and inactivation of the TRPA1 channel, which still remain a matter of controversy.

The obvious candidates for a domain through which Ca^{2+} can modulate TRPA1 are acidic residues on the intracellular side of TRPA1. Within the C terminus, a highly conserved sequence of acidic amino acids, ^{1077}ETEDDD^{1082}, shares the sequence similarity with the Ca^{2+}- binding domain found in the hBest1 channel[126] or so-called Ca^{2+} bowl

domain of the superfamily of BK channels[127]. To confirm the involvement of the ^{1077}ETEDDD^{1082} motif in Ca^{2+}- mediated modulation we used site-directed mutagenesis, whole-cell electrophysiology, homology modeling and molecular dynamics simulations.

As the first step, all negatively charged residues were individually mutated to alanine, a neutral amino acid. Except for E1077A, none of the mutant exhibited a substantially decreased relative sensitivity to CA compared to WT TRPA1 (Fig. 18A top, p. 52). However, the kinetics of the Ca^{2+} -dependent potentiation was dramatically changed in four out of the six charge-neutralized mutants: E1073A, D1080A, D1081A and D1082A (Fig. 18B, p. 52). Among them, the most affected mutant was D1080A. In five of ten D1080A-expressing cells that were treated with 2 mM Ca^{2+} and in three out of seven cells treated with 10 mM Ca^{2+}, no potentiation at all was observed within the time interval tested (3-4 min) (Fig. 18A bottom, p. 52). Instead, the CA-induced currents decayed in the presence of Ca^{2+} to their initial value obtained before the agonist was applied to these cells. Interestingly, under the conditions with 100 μM intracellular calcium, the D1080A mutant produced robust currents in response to CA in Ca^{2+} -free bath solution, and after the addition of external 10 mM Ca^{2+}, the currents were consistently potentiated without any delay. In contrast, Ca^{2+} -induced responses through wild-type channels dialyzed with the same internal solution were mostly inactivated immediately after the addition of 10 mM Ca^{2+}, suggesting that the mutation D1080A most likely has an effect on Ca^{2+} affinity.

This observation further supports the idea that the whole region containing the negatively charged cluster is structurally important and involved in the Ca^{2+} -dependent modulation of TRPA1. Therefore, we utilized MD simulations to probe the Ca^{2+} -binding capability of the acidic region from TRPA1, using Ca^{2+} activation apparatus of the human BK channel[127] as the template protein (pdb code 3MT5). After replacing the stretch of 10 consecutive residues ^{889}QFLDQDDDDD^{898} in the structure of the Ca^{2+} -binding domain of BK with 10 residues from human TRPA1 (^{1074}IISETEDDDS^{1083}), the MD simulations confirmed that this region is capable of binding Ca^{2+}. Furthermore, we showed that the two residues D1080 and D1082 use oxygen atoms from their side chains for direct contact with calcium ions, which is in a good agreement with our experimental data (Fig. 18C, p. 52).

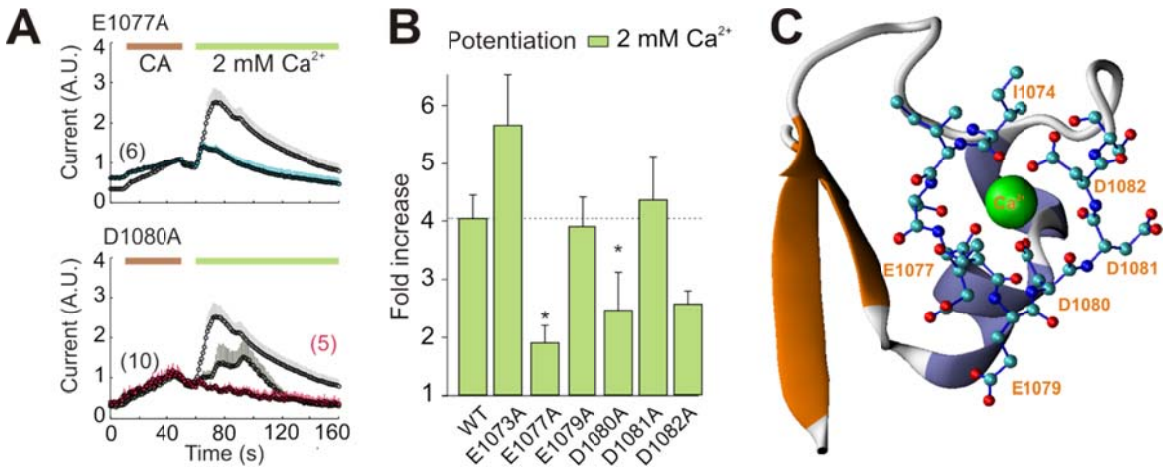

Figure 18. Negatively charged motif ^{1074}IISETEDDDS^{1083} is involved in Ca^{2+}-dependent modulation of human TRPA. ***(A)*** Average TRPA1 currents evoked in response to 40 s exposure to 100 μM cinnamaldehyde (CA) and subsequent addition of 2 mM Ca^{2+} as indicated by horizontal bars. The currents are normalized to their maximal cinnamaldehyde responses obtained prior to the addition of Ca^{2+} to the bath solution. For D1080A, the average current for nonpotentiated cells (in red) is overlaid onto the average current from all cells. ***(B)*** Calcium-induced potentiation was measured as the fold increase in current, measured at +80 mV, following the addition of 2 mM extracellular Ca^{2+}. The *asterisks* indicate significant differences between mutant and wild-type TRPA1. ***(C)*** Illustration of calcium-binding site in hSlo1-TRPA1 chimera with surrounding structures. Residues from the TRPA1 protein are shown in ball and stick representation.

To further investigate functional properties of the C-terminal Ca^{2+} -binding motif, we constructed additional mutants of glutamate residues E1077 and E1079 to positively charged lysine. Both mutations of the glutamate 1077, E1077K and E1077A, induced a dramatic increase in the amplitude of the outward currents induced by voltage ramps in control Ca^{2+} -free solution. Also, their conductance-voltage relationships were significantly shifted toward less depolarizing potentials. We reasoned that this sensitizing effect might reflect either a gain-of-function (constitutively active) phenotype or tonic activation due to an increased expression of the mutant channels on the cell surface.

In fact, a similar phosphorylatable acidic cluster has been reported to control the trafficking and surface expression of TRPA1-related TRPP2 and TRPV4 channels[128]. Within our region of interest, a sequence prediction analysis revealed two strong phosphorylation motifs containing serine 1076 and threonine 1078, both predicted to be targeted by casein kinase CK2. To mimic non-phosphorylated and phosphorylated state of these two residues, we constructed four additional alanine and aspartate mutants. We

performed a series of experiments, which detected altered phenotypes, but we were able to conclude that this particular part of TRPA1 seems to be unlikely involved in trafficking to the membrane. Moreover, we identified one more gain-of-function mutant T1078D whose sensitivity to membrane voltage was increased while its responsiveness to CA remained unchanged. While T1078D is located in the primary sequence far from the membrane proximal regions, it is unlikely a part of the voltage sensor and the observed changes in its voltage modulation are most likely caused by altered allosteric coupling between the activation sites (voltage sensor, Ca^{2+} sensor) and movement of the gate. However, the role of threonine T1078 in TRPA1 phosphorylation cannot be excluded.

5.5. Functional role of the distal C terminus of hTRPA1

As the final step of the study, we constructed two C-terminal truncation mutants, TRPA1-Δ20 and TRPA1-Δ26 to investigate the role of the distal part of the hTRPA1 carboxy terminus. In the TRPA1-Δ20 mutant, stop codon was introduced at N1100, which removed the last predicted C-terminal α-helix H6. In the TRPA1-Δ26 mutant, stop codon was introduced at E1094 (within the H5 helix) to preserve the structure of the loop containing the calcium-binding motif ^{1074}IISETEDDDS^{1083} (Fig. 19A, p. 54).

Mutation TRPA1-Δ26 did not produce measurable currents in response to any of the stimuli tested, indicating an important functional role of the predicted H5 helix (Fig. 19B and 19C, p. 54). In contrast, the TRPA1-Δ20 truncation mutant was functional. Unlike the wild-type channel, this mutant exhibited strikingly slower inactivation upon the addition of Ca^{2+} while it exhibited normal degree of Ca^{2+} -potentiation and normal responsiveness to voltage and CA (Fig. 19B and 19D, p. 54). This set of experiments identified the distal C terminus as a critical modulatory domain of TRPA1 involved in its Ca^{2+} -dependent inactivation.

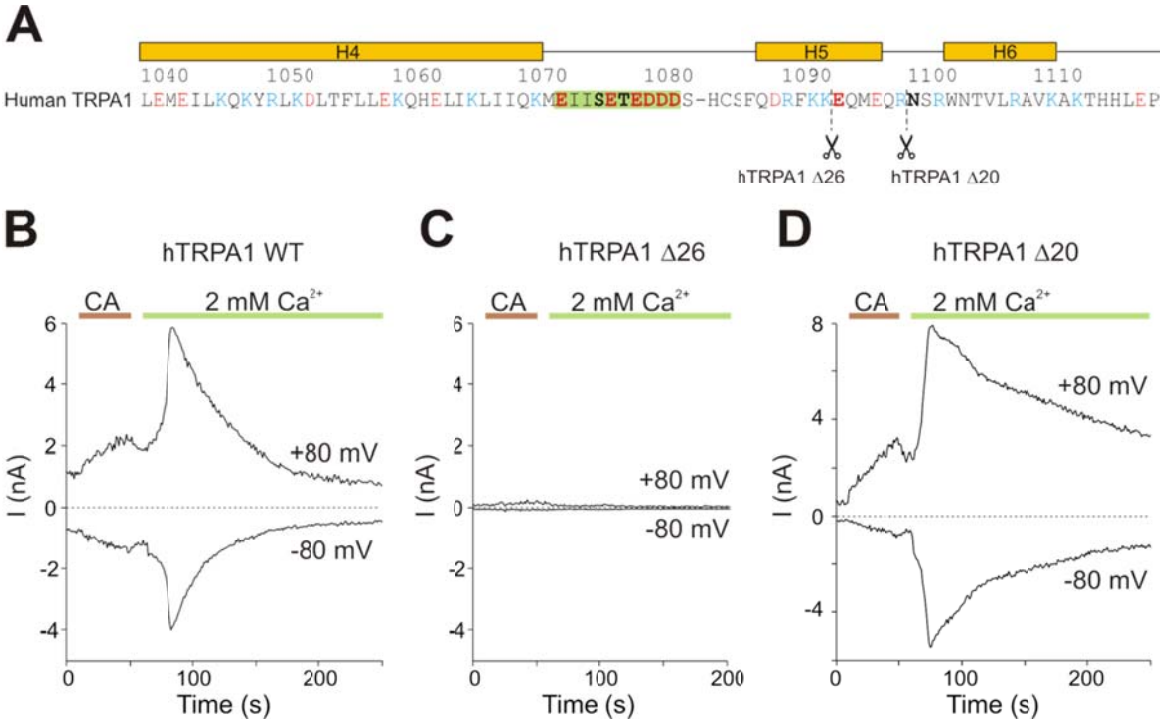

Figure 19. Truncations in C terminus reveal region involved in Ca^{2+}-dependent inactivation. ***(A)*** Amino acid sequence of the distal C terminus. Predicted secondary structure for hTRPA1 is indicated above the alignment. The region of interest is boxed. Residues mutated in this study are indicated in bold. ***(B)*** Time course of representative whole-cell currents through wild-type hTRPA1 measured at -80 mV and +80 mV. The application of 100 µM cinnamaldehyde (CA) and subsequent addition of 2 mM Ca^{2+} are indicated above. ***(C and D)*** Voltage-ramp protocol as in (A) used for truncation mutants. Note the obviously slower inactivation of the TRPA1-Δ20 truncation mutant upon the addition of 2 mM Ca^{2+} compared with WT.

6. Conclusions

The amount of new findings in the field of TRP channels´ research has dramatically increased in last few years. Whereas our former studies (see Publications 2 and 3) were created in the time period before the cryo-EM structure has been resolved, the results of our latest study could be interpreted in the context of this structure. However, the latest structural model does not contain the most distal N and C termini of the TRPA1 protein, probably because of a high flexibility of these regions, thus the functional studies we performed can still bring new insight into the TRPA1 gating mechanisms.

A central observation of our first study is that the most conserved N-terminal consensus T/SPLH tetrapeptide motifs, which initiate the helix–turn–helix conformation of the repeats AR2, AR6, AR11, AR12 and AR13, are required for the proper functioning of TRPA1 and distinctly contribute to its multimodal activation. While the stabilizing mutations of AR2 and its neighboring AR3 affect voltage-dependent TRPA1 channel gating, a destabilizing mutation within AR6, T214D, affects both voltage- and Ca^{2+}-dependent modulation. We also show that strict conservation of the T/SPLH motifs in AR11-AR13 is required for functional interactions, and most likely not for targeting TRPA1 to the plasma membrane.

Our results suggest that the conserved T/SPLH motifs are not likely to be phosphorylated by Cdk5. The only residue fulfilling the consensus requirement and upregulating the function of TRPA1 under phospho-mimicking conditions is T673, which is outside the ARD. Also, the specific result of our study that the co-expression of p35 or Cdk5 with p35 significantly increased TRPA1-mediated responses to cinnamaldehyde is an important observation that was not previously reported.

Homology modeling and molecular dynamics simulations revealed a salt bridge between residues E854 within the S4-S5 linker of one TRPA1 subunit and K868 in S5 domain from another subunit, which stabilizes the channel open state. We suppose that it is primarily disturbance of this interaction what causes changes in activation while of the N855S mutant channel, which underlies the familial episodic pain syndrome.

We confirmed the binding capability of the C-terminal acidic cluster E1077 – D1082 for Ca^{2+} and its contribution to Ca^{2+} -dependent modulation of TRPA1. Moreover, we found that intact end (last 20 AA) of C terminus is essential for proper calcium-dependent inactivation of the TRPA1 channel.

Taken together, our results contribute to the understanding of how the TRPA1 channel operates and how it may be regulated in cells.

7. Bibliography

1. Nilius, B. & Flockerzi, V. *Mammalian Transient Receptor Potential (TRP) Cation Channels. Volume II*. *Handbook of Experimental Pharmacology* **223,** (2014).
2. Caterina, M. J. *et al.* The capsaicin receptor: a heat-activated ion channel in the pain pathway. *Nature* **389,** 816–824 (1997).
3. Clapham, D. E. TRP channels as cellular sensors. *Nature* **426,** 517–524 (2003).
4. Pedersen, S. F., Owsianik, G. & Nilius, B. TRP channels: An overview. *Cell Calcium* **38,** 233–252 (2005).
5. Vannier, B., Zhu, X., Brown, D. & Birnbaumer, L. The membrane topology of human transient receptor potential 3 as inferred from glycosylation-scanning mutagenesis and epitope immunocytochemistry. *J. Biol. Chem.* **273,** 8675–8679 (1998).
6. Jaquemar, D., Schenker, T. & Trueb, B. An Ankyrin-like Protein with Transmembrane Domains Is Specifically Lost after Oncogenic Transformation of Human Fibroblasts. *Biochemistry* **274,** 7325–7333 (1999).
7. Story, G. M. *et al.* ANKTM1, a TRP-like channel expressed in nociceptive neurons, is activated by cold temperatures. *Cell* **112,** 819–829 (2003).
8. Kremeyer, B. *et al.* A Gain-of-Function Mutation in TRPA1 Causes Familial Episodic Pain Syndrome. *Neuron* **66,** 671–680 (2010).
9. Binder, A. *et al.* Transient receptor potential channel polymorphisms are associated with the somatosensory function in neuropathic pain patients. *PLoS One* **6,** (2011).
10. Woolf, C. J. & Ma, Q. Nociceptors-Noxious Stimulus Detectors. *Neuron* **55,** 353–364 (2007).
11. Saito, S. & Tominaga, M. Functional diversity and evolutionary dynamics of thermoTRP channels. *Cell Calcium* **57,** 214–221 (2015).
12. Vriens, J. *et al.* TRPM3 Is a Nociceptor Channel Involved in the Detection of Noxious Heat. *Neuron* **70,** 482–494 (2011).
13. Fernández-Carvajal, A., Fernández-Ballester, G., Devesa, I., González-Ros, J. M. & Ferrer-Montiel, A. New strategies to develop novel pain therapies: Addressing thermoreceptors from different points of view. *Pharmaceuticals* **5,** 16–48 (2011).
14. Smith, G. D. *et al.* TRPV3 is a temperature-sensitive vanilloid receptor-like protein. *Nature* **418,** 186–190 (2002).
15. Güler, A. D. *et al.* Heat-evoked activation of the ion channel, TRPV4. *J. Neurosci.* **22,** 6408–6414 (2002).
16. Benham, C. D., Gunthorpe, M. J. & Davis, J. B. TRPV channels as temperature sensors. *Cell Calcium* **33,** 479–487 (2003).
17. Tominaga, M. *et al.* The cloned capsaicin receptor integrates multiple pain-producing stimuli. *Neuron* **21,** 531–543 (1998).
18. Caterina, M. J., Rosen, T. a, Tominaga, M., Brake, a J. & Julius, D. A capsaicin-receptor homologue with a high threshold for noxious heat. *Nature* **398,** 436–441 (1999).
19. Togashi, K. *et al.* TRPM2 activation by cyclic ADP-ribose at body temperature is involved in insulin secretion. *EMBO J.* **25,** 1804–1815 (2006).
20. Talavera, K. *et al.* Heat activation of TRPM5 underlies thermal sensitivity of sweet taste. *Nature* **438,** 1022–5 (2005).
21. Zimmermann, K. *et al.* Transient receptor potential cation channel, subfamily C, member 5 (TRPC5) is a cold-transducer in the peripheral nervous system. *Proc. Natl. Acad. Sci. U. S. A.* **108,** 18114–9 (2011).
22. McKemy, D. D., Neuhausser, W. M. & Julius, D. Identification of a cold receptor

reveals a general role for TRP channels in thermosensation. *Nature* **416,** 52–58 (2002).
23. Chuang, H. H., Neuhausser, W. M. & Julius, D. The super-cooling agent icilin reveals a mechanism of coincidence detection by a temperature-sensitive TRP channel. *Neuron* **43,** 859–869 (2004).
24. Peier, A. M. *et al.* A TRP channel that senses cold stimuli and menthol. *Cell* **108,** 705–715 (2002).
25. Kobayashi, K. *et al.* Distinct expression of TRPM8, TRPA1, and TRPV1 mRNAs in rat primary afferent neurons with Aδ/C-fibers and colocalization with Trk receptors. *J. Comp. Neurol.* **493,** 596–606 (2005).
26. Bautista, D. M. *et al.* TRPA1 Mediates the Inflammatory Actions of Environmental Irritants and Proalgesic Agents. *Cell* **124,** 1269–1282 (2006).
27. Kwan, K. Y. *et al.* TRPA1 Contributes to Cold, Mechanical, and Chemical Nociception but Is Not Essential for Hair-Cell Transduction. *Neuron* **50,** 277–289 (2006).
28. Karashima, Y. *et al.* TRPA1 acts as a cold sensor in vitro and in vivo. *Proc. Natl. Acad. Sci. U. S. A.* **106,** 1273–1278 (2009).
29. Bandell, M. *et al.* Noxious cold ion channel TRPA1 is activated by pungent compounds and bradykinin. *Neuron* **41,** 849–857 (2004).
30. Sawada, Y., Hosokawa, H., Hori, A., Matsumura, K. & Kobayashi, S. Cold sensitivity of recombinant TRPA1 channels. *Brain Res.* **1160,** 39–46 (2007).
31. Zurborg, S., Yurgionas, B., Jira, J. a, Caspani, O. & Heppenstall, P. a. Direct activation of the ion channel TRPA1 by Ca2+. *Nat. Neurosci.* **10,** 277–279 (2007).
32. Nagata, K., Duggan, A., Kumar, G. & García-Añoveros, J. Nociceptor and Hair Cell Transducer Properties of TRPA1, a Channel for Pain and Hearing. *J. Neurosci.* **25,** 4052–4061 (2005).
33. de Oliveira, C. *et al.* Transient receptor potential channel ankyrin-1 is not a cold sensor for autonomic thermoregulation in rodents. *J. Neurosci.* **34,** 4445–52 (2014).
34. Moparthi, L. *et al.* Human TRPA1 is intrinsically cold- and chemosensitive with and without its N-terminal ankyrin repeat domain. *Proc. Natl. Acad. Sci. U. S. A.* **111,** 16901–6 (2014).
35. Klionsky, L. *et al.* Species-specific pharmacology of Trichloro(sulfanyl)ethyl benzamides as transient receptor potential ankyrin 1 (TRPA1) antagonists. *Mol. Pain* **3,** 39 (2007).
36. Jordt, S.-E. *et al.* Mustard oils and cannabinoids excite sensory nerve fibres through the TRP channel ANKTM1. *Nature* **427,** 260–265 (2004).
37. Cordero-Morales, J. F., Gracheva, E. O. & Julius, D. PNAS Plus: Cytoplasmic ankyrin repeats of transient receptor potential A1 (TRPA1) dictate sensitivity to thermal and chemical stimuli. *Proc. Natl. Acad. Sci.* **108,** E1184–E1191 (2011).
38. Chen, J. *et al.* Species differences and molecular determinant of TRPA1 cold sensitivity. *Nat. Commun.* **4,** 2501 (2013).
39. Saito, S. *et al.* Analysis of transient receptor potential ankyrin 1 (TRPA1) in frogs and lizards illuminates both nociceptive heat and chemical sensitivities and coexpression with TRP vanilloid 1 (TRPV1) in ancestral vertebrates. *J. Biol. Chem.* **287,** 30743–30754 (2012).
40. Gracheva, E. O. *et al.* Molecular basis of infrared detection by snakes. *Nature* **464,** 1006–11 (2010).
41. Saito, S. *et al.* Heat and noxious chemical sensor, chicken TRPA1, as a target of bird repellents and identification of its structural determinants by multispecies functional comparison. *Mol. Biol. Evol.* **31,** 708–722 (2014).

42. Zhong, L. *et al.* Thermosensory and Nonthermosensory Isoforms of Drosophila melanogaster TRPA1 Reveal Heat-Sensor Domains of a ThermoTRP Channel. *Cell Rep.* **1,** 43–55 (2012).
43. Hamada, F. N. *et al.* An internal thermal sensor controlling temperature preference in Drosophila. *Nature* **454,** 217–220 (2008).
44. Corfas, R. A. & Vosshall, L. B. The cation channel TRPA1 tunes mosquito thermotaxis to host temperatures. *Elife* **4,** (2015).
45. Prober, D. A. *et al.* Zebrafish TRPA1 channels are required for chemosensation but not for thermosensation or mechanosensory hair cell function. *J. Neurosci.* **28,** 10102–10110 (2008).
46. Basbaum, A. I., Bautista, D. M., Scherrer, G. & Julius, D. Cellular and Molecular Mechanisms of Pain. *Cell* **139,** 267–284 (2009).
47. Bourinet, E. *et al.* Calcium-permeable ion channels in pain signaling. *Physiol. Rev.* **94,** 81–140 (2014).
48. Mizumura, K., Sugiura, T., Katanosaka, K., Banik, R. K. & Kozaki, Y. Excitation and sensitization of nociceptors by bradykinin: What do we know? *Exp. Brain Res.* **196,** 53–65 (2009).
49. Andrade, E. L., Meotti, F. C. & Calixto, J. B. TRPA1 antagonists as potential analgesic drugs. *Pharmacol. Ther.* **133,** 189–204 (2012).
50. Doerner, J. F., Gisselmann, G., Hatt, H. & Wetzel, C. H. Transient receptor potential channel A1 is directly gated by calcium ions. *J. Biol. Chem.* **282,** 13180–13189 (2007).
51. Wang, S. *et al.* Phospholipase C and protein kinase A mediate bradykinin sensitization of TRPA1: A molecular mechanism of inflammatory pain. *Brain* **131,** 1241–1251 (2008).
52. Dai, Y. *et al.* Sensitization of TRPA1 by PAR2 contributes to the sensation of inflammatory pain. *J. Clin. Invest.* **117,** 1979–1987 (2007).
53. Fischer, M. J. M. *et al.* Direct evidence for functional TRPV1/TRPA1 heteromers. *Pflugers Arch. Eur. J. Physiol.* **466,** 2229–2241 (2014).
54. Weng, H. J. *et al.* Tmem100 Is a Regulator of TRPA1-TRPV1 Complex and Contributes to Persistent Pain. *Neuron* **85,** 833–846 (2015).
55. Cvetkov, T. L., Huynh, K. W., Cohen, M. R. & Moiseenkova-Bell, V. Y. Molecular architecture and subunit organization of TRPA1 ion channel revealed by electron microscopy. *J. Biol. Chem.* **286,** 38168–38176 (2011).
56. Paulsen, C. E., Armache, J., Gao, Y., Cheng, Y. & Julius, D. Structure of the TRPA1 ion channel suggests regulatory mechanisms. *Nature* **520,** 511–517 (2015).
57. Liao, M., Cao, E., Julius, D. & Cheng, Y. Structure of the TRPV1 ion channel determined by electron cryo-microscopy. *Nature* **504,** 107–12 (2013).
58. Cao, E., Liao, M., Cheng, Y. & Julius, D. TRPV1 structures in distinct conformations reveal activation mechanisms. *Nature* **504,** 113–8 (2013).
59. Payandeh, J., Scheuer, T., Zheng, N. & Catterall, W. a. The crystal structure of a voltage-gated sodium channel. *Nature* **475,** 353–358 (2011).
60. Long, S. B., Campbell, E. B. & Mackinnon, R. Crystal structure of a mammalian voltage-dependent Shaker family K+ channel. *Science* **309,** 897–903 (2005).
61. Palovcak, E., Delemotte, L., Klein, M. L. & Carnevale, V. Comparative sequence analysis suggests a conserved gating mechanism for TRP channels. *J. Gen. Physiol.* **146,** 37–50 (2015).
62. Wang, Y. Y., Chang, R. B., Waters, H. N., McKemy, D. D. & Liman, E. R. The nociceptor ion channel TRPA1 is potentiated and inactivated by permeating calcium ions. *J. Biol. Chem.* **283,** 32691–32703 (2008).

63. Voets, T., Janssens, A., Droogmans, G. & Nilius, B. Outer Pore Architecture of a Ca2+-selective TRP Channel. *J. Biol. Chem.* **279,** 15223–15230 (2004).
64. Wan, X. *et al.* Bimodal voltage dependence of TRPA1: Mutations of a key pore helix residue reveal strong intrinsic voltage-dependent inactivation. *Pflugers Arch. Eur. J. Physiol.* **466,** 1273–1287 (2014).
65. Raybaud, A. *et al.* The role of the GX9GX3G motif in the gating of high voltage-activated Ca2+ Channels. *J. Biol. Chem.* **281,** 39424–39436 (2006).
66. Benedikt, J., Samad, A., Ettrich, R., Teisinger, J. & Vlachova, V. Essential role for the putative S6 inner pore region in the activation gating of the human TRPA1 channel. *Biochim. Biophys. Acta - Mol. Cell Res.* **1793,** 1279–1288 (2009).
67. Brewster, M. S. J. & Gaudet, R. How the TRPA1 receptor transmits painful stimuli: Inner workings revealed by electron cryomicroscopy. *BioEssays* **37,** 1184–1192 (2015).
68. Guo, Y. *et al.* Contributions of conserved TPLH tetrapeptides to the conformational stability of ankyrin repeat proteins. *J. Mol. Biol.* **399,** 168–181 (2010).
69. Yuan, C. *et al.* The study of pH-dependent stability shows that the TPLH-mediated hydrogen-bonding network is important for the conformation and stability of human gankyrin. *Biochemistry* **52,** 4848–4857 (2013).
70. Sotomayor, M., Corey, D. P. & Schulten, K. In search of the hair-cell gating spring: Elastic properties of ankyrin and cadherin repeats. *Structure* **13,** 669–682 (2005).
71. Gaudet, R. A primer on ankyrin repeat function in TRP channels and beyond. *Mol. Biosyst.* **4,** 372–9 (2008).
72. Phelps, C. B., Wang, R. R., Choo, S. S. & Gaudet, R. Differential regulation of TRPV1, TRPV3, and TRPV4 sensitivity through a conserved binding site on the ankyrin repeat domain. *J. Biol. Chem.* **285,** 731–740 (2010).
73. Walker, R. G., Willingham, a T. & Zuker, C. S. A Drosophila mechanosensory transduction channel. *Science* **287,** 2229–2234 (2000).
74. Howard, J. & Bechstedt, S. Hypothesis: A helix of ankyrin repeats of the NOMPC-TRP ion channel is the gating spring of mechanoreceptors [1]. *Curr. Biol.* **14,** 224–226 (2004).
75. Corey, D. P. *et al.* TRPA1 is a candidate for the mechanosensitive transduction channel of vertebrate hair cells. *Nature* **432,** 723–730 (2004).
76. Hinman, a a, Chuang, H. H. a B., Bautista, D. M. a & Julius, D. a. TRP channel activation by reversible covalent modification. *Proc. Natl. Acad. Sci. U. S. A.* **103,** 19564–19568 (2006).
77. Macpherson, L. J. *et al.* Noxious compounds activate TRPA1 ion channels through covalent modification of cysteines. *Nature* **445,** 541–545 (2007).
78. Wang, L., Cvetkov, T. L., Chance, M. R. & Moiseenkova-Bell, V. Y. Identification of in vivo disulfide conformation of TRPA1 ion channel. *J. Biol. Chem.* **287,** 6169–6176 (2012).
79. Nilius, B., Prenen, J. & Owsianik, G. Irritating channels: the case of TRPA1. *J. Physiol.* **589,** 1543–1549 (2011).
80. Jabba, S. *et al.* Directionality of temperature activation in mouse TRPA1 ion channel can be inverted by single-point mutations in ankyrin repeat six. *Neuron* **82,** 1017–1031 (2014).
81. Samad, A. *et al.* The C-terminal basic residues contribute to the chemical- and voltage-dependent activation of TRPA1. *Biochem. J.* **433,** 197–204 (2011).
82. Venkatachalam, K. & Montell, C. TRP channels. *Annu. Rev. Biochem.* **76,** 387–417 (2007).
83. Woolfson, D. N. The design of coiled-coil structures and assemblies. *Advances in*

Protein Chemistry **70,** 79–112 (2005).
84. Kim, D. & Cavanaugh, E. J. Requirement of a soluble intracellular factor for activation of transient receptor potential A1 by pungent chemicals: role of inorganic polyphosphates. *J. Neurosci.* **27,** 9 (2007).
85. Salas, M. M., Hargreaves, K. M. & Akopian, A. N. TRPA1-mediated responses in trigeminal sensory neurons: Interaction between TRPA1 and TRPV1. *Eur. J. Neurosci.* **29,** 1568–1578 (2009).
86. Dhavan, R. & Tsai, L. H. A decade of CDK5. *Nat. Rev. Mol. Cell Biol.* **2,** 749–759 (2001).
87. Tsai, L. H., Delalle, I., Caviness, V. S., Chae, T. & Harlow, E. P35 Is a Neural-Specific Regulatory Subunit of Cyclin-Dependent Kinase 5. *Nature* **371,** 419–423 (1994).
88. Humbert, S., Dhavan, R. & Tsai, L. P39 Activates Cdk5 in Neurons, and Is Associated With the Actin Cytoskeleton. *J. Cell Sci.* **113 (Pt 6,** 975–983 (2000).
89. Lew, J. *et al.* A brain-specific activator of cyclin-dependent kinase 5. *Nature* **371,** 423–426 (1994).
90. Ohshima, T. *et al.* Targeted disruption of the cyclin-dependent kinase 5 gene results in abnormal corticogenesis, neuronal pathology and perinatal death. *Proc. Natl. Acad. Sci. U. S. A.* **93,** 11173–11178 (1996).
91. Tanaka, T. *et al.* Neuronal cyclin-dependent kinase 5 activity is critical for survival. *J. Neurosci.* **21,** 550–8 (2001).
92. Ko, J. *et al.* P35 and P39 Are Essential for Cyclin-Dependent Kinase 5 Function During Neurodevelopment. *J. Neurosci.* **21,** 6758–6771 (2001).
93. Songyang, Z. *et al.* A structural basis for substrate specificities of protein Ser/Thr kinases: primary sequence preference of casein kinases I and II, NIMA, phosphorylase kinase, calmodulin-dependent kinase II, CDK5, and Erk1. *Mol. Cell. Biol.* **16,** 6486–93 (1996).
94. Liu, J., Du, J., Yang, Y. & Wang, Y. Phosphorylation of TRPV1 by cyclin-dependent kinase 5 promotes TRPV1 surface localization, leading to inflammatory thermal hyperalgesia. *Exp. Neurol.* **273,** 253–262 (2015).
95. Jendryke, T. *et al.* TRPV1 function is modulated by Cdk5-mediated phosphorylation: insights into the molecular mechanism of nociception. *Sci. Rep.* **6,** 22007 (2016).
96. Sulak, M. A. Modulation of transient receptor potential cation channel, subfamily A, member 1 (TRPA1) activity by CDK5. (Kent State University, 2011).
97. Macpherson, L. J. *et al.* The pungency of garlic: Activation of TRPA1 and TRPV1 in response to allicin. *Curr. Biol.* **15,** 929–934 (2005).
98. Matta, J. a *et al.* General anesthetics activate a nociceptive ion channel to enhance pain and inflammation. *Proc. Natl. Acad. Sci. U. S. A.* **105,** 8784–9 (2008).
99. Fischer, M. J. M. *et al.* The general anesthetic propofol excites nociceptors by activating TRPV1 and TRPA1 rather than GABAA receptors. *J. Biol. Chem.* **285,** 34781–34792 (2010).
100. Laursen, W. J., Bagriantsev, S. N. & Gracheva, E. O. *TRPA1 Channels: Chemical and Temperature Sensitivity*. *Current Topics in Membranes* **74,** (Elsevier, 2014).
101. Takahashi, N. *et al.* TRPA1 underlies a sensing mechanism for O2. *Nat. Chem. Biol.* **7,** 701–11 (2011).
102. Miyamoto, T., Dublin, A. E., Petrus, M. J. & Patapoutian, A. TRPV1 and TRPA1 mediate peripheral nitric oxide-induced nociception in mice. *PLoS One* **4,** (2009).
103. Cavanaugh, E. J., Simkin, D. & Kim, D. Activation of transient receptor potential A1 channels by mustard oil, tetrahydrocannabinol and Ca2+ reveals different

functional channel states. *Neuroscience* **154,** 1467–1476 (2008).
104. Xiao, B. *et al.* Identification of transmembrane domain 5 as a critical molecular determinant of menthol sensitivity in mammalian TRPA1 channels. *J. Neurosci.* **28,** 9640–9651 (2008).
105. Karashima, Y. *et al.* Bimodal action of menthol on the transient receptor potential channel TRPA1. *J. Neurosci.* **27,** 9874–9884 (2007).
106. Talavera, K. *et al.* Nicotine activates the chemosensory cation channel TRPA1. *Nat. Neurosci.* **12,** 1293–1299 (2009).
107. Nagatomo, K. & Kubo, Y. Caffeine activates mouse TRPA1 channels but suppresses human TRPA1 channels. *Proc. Natl. Acad. Sci. U. S. A.* **105,** 17373–8 (2008).
108. Nagatomo, K., Ishii, H., Yamamoto, T., Nakajo, K. & Kubo, Y. The Met268Pro mutation of mouse TRPA1 changes the effect of caffeine from activation to suppression. *Biophys. J.* **99,** 3609–3618 (2010).
109. Bobkov, Y. V., Corey, E. a. & Ache, B. W. The pore properties of human nociceptor channel TRPA1 evaluated in single channel recordings. *Biochim. Biophys. Acta - Biomembr.* **1808,** 1120–1128 (2011).
110. Hynkova, A. Modulation of the ankyrin receptor TRPA1 by divalent cations. (Charles University in Prague, 2012).
111. Hu, H., Bandell, M., Petrus, M. J., Zhu, M. X. & Patapoutian, A. Zinc activates damage-sensing TRPA1 ion channels. *Nat. Chem. Biol.* **5,** 183–190 (2009).
112. Karashima, Y. *et al.* Agonist-induced changes in Ca2+ permeation through the nociceptor cation channel TRPA1. *Biophys. J.* **98,** 773–783 (2010).
113. Schmidt, M., Dubin, A. E., Petrus, M. J., Earley, T. J. & Patapoutian, A. Nociceptive Signals Induce Trafficking of TRPA1 to the Plasma Membrane. *Neuron* **64,** 498–509 (2009).
114. Benedikt, J., Teisinger, J., Vyklicky, L. & Vlachova, V. Ethanol inhibits cold-menthol receptor TRPM8 by modulating its interaction with membrane phosphatidylinositol 4,5-bisphosphate. *J. Neurochem.* **100,** 211–224 (2007).
115. Dittert, I. *et al.* Improved superfusion technique for rapid cooling or heating of cultured cells under patch-clamp conditions. *J. Neurosci. Methods* **151,** 178–185 (2006).
116. Chaudhury, S., Bal, M., Belugin, S., Shapiro, M. S. & Jeske, N. a. AKAP150-mediated TRPV1 sensitization is disrupted by calcium/calmodulin. *Mol. Pain* **7,** 34 (2011).
117. Krieger, E. & Vriend, G. YASARA View — molecular graphics for all devices — from smartphones to workstations. *Bioinformatics* **30,** 2981–2982 (2014).
118. Arnold, K., Bordoli, L. & Schwede, T. The SWISS-MODEL workspace : a web-based environment for protein structure homology modelling. *Bioinformatics* **22,** 195–201 (2006).
119. Kopp, J. & Schwede, T. The SWISS-MODEL Repository : new features and functionalities. *Nucleic Acids Res.* **34,** 315–318 (2006).
120. Zhang, Y. I-TASSER server for protein 3D structure prediction. *BMC Bioinformatics* **9,** 40 (2008).
121. Bordoli, L. *et al.* Protein structure homology modeling using SWISS-MODEL workspace. *Nat. Protoc.* **4,** 1–13 (2009).
122. Kiefer, F., Arnold, K., Kunzli, M., Bordoli, L. & Schwede, T. The SWISS-MODEL Repository and associated resources. *Nucleic Acids Res.* **37,** 387–392 (2009).
123. Roy, A., Kucukural, A. & Zhang, Y. I-TASSER: a unified platform for automated protein structure and function prediction. *Nat. Protoc.* **5,** 725–738 (2011).

124. Yang, J. *et al.* The I-TASSER Suite: protein structure and function prediction. *Nat. Methods* **12,** 7–8 (2015).
125. Lee, W., Strumpfer, J., Bennett, V., Schulten, K. & Marszalek, P. E. Mutation of conserved histidines alters tertiary structure and nanomechanics of consensus ankyrin repeats. *J. Biol. Chem.* **287,** 19115–19121 (2012).
126. Xiao, Q., Prussia, A., Yu, K., Cui, Y. & Hartzell, H. C. Regulation of bestrophin Cl channels by calcium: role of the C terminus. *J. Gen. Physiol.* **132,** 681–92 (2008).
127. Yuan, P., Leonetti, M. D., Pico, A., Hsiung, Y. & MacKinnon, R. Structure of the human BK channel Ca2+-activation apparatus at 3.0 A resolution. *Science* **329,** 182–6 (2010).
128. Köttgen, M. *et al.* Trafficking of TRPP2 by PACS proteins represents a novel mechanism of ion channel regulation. *EMBO J.* **24,** 705–16 (2005).

8. List of publications

1) **Hynkova A.**, Marsakova L., Vaskova J., Vlachova V.
N-terminal tetrapeptide T/SPLH motifs contribute to multimodal activation of human TRPA1 channel
Scientific Reports, 6:28700, 2016

2) Zima V., Witschas K., **Hynkova A.**, Zimova L, Barvik I., Vlachova V.
Structural modeling and patch-clamp analysis of painrelated mutation TRPA1-N855S reveals inter-subunit salt bridges stabilizing the channel open state.
Neuropharmacology, 93: 294-307, 2015

3) Sura L., Zima V., Marsakova L., **Hynkova A.**, Barvik I., Vlachova V.
C-terminal acidic cluster is involved in Ca^{2+}-induced regulation of human transient receptor potential ankyrin 1 channel.
The Journal of Biological Chemistry, 287(22):18067-77, 2012

4) Boukalova S., Touska F., Marsakova L., **Hynkova A.**, Sura L., Chvojka S., Dittert I., Vlachova V.
Gain-of-function mutations in the transient receptor potential channels TRPV1 and TRPA1: how painful?
Physiological Research, 63 Suppl 1:S205-13, 2014

Publication 1

Hynkova A., Marsakova L., Vaskova J., Vlachova V.

N-terminal tetrapeptide T/SPLH motifs contribute to multimodal activation of human TRPA1 channel

Scientific Reports, 6:28700, 2016

The extent of participation: Preparation of all mutant constructs, most of the electrophysiological experiments, biotinylation assay, data analysis, writing of the manuscript.

SCIENTIFIC REPORTS

OPEN

N-terminal tetrapeptide T/SPLH motifs contribute to multimodal activation of human TRPA1 channel

Received: 15 March 2016
Accepted: 08 June 2016
Published: 27 June 2016

Anna Hynkova, Lenka Marsakova, Jana Vaskova & Viktorie Vlachova

Human transient receptor potential ankyrin channel 1 (TRPA1) is a polymodal sensor implicated in pain, inflammation and itching. An important locus for TRPA1 regulation is the cytoplasmic N-terminal domain, through which various exogenous electrophilic compounds such as allyl-isothiocyanate from mustard oil or cinnamaldehyde from cinnamon activate primary afferent nociceptors. This major region is comprised of a tandem set of 17 ankyrin repeats (AR1-AR17), five of them contain a strictly conserved T/SPLH tetrapeptide motif, a hallmark of an important and evolutionarily conserved contribution to conformational stability. Here, we characterize the functional consequences of putatively stabilizing and destabilizing mutations in these important structural units and identify AR2, AR6, and AR11-13 to be distinctly involved in the allosteric activation of TRPA1 by chemical irritants, cytoplasmic calcium, and membrane voltage. Considering the potential involvement of the T/SP motifs as putative phosphorylation sites, we also show that proline-directed Ser/Thr kinase CDK5 modulates the activity of TRPA1, and that T673 outside the AR-domain is its only possible target. Our data suggest that the most strictly conserved N-terminal ARs define the energetics of the TRPA1 channel gate and contribute to chemical-, calcium- and voltage-dependence.

Human transient receptor potential (TRP) subtype A1 (TRPA1) is an intrinsically cold and chemosensitive ion channel whose physiological role has been implicated in nociception, inflammatory pain, and itching[1–5]. This channel is one of the key sensors for various pungent and irritant compounds, being activated by thiol-reactive electrophiles and oxidants, but also by a number of nonelectrophilic chemicals, including menthol, nicotine, carvacrol, clotrimazole, and certain cannabinoids (for a review, see[6]). Moreover, TRPA1 is also dynamically modulated by permeating calcium ions[7–9] and partially activated by strong depolarization[10,11]. While members of the TRP channel superfamily share a general tetrameric six-transmembrane (S1-S6) architecture and likely a similar mechanism of pore-opening[12], all the stimuli that trigger this gating mechanism differ substantially and are mediated or modulated by large cytoplasmic N and C termini that flank the relatively well conserved transmembrane domain (Fig. 1). The recent high-resolution structure of TRPA1 clearly indicates that chemical signals initiated by various stimuli might indeed be readily conveyed through cytoplasmic domains to the intracellular channel gate[13–15].

TRPA1 is unique among mammalian TRP channels in bearing an extensive cytoplasmic amino terminus (720 of 1119 amino acids), comprised of a prominent ankyrin repeat domain (ARD; 1–649) consisting of a tandem array of 17 ankyrin repeats (AR1–AR17), and a linker that connects ARD with the first transmembrane segment[13,14,16]. The N-terminus has been long known to be an immediate detector and integrator of the TRPA1 activation stimuli. Initial mutagenesis studies proposed that membrane-permeable electrophilic molecules such as allyl isothiocyanate (AITC) or cinnamaldehyde (CA) react with free sulfhydryl groups on specific cysteines and the primary amine of lysines (C621, C641, C665, K710 in human and C415, C422 and C622 in mouse), inducing conformational changes leading to channel opening[17–19]. ARD has also been thought to regulate the activity of TRPA1 from a canonical EF-hand-like Ca^{2+} binding domain beginning at aspartate D468 in AR12[7,8]. Although this hypothesis has been disputed by others[9,20], an AR cluster centered around AR11 was shown to act as an important determinant of Ca^{2+}-dependent desensitization[21]. The importance of the integrity of the ARD region was also supported by human genetic data indicating that a single nucleotide polymorphism in the *Trpa1* gene, which results in a substitution in AR4 (E179K), is associated with paradoxical heat sensation[22,23].

Department of Cellular Neurophysiology, Institute of Physiology of the Czech Academy of Sciences, Videnska 1083, 142 20 Prague 4, Czech Republic. Correspondence and requests for materials should be addressed to V.V. (email: viktorie.vlachova@fgu.cas.cz)

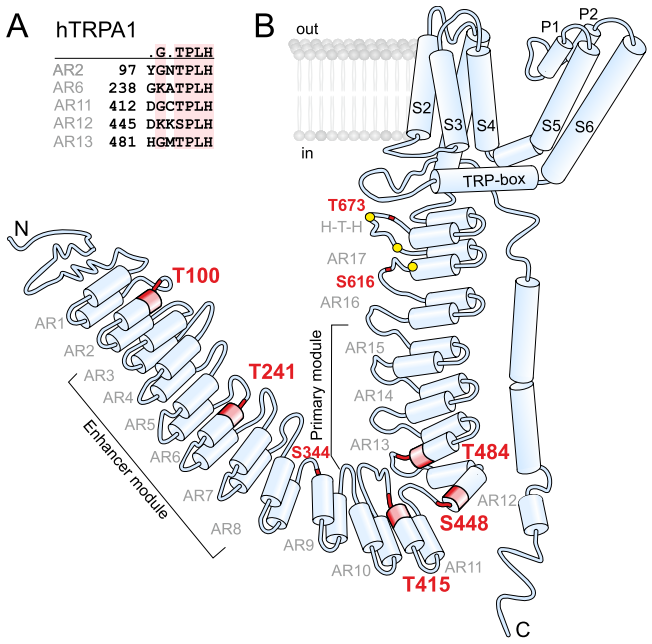

Figure 1. Topology of human TRPA1 channel subunit. (**A**) Sequence alignment of highly conserved T/SPLH motifs in the N-terminal ankyrin repeats (AR) of human TRPA1 (hTRPA1). (**B**) Schematic of one hTRPA1 channel subunit (according to Paulsen *et al.*[13],). TRP-box denotes TRP-like domain, H-T-H indicates helix-turn-helix motif. Conserved threonines and serine from T/SPLH tetrapeptide motifs and T/S residues mutated in this study are indicated in red, reactive cysteine residues (C621, C641 and C665) are represented by yellow circles.

A systematic study based on a series of chimeras between human and rattlesnake TRPA1 proposed two spatially distinct, independent and transferable AR modules, the primary module AR10–AR15, and the enhancer module AR3–AR8 (Fig. 1B), that are each capable of conferring thermal or electrophilic sensitivity to the respective, otherwise insensitive orthologue[21]. In addition, AR6 is uniquely sensitive to changes in the coupling of temperature stimuli to the channel gate, and a single-point mutation in AR6 induced temperature activation without changing the sensitivity to chemical agonists in mouse TRPA1[24]. The recently resolved high-resolution three-dimensional structure of the TRPA1 channel provides important support for the modularity of ARD by showing that AR12–AR16 are structurally integrated with the C-terminal tetrameric parallel coiled-coil, whereas the extended ARD (most likely AR1–AR11) is suspended below the membrane and forms a crescent-shaped structure[13,16]. All the results point to the widely accepted assumption that through evolution, the TRPA1 channel has acquired highly conserved discrete protein sub-structures that underlie its specific and species-dependent functional properties.

Recently, the N-terminus of TRPA1 has been surprisingly shown to be dispensable for a functional channel[25]. Purified human TRPA1 reconstituted into lipid bilayers can be readily activated by electrophiles, non-electrophiles as well as by cold without its N-terminal ARD (Δ1–688 TRPA1) and the channel does not seem to need Ca^{2+} or accessory proteins for its responses. Thus, the role of the N-terminus now appears to be less clear than previously assumed and may consist of forming multi-ligand binding sites, interacting with other proteins, including self-association with other non-contiguous structures of the TRPA1 channel homotetramer[26], the proper targeting of the protein into the plasma membrane[20,25], and, importantly, in the direct regulation of the channel's gating[25].

Structurally, the predicted ankyrin repeats (ARs) comprising the ARD N-terminal region in TRPA1 are characteristic ~33-amino acid motifs, each adopting a helix-turn-helix-extended loop secondary structure topology, stacking together in a close to linear fashion and producing a distinctive modular and elongated architecture[26,27]. Five of the ARs contain a strictly conserved T/SPLH tetrapeptide motif (Fig. 1A and Supplementary Fig. S1), a hallmark of the consensus ankyrin repeat sequence contributing substantially to local conformational stability[28,29]. In such a motif, proline initiates the first α-helix, whereas the pair of threonine and histidine forms intra- and inter-repeat hydrogen bonds (see Fig. 2A).

In this study, we hypothesize that the strict conservation within the evolutionarily conserved T/SPLH motifs in AR2, AR6, and AR11-13 across different species suggests that an especially precisely tuned stability of these N-terminal modules is essential for the proper functioning of the TRPA1 channel. Thus, we set out to characterize the functional consequences of stabilizing and destabilizing mutations in these important structural units.

Results

Mutations affecting the conformational stability of ankyrin repeat 2 affect voltage-dependent TRPA1 channel gating. To examine how the conserved TPLH motif in ankyrin repeat 2 contributes to the functioning of the TRPA1 channel, we constructed three mutants: T100A, T100D, and M131G/A133T, that

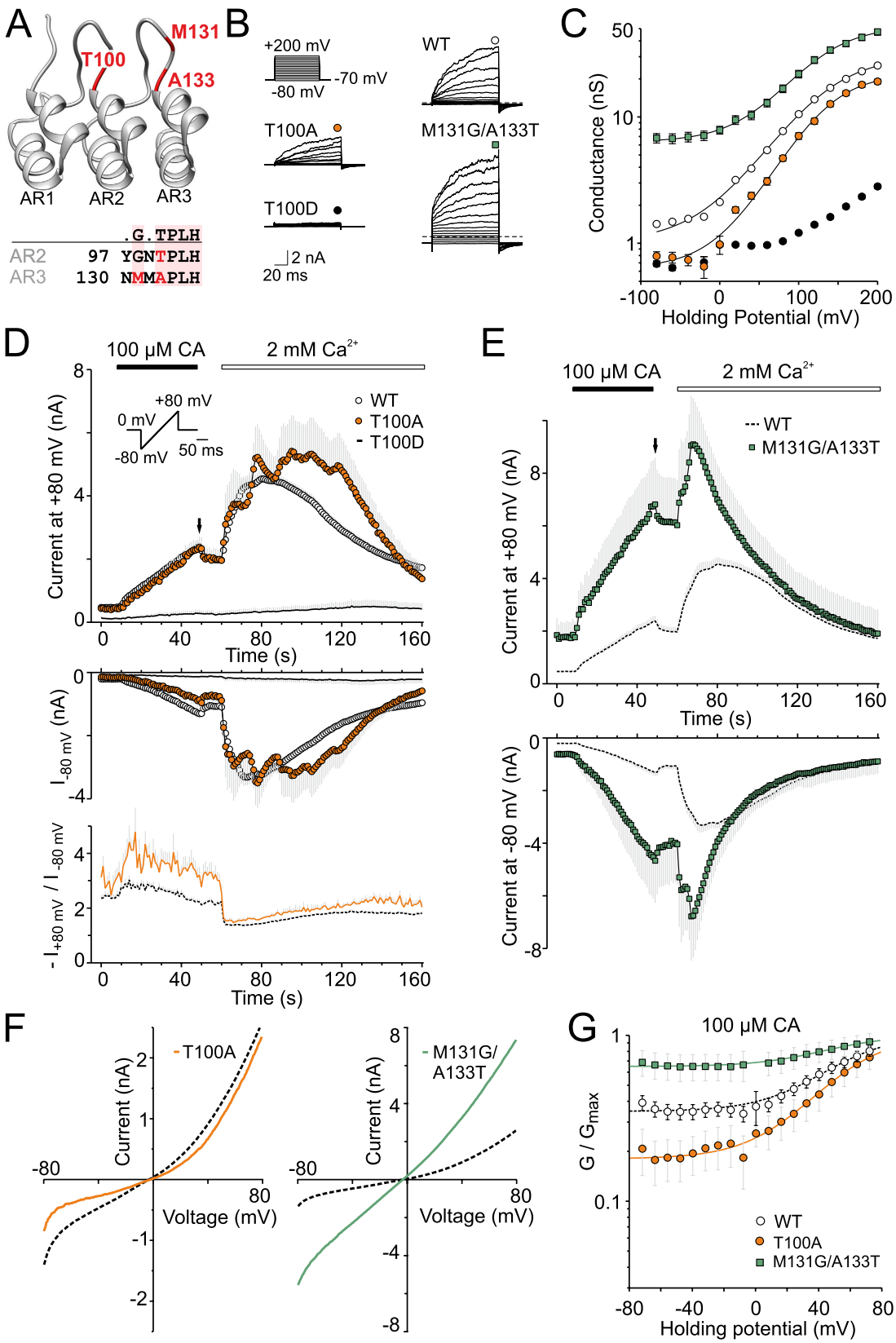

Figure 2. Mutations affecting the conformational stability of the ankyrin repeat 2 and 3 affect voltage-dependent TRPA1 channel gating. (**A**) Homology model of the first three N-terminal ankyrin repeats (AR) of hTRPA1 based on human ankyrinR (pdb code 1N11). In the consensus T/SPLH motif, the hydroxyl from the threonine/serine side-chain forms a hydrogen bond with a nitrogen atom from the histidine side-chain and results in a sharp turn prior to the first helix in the AR. Glycine two residues prior to T/SPLH allows for the compact L shape of the AR. Residues mutated in this study are indicated in red. (**B**) Representative

current traces in response to indicated voltage step protocol (100 ms voltage steps from −80 mV to +200 mV; increment +20 mV; holding potential −70 mV) recorded in control extracellular solution ~1 min after whole-cell formation. (**C**) Average conductances obtained from voltage-step protocols as in B. Data represent the means ± S.E.M. ($n = 128$ for WT and 7–26 for mutants), solid lines are best fits to a Boltzmann function as described in Methods. In some cases, the error bars are smaller than the symbol. (**D**) Time course of average currents through wild-type (solid circles, $n = 70$), T100A (filled circles, $n = 9$) and T100D (solid line, $n = 9$) mutants measured at +80 mV and −80 mV. The average currents are shown with gray bars indicating S.E.M. The application of 100 μM cinnamaldehyde (CA) and subsequent addition of 2 mM Ca^{2+} are indicated above. Below, average rectification of currents shown above, plotted as a function of time. Inset: voltage-ramp protocol. (**E**) Time course of average CA-induced currents in M131G/A133T. The average current for WT is shown in dashed line with gray bars indicating S.E.M. (**F**) Average current-voltage relationships of traces measured at times indicated by an arrow in panels D and E for wild-type (dashed line) and indicated mutants. (**G**) Voltage-independent gating in M131G/A133T. Average conductances obtained from voltage ramp protocol (shown in panel D) normalized to G_{max}. Dashed line for wild-type and solid lines for mutants are best fits to a Boltzmann function.

were intended to either destabilize or stabilize the conformation of the ankyrin repeat AR2 (Fig. 2A). We anticipated that the alanine mutation at T100 could lower the structural stability, most likely due to eliminating the intra-repeat hydrogen bonds (T100 H^N-H103 $N^{\delta 1}$, T100 $O^{\gamma 1}$-H103 H^N and T100 $H^{\gamma 1}$-H103 $N^{\delta 1}$)[29] and that the TPLH-mediated hydrogen-bonding network would be impacted even more by introducing a charged residue at this position. We also hypothesized that if the strictly conserved TPLH motif in AR2 contributes to channel functioning, then introducing a T/SxxH consensus sequence into the adjacent AR3 might have stabilizing effects through inter-repeat interactions, and thus be structurally and/or functionally beneficial.

To characterize the phenotypes of the mutants, we used whole-cell patch clamp recordings from transiently transfected HEK293T cells and assessed their voltage-dependent activation properties using a voltage step protocol from −80 mV to +200 mV, in 20 mV increments (Fig. 2B). The mutants expressed functional channels, however their responses to depolarizing voltage steps and their chemical sensitivities were dramatically different. Figure 2C compares the average conductance-to-voltage (G-V) relationships of voltage-dependent gating for the wild type and the mutant channels. For wild-type TRPA1, the Boltzmann fit gave a half-maximal activation voltage (V_{50}) of 129 ± 2 mV and an apparent number of gating charges (z) of 0.72 ± 0.02 e_0 ($n = 128$). The estimated V_{50} and z were neither significantly changed in T100A (135 ± 6 mV; $z = 0.80 \pm 0.09$ e_0; $n = 9$) nor in the M131G/A133T double mutant channels (124 ± 6 mV; $z = 0.73 \pm 0.04$ e_0; $n = 7$). Apparent differences, however, were seen at hyperpolarizing voltages. The T100A mutant exhibited a decreased basal conductance at negative membrane potentials, indicating a disturbed closed–open equilibrium in favor of the closed state. In contrast, the double mutation M131G/A133T resulted in a gain of function phenotype, where the channel displayed significant voltage-independent gating at negative membrane potentials (G_{min} of 14 ± 1% of G_{max}; $n = 7$), suggesting that the energy required to activate the pore opening is reduced.

To test the chemical sensitivity of the mutants, we employed a standard protocol in which whole-cell membrane currents were measured first in the absence of extracellular Ca^{2+} and in the presence of the partial agonist cinnamaldehyde (CA, 100 μM for 40 s). The agonist was then washed out for 10 s, and Ca^{2+} at a concentration of 2 mM was added to the extracellular solution (Fig. 2D,E). The membrane potential was ramped up each second from –80 mV to +80 mV (1 V/s). Intracellular Ca^{2+} was buffered to low levels with 5 mM EGTA in the patch pipette to assess the effects of permeating calcium ions[9]. Such a protocol enabled us to explore the sensitivity of individual mutants not only to an electrophilic agonist, which most likely leads to the persistent activation of TRPA1[17,18] but also to permeating calcium ions that activate and subsequently inactivate the channel through largely unknown mechanisms[7,8,21]. In agreement with previous reports, cinnamaldehyde at a concentration of 100 μM evoked slowly developing currents in wild-type TRPA1 (2.5 ± 0.2 nA at +80 mV after 40 s; $n = 70$) which slightly relaxed (by ~10%) to a lower sustained level upon washout. The addition of 2 mM Ca^{2+} to the bath solution induced, with a delay of ~13 s, a marked potentiation that was followed by an almost complete inactivation within 1 minute. During the 40 s-application of cinnamaldehyde, the T100A-mediated whole-cell outward currents were almost identical to those of the wild-type channels, but significantly reduced in an inward direction (Fig. 2D,F), matching the above-described reduction in voltage-induced currents at hyperpolarizing membrane potentials measured in control extracellular solution. Compared to the wild type, the delay in the onset of the second, Ca^{2+}-dependent phase of the currents was almost twice as long (median value of 30 s; $n = 9$ versus 18 s for wild-type channels; $n = 70$), indicating that the reduction in inward current led to a reduction in the amount of calcium that enters the cell. The T100D mutation did not give voltage-sensitive channels in the range of voltages explored, and only four of the nine tested cells revealed detectable, but minimal, responses induced by cinnamaldehyde at positive membrane potentials (Fig. 2D). The double mutant M131G/A133T channels displayed much larger responses to cinnamaldehyde at both negative and positive holding potentials (Fig. 2E), a linear current-voltage relationship after 40 s of exposure (Fig. 2F), and about 70% voltage-independent activation (Fig. 2G). Both the delay and the degree of Ca^{2+}-induced potentiation were significantly reduced compared to wild-type channels (Fig. 2E). These observations confirm the previously proposed role of the cytoplasmic N-terminal ankyrin repeat-rich region in the regulation of TRPA1 and identify AR2 to be a domain contributing to voltage-dependent gating.

Specific mutation in conserved TPLH motif in ankyrin repeat six affects voltage- and Ca^{2+}-dependent modulation. Previous findings have implicated ankyrin repeat six in determining the

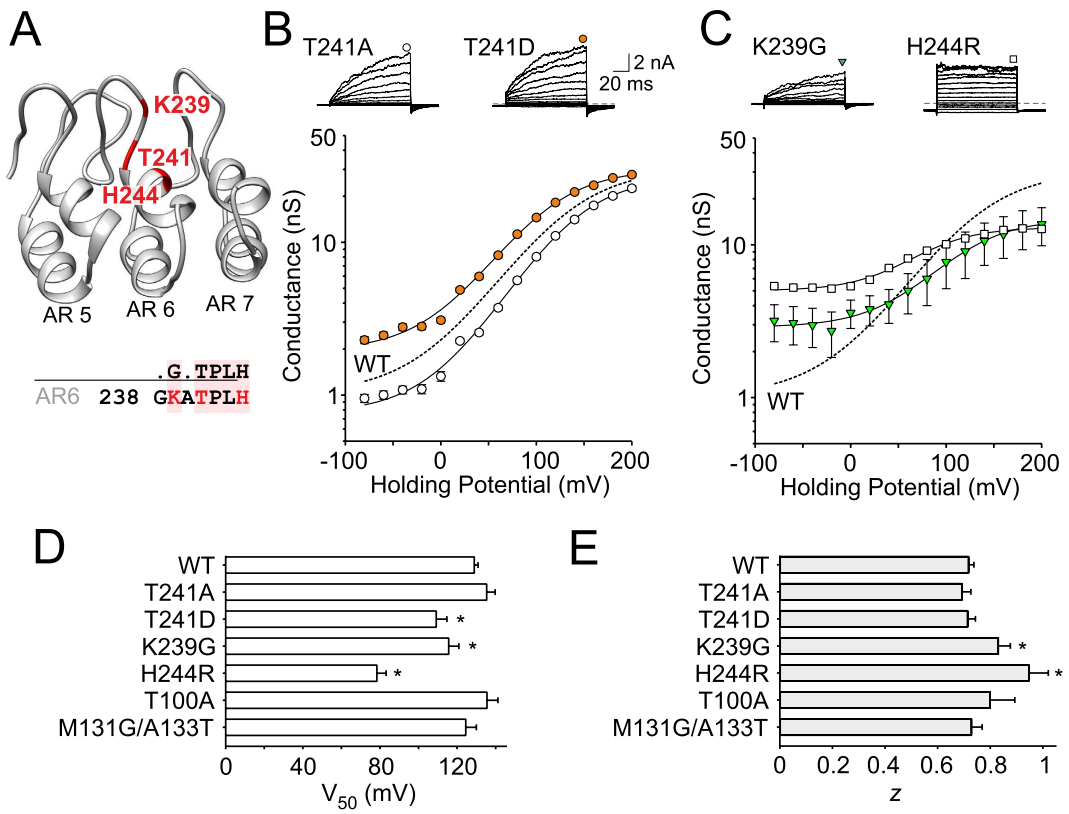

Figure 3. Specific mutation in the conserved TPLH motif in the ankyrin repeat six affects voltage-dependent modulation. (**A**) Homology model of the ankyrin repeats 5 to 7 of hTRPA1 based on human ankyrinR (pdb code 1N11). Residues mutated in this study are indicated in red. (**B**,**C**) Representative current traces in response to voltage step protocol (holding potential −70 mV; 100 ms voltage steps from −80 mV to +200 mV; increment +20 mV) recorded in control extracellular solution ~1 min after whole-cell formation. Representative current traces for wild-type TRPA1 are shown in Fig. 2B. The H244R mutation produced non-zero current at −70 mV at the beginning and the end of each voltage step during the voltage-step protocol (the dashed line depicts the −70 mV baseline), indicating the constitutive activity. Below, average conductances obtained from voltage step protocols shown above. Solid lines are best fits to a Boltzmann function. The dashed line represents the fit obtained from data for wild-type TRPA1 shown in Fig. 2C. Note, both mutations, the stabilizing K239G and destabilizing H244R, reduce the responses of TRPA1 to voltage. (**D**) Summary of half-maximal activation voltage (V_{50}) of wild-type hTRPA1 and individual mutants from experiments as in (**B**,C) and Fig. 2C. The asterisks indicate significant differences between mutant and wild-type TRPA1 (*$P < 0.05$, $n = 138$ for WT and 7–27 for mutant channels). (**E**) Summary of apparent number of gating charges (z) of wild-type hTRPA1 and individual mutants from experiments as in (**B**,**C**) and Fig. 2C. The asterisks indicate significant difference from wild-type TRPA1 (*$P < 0.05$).

temperature sensitivity of mouse TRPA1 and suggested its direct role in coupling the activating stimuli to gate opening[24]. To determine the functional role of the conserved TPLH motif in AR6 of human TRPA1, we first tested the T241A and T241D mutants (Fig. 3A,B) and found them to be both functional, which suggests that strict TPLH conservation is not crucial for TRPA1 functioning. The T241D mutation caused a leftward shift in the voltage-dependent activation curve, decreasing the V_{50} by ~20 mV without affecting the gating charge (0.68 ± 0.06 e_0, $n = 16$). This mutant clearly displayed significant voltage-independent gating at hyperpolarized potentials (Fig. 3B), supporting the possible role of AR6 in defining the energetics of the channel gate.

In further attempts to either strengthen or weaken the AR6 consensus sequence, we next constructed two additional mutants. The first, K239G, was anticipated to improve the ankyrin fold and allow for a more compact L shape of the repeat AR6. The second mutant, H244R, was designed to perturb AR6 by decreasing its mechanical stability[30]. Both the mutants yielded smaller currents in response to depolarizing voltages and also smaller maximal responses to chemical activators (Fig. 3C and see Fig. 4B below). This reduction, however, was probably not the result of their lower expression levels at the plasma membrane, because both the mutants displayed a significantly enhanced conductance at negative membrane potentials (G_{min} of $26 \pm 6\%$ and $44 \pm 1\%$ of G_{max}; $n = 14$ and 25), a leftward shift in the half-activation potential and an increased apparent number of gating charges (Fig. 3D,E), all of which strongly support functional changes. We observed that HEK293T cells transfected with H244R exhibited constitutive inward currents after the whole-cell configuration was established at −70 mV, which indicates a constitutive activity of the mutant channel.

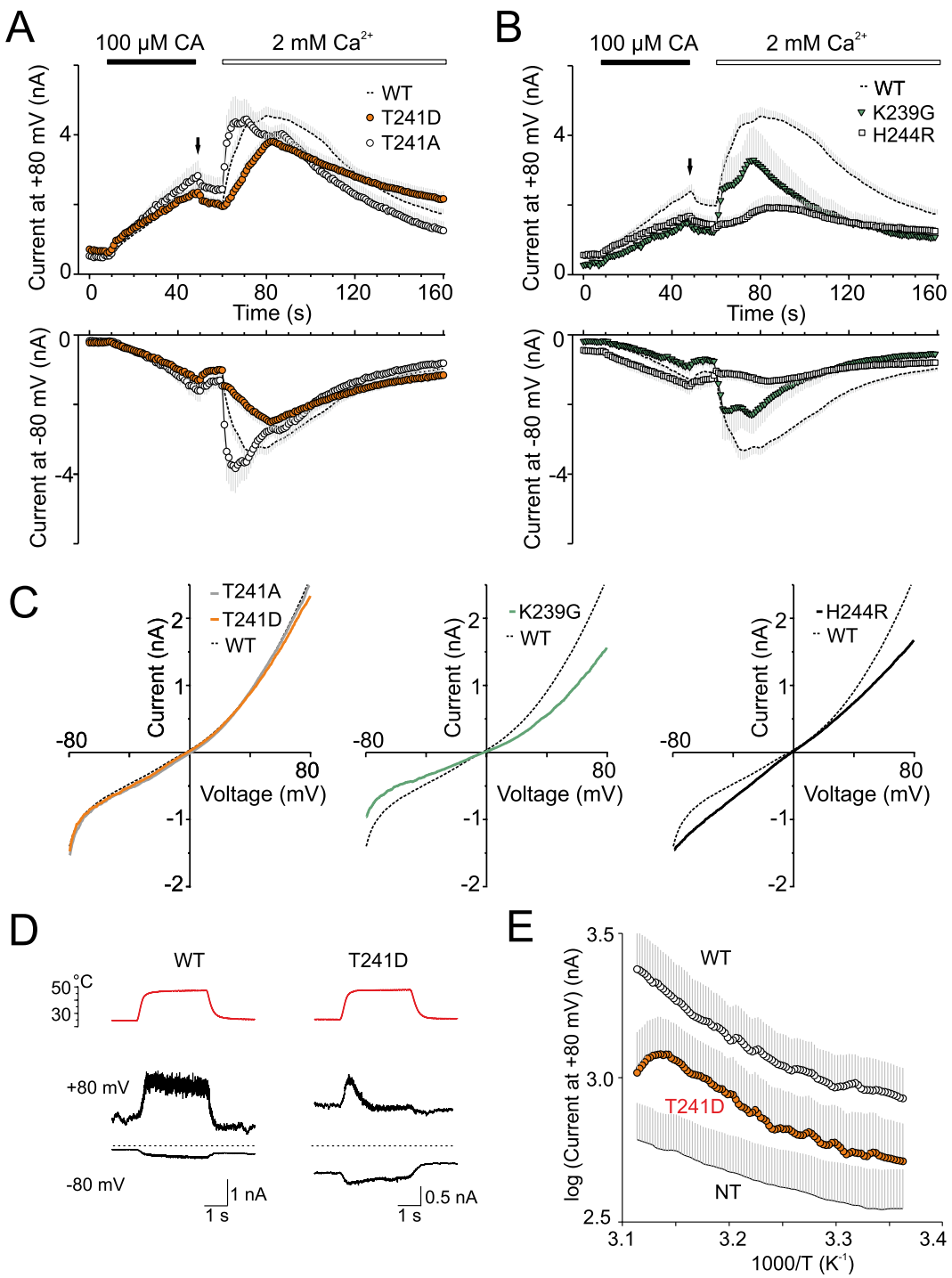

Figure 4. Multimodal gating of TRPA1 depends on the stability of ankyrin repeat 6. (**A**,**B**) Time course of average whole-cell currents induced by 100 μM cinnamaldehyde (CA) in Ca^{2+}-free solution and then exposed to 2 mM Ca^{2+}, measured at +80 mV and at −80 mV in wild-type (dashed line) and indicated mutants. The application of CA and subsequent addition of 2 mM Ca^{2+} are indicated above. (**C**) Average current-voltage relationships of traces measured at times indicated by an arrow in panels A and B for wild-type (dashed line) and individual mutants T241A (gray line), T241D (orange line), K239G (green line) and H244R (black solid line). (**D**) Time course of representative whole-cell current responses to application of 25–47 °C heat step recorded from cells expressing wild-type and mutant hTRPA1 at +80 mV and −80 mV as indicated. The upper row of records (red lines) shows the temperatures of superfusing solution (ECS) measured by a thermocouple inserted into the shared outlet capillary of the drug application system. (**E**) Arrhenius plot of average heat-induced whole-cell currents obtained from wild-type TRPA1 ($n = 9$), the T241D mutant ($n = 7$) and from non-transfected HEK293T cells (NT, $n = 6$) measured at +80 mV.

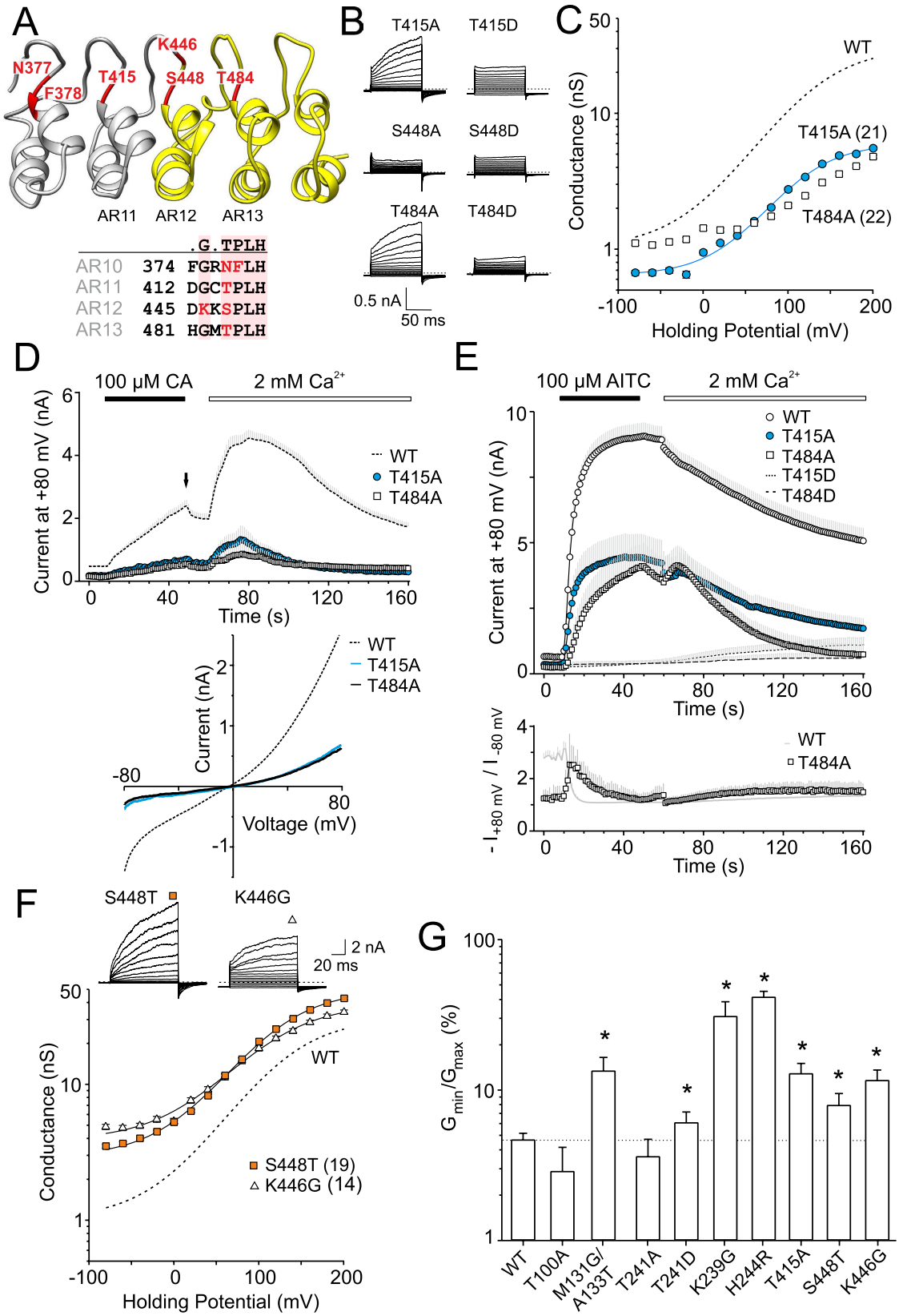

Figure 5. A short range stability of the ankyrin repeat 12 determines the gating and calcium regulation of human TRPA1. (**A**) Homology model of the ankyrin repeats 10 to 14 of hTRPA1. The grey part is based on ankyrinR (pdb code 1N11), the yellow part is based on the published structure of hTRPA1 ([13]; pdb code 3J9P). (**B**) Representative current traces in response to voltage step protocol. Representative current traces for wild-type TRPA1 are shown in Fig. 2B. (**C**) Average conductances obtained from voltage step protocols as in B. Solid line is the best fit to a Boltzmann function. The dashed line represents the fit obtained for wild-type TRPA1

shown in Fig. 2C. Only the voltage-sensitive mutants are shown; *n* indicated in brackets. (**D**) Time course of average whole-cell currents through the wild-type hTRPA1 and the T415A ($n = 8$) and T484A ($n = 11$) mutants measured at +80 mV (protocol shown in Fig. 2D). The application of 100 μM cinnamaldehyde (CA) and subsequent addition of 2 mM Ca^{2+} are indicated above. Below, average current-voltage relationships of traces measured at times indicated by an arrow in panel above. (**E**) Time course of average whole-cell currents through wild-type and mutant hTRPA1 measured at +80 mV. The application of 100 μM allyl isothiocyanate (AITC) and subsequent addition of 2 mM Ca^{2+} are indicated above. Gray bars indicate S.E.M. from 33 (WT), 16 (T415A) and 10 (T484A) cells. T415D and T484D were insensitive to AITC ($n = 13$ and 10). Below, average rectification of currents through WT and T484A shown above. (**F**) Representative current traces in response to voltage step protocol (as shown in Fig. 2B) recorded in control extracellular solution. Below, average conductances obtained from currents as shown above (*n* indicated in brackets). Solid lines are best fits to a Boltzmann function. The dashed line represents the fit obtained from data for wild-type TRPA1. (**G**) Summary of voltage-independent component of voltage-induced gating for wild-type ($n = 138$) and individual mutants shown in this study ($n = 7$–27). The asterisks indicate significant ($^*P < 0.05$) differences between mutant and wild-type TRPA1.

During the 40-s application of cinnamaldehyde, the T241D-mediated whole-cell currents were no different from those of the wild-type channels. Compared to wild-type TRPA1, the onset of the subsequent Ca^{2+}-induced potentiation was not delayed, but it was apparently slowed (Fig. 4A). The average maximum rise slope of Ca^{2+}-induced outward currents through the T241D channels was 0.37 ± 0.04 nA/s at +80 mV ($n = 12$), whereas in wild-type channels it was 1.2 ± 0.1 nA/s ($n = 70$). T241A was not much different from wild-type TRPA1, indicating a resilient nature of the hydrogen-bonding network in the AR6 region. In H244R, the inward currents induced after a 40-s application of cinnamaldehyde reached a similar maximum amplitude to that of the wild type (Fig. 4B,C). Both the mutations thus seemed to reduce the energy required to activate the pore opening at hyperpolarizing potentials and influence the energetic coupling of putative voltage sensor activation to gate opening. The conserved TPLH motif in AR6 has a lesser contribution to channel functioning than that in AR2 in terms of alanine or aspartate substitution. On the other hand the K239G mutation, which conforms to the consensus glycine two residues prior to the TPLH motif, had a serious mutagenic impact, most likely due to eliminating important interactions in the loop preceding AR6.

Multimodal gating of TRPA1 depends on the stability of ankyrin repeat six. In a recently published study based on an unbiased screen of a random mutant library of mouse TRPA1, Jabba *et al.*[24] revealed that AR6 is uniquely sensitive to changes in the coupling of temperature stimuli to the channel gate. The authors demonstrated that a single-point mutation in AR6 of mouse TRPA1 at position S250 (N249 in human TRPA1) induced temperature activation and temperature sensitivity of voltage-dependent activation, without changing the sensitivity to chemical agonists. In our study, we therefore asked whether the T241D mutant, which exhibited a depolarizing shift in voltage-dependent activation, also has a changed temperature sensitivity. We applied 3-sec heat steps from 25 °C to 50 °C (initial rate of ~25 °C s^{-1}) and measured whole-cell currents from wild-type and mutant T241D channels at −80 mV and at +80 mV. As shown in Fig. 4D, both channels generated only faint currents at −80 mV. At +80 mV, increasing bath temperature elicited outward currents that persisted during heating in wild-type TRPA1, but in T241D the outward currents rapidly inactivated at temperatures above ~45 °C. In both channels, the currents exhibited only a weak temperature dependence (maximum Q_{10} of 2.5 in the wild type and 2.3 in T241D; Fig. 4E).

Taken together, these findings imply that destabilizing mutations in the conserved TPLH motif of AR6 create functional channels that are gated in a less voltage-dependent manner, distinctly affecting their chemical activation and Ca^{2+}-dependent modulation. Our observations also support the previous identification of AR6 as a sensitive modulator of thermal activation[24].

Short-range stability of ankyrin repeat 12 determines the gating and calcium regulation of human TRPA1. The multiple alignment of all available TRPA1 sequences from different vertebrate species shows that the T/SPLH motifs are strictly conserved in the stretch of three adjacent repeats AR11-AR13 (Supplementary Fig. S1). In the recently resolved cryo-EM structure, this tandem repeat region is part of a crescent-shaped density assembled into a propeller-like structure that is only loosely associated with the rest of the tetrameric channel complex[13]. Such a non-canonical arrangement of the ankyrin repeat domain has been attributed to the observation that AR10 substantially deviates from the ankyrin repeat consensus and contributes to forming a sharp and flexible kink before repeat 12[16]. Indeed, in support of this prediction, we did not observe any measurable currents through the N377T/F378P channels in response to either of the stimuli when we aimed to conform to the consensus signature by mutating a highly conserved ^{377}NFLH motif in AR10 (data not shown). Thus, it is conceivable that precisely tuned stability within the evolutionarily conserved T/SPLH motifs in the ankyrin repeat cluster AR11-AR13 is essential for the proper functioning of TRPA1.

To explore this hypothesis, we next assessed the consequences of individual substitutions of T415, S448 and T484 with alanine or aspartate (Fig. 5A). Only the alanine mutations were tolerated at T415 and T484, and resulted in channels with altered voltage dependency, significantly lower chemical responsiveness, and gating kinetics (Fig. 5B–E). Compared to wild-type TRPA1, these two mutants exhibited much smaller responses to cinnamaldehyde, and the addition of Ca^{2+} to the bath solution induced only a weak potentiation (Fig. 5D). Also, the full agonist allyl isothiocyanate (AITC; 100 μM) induced smaller and, in T484A, also slower responses (Fig. 5E). In agreement with previous studies, AITC elicited rapidly developing membrane currents in wild-type TRPA1, characterized by a mean time activation constant τ_{on} of 5.0 ± 0.1 s ($n = 33$). After agonist washout, the addition of

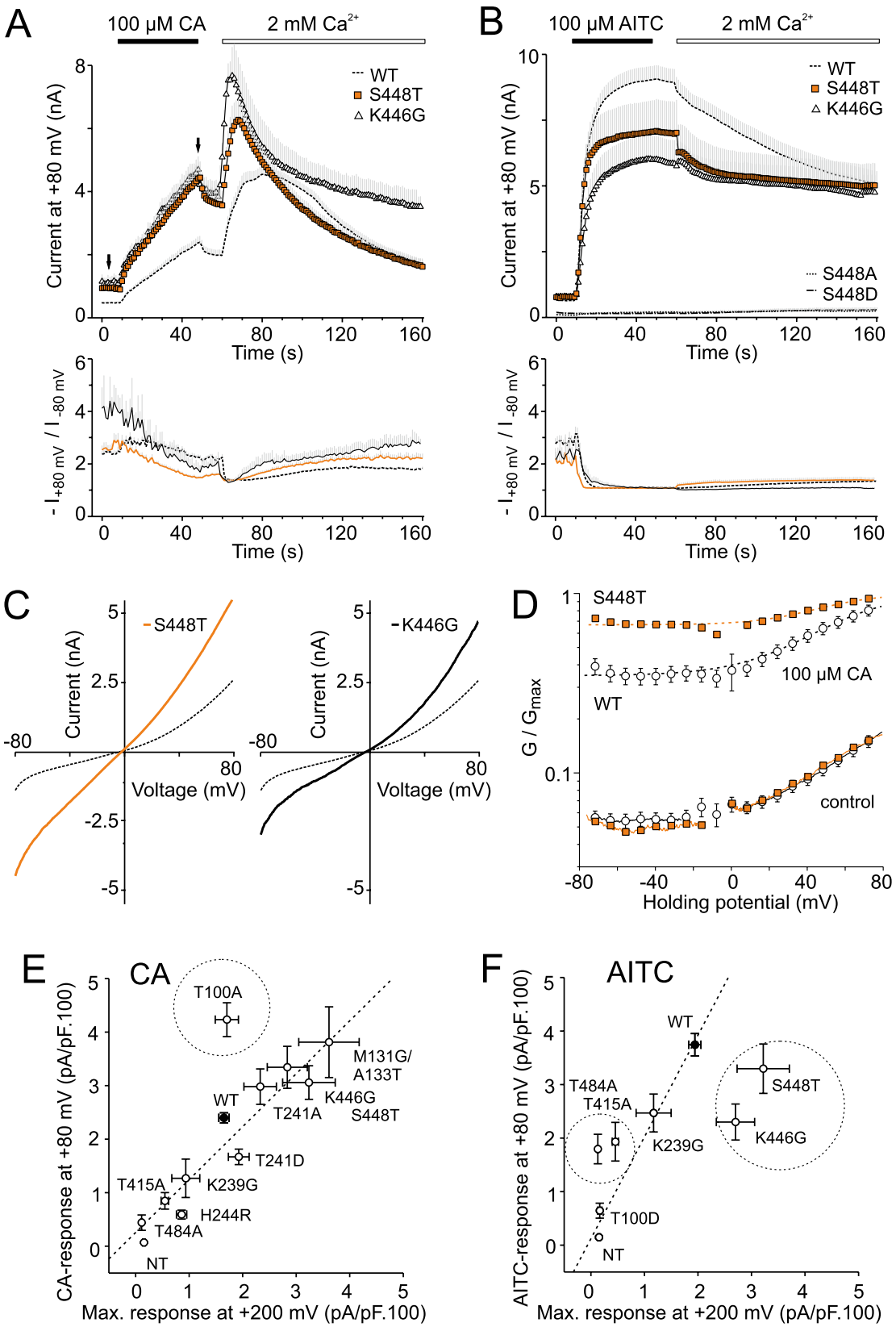

Figure 6. Strict conservations of the T/SPLH motifs in AR11-AR13 are required for functional interactions and not for targeting TRPA1 to the plasma membrane. (**A**,**B**) Time course of average whole-cell currents through wild-type and mutant hTRPA1 measured at +80 mV. The application of 100 µM cinnamaldehyde (CA, in panel (A)) or 100 µM allyl isothiocyanate (AITC, in panel (B)) and subsequent addition of 2 mM Ca^{2+} are indicated above. Below, average rectification of currents shown above. Note, the S448T ($n = 18$) and K446G ($n = 5$) mutants exhibit greater currents than WT in CA but not in the presence of AITC. Mutations S448A and

S448D were AITC-insensitive ($n = 9$ and 9). (**C**) Average current-voltage relationships of traces measured after 40 s application of 100 μM CA at time indicated by an arrow in panel A for wild-type (dashed line) and indicated mutants. (**D**) Average conductances obtained for WT (open circles) and for S448T (orange squares) from voltage ramp protocol before (control) and after 40 s application of 100 μM CA at times indicated by arrows in panel A, normalized to G_{max}. Dashed lines are best fits to a Boltzmann function. The *G-V* curves for CA-dependent gating of S448T exhibited significantly different parameters ($V_{50} = 48$ mV, $G_{min} = 0.67$, $z = 1.5$ e_0, $n = 14$) than wild-type TRPA1 ($V_{50} = 54$ mV, $G_{min} = 0.35$, $z = 1.2$ e_0, $n = 91$). (**E**) Correlation of the maximum conductances induced by depolarizing voltage (+200 mV; see voltage-step protocol in Fig. 2B) against the maximum outward responses induced by cinnamaldehyde (measured at time indicated by an arrow in Fig. 2D,E) for all responsive mutants and for non-transfected cells (NT; $n = 14$). T100A indicated by a dashed circle diverges from linear relationship. (**F**) Correlation of the maximum current densities induced by depolarizing voltage against the maximum responses induced by AITC. Mutations indicated by dashed circles diverge from linear relationship.

2 mM Ca^{2+} to the bath solution induced a marked inactivation (to 53 ± 5% of maximal response, after 100 s). The average AITC-induced currents through T415A were smaller, but τ_{on} and the extent of Ca^{2+}-dependent inactivation were not significantly different from wild-type channels (4.7 ± 0.2 s; to 42 ± 6% of maximal response; $n = 16$). In contrast, T484A-mediated currents exhibited a mean time activation constant τ_{on} of 12.6 ± 0.4 s ($n = 10$) and almost complete Ca^{2+}-dependent inactivation (19 ± 4%). The lower sensitivity of T484A is also visible in the higher rectification ratio during a 40-s application of AITC (Fig. 5E, lower graph). This result indicates that T484 in AR13 is structurally required for the normal functioning of the TRPA1 channel.

In S448A and S448D, AITC failed to induce any appreciable currents at any examined membrane potential (Fig. 6B), indicating that this strictly conserved serine is crucial either for conformational stability, function or expression. To distinguish between these possibilities, we aimed to improve the stability of AR12 by constructing two consensus-based mutations, S448T and K446G. We hypothesized that if S448 contributes substantially to ARD stability through intra- and inter-repeat hydrogen bonding, then the threonine at this position could improve ancillary interactions in its microenvironment by hydrophobic interactions associated with the threonine methyl group[29]. The second mutation introducing glycine at position K446 was anticipated to better stabilize the ankyrin fold by stabilizing its L-shaped conformation and further allowing for a better intrinsic stability of AR12 and the interfacial stability between neighboring ARs. Notably, both the mutations produced functional channels that exhibited greater currents in response to depolarizing voltage steps and a significant conductance at negative membrane potentials, indicating the presence of a strong voltage-independent component (Fig. 5F,G). Moreover, we noticed that HEK293T cells transfected with K446G (but not with S448T) exhibited a much greater extent of cell rounding and detachment than cells expressing wild-type channels, which indicates a constitutive activity of the mutant channel (Supplementary Fig. S2). The estimated V_{50} and z were not significantly different from wild-type TRPA1, being 122 ± 4 mV and 122 ± 8 mV and 0.66 ± 0.04 e_0 and 0.64 ± 0.04 e_0 for K446G and S448T ($n = 14$ and 19). A bar graph in Fig. 5G compares the average values of the voltage-independent component (G_{min}/G_{max}) for the examined T/SPLH mutants and suggests that the stretch of canonical ankyrin repeats AR11-13 tightly modulates the transition between the closed and open state of the channel in a manner that is independent of voltage sensor activation.

A remarkable finding was an apparent difference between the characteristic currents induced by cinnamaldehyde and AITC in S448T and K446G (Fig. 6A,B). The currents induced by 100 μM cinnamaldehyde were significantly greater and, upon the addition of Ca^{2+} to the bath solution, reached amplitudes that were ~1.4-fold and 1.7-fold the amplitude of the wild-type channels. The currents resembled wild-type TRPA1 in terms of the extent of Ca^{2+}-dependent desensitization (Fig. 6A). In a striking contrast, the maximum currents induced by AITC were smaller than in the wild-type channels and exhibited only a slight calcium-dependent desensitization (to 72 ± 5% and 84 ± 6% of the maximal response; $n = 6$ and 10; Fig. 6B).

Although the voltage causing half-maximal activation (V_{50}) in S448T was not different from the wild type, the voltage-independent component of cinnamaldehyde-induced activation was different (Fig. 6C). Figure 6D shows the average conductance-to-voltage (*G-V*) relationships of voltage-dependent gating calculated by normalizing *G-V* curves with the G_{max} value obtained after a 40-s exposure to 100 μM cinnamaldehyde. The S448T mutant clearly exhibits a much stronger voltage-independent component of gating at negative membrane potentials, indicating that cinnamaldehyde alone, which is a sub-maximal stimulus for TRPA1, is sufficient to produce almost voltage-independent gating in S448T.

Taken together, our data support the previous suggestion that calcium-dependent desensitization of AITC-induced responses is specified by an AR cluster centered around AR11[21]. Moreover, we show that subtle changes in AR12 stability affect the Ca^{2+}-dependent desensitization to varying degrees according to the mode of chemical activation, and increase the voltage-independent component of TRPA1 channel gating.

Strict conservation of the T/SPLH motifs in AR11-AR13 are required for functional interactions and not for targeting TRPA1 to the plasma membrane. Our results demonstrate that the strictly conserved T/SPLH motifs are distinctly involved in multimodal activation of human TRPA1 channel, and mutations at these positions may perturb intra- or inter-domain interactions, leading to altered activation profiles. We show that a subtle change in the structural stability of the AR11-13 stretch leads to qualitative changes in voltage-, cinnamaldehyde- and AITC-induced gating. On the other hand, changes in plasma membrane expression may also affect the qualitative behavior of the TRPA1 channel[23,31]. The increase in current responses in the S448T construct was surprising, since threonine is a conservative substitution, therefore we assessed the extent to which the mutation's effects might reflect changes in surface expression. We used cell-surface biotinylation

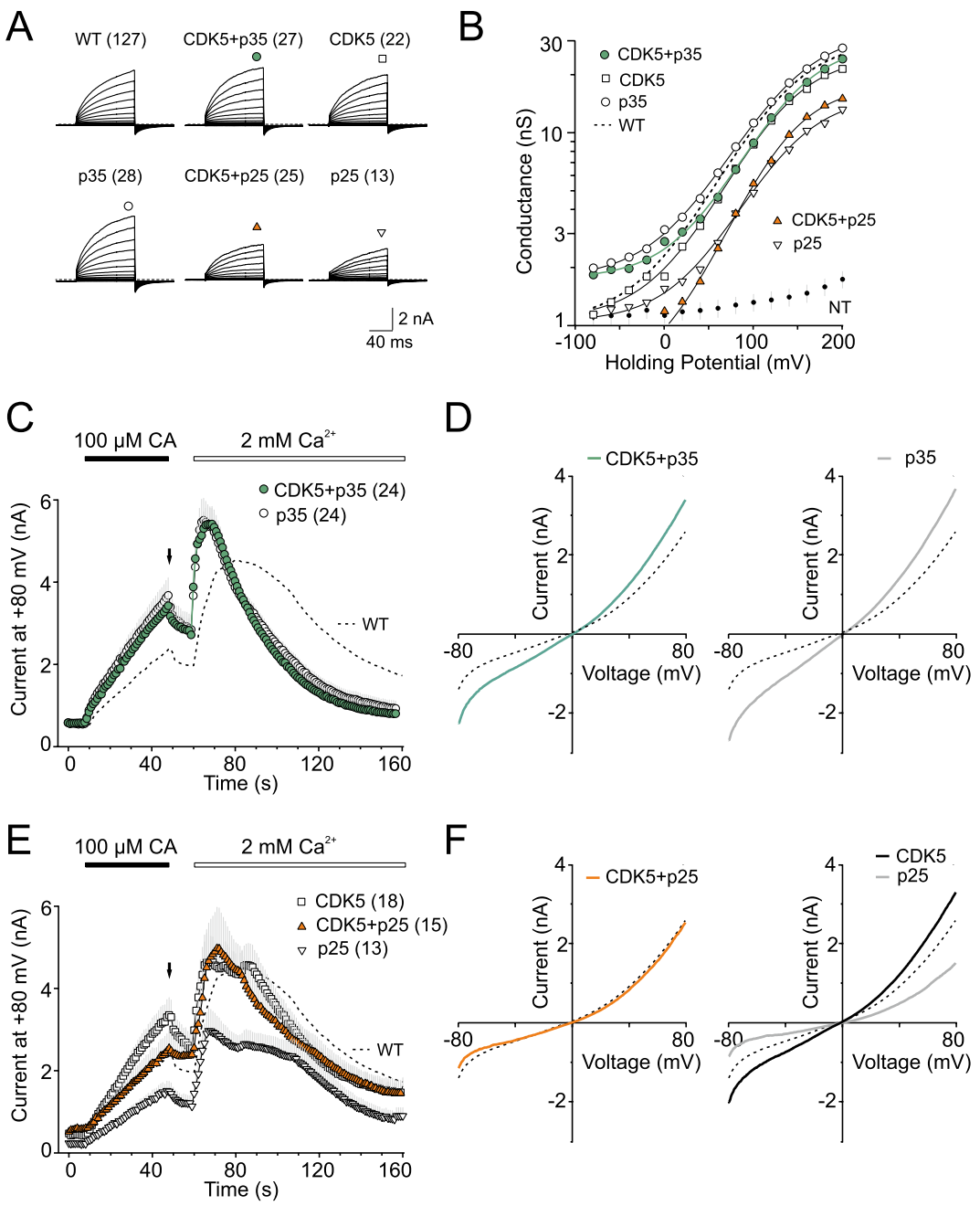

Figure 7. Conserved T/SPLH motifs as putative phosphorylation sites. (**A**) Average current traces in response to indicated voltage step protocol (holding potential −70 mV; 100 ms voltage steps from −80 mV to +200 mV; increment +20 mV) recorded in control extracellular solution ~1 min after whole-cell formation, *n* is indicated in brackets. Note, the presence of p25 protein in the cells had a cytotoxic effect, which resulted in reduced responses of TRPA1. (**B**) Average conductances obtained from voltage step protocols as in A. Solid lines are best fits to a Boltzmann function. The dashed line represents the fit obtained from data for wild-type TRPA1 shown in Fig. 2C. (**C**,**E**) Time course of average whole-cell currents induced by 100 μM cinnamaldehyde (CA) in Ca^{2+}-free solution and then exposed to 2 mM Ca^{2+}, measured at +80 mV in wild-type (dashed line) and wild-type co-expressed with indicated proteins; *n* is indicated in brackets. The application of CA and subsequent addition of 2 mM Ca^{2+} are indicated above. (**D**,**F**) Average current-voltage relationships of traces measured after 40 s application of 100 μM CA at time indicated by arrows in panels C and E for wild-type (dashed line) and indicated proteins.

assay to examine the surface expression of the wild-type and two mutant proteins: the gain-of-function mutant S448T, and T415A as a loss-of-function control. As shown in Supplementary Figure S2, immunoblots of S448T and T415A confirmed that the proteins were processed and targeted to the membrane to a comparable extent to that of wild-type TRPA1. Thus, the changes in functionality are most likely due to structural changes. Additional

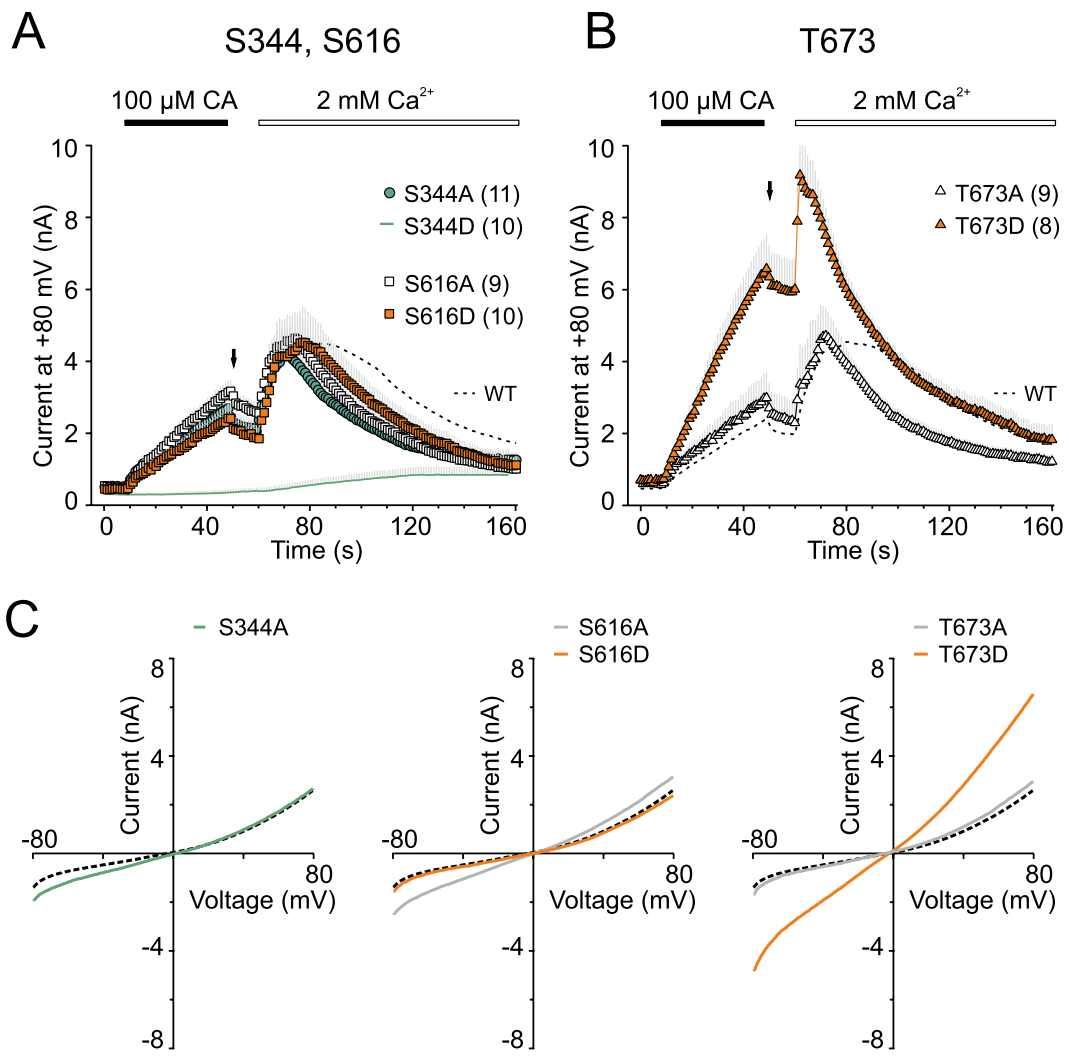

Figure 8. Phospho-mimicking and phospho-null substitutions at S344, S616 and T673. (**A**,**B**) Time course of average whole-cell currents induced by 100 µM cinnamaldehyde (CA) in Ca^{2+}-free solution and then exposed to 2 mM Ca^{2+}, measured at +80 mV in wild-type (dashed line) and indicated mutants; *n* is indicated in brackets. The application of CA and subsequent addition of 2 mM Ca^{2+} are indicated above. Note, the aspartate mutation of S344 resulted in a loss-of-function phenotype, the T673D mutant is a gain-of-function phenotype. (**C**) Average current-voltage relationships of traces measured after 40 s application of 100 µM CA at times indicated by arrows in panels A and B for wild-type (dashed line) and indicated functional mutants.

support for this hypothesis stems from the bi-directional scatter plots shown in Fig. 6E,F. These graphs correlate, for each mutant, the maximum conductances induced by depolarizing voltage (+200 mV) against the maximum responses induced by cinnamaldehyde or AITC. Voltage, cinnamaldehyde and intracellular calcium, which are all sub-maximal stimuli for TRPA1, interact allosterically to enhance channel opening. The observation that alanine substitution at threonine T100 diverges from a linear relationship suggests the involvement of this residue in coupling the voltage-sensing domain to TRPA1 channel opening. On the other hand, AITC is a full agonist of TRPA1, and mutations within the ankyrin repeat stretch AR11-AR13 seem to primarily affect the energetics of gating in the absence of membrane depolarization (seen in Fig. 5F,G), and coupling between the AITC-interacting region and the channel gate (seen in Figs 5E and 6B).

Conserved T/SPLH motifs as putative phosphorylation sites. In general, the variable molecular surfaces formed by the assembly of ankyrin repeats and their modular architecture render AR proteins highly versatile and prone to binding with other biologically important proteins[26,32]. The extensive N-terminal ankyrin repeat domain of TRPA1 has been proposed to interact with several proteins that modulate the channel's functioning, cytoplasmic levels, turnover, or trafficking[31,33–35]. Evidence has also been presented that the N-terminus may be involved in phosphorylation-mediated regulation of the channel downstream of the phospholipase C and Src tyrosine kinase signaling pathways[36,37]. In the context of our study, we considered that some of the serines or threonines from the N-terminal T/SPLH motifs may represent potential phosphorylation sites, particularly for proline-directed Ser/Thr kinases. Among these, cyclin-dependent kinase 5 (CDK5) is a neuron-specific kinase

of great functional relevance, known to regulate nociceptive signaling via the N-terminus of the TRPA1-related channel TRPV1[38,39]. Bioinformatics analysis of the human TRPA1 primary sequence predicts T100, T241, T415, S448, and T484 to be consensus sites for CDK5 at a high stringency level, some of these sites with even better scores than that predicted for threonine T407 in human TRPV1, the residue which is directly phosphorylated by CDK5[38] (Supplementary Table S1).

At first sight, the serine and threonine residues constituting the conserved T/SPLH motifs examined above are not likely to be involved in the phosphorylation of TRPA1, because the phosphonull alanine mutations and phosphorylation mimicking aspartate mutations did not lead to opposite changes in the functioning of the channel. However, structural changes around these residues, such as the M131G/A133T mutation, may affect phosphorylation at the contiguous sites - in a constitutive or activity-dependent manner. At the same time, the prediction shows that threonine substitution at S448 may also affect the prediction score. Therefore, as the first logical step, we tested the relevance of these considerations by assessing whether the co-expression of TRPA1 with CDK5 and p35, a CDK5-specific activator, may modulate voltage-dependent channel activation. As shown in Fig. 7A,B, co-expression of CDK5/p35 resulted in no change in the maximal responses to depolarizing voltage, and only a slight increase in voltage-independent gating at hyperpolarized potentials. Similar effects have been also observed in cells co-expressing TRPA1 with p35 alone, but not in those expressing TRPA1 with CDK5. The co-expression of p35 alone or with CDK5 significantly increased TRPA1-mediated responses to cinnamaldehyde (Fig. 7C,D). Some authors suggest that CDK5 is present and functionally relevant in HEK293 cells[40], while others have reported that HEK293 cells only express CDK5 at low levels and they lack endogenous CDK5 activity[41]. Thus, our result indicates that TRPA1 may be a substrate for the CDK5/p35 complex and/or its interaction with p35 may stabilize the activated state.

Proteolytic cleavage of p35 to p25 results in the cytosolic redistribution of CDK5, and therefore we also tested the effects of CDK5/p25 co-expression on TRPA1. Generally, we observed clear hallmarks of cytotoxicity in cells overexpressing p25, with or without TRPA1, which is an observation consistent with the literature[42]. The co-expression of TRPA1 with CDK5/p25 induced a less significant toxicity than that seen when TRPA1 was co-expressed with p25 alone, an explanation for this could be that the inclusion of CDK5 partially buffered the detrimental effects mediated by p25 alone. Intriguingly, CDK5 alone led to an increased responsiveness of TRPA1 to cinnamaldehyde, but co-transfection with p25 abolished this effect (Fig. 7E,F). Thus, given these findings, we cannot unambiguously exclude some specific effects of CDK5.

Within the N-terminal region of TRPA1, a sequence prediction analysis also reveals three additional putative phosphorylation sites for CDK5, containing S344, S616 and T673 (as shown in Table S1). To test the functional role of these residues and to obtain a complete picture of the role of the T/SP motifs in the N-terminus of TRPA1, we constructed six additional mutants in which either serine or threonine were replaced by either alanine or aspartate to mimic the non-phosphorylated and phosphorylated forms of the TRPA1 protein, respectively. As shown in Fig. 8, only two mutations caused significant changes in TRPA1 channel's activity: the S344D mutation failed to produce any appreciable currents, suggesting either a structural disturbance around the AR9 repeat or a failure of functional expression as a specific result of the phosphomimicking substitution. On the other hand, the T673D mutation resulted in channels whose responses to cinnamaldehyde were increased almost threefold (from 2.4 ± 0.2 nA to 6.6 ± 1 nA at $+80$ mV; $n = 70$ and $n = 8$). According to the recently resolved TRPA1 structure, T673 is solvent-accessible and located in a flexible loop connecting the β-strands to the helix-turn-helix motif preceding the pre-S1 helix, i.e., well situated in a locus especially important for the detection, integration and transmission of activation stimuli[13]. This, together with our finding that the mutant T673A channels remained largely unchanged, indicates that this location, the resolution of which would require more detailed measurements and modeling, may indeed represent a candidate target for Ser/Thr phosphorylation and further studies are needed to explore this possibility.

Discussion

A central observation of this study is that the most conserved N-terminal consensus T/SPLH tetrapeptide motifs, which initiate the helix–turn–helix conformation of the repeats AR2, AR6, AR11, AR12 and AR13, are required for the proper functioning of TRPA1 and distinctly contribute to its multimodal activation. The extensive N-terminal ankyrin repeat domain, according to which this channel has been dubbed, represents almost 74% of the cytoplasmic portion and 57% of the whole protein. Although the N-terminus is likely to be dispensable for a functional channel[25], it is hard to believe that evolution has allocated such a large and structurally organized proportion of a protein merely for auxiliary functions such as trafficking, subcellular localization, homotetramerization, or a number of poly-specific interactions. Indeed, for examples, AR6 dictates the directionality of temperature activation to mouse TRPA1[24] and two isoforms of a *Drosophila melanogaster* TRPA1 ortholog, which arise from alternative splicing of the N-terminal region, enable flies to detect electrophilic compounds, but only one of them is highly sensitive to temperature[43].

It has been well demonstrated that the two N-terminal AR modules, the primary AR10-AR15 and the enhancer AR3-AR8, are independent and transferable, each capable of bestowing thermal or electrophilic sensitivity to the human TRPA1 channel[21]. However the extent to which the individual ankyrin repeats correspond to functional units still needs to be fully elucidated and understood. Previous mutagenesis and chimaeric studies have identified regions within the N-terminal ARD that dictate the pronounced specificity of the temperature, electrophilic, non-electrophilic, and oxidative sensitivity of TRPA1[7,8,17,18,24,44]. Mutations within the ARD frequently rendered the TRPA1 channel non-functional and any mutation of AR consensus residues had been thought to result in an unstable protein[26]. To theoretically estimate the putative effects of mutations on the stability of ARD, we used the program FoldX that calculates the folding energies of proteins and the effects of a point mutation on the stability of a protein (see Supplementary Methods). Theoretical energy measurements around

ankyrin repeat 2 predicted the average free energy change $\Delta\Delta G = 1.05$ kcal/mol for T100A and 4.63 kcal/mol for T100D, indicating the respective smaller and greater destabilizing effects of the mutations. In contrast, the double mutant M131G/A133T resulted in the average free energy change $\Delta\Delta G = -5.61$ kcal/mol. These predictions correlate very well with the functional profiles shown in Fig. 2.

The putatively destabilizing mutations in AR6, T241A and T241D, had pronounced effects on the estimated free energy changes ($\Delta\Delta G = 1.74$ and 5.53 kcal/mol). However, both of these mutants were functional. On the other hand, mutations predicted to either destabilize or stabilize AR6 (H244R; $\Delta\Delta G = 2.95$ kcal/mol and K239G; $\Delta\Delta G = -3.61$ kcal/mol) led to similar phenotypes with constitutive activity and changes in voltage dependence (Fig. 3C–E), suggesting that AR6 contributes to the energetics of the channel gate under resting conditions. The functional role of the extended loop preceding AR6 appears to be more important than the TPLH-mediated hydrogen-bonding network. When mutated, this region may sterically hinder and destabilize the channel gate upon depolarization. The T241D mutation, expected to be the most disruptive, changed the parameters of Ca^{2+}-dependent potentiation (Fig. 4A) which may reflect perturbations in coupling between the calcium sensing domain and gate opening.

The recent study by Moparthi *et al.*[25] implicated the N-terminal ARD region as an important gating modifier that may regulate the channel's behavior in a voltage-dependent manner. The ankyrin repeats around AR2 and AR6 are sequentially distant from the transmembrane region expected to 'sense' the membrane electrical field, but they may contribute to voltage-dependent gating through interactions with the TRPA1 protein itself, membrane or membrane-associated factors[13,16]. The recently resolved structure of TRPA1 provides a mechanistic explanation of how the proximal part of ARD can communicate with the channel gate[13]: the information from the ARD can be transduced through the overlying helix-turn-helix motif of the linker region that forms a network of packed interactions with the TRP-like domain (Fig. 1B). From the structure, it is also apparent that the mutational consequences for the canonical ankyrin cluster AR11-AR13 cannot be easily interpreted, because the region including AR11 is represented by only a weak electron density map and contains a flexible kink before AR12. If the T/SPLH motifs in AR11-AR13 assumed an ideal conformation in the context of the tertiary fold, the alanine and aspartate mutations at T415 would consistently change the free energy by -0.6 and 3.2 kcal/mol and would lead to only moderate changes at T484 ($\Delta\Delta G$ from -1.03 to 1.36 kcal/mol). The conservative substitution S448T would yield $\Delta\Delta G = -1.12$ kcal/mol, i.e. it should have a slightly stabilizing impact. One of the most surprising findings for us was that such a subtle change in AR12 led to a gain-of-function phenotype distinctly affecting the polymodal gating of the channel (Fig. 6). Serine is statistically three times less favored than threonine in T/SPLH tetrapeptides[29], and thus the role of S448 in TRPA1 is likely to be specific and may be evolutionarily fine-tuned. The ^{448}SPLH motif, strictly conserved in mammals, birds and reptiles, aligns with SALH in zebrafish, TALH in the nematode worm *Caenorhabditis elegans*, and TPLH in hymenoptera- specific TRPA. A strikingly conserved quadruplet of asparagines followed by glutamate, instead of ^{443}SKDKK in human TRPA1, precedes the SPLH motif in insects.

We show that strict conservation of the T/SPLH motifs in AR11-AR13 is required for functional interactions, and most likely not for targeting TRPA1 to the plasma membrane. Although changes in plasma membrane expression may also affect the qualitative behavior of the TRPA1 channel[23,31], we believe that the S448T mutation results in a gain-of-function by mainly impacting the transition between the closed and open state of the channel in a way that is independent of the putative voltage sensor (Fig. 5F). When the channel is partially activated by cinnamaldehyde, S448 may contribute to allosteric coupling between the voltage-sensing domain and the gate, as can be inferred from Fig. 6D. To further characterize the impact of the S448T mutation on voltage-dependent gating, we used the allosteric model for voltage-sensor/gate allosteric coupling proposed by[45,46] (Equation 1 in Supplementary Methods). By fitting the normalized *G-V* curves for voltage activation, we obtained the values of the equilibrium constant for gate opening L and the allosteric coupling factor D. For wild-type TRPA1, these values were $L = 0.06$ and $D = 166$ (Supplementary Fig. S3 and Table S2). The S448T mutation increased the equilibrium constant L by 67% and decreased the allosteric coupling factor D by only 16%. Even more pronounced effects were obtained for K446G, for which L was increased by 166%, whereas D was reduced by 46% compared to the wild-type. Taken together, these findings suggest that an increase in the structural stability of AR12 predominantly impacts the energetics of channel opening and modestly interferes with the allosteric mechanism of coupling the putative voltage-sensing domain and gate opening.

When designing this study, we considered that the strictly conserved T/SPLH motifs are consistent with the consensus phosphorylation sequence of proline-directed Ser/Thr kinases (T/SPXK/H/R). Phosphorylation has been shown to substantially regulate the subcellular targeting, biophysical properties and gating of many TRP channels[47], to date very little is known about this kind of modification in TRPA1. Therefore for our substitution at the T/S position we used aspartate, which both mimics phosphorylation as well as being anticipated to sufficiently destabilize the ankyrin repeat's conformation. The data obtained with aspartate mutants compared with their phospho-null counterparts suggest that the strict conservation of the T/SPLH motifs in ARD is not to enable or improve phosphorylation. The only residue fulfilling the consensus requirement and upregulating the function of TRPA1 under phospho-mimicking conditions is T673, which is outside the ARD. Also, the specific result of our study that the co-expression of p35 or CDK5 with p35 significantly increased TRPA1-mediated responses to cinnamaldehyde is an important observation that was not previously reported and is relevant to the putative roles of the N-terminal T/SPXH motifs.

We believe that the information provided by this study will facilitate our future understanding of how TRPA1 operates, how is used for signal transduction and how it is regulated in native cells.

Methods

Expression and constructs of hTRPA1 channel. Human embryonic kidney 293T (HEK293T) cells were cultured in Opti-MEM I media (Invitrogen) supplemented with 5% fetal bovine serum as described previously[48]. Cells were transiently co-transfected with 400 ng of cDNA plasmid encoding wild-type (WT) or mutant human

TRPA1 (wild type in the pCMV6-XL4 vector, OriGene) and with 200 ng of GFP plasmid (TaKaRa) per 1.6 mm dish using the magnet-assisted transfection (IBA GmbH.) technique. In the experiments with CDK5, the WT was co-expressed with CDK5 and p25 (p35) in the cDNA ratio 250:250:125 (400:250:150). A 1:1 cDNA ratio was used for the co-expression of the WT with CDK5, p25 or p35. The plasmids pcDNA3-CDK5-GFP, pcDNA3.1-P25C-GFP and pCMV-P35 were obtained from the plasmid repository Addgene. The cells were used 24–48 h after transfection. At least three independent transfections were used for each experimental group. The wild-type channel was regularly tested in the same batch as the mutants. The mutants were generated by PCR using a QuikChange Site-Directed Mutagenesis Kit (Stratagene) and confirmed by DNA sequencing (GATC Biotech).

Electrophysiology. Whole-cell membrane currents were recorded by employing an Axopatch 200B amplifier and pCLAMP 10 software (Molecular Devices). Patch electrodes were pulled from a glass tube with a 1.65-mm outer diameter. The tip of the pipette was heat-polished, and its resistance was 3–5 MΩ. Series resistance was compensated by at least 70% in all recordings. The experiments were performed at room temperature (23–25 °C). Only one recording was performed on any one coverslip of cells to ensure that recordings were made from cells not previously exposed to chemical stimuli. A system for rapid superfusion and heating of the cultured cells was used for drug application[49]. The extracellular bath solutions contained: 150 mM NaCl and 10 mM HEPES, with an added 2 mM HEDTA for the Ca^{2+}-free solution, and 2 mM $CaCl_2$ for the Ca^{2+}-containing solutions, adjusted to pH 7.3 with NaOH, 300 mOsm. The *I-V* relationships were measured in control bath solution containing 160 mM NaCl, 2.5 mM KCl, 1 mM $CaCl_2$, 2 mM $MgCl_2$, 10 mM HEPES, 10 mM glucose, adjusted to pH 7.3 and 320 mOsm. The whole-cell pipette solution contained the high buffer internal solution: 145 mM CsCl, 5 mM EGTA, 3 mM $CaCl_2$, 10 mM HEPES, 2 mM MgATP, pH 7.3, adjusted with CsOH, 290 mOsm. Cinnamaldehyde and allyl isothiocyanate solution was prepared prior to use from a 0.1 M stock solution in Me_2SO. All of the chemicals were purchased from Sigma-Aldrich.

Statistical analysis. All of the electrophysiological data were analyzed using pCLAMP 10 (Molecular Devices), and curve fitting and statistical analyses were done in SigmaPlot 10 (Systat Software Inc.). Conductance-voltage (*G-V*) relationships were obtained from steady-state whole cell currents measured at the end of voltage steps from −80 to +200 mV in increments of +20 mV, or from currents recorded by voltage ramp protocol in the presence of 100 μM cinnamaldehyde for 40 s. Voltage-dependent gating parameters were estimated by fitting the conductance $G = I/(V - V_{rev})$ as a function of the test potential V to the Boltzmann equation: $G = [(G_{max} - G_{min})/(1 + \exp(-zF(V - V_{50})/RT))] + G_{min}$, where z is the apparent number of gating charges, V_{50} is the half-activation voltage, G_{min} and G_{max} are the minimum and maximum whole cell conductance, V_{rev} is the reversal potential, and F, R, and T have their usual thermodynamic meanings. Statistical significance was determined by Student's *t*-test or the analysis of variance, as appropriate; differences were considered significant at $P < 0.05$ where not stated otherwise. For statistical analysis of the voltage-independent component of gating (G_{min}/G_{max}) data, a logarithmic transformation was used to achieve a normal distribution. The data are presented as means ± S.E.M.

References

1. Story, G. M. *et al.* ANKTM1, a TRP-like channel expressed in nociceptive neurons, is activated by cold temperatures. *Cell* **112,** 819–829 (2003).
2. Nilius, B., Appendino, G. & Owsianik, G. The transient receptor potential channel TRPA1: from gene to pathophysiology. *Pflugers Archiv* (*European Journal of Physiology*) **464,** 425–458 (2012).
3. Moran, M. M. Transient receptor potential ankyrin 1 as a target for perioperative pain management. *Anesthesiology* **117,** 8–9 (2012).
4. Wilson, S. R. *et al.* The ion channel TRPA1 is required for chronic itch. *J Neurosci* **33,** 9283–9294 (2013).
5. Laursen, W. J., Bagriantsev, S. N. & Gracheva, E. O. TRPA1 channels: chemical and temperature sensitivity. *Curr Top Membr* **74,** 89–112 (2014).
6. Zygmunt, P. M. & Hogestatt, E. D. Trpa1. *Handb Exp Pharmacol* **222,** 583–630 (2014).
7. Doerner, J. F., Gisselmann, G., Hatt, H. & Wetzel, C. H. Transient receptor potential channel A1 is directly gated by calcium ions. *J Biol Chem* **282,** 13180–13189 (2007).
8. Zurborg, S., Yurgionas, B., Jira, J. A., Caspani, O. & Heppenstall, P. A. Direct activation of the ion channel TRPA1 by Ca^{2+}. *Nat Neurosci* **10,** 277–279 (2007).
9. Wang, Y. Y., Chang, R. B., Waters, H. N., McKemy, D. D. & Liman, E. R. The Nociceptor Ion Channel TRPA1 Is Potentiated and Inactivated by Permeating Calcium Ions. *J Biol Chem* **283,** 32691–32703 (2008).
10. Baez-Nieto, D., Castillo, J. P., Dragicevic, C., Alvarez, O. & Latorre, R. Thermo-TRP channels: biophysics of polymodal receptors. *Adv Exp Med Biol* **704,** 469–490 (2011).
11. Wan, X. *et al.* Bimodal voltage dependence of TRPA1: mutations of a key pore helix residue reveal strong intrinsic voltage-dependent inactivation. *Pflugers Arch* **466,** 1273–1287 (2014).
12. Palovcak, E., Delemotte, L., Klein, M. L. & Carnevale, V. Comparative sequence analysis suggests a conserved gating mechanism for TRP channels. *The Journal of general physiology* **146,** 37–50 (2015).
13. Paulsen, C. E., Armache, J. P., Gao, Y., Cheng, Y. & Julius, D. Structure of the TRPA1 ion channel suggests regulatory mechanisms. *Nature* **520,** 511–517 (2015).
14. Cvetkov, T. L., Huynh, K. W., Cohen, M. R. & Moiseenkova-Bell, V. Y. Molecular architecture and subunit organization of TRPA1 ion channel revealed by electron microscopy. *J Biol Chem* **286,** 38168–38176 (2011).
15. Wang, L., Cvetkov, T. L., Chance, M. R. & Moiseenkova-Bell, V. Y. Identification of *in vivo* disulfide conformation of TRPA1 ion channel. *J Biol Chem* **287,** 6169–6176 (2012).
16. Brewster, M. S. & Gaudet, R. How the TRPA1 receptor transmits painful stimuli: Inner workings revealed by electron cryomicroscopy. *BioEssays: News and Reviews in Molecular, Cellular and Developmental Biology* **37,** 1184–1192 (2015).
17. Hinman, A., Chuang, H. H., Bautista, D. M. & Julius, D. TRP channel activation by reversible covalent modification. *Proc Natl Acad Sci USA* **103,** 19564–19568 (2006).
18. Macpherson, L. J. *et al.* Noxious compounds activate TRPA1 ion channels through covalent modification of cysteines. *Nature* **445,** 541–545 (2007).
19. Caterina, M. J. Chemical biology: sticky spices. *Nature* **445,** 491–492 (2007).
20. Nilius, B., Prenen, J. & Owsianik, G. Irritating channels: the case of TRPA1. *Journal of Physiology* **589,** 1543–1549 (2011).

21. Cordero-Morales, J. F., Gracheva, E. O. & Julius, D. Cytoplasmic ankyrin repeats of transient receptor potential A1 (TRPA1) dictate sensitivity to thermal and chemical stimuli. *Proceedings of the National Academy of Sciences of the United States of America* **108,** E1184–1191 (2011).
22. Binder, A. *et al.* Transient receptor potential channel polymorphisms are associated with the somatosensory function in neuropathic pain patients. *PLoS One* **6,** e17387 (2011).
23. May, D. *et al.* Differential expression and functionality of TRPA1 protein genetic variants in conditions of thermal stimulation. *J Biol Chem* **287,** 27087–27094 (2012).
24. Jabba, S. *et al.* Directionality of temperature activation in mouse TRPA1 ion channel can be inverted by single-point mutations in ankyrin repeat six. *Neuron* **82,** 1017–1031 (2014).
25. Moparthi, L. *et al.* Human TRPA1 is intrinsically cold- and chemosensitive with and without its N-terminal ankyrin repeat domain. *Proc Natl Acad Sci USA* **111,** 16901–16906 (2014).
26. Gaudet, R. A primer on ankyrin repeat function in TRP channels and beyond. *Mol Biosyst* **4,** 372–379 (2008).
27. Sotomayor, M., Corey, D. P. & Schulten, K. In search of the hair-cell gating spring elastic properties of ankyrin and cadherin repeats. *Structure* **13,** 669–682 (2005).
28. Yuan, C. *et al.* The study of pH-dependent stability shows that the TPLH-mediated hydrogen-bonding network is important for the conformation and stability of human gankyrin. *Biochemistry* **52,** 4848–4857 (2013).
29. Guo, Y. *et al.* Contributions of conserved TPLH tetrapeptides to the conformational stability of ankyrin repeat proteins. *J Mol Biol* **399,** 168–181 (2010).
30. Lee, W., Strumpfer, J., Bennett, V., Schulten, K. & Marszalek, P. E. Mutation of conserved histidines alters tertiary structure and nanomechanics of consensus ankyrin repeats. *J Biol Chem* **287,** 19115–19121 (2012).
31. Schmidt, M., Dubin, A. E., Petrus, M. J., Earley, T. J. & Patapoutian, A. Nociceptive signals induce trafficking of TRPA1 to the plasma membrane. *Neuron* **64,** 498–509 (2009).
32. Li, J., Mahajan, A. & Tsai, M. D. Ankyrin repeat: a unique motif mediating protein-protein interactions. *Biochemistry* **45,** 15168–15178 (2006).
33. Dai, Y. *et al.* Sensitization of TRPA1 by PAR2 contributes to the sensation of inflammatory pain. *J Clin Invest* **117,** 1979–1987 (2007).
34. Staruschenko, A., Jeske, N. A. & Akopian, A. N. Contribution of TRPV1-TRPA1 interaction to the single channel properties of the TRPA1 channel. *J Biol Chem* **285,** 15167–15177 (2010).
35. Stokes, A. *et al.* TRPA1 is a substrate for de-ubiquitination by the tumor suppressor CYLD. *Cell Signal* **18,** 1584–1594 (2006).
36. Morgan, K., Sadofsky, L. R. & Morice, A. H. Genetic variants affecting human TRPA1 or TRPM8 structure can be classified *in vitro* as 'well expressed', 'poorly expressed' or 'salvageable'. *Biosci Rep* **35,** doi:10.1042/BSR20140061 (2015).
37. Zhang, X., Li, L. & McNaughton, P. A. Proinflammatory mediators modulate the heat-activated ion channel TRPV1 via the scaffolding protein AKAP79/150. *Neuron* **59,** 450–461 (2008).
38. Pareek, T. K. *et al.* Cyclin-dependent kinase 5 modulates nociceptive signaling through direct phosphorylation of transient receptor potential vanilloid 1. *Proc Natl Acad Sci USA* **104,** 660–665 (2007).
39. Liu, J., Du, J., Yang, Y. & Wang, Y. Phosphorylation of TRPV1 by cyclin-dependent kinase 5 promotes TRPV1 surface localization, leading to inflammatory thermal hyperalgesia. *Exp Neurol* **273,** 253–262 (2015).
40. Gallazzini, M., Yu, M. J., Gunaratne, R., Burg, M. B. & Ferraris, J. D. c-Abl mediates high NaCl-induced phosphorylation and activation of the transcription factor TonEBP/OREBP. *FASEB Journal: Official Publication of the Federation of American Societies for Experimental Biology* **24,** 4325–4335 (2010).
41. Zheng, Y. L., Li, B. S., Amin, N. D., Albers, W. & Pant, H. C. A peptide derived from cyclin-dependent kinase activator (p35) specifically inhibits Cdk5 activity and phosphorylation of tau protein in transfected cells. *Eur J Biochem* **269,** 4427–4434 (2002).
42. Dhavan, R. & Tsai, L. H. A decade of CDK5. *Nat Rev Mol Cell Biol* **2,** 749–759 (2001).
43. Zhong, L. *et al.* Thermosensory and nonthermosensory isoforms of Drosophila melanogaster TRPA1 reveal heat-sensor domains of a thermoTRP Channel. *Cell Rep* **1,** 43–55 (2012).
44. Takahashi, N. *et al.* TRPA1 underlies a sensing mechanism for O2. *Nat Chem Biol* **7,** 701–711 (2011).
45. Horrigan, F. T. & Aldrich, R. W. Coupling between voltage sensor activation, Ca^{2+} binding and channel opening in large conductance (BK) potassium channels. *The Journal of General Physiology* **120,** 267–305 (2002).
46. Brauchi, S., Orio, P. & Latorre, R. Clues to understanding cold sensation: thermodynamics and electrophysiological analysis of the cold receptor TRPM8. *Proc Natl Acad Sci USA* **101,** 15494–15499 (2004).
47. Voolstra, O. & Huber, A. Post-Translational Modifications of TRP Channels. *Cells* **3,** 258–287 (2014).
48. Benedikt, J., Teisinger, J., Vyklicky, L. & Vlachova, V. Ethanol inhibits cold-menthol receptor TRPM8 by modulating its interaction with membrane phosphatidylinositol 4, 5-bisphosphate. *J Neurochem* **100,** 211–224 (2007).
49. Dittert, I. *et al.* Improved superfusion technique for rapid cooling or heating of cultured cells under patch-clamp conditions. *J Neurosci Methods* **151,** 178–185 (2006).

Acknowledgements

The authors thank Dr. Li-Huei Tsai (Howard Hughes Medical Institute, Massachusetts Institute of Technology, Cambridge, MA) for CDK5, p25 and p35 plasmids. The authors are sincerely grateful to Professor Klaus Schulten (Beckman Institute) and Professor Marcos Sotomayor (The Ohio State University) for providing the model of the TRPA1 ankyrin repeats, and Lucie Zimova for insightful critiques. This work was supported by the Czech Science Foundation (15-15839S) and the Grant Agency of Charles University (GA UK 888513 and 365215).

Author Contributions

A.H. and V.V. designed the experiments, A.H., J.V. and L.M. performed the experiments, and V.V. and A.H. wrote the paper.

Additional Information

Supplementary information accompanies this paper at http://www.nature.com/srep

Competing financial interests: The authors declare no competing financial interests.

How to cite this article: Hynkova, A. *et al.* N-terminal tetrapeptide T/SPLH motifs contribute to multimodal activation of human TRPA1 channel. *Sci. Rep.* **6**, 28700; doi: 10.1038/srep28700 (2016).

Publication 2

Zima V., Witschas K., **Hynkova A.**, Zimova L, Barvik I., Vlachova V.

Structural modeling and patch-clamp analysis of painrelated mutation TRPA1-N855S reveals inter-subunit salt bridges stabilizing the channel open state.

Neuropharmacology, 93: 294-307, 2015

The extent of participation: Preparation of all mutant constructs, electrophysiological experiments, help with finalization of the manuscript.

Neuropharmacology 93 (2015) 294–307

Contents lists available at ScienceDirect

Neuropharmacology

journal homepage: www.elsevier.com/locate/neuropharm

Structural modeling and patch-clamp analysis of pain-related mutation TRPA1-N855S reveal inter-subunit salt bridges stabilizing the channel open state

Vlastimil Zíma [b, 1], Katja Witschas [a, 1], Anna Hynkova [a, c, 1], Lucie Zímová [a], Ivan Barvík [b], Viktorie Vlachova [a, *]

[a] Department of Cellular Neurophysiology, Institute of Physiology of the Czech Academy of Sciences, Videnska 1083, 14220 Prague 4, Czech Republic
[b] Division of Biomolecular Physics, Institute of Physics, Faculty of Mathematics and Physics, Charles University in Prague, Ke Karlovu 5, 121 16 Prague 2, Czech Republic
[c] Department of Biochemistry, Faculty of Science, Charles University in Prague, Albertov 6, 128 43 Prague 2, Czech Republic

ARTICLE INFO

Article history:
Received 30 October 2014
Received in revised form
14 January 2015
Accepted 16 February 2015
Available online 25 February 2015

Keywords:
Ankyrin receptor subtype 1
Transient receptor potential
S4–S5-linker
Mutagenesis
Homology modeling
Molecular dynamics

ABSTRACT

The ankyrin transient receptor potential channel TRPA1 is a polymodal sensor for noxious stimuli, and hence a promising target for treating chronic pain. This tetrameric six-transmembrane segment (S1–S6) channel can be activated by various pungent chemicals, such as allyl isothiocyanate or cinnamaldehyde, but also by intracellular Ca^{2+} or depolarizing voltages. Within the S4–S5 linker of human TRPA1, a gain-of-function mutation, N855S, was recently found to underlie familial episodic pain syndrome, manifested by bouts of severe upper body pain, triggered by physical stress, fasting, or cold. To clarify the structural basis for this channelopathy, we derive a structural model of TRPA1 by combining homology modeling, molecular dynamics simulations, point mutagenesis and electrophysiology. In the vicinity of N855, the model reveals inter-subunit salt bridges between E854 and K868. Using the heterologous expression of recombinant wild-type and mutant TRPA1 channels in HEK293T cells, we indeed found that the charge-reversal mutants E854R and K868E exhibited dramatically reduced responses to chemical and voltage stimuli, whereas the charge-swapping mutation E854R/K868E substantially rescued their functionalities. Moreover, mutation analysis of highly conserved charged residues within the S4–S5 region revealed a gain-of-function phenotype for R852E with an increased basal channel activity, a loss of Ca^{2+}-induced potentiation and an accelerated Ca^{2+}-dependent inactivation. Based on the model and on a comparison with the recently revealed atomic-level structure of the related channel TRPV1, we propose that inter-subunit salt bridges between adjacent S4–S5 regions are crucial for stabilizing the conformations associated with chemically and voltage-induced gating of the TRPA1 ion channel.

1. Introduction

The channelopathies that underlie monogenic human diseases are of constantly increasing clinical relevance as our knowledge of the structure and function of ion channels grows. Transient Receptor Potential Ankyrin receptor-1 (TRPA1) is one of the few ion channels to have been recently linked to a heritable human pain disorder (Kremeyer et al., 2010), and hence is viewed as a potential specific and tractable drug target for treating chronic pain (Andrade et al., 2012; Moran, 2012). This polymodal nonselective cation channel is expressed at high levels in primary nociceptive sensory neurons, where it acts as a molecular transducer for a variety of environmental irritants such as cinnamaldehyde, allyl isothiocyanate or lipid peroxidation products, and, from the cytoplasmic side, is critically regulated by Ca^{2+} ions (Doerner et al., 2007; Nilius et al., 2012; Wang et al., 2008; Zurborg et al., 2007). The molecular

Abbreviations: AITC, allyl isothiocyanate; CA, cinnamaldehyde; HEK293T cell, human embryonic kidney-293 cell expressing the large T-antigen of SV40 (simian virus 40); TRP, transient receptor potential; TRPA, TRP ankyrin; MD, molecular dynamics.

* Corresponding author. Tel.: +420 29644 2711; fax: +420 29644 2488.
E-mail address: vlachova@biomed.cas.cz (V. Vlachova).

[1] These authors contributed equally to the manuscript.

http://dx.doi.org/10.1016/j.neuropharm.2015.02.018
0028-3908/

architecture of the transmembrane region of TRPA1 is assumed to be analogous to the large family of voltage-gated channels in which each subunit of the homotetrameric channel contains six membrane-spanning domains (S1–S6) with the S1–S4 sensor and the pore-forming region consisting of the S5 and S6 segments and the P-loop between them (Owsianik et al., 2006) (Fig. 1A). In the S4–S5 linker of human TRPA1, the missense mutation N855S that leads to increased channel activity has been recently found to be a cause of familial episodic pain syndrome manifested as paroxysmal pain induced by tiredness, fasting or cold (Kremeyer et al., 2010). Multiple sequence alignment of 22 TRPA1 proteins from distinct species (Fig. 1B) shows that N855 is replaced by lysine in cows and goats, by serine in frogs and boas, and by arginine in zebrafish. On the other hand, the charged residues in the immediate vicinity of N855, R852 and E854, are conserved unanimously, indicating an important functional role under evolutionary constraint, whereas E864, conserved in mammals, is shifted right by one position in non-mammalian organisms. In human TRPA1, the N855S mutation shifts activation toward more negative voltages and changes the channel's gating through a Ca^{2+}-dependent mechanism, resulting in an increase in inward currents through the activated channels at normal resting membrane potentials (Kremeyer et al., 2010). Although the functional impact of this mutation has been established in the original study, its structural basis is less understood.

Here we apply homology modeling, molecular dynamics simulation, mutagenesis and electrophysiology, to explore the possibility that the S4–S5 domain is specifically involved in TRPA1 activation, and thus important for the conformational coupling between the S1–S4 sensor activation and gate opening. We identified a charged residue in the immediate vicinity of N855 that,

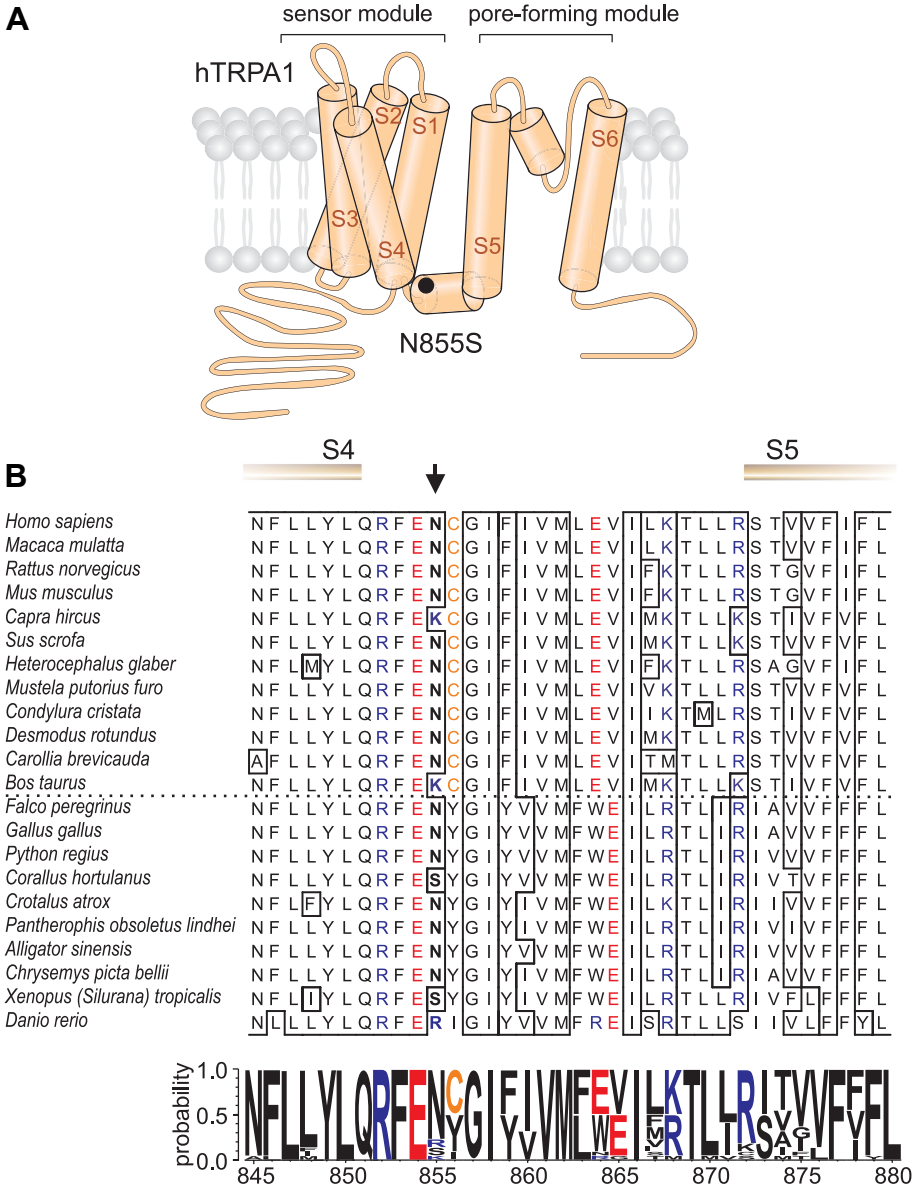

Fig. 1. Topology of pore-forming TRPA1 channel subunit and sequence alignment of selected TRPA1 proteins. (A) Schematic of human TRPA1 channel subunit with indicated positions of gain-of-function mutation in S4–S5 linker. (B) Multiple sequence alignment of S4–S5 linker from representative TRPA1 protein orthologs. Negatively and positively charged residues and cysteine C856 are shown in color. Below, amino acid sequence conservation within S4–S5 linker of TRPA1 proteins represented as sequence logo generated using WebLogo server (Crooks et al., 2004). The height of the particular amino acid at each position indicates its probability of occurrence at that position. Note that the charged residues R852 and E854 in the immediate vicinity of N855 are conserved unanimously, whereas E864, conserved in mammals, is shifted by one position to the right in non-mammalian organisms. (For interpretation of the references to color in this figure legend, the reader is referred to the web version of this article.)

when mutated, produced phenotypes with an increased basal channel activity and sensitivity to chemical stimuli in which Ca^{2+} did not potentiate and, instead, promoted rapid inactivation of the currents. Notably, our data also identify two conserved residues in the S4–S5 region that are critical for maintaining functionally important inter-subunit interactions within the tetramer. We thus provide novel mechanistic insights into the unique structural requirements for human TRPA1 channel multimodal gating.

2. Materials and methods

2.1. Homology modeling of TRPA1 based on Kv1.2-2.1 crystal structure

Sequence alignments produced using ClustalW (Larkin et al., 2007) were manually adjusted, with particular attention paid to the S4–S5 linker (amino acids 854–868) and the selectivity filter (amino acids 912–917), for which a partial sequence alignment proposed in Wang et al. (2008) was respected. The positions of the transmembrane helices in human TRPA1 (hTRPA1) predicted by TOPCONS (Bernsel et al., 2009) were checked against the positions of the transmembrane helices in Kv1.2-2.1 assigned by the DSSP algorithm (Kabsch and Sander, 1983). Candidate homology models (20 structures) of the hTRPA1 monomer were built with the software package MODELLER (Eswar et al., 2006; Marti-Renom et al., 2000) using the Kv1.2-2.1 chimera (PDB code 2R9R; (Long et al., 2007)) as a template. The best structure was selected according to the MODELLER objective function and visual inspection of the resulting structures. The homology model of the TRPA1 monomer was tetramerized by rotating around the z-axis by 90/180/270°. Two sodium ions were inserted into the selectivity filter at the positions of two of the potassium ions known from the Kv1.2-2.1 template crystal structure (Long et al., 2007). The state of wild-type TRPA1 obtained after 5 ns of the first equilibration MD run was used to prepare mutated TRPA1 tetramers with the point mutations N855R and E854R/K868E by means of the psfgen plugin for VMD (Humphrey et al., 1996). Finally, Kv1.2-2.1 was built with K308E/R322K mutations representing the E854 and K868 of TRPA1.

2.2. Homology modeling of TRPV1-A1 chimeras based on TRPV1 cryoEM structure

TRPV1-A1 chimeric structures, where the S4–S5 linker from TRPA1 (i.e. amino acids 854–868) replaced the corresponding parts of the rat TRPV1 tetrameric structure (i.e. amino acids 560–575), were built with the software package MODELLER (Eswar et al., 2006; Marti-Renom et al., 2000) using a high-resolution cryo-EM structure of apo TRPV1 (PDB code 3J5P (Liao et al., 2013)). The state of TRPV1-A1 obtained after 5 ns of the first equilibration MD run was used to prepare mutated TRPV1-A1 tetramers with the point mutations N855S, N855V by means of the psfgen plugin for VMD (Humphrey et al., 1996).

2.3. Molecular dynamic simulations

All TRPA1, TRPV1, TRPV1-A1 and Kv1.2-2.1-K308E/R322K tetrameric structures were independently inserted into the patch of the POPC bilayer and solvated in TIP3P (Jorgensen et al., 1983) water molecules forming a cylindric simulated system with its z-axis parallel to the z-axis of the tetramer. All-atom structure and topology files were generated using VMD. Forces were computed using the CHARMM 27 force field for proteins, lipids and ions (Beglov and Roux, 1994; MacKerell et al., 1998; Schlenkrich et al., 1996). Simulated systems were energy-minimized, heated up to 310 K and equilibrated for 5 ns under cylindric boundary conditions. Symmetry restraints of 10 kcal mol^{-1} $Å^{-2}$ were applied to all alpha carbons. Moreover, additional constraints of 10 kcal mol^{-1} $Å^{-2}$ were applied to fix backbone atoms in the selectivity filter. Simulated systems were reduced to an orthorhombic cell, resolvated to ensure a solvent layer of at least 10 Å on both sides of the membrane and neutralized in 0.5 M NaCl. This gives a periodic box with a size of ~130 Å, ~130 Å, ~90/110 Å for a simulated system consisting of ~180,000 atoms. Mutated proteins were derived from wild-type TRPA1, TRPV1-A1 and Kv1.2-2.1 channels. All simulated systems were again energy-minimized, heated and equilibrated without any additional constraints for another 5 ns under periodic boundary conditions in the isothermal-isobaric ensemble. All MD simulations were produced using the software package NAMD 2.9 (Phillips et al., 2005) running on a local workstation equipped with an NVIDIA graphics processing unit (GPU). The Particle-mesh Ewald (PME) method with a grid size of 144 × 144 × 108/128 was employed for long-range electrostatic forces (Cheatham et al., 1995). The cutoff for non-bonded interactions was set to 12 Å. The SETTLE algorithm (tolerance $1e^{-8}$) was applied to constrain bonds in water molecules (Ryckaert et al., 1977). Langevin dynamics was used for temperature control with the target temperature set to 310 K. The Langevin piston method was applied to achieve an effective pressure control with a target pressure of 1 atm (Phillips et al., 2005). The integration timestep was set to 1 fs. Data were recorded every 5 ps, analyzed using the CPPTRAJ module from the Amber Tools suite (Roe and Cheatham, 2013). MD trajectories were visualized using the software package VMD 1.9 (Humphrey et al., 1996). The molecular images were created with YASARA (YASARA Biosciences). Further details of the modeling procedures, illustrations of sequence alignments and coordinates of all structural models presented in this work are available from V.Z. and I.B. upon request.

2.4. Expression and constructs of hTRPA1 channel

Human embryonic kidney 293T (HEK293T) cells were cultured in Opti-MEM I medium (Invitrogen) supplemented with 5% FBS as described previously (Susankova et al., 2007). The cells were transiently co-transfected with 400 ng of cDNA plasmid encoding wild-type or mutant human TRPA1 (wild type in the pCMV6-XL4 vector, OriGene, Rockville, MD) and with 200 ng of GFP plasmid (TaKaRa, Japan) per 1.6-mm dish using the magnet-assisted transfection technique (IBA GmbH, Goettingen, Germany). The cells were used 24–48 h after transfection. At least three independent transfections were used for each experimental group. The wild-type channel was regularly tested in the same batch as the mutants. The mutants were generated by PCR using the QuikChange XL Site-Directed Mutagenesis Kit (Stratagene, Heidelberg, Germany) and confirmed by DNA sequencing (GATC Biotech, Germany).

2.5. Electrophysiology

Whole-cell membrane currents were recorded by employing an Axopatch 200B amplifier and pCLAMP 10 software (Molecular Devices, Sunnyvalle, CA). Patch electrodes were pulled from a glass tube with a 1.65-mm outer diameter. The tip of the pipette was heat-polished, and its resistance was 3–5 MΩ. Series resistance was compensated by at least 70% in all recordings. The experiments were performed at room temperature (23–25 °C). Only one recording was performed on any one coverslip of cells to ensure that recordings were made from cells not previously exposed to chemical stimuli. The extracellular bath solutions contained: 150 mM NaCl and 10 mM HEPES, with an added 2 mM HEDTA for the Ca^{2+}-free solution, and 2 mM $CaCl_2$ for the Ca^{2+}-containing solution, adjusted to pH 7.3 with NaOH, 300 mOsm. The *I–V* relationships were measured in a bath solution containing 160 mM NaCl, 2.5 mM KCl, 1 mM $CaCl_2$, 2 mM $MgCl_2$, 10 mM HEPES, 10 mM glucose, adjusted to pH 7.3 and 320 mOsm. The whole-cell pipette solution contained the high buffer internal solution: 145 mM CsCl, 5 mM EGTA, 3 mM $CaCl_2$, 10 mM HEPES, 2 mM MgATP, pH 7.3, adjusted with CsOH, 290 mOsm. Cinnamaldehyde and allyl isothiocyanate solutions were prepared prior to use from a 0.1 M stock solution in Me_2SO. All of the chemicals were purchased from Sigma–Aldrich (St. Louis, MO). A system for rapid superfusion of the cultured cells was used for drug application (Dittert et al., 2006).

2.6. Statistical analysis

All of the electrophysiological data were analyzed using pCLAMP 10 (Molecular Devices), and curve fitting and statistical analyses were done in SigmaPlot 10 (Systat Software Inc., San Jose, CA). Conductance–voltage (*G–V*) relationships were obtained from steady-state whole-cell currents measured at the end of voltage steps from −80 to +200 mV in increments of +20 mV. Voltage-dependent gating parameters were estimated by fitting the conductance $G = I/(V - V_{rev})$ as a function of the test potential V to the Boltzmann equation: $G = [(G_{max} - G_{min})/(1 + \exp(-zF(V - V_{½})/RT))] + G_{min}$, where z is the apparent number of gating charges, $V_{½}$ is the half-activation voltage, G_{min} and G_{max} are the minimum and maximum whole cell conductance, V_{rev} is the reversal potential, and F, R, and T have their usual thermodynamic meaning. Statistical significance was determined by Student's *t* test or one-way analysis of variance; differences were considered significant at $p < 0.05$, where not stated otherwise. For statistical analysis of τ_{on} data, a logarithmic transformation was used to achieve a normal distribution. The data are presented as means ± S.E.

3. Results

3.1. Structural modeling of TRPA1 based on Kv1.2-2.1 paddle chimera template structure reveals inter-subunit interactions

The crystal structures of potassium voltage-gated (Kv) channels in the open state (Long et al., 2007) and the electron cryo-microscopic structure of the TRPV1 ion channel, in both the activated (open) and resting (closed) state (Cao et al., 2013; Liao et al., 2013), provide two suitable structural templates for structural modeling of the TRPA1 channel. First, we built an initial homology model of the transmembrane part of human TRPA1 (M689-D963) based on the Kv1.2-2.1 paddle chimera template structure (PDB entry 2R9R; (Long et al., 2007)) (Fig. 2A, B). The molecular dynamics (MD) trajectory reached 30 ns and the root mean square deviation (RMSD) measured for individual monomers and for the channel complex indicated that the model was stable (Fig. 2C). In this model, the side chains of N855 pointed towards the S4–S5 segments of adjacent TRPA1 monomers (and not to the S1 helix as

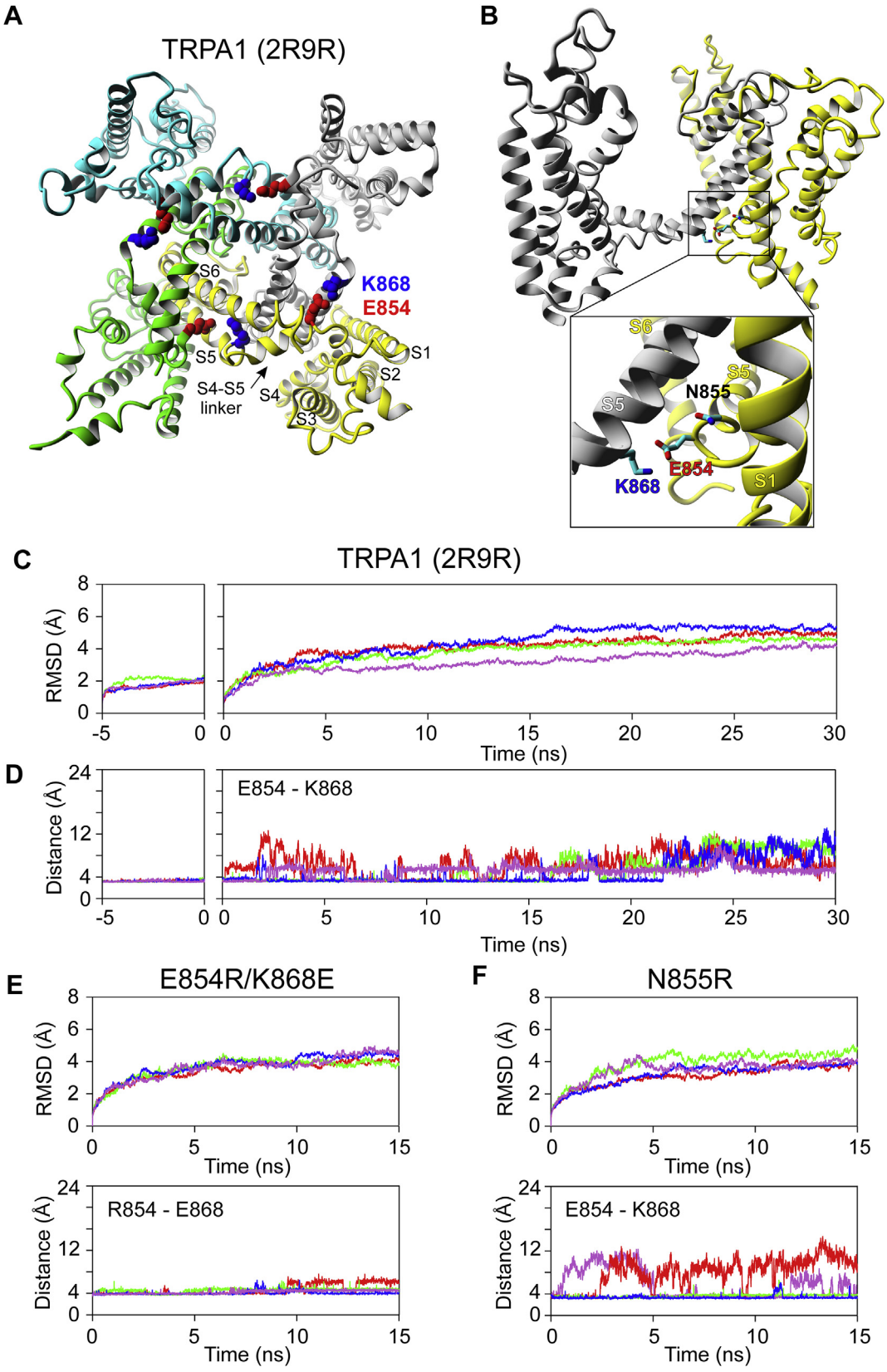

Fig. 2. Homology model of transmembrane region of human TRPA1 based on 2R9R structure reveals inter-subunit interactions. (A) Intracellular view of homology model of TRPA1 channel based on Kv1.2-2.1 paddle chimera (Long et al., 2007) with E854 and K868 residues indicated. The monomers are colored and one of them (yellow) is labeled. (B) Charged residues E854 and K868 forming salt bridges in immediate vicinity of N855 shown in side view of two TRPA1 subunits. The inset shows the predicted interaction in more detail. (C) Molecular dynamics simulation results obtained for TRPA1 model based on 2R9R structure. The root mean square deviation (RMSD) values, over backbone atoms for each monomer, obtained after 5 ns of the first equilibration MD run (time from −5 to 0 ns) were used to prepare mutated TRPA1 tetramers with point mutations N855R and E854R/K868E shown in *E* and *F*. Time evolution of RMSD values and (D), distances separating side chains of E854 and K868 produced for TRPA1 homology models. Values lower than ~4 Å indicate the existence of inter-subunit salt bridges. (E) Time evolutions of RMSD values (upper plot) and distances (lower plot) separating side chains at positions 854 and 868 for charge-swapping mutant and (F) N855R mutant of TRPA1 homology model. (For interpretation of the references to color in this figure legend, the reader is referred to the web version of this article.)

proposed in Zayats et al. (2013)). Notably, we saw more or less stable inter-subunit salt bridges in the immediate vicinity of N855 that were formed between the side chains of amino acids at positions E854 and K868, and these interactions were stable for 22 ns of MD simulation (Fig. 2D). To further corroborate these findings, the E854R/K868E charge-swapping mutation and the substitution N855R that introduced a positive charge at position 855 were also tested by MD simulations (Fig. 2E, F). Importantly, two or three inter-subunit salt bridges were retained all the way through every simulation. In E854R/K868E, the average distances separating side chains at positions 854 and 868 exhibited even lower fluctuations around their mean values (4.05–4.6 Å; Fig. 2E) than the wild-type TRPA1 (3.4–5.5 Å; Fig. 2D), further supporting the contribution of these two sites to inter-subunit stability. The structures obtained at the end of 15 ns of MD simulations were not significantly different from the wild-type channel, indicating that the structural effects caused by the substitutions are too subtle to be captured by the models. However, given the immediate proximity of N855 to E854, these results suggest that the functional changes observed in the N855S mutant by Kremeyer et al. (2010) may originate, at least in part, from changes in inter-subunit interactions.

3.2. Structural modeling based on the high-resolution cryo-EM structure of TRPV1 channel confirms the proximity of E854 and K868

TRPA1 shares a very low sequence identity of about 10% with the structure of Kv1.2-2.1, which complicates the modeling and may lead to errors in mapping structural features from the templates to the model. To reduce the ambiguity, we aligned the TRPA1 sequence with the sequence of the related TRPV1 protein. For this channel, high-resolution cryo-EM structures have been recently solved in the closed state (PDB entry 3J5P) and in two open conformations (3J5Q, 3J5R) (Cao et al., 2013; Liao et al., 2013), one with the TRPV1-specific agonist capsaicin and the other with two strong activators: resiniferatoxin and double-knot toxin. Although the overall sequence identity between the transmembrane parts of TRPA1 and TRPV1 is again not high (~20%), in the S4–S5 linker region it reaches almost 50% (Fig. 3A). A comparison of the sequences allows a direct assignment of the TRPV1 counterparts for charged and conserved amino acids in **TRPA1**: **R852** – G558, **E854** – Q560, **N855** – Q561, **E864** – E570, **K868** – R575, **R872** – R579. In TRPV1, R579 from S5 interacts directly with Q561 from the S4–S5 linker of an adjacent subunit, in addition to the inter-subunit cation-π interaction with Y565 (Liao et al., 2013). This promotes the hypothesis that inter-subunit interactions involving cognate residues in TRPA1, N855 and R872, may underlie the gain-of-function effects observed with the N855S mutation. To further explore this possibility, we built another homology model, this time based directly upon the 3J5P apo structure of TRPV1, in which only the S4–S5 linker (Q560-R575) was replaced by the homologous region E854-K868 from TRPA1 (Fig. 3B–F). RMSD values revealed substantial conformational fragility and occasional reorganizations that occurred in the peripheral areas (helices S1–S3) of the TRPV1-A1 chimera subunits (Fig. 3B), as in the molecular dynamic simulation of the TRPV1 template structure (Fig. 3F). Inter-subunit salt bridges E854-K868 were not formed spontaneously during MD simulations (Fig. 3B, E), although the side chains occasionally got much closer to each other than in the initial cryo-EM structure. In the subsequent set of MD simulations, modest harmonic constraints of 10 kcal mol^{-1} $Å^{-2}$ were applied to E854 and K868 side chains in the preliminary MD run (Fig. 3C). The inter-subunit salt bridges then formed, however they only survived a limited time in subsequent production MD runs. MD simulations were also performed with the N855S and N855V mutants, in addition to the TRPV1-A1 chimeric structures, however, we did not observe any significant changes in the time course of RMSD or the average distances separating side chains at positions 854 and 868 (data not shown). The results from this series of simulations support the proximity and mutual orientation of the E854 and K868 residues and indicate that either the conformational states of TRPV1 may be different from those of TRPA1, or that the formation of inter-subunit salt-bridges between these residues is state-dependent or not critical for the channel's conformational stability.

3.3. Structural alignment between Kv1.2-2.1 and TRPV1 enables the alignment of the target TRPA1 sequence to be refined

In the final step of the modeling, we exploited the cryo-EM structure of TRPV1 to further reduce inaccuracies in the initial target-template sequence alignment between Kv1.2-2.1 and TRPA1. Using the structural alignment of the Kv1.2-2.1 crystal structure (Long et al., 2007) with the cryo-EM apo structure 3J5P of TRPV1 (Liao et al., 2013), we adjusted the sequence alignment between the S4–S5 regions of Kv1.2-2.1 and TRPA1, which resulted in a shift by just one position (Fig. 3A). In the refined alignment, E854 and K868 correspond to K308 and R322 in Kv1.2-2.1, not to G309 and E323, as proposed in our initial alignment. In Kv1.2-2.1, the R322 side chain points towards the K308 side chain. Both positively charged side chains may be located so close to each other due to the presence of the negatively charged side chain of E416 from helix S6. In order to explore how the target-template sequence alignment influences the formation of putative inter-subunit salt bridges, we ran MD simulations of Kv1.2-2.1 with the point mutations K308E and R322K (Fig. 3G). Over the entire MD trajectories, RMSDs for all Kv1.2-2.1-K308E/R322K monomers reached very low values of about 2 Å, corresponding to values that were only observed in previous MD simulations with “stable” TRPV1-A1 monomers (compare Fig. 3B, C). The inter-subunit salt bridges between E308 and K322 had similar stabilities to those observed in the TRPA1 homology model based on the original sequence alignment (compare Figs. 3G and 2C and D). Thus overall, our simulation data on TRPA1 indicates the existence of inter-subunit salt bridges between E854 and K868 and supports the hypothesis that the main mechanism underlying the changes in the channel's activation caused by the pathological N855S mutation is a disturbance of this important subunit–subunit interaction. In addition, the data indicates that, despite a substantial sequence homology shared by the S4–S5 linkers of TRPA1 and TRPV1, the functional roles of cognate residues may differ.

3.4. Electrophysiological measurements support the predicted E854–K868 interaction

To examine whether the predicted inter-subunit interactions contribute to the functionality of the TRPA1 channel, we constructed charge-neutralizing (E854A, K868A) and charge-reversing (E854R, K868E) mutants of human TRPA1 and characterized their phenotypes using whole-cell patch clamp recordings from transiently transfected HEK293T cells. We hypothesized that if specific interactions between opposite charges are required for proper functioning, the charge-swapping double mutant might functionally rescue the channel. We thus also tested the functional properties of the TRPA1 double mutant E854R/K868E. The voltage-dependent activation properties were assessed using a voltage step protocol from −80 mV to +200 mV (Fig. 4A). To compare the energetic effects of mutations at hyperpolarizing voltages, where voltage sensors are close to the resting state, the conductances were plotted on a log scale (Fig. 4B). The E854A and E854R mutants expressed AITC-sensitive channels (as shown below), however,

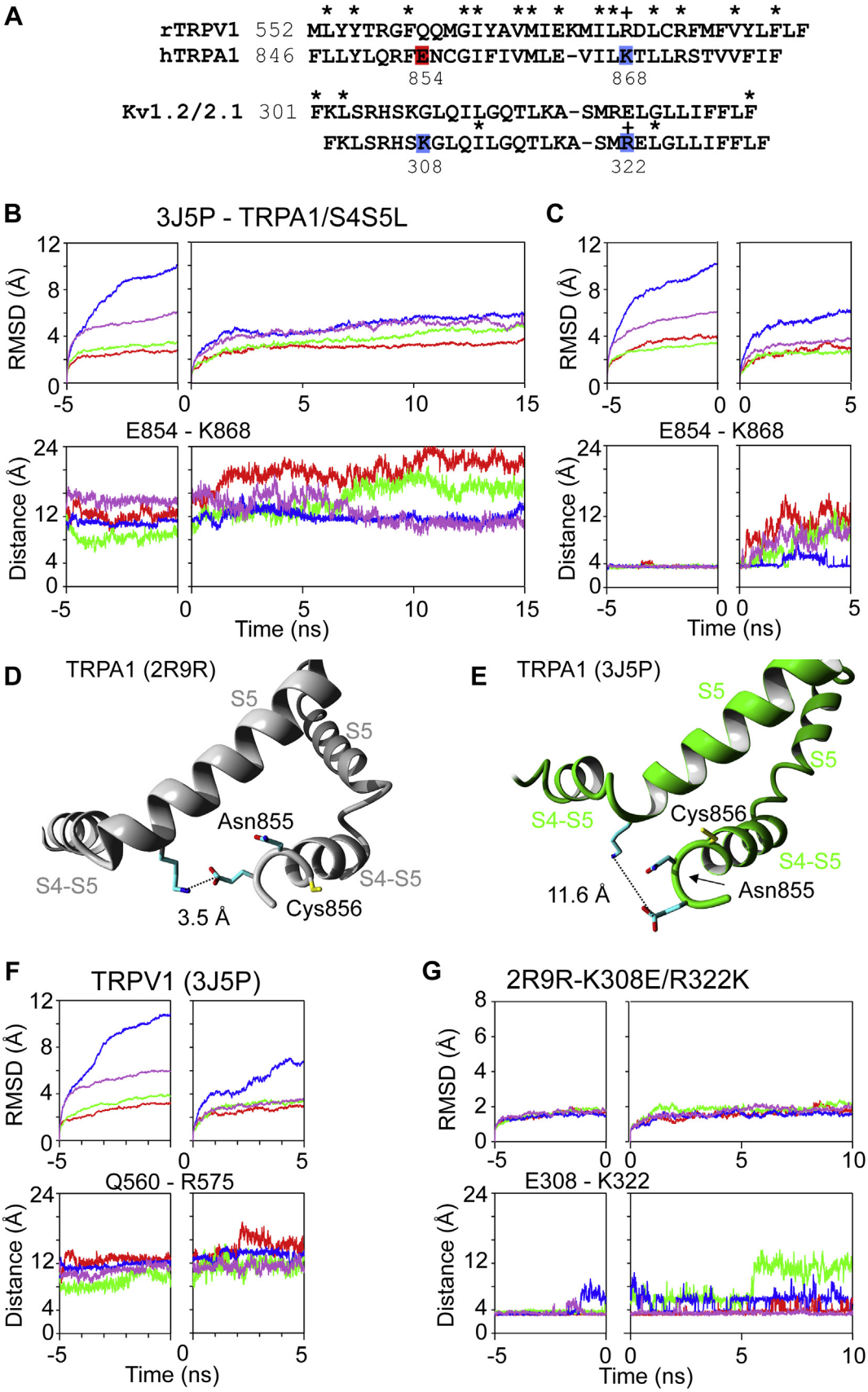

Fig. 3. Homology model of TRPA1 based on 3J5P structure of TRPV1 supports spatial proximity of E854 and K868, but their distances are not sufficient to form inter-subunit salt bridges. (A) Alignments of S4–S5 region of TRPV1 with TRPA1 and two alternative alignments with Kv1.2-2.1. (B) Time evolution of RMSD values (upper plot) and distances separating side chains of E854 and K868 (lower plot), produced for TRPV1-A1 chimera based on 3J5P template structure. Left, the RMSD values obtained for 5 ns of the equilibration

their responses to depolarizing voltage steps were smaller in amplitude and their steady-state activation curves were dramatically shifted toward more positive potentials. Mutations at K868 elicited an increased basal conductance at negative potentials, indicating a disturbed closed–open equilibrium in favor of the open state. The conductance of K868A and K868E was virtually independent of the applied voltage, indicating that a less stringent interaction between the activation gate and the presumed voltage-sensing domain could destabilize the closed conformation of the mutant channels. The charge-swapping mutation E854R/K868E restored normal channel closure at hyperpolarizing voltages, although it did not rescue normal voltage dependency. These data indicate that substitutions at E854 and K868 result in channels with altered gating kinetics.

To test the chemical sensitivity of the TRPA1 mutants, we used a protocol in which whole-cell membrane currents were measured first in the absence of extracellular Ca^{2+} and in the presence of the full agonist allyl isothiocyanate (AITC, 100 μM for 40 s). The agonist was then washed out for 10 s, and Ca^{2+} at a concentration of 2 mM was added to the extracellular solution (Fig. 4C). The membrane potential was ramped every second from −80 mV to +80 mV (1 V/s) (Fig. 4D). Intracellular Ca^{2+} was buffered to low levels with 5 mM EGTA in the patch pipette to assess the effects of permeating calcium ions (Wang et al., 2008). This protocol enabled us to explore not only the sensitivity of individual mutants to electrophilic agonists that lead to persistent activation of TRPA1 (Hinman et al., 2006; Macpherson et al., 2007) but also to permeating Ca^{2+} that activates the channel through a different mechanism (Doerner et al., 2007; Zurborg et al., 2007). In wild-type TRPA1, AITC elicited rapidly developing membrane currents characterized by a mean time activation constant τ_{on} of 5.6 ± 0.7 s (n = 20). After agonist washout, the addition of 2 mM Ca^{2+} to the bath solution induced a marked (58 ± 6%) inactivation. As expected from previous findings (Wang et al., 2008), the TRPA1 currents were inactivated with a similar kinetics and to a similar extent as when Ca^{2+} was added in the continuous presence of AITC (Fig. 4E). Compared with wild-type TRPA1, all the single mutants exhibited much smaller responses to AITC (Figs. 4C, F and 5A). The currents through the E854 single mutant channels had much slower activation kinetics (Fig. 5B), whereas the degree of Ca^{2+}-induced inactivation was similar to wild-type channels (Fig. 5C). In contrast, mutations at K868 generated AITC-induced responses with an onset comparable to the wild-type channels, however, the addition of Ca^{2+} to the bath solution failed to induce any potentiation and only slightly inactivated the currents (22 ± 4% in K868A and 16 ± 9% in K868E; n = 7 and 16) (Fig. 5C). The E854R/K868E double mutation generated currents with an apparently slower onset, but with maximal amplitudes not significantly different from wild-type channels (Figs. 4C and 5A). Upon the addition of Ca^{2+} to the bath solution, this construct exhibited a potentiation that was followed by a more pronounced inactivation than with wild-type TRPA1. As previously shown, current–voltage relationships of TRPA1 responses to AITC become more linear with stronger activation, and less linear as they inactivate (Kremeyer et al., 2010; Wang et al., 2008). Both the wild-type and the double-mutant channels exhibited close-to-linear current–voltage relationships at peak response (Fig. 4D*a*), indicating that a combination of 100 μM AITC with 2 mM Ca^{2+} activates channels to their near-maximum activation capacity. In contrast to wild-type channels, the whole-cell currents through the E854R/K868E double mutant displayed marked outward rectification at the end of the 100 s application of Ca^{2+} (Fig. 4D*b*). The finding that the charge-swapping mutation E854R/K868E substantially rescues the functionality of TRPA1 supports the hypothesis that inter-subunit salt bridges are again formed between the side chains of amino acids at these two positions which indicates the spatial proximity of these two sites.

3.5. Mutations at R852 reveal a gain-of-function phenotype

Mutations at position K868 destabilized the closed, resting conformation of the channel and strongly reduced responses to all stimuli. We reasoned that if this residue is spatially close to E854, then introducing an additional negative charge to the vicinity of E854 could affect the electrostatic attraction between these two residues and thus change the channel's gating equilibrium. Therefore, we next measured voltage-induced currents from the R852E mutant and from the R852A mutant as a control (Fig. 6A, B). For wild-type TRPA1, the Boltzmann fit gave a half-maximal activation voltage ($V_{1/2}$) of 127 ± 2 mV and an apparent number of gating charges (z) of 0.59 ± 0.02 (n = 45). In R852E, $V_{1/2}$ was significantly shifted toward less depolarizing voltages (98 ± 2 mV; z = 0.68 ± 0.04; n = 31), suggesting that the energy required to activate the voltage sensor and pore opening is reduced. In contrast, the open probabilities of R852A were apparently below 0.5 for voltage protocols up to +200 mV, so that values for $V_{1/2}$ and z could only be estimated from the averaged conductances (176 ± 3 mV; n = 32). As predicted, R852E exhibited increased basal activity, however, it exhibited similar AITC-induced maximum current amplitudes and Ca^{2+}-dependent inactivation to the wild-type channels at both positive and negative membrane potentials (Fig. 6C). The R852A mutant exhibited smaller and slower responses to AITC and markedly increased outward rectification upon the addition of 2 mM Ca^{2+} to the bathing solution (Fig. 6D, below). The finding that the alanine mutation produced stronger effects on chemical activation than the charge-reversing mutation indicates the importance of polarity, chain length or both but, in any case, points to a specific role for R852 in the Ca^{2+}-dependent modulation of TRPA1. To explore this observation further, we used cinnamaldehyde (CA) as a partial agonist of TRPA1, which enabled us to assess the potentiating and inactivating effects of permeating Ca^{2+} (Fig. 7A). Cinnamaldehyde, at a concentration of 100 μM, evoked slowly developing currents in wild-type TRPA1 (2.2 ± 0.2 nA at +80 mV after 40 s; n = 25) that slightly relaxed (by 10 ± 3%) to a lower sustained level upon washout. The addition of 2 mM Ca^{2+} to the bath solution induced a marked potentiation that was followed by an almost complete inactivation within 1 min. The R852E mutant produced a very different and striking pattern of responses. During the 40 s application of CA, the currents became close to saturation, which would indicate an increased sensitivity to the agonist. Adding 2 mM Ca^{2+} to the bathing solution immediately inhibited the currents and only a small and delayed potentiation was observed.

To explore whether the replacement of the lysine amino group at K868 with the larger arginine guanidinium group could influence the functionality of the R852E mutant channel, we next compared the CA-induced currents recorded from the K868R and R852E/K868R mutants (Fig. 7B, C). The currents through K868R were

MD run. (C) Modest harmonic constraints of 10 kcal mol^{-1} $Å^{-2}$ were applied to E854 and K868 side chains in preliminary MD run (from −5 to 0 ns) for TRPV1-A1 chimera structure. Note that the inter-subunit salt bridges formed, however they only survived a limited time in the subsequent production MD run. (D) Side chains of residues E854, N855, C856 and K868 are shown on homology models based on 2R9R and (E) 3J5P template structures in enlarged views of adjacent S4/S4–S5 regions. (F) Time evolution of RMSD values (upper plot) and distances separating side chains of Q560 and R575 (E854 and K868 in TRPA1; lower plot) produced for TRPV1 cryo-EM structure 3J5P. Left, RMSD values obtained for 5 ns of equilibration MD run. (G) Molecular dynamics simulation results obtained for Kv1.2-2.1 structure with point mutations K308E and R322K. Lower plot, time evolution of distances between E308 and K322 (E854 and K868 in TRPA1). Values lower than ~4 Å indicate the existence of inter-subunit salt bridges.

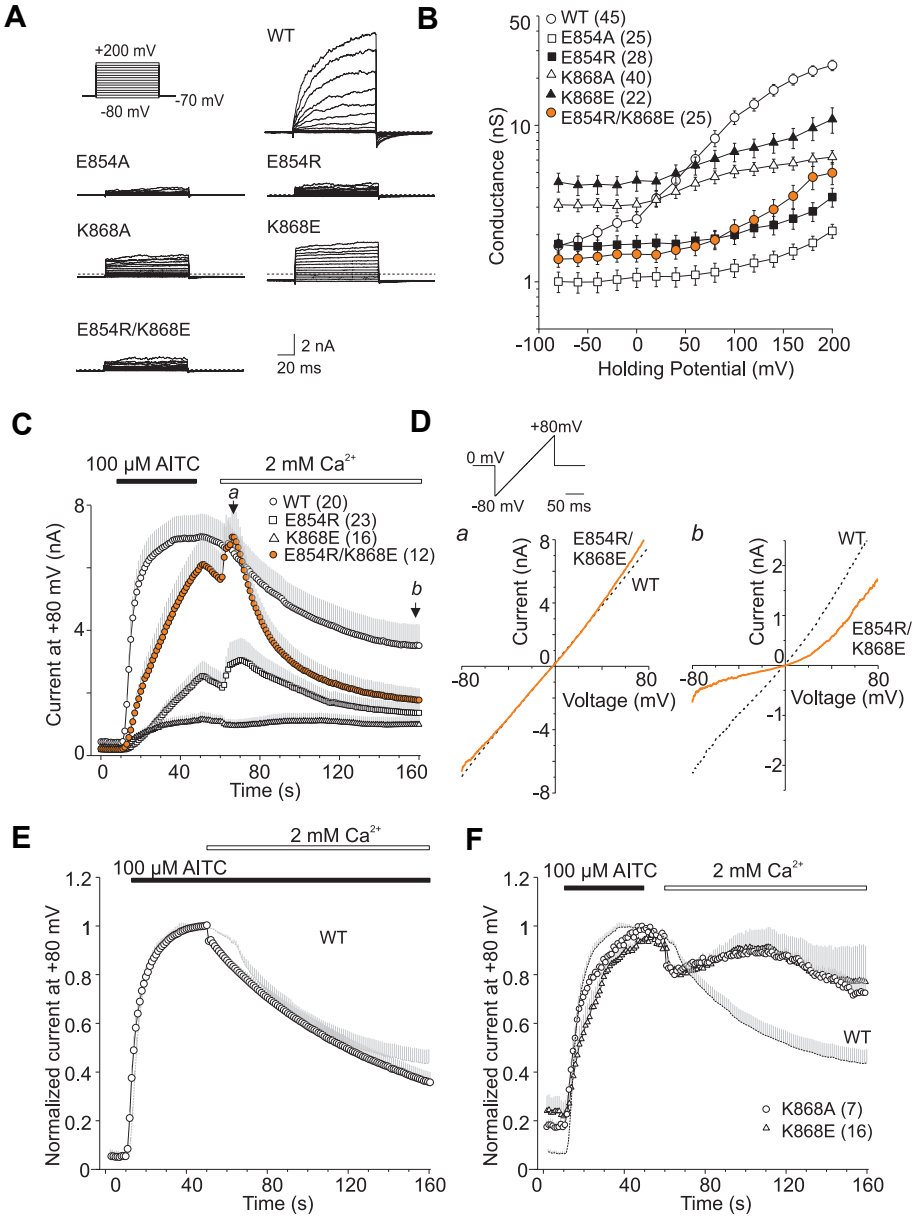

Fig. 4. Charge-swap mutation E854R/K868E in S4–S5 linker rescues chemical sensitivity of TRPA1. (A) Representative current traces in response to indicated voltage step protocol (holding potential −70 mV; 100 ms voltage steps from −80 mV to +200 mV; increment +20 mV) recorded in control extracellular solution ~1 min after whole-cell formation. (B) Average conductances obtained from voltage step protocols as in *A*. Note, a logarithmic scale is used to compare the energetic effects of mutations at hyperpolarizing voltages. (C) Time course of average whole-cell currents induced by 100 μM allyl isothiocyanate (AITC) in Ca^{2+}-free solution and then exposed to 2 mM Ca^{2+} in bath solution, measured at +80 mV in wild-type and indicated mutants. The application of AITC and subsequent addition of 2 mM Ca^{2+} are indicated above. (D) Representative current–voltage relationships of traces measured at times indicated by *a* and *b* in panel (C) for wild-type (dashed line) and E854R/K868E double-mutant TRPA1. Inset shows voltage-ramp protocol used for measuring currents. (E) TRPA1 currents evoked in response to AITC and the subsequent addition of 2 mM Ca^{2+} to the bath solution ($n = 6$). The currents were scaled by the magnitude of the response to AITC and, therefore the y axis is represented by an arbitrary unit. The average normalized current for the wild type recorded with protocol such as in (C) is shown for comparison (dashed line; $n = 18$). Gray bars indicate S.E.M. (F) The average currents recorded from K868A and K868E are expanded and normalized to illustrate more clearly the differences in activation and inactivation rate. Data represent mean ± S.E.M.; *n* indicated in brackets. The average normalized current for the wild type is overlaid for comparison (dashed line with gray bars indicating S.E.M.; $n = 18$).

comparable to the wild-type channels. In contrast, the double mutation generated currents with larger responses to CA and, upon the addition of Ca^{2+}, the currents became less inactivated than in R852E (compare the average currents at the end of recordings in Fig. 7A and B, upper panels). These findings indicate that the R852 residue, which is totally conserved across all TRPA1 channels (Fig. 1B) and does not have a structurally equivalent counterpart in TRPV1 (G558), is clearly involved in the transduction of voltage and chemical stimuli and participates in the Ca^{2+}-dependent regulation of TRPA1. Moreover, we demonstrate that the functionality of the R852E mutant can be affected by the conservative mutation at K868, which indicates that the two residues are on the same allosteric pathway.

3.6. N855 and R872 are not likely to be involved in roles analogous to those of the cognate residues from TRPV1

The transmembrane part of the TRPA1 channel is structurally related to the TRPV1 channel for which the structure was recently

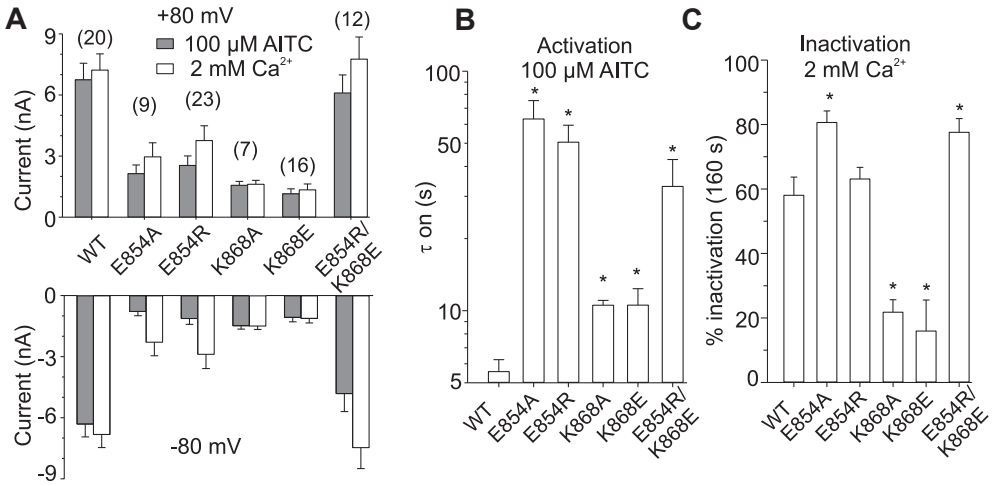

Fig. 5. Summary of the effects of mutations on AITC-induced currents. (A) Average maximum AITC-induced currents from experiments as in Fig. 4C, measured at +80 mV and at −80 mV in absence of Ca^{2+} and then in the presence of 2 mM Ca^{2+} from wild-type and mutant TRPA1. Data represent mean ± S.E.M.; *n* indicated in brackets. (B) Mean time activation constant (τ_{on}), obtained by fitting onset of AITC responses at +80 mV to single exponential function. Asterisks indicate significant difference from wild-type TRPA1 (*$P = 0.01$, unpaired *t*-test). (C) Degree of Ca^{2+}-induced inactivation at +80 mV, expressed as % reduction in current reached at end of Ca^{2+} application relative to peak current.

solved to 3.4 Å resolution using single-particle electron cryo-microscopy (Liao et al., 2013). In TRPV1, Q561 interacts directly with R579 from S5 from an adjacent subunit. Mutation Q561R caused a gain of function of the channel and strong toxicity when expressed in *Saccharomyces cerevisiae* (Myers et al., 2008). On the other hand, R579 has been shown to contribute to the voltage-, lipid- and cholesterol-dependent modulation of the TRPV1 channel (Picazo-Juarez et al., 2011) and the R579E mutation was completely nonfunctional (Boukalova et al., 2010). The corresponding residues in TRPA1 are N855 and R872, and thus we next examined the properties of the N855R and R872E mutants (Fig. 8A–D). Interestingly, neither the mid-point of activation (131 ± 5 mV) nor the slope of the Boltzmann curve ($z = 0.60 \pm 0.02$; $n = 17$) was affected in N855R, compared with wild-type TRPA1 (Fig. 8A), which indicates that this residue is situated outside the membrane electric field. Outward conductances elicited at +200 mV in the absence of agonist were 27 ± 4 nS ($n = 17$), comparable to those observed in the wild-type channel (24 ± 2 nS; $n = 45$). The N855R mutant, however, responded more strongly to CA in Ca^{2+}-free bath solution, which was also reflected in a decrease in the outward rectification of the currents (Fig. 8C). The addition of 2 mM Ca^{2+} increased the CA-induced currents to similar maximum amplitudes (6.6 ± 0.9 nA; n = 9) as in the wild-type channels (6.8 ± 0.4 nA; $n = 25$). The subsequent Ca^{2+}-induced inactivation was faster, but without significant changes in the outward rectification, suggesting a similar degree of inactivation as in the wild-type channel. A simplistic interpretation is that mutations at N855 increase the strength of coupling between the CA-sensing domain and the pore domain.

The R872E construct produced voltage-induced currents that were smaller than those in wild-type channels, however, in contrast to most of the other low-responder phenotypes, its average conductance–voltage relationship was markedly shifted toward less depolarizing voltages (91 ± 2 mV; $z = 0.79 \pm 0.05$; $n = 10$; Fig. 8B). The amplitudes of the voltage-induced currents at +200 mV were about 5-fold lower, whereas the AITC-induced currents reached about one half of the maximum currents recorded from the wild-type channels (Fig. 8B and D). These data suggest that the two residues, N855 and R872, are not likely to play identical roles to Q561 and R579 in TRPV1. The N855R mutation, in contrast to Q561R, does not represent a prototypical gain-of-function channel as it is not spontaneously active at resting membrane potentials, and its half-maximal voltage for activation is no different from the wild-type channel. Moreover, the R872E mutant is fully functional and its leftward shift in the voltage–current relationship indicates that the mutation shifts the gating equilibrium to favor the open state, whereas the analogous mutation R579E leads to a non-functional channel in TRPV1.

4. Discussion

In this study, we propose a possible mechanism explaining the gain-of-function phenotype of the N855S mutation in the ankyrin TRPA1 channel, associated with familial episodic pain syndrome in humans (Kremeyer et al., 2010). Using data from structural modeling and whole-cell voltage-clamp recordings, we propose that it is a change in the electrostatic environment experienced by neighboring charged residues which causes a depolarized shift in the voltage-dependence of CA-induced responses and changes the N855S channel's gating through a Ca^{2+}-sensitive mechanism.

The first key finding of our study is the identification of inter-subunit interactions between the two highly conserved charged residues, E854, the neighboring residue of N855, and K868, from the S5 helix of an adjacent subunit. By using comparative modeling based on alternative alignments and two alternative templates, we consistently find that the two residues E854 and K868 are in close proximity and may form salt bridges. In our model based on the 3J5P structure of TRPV1 (Liao et al., 2013), inter-subunit salt bridges E854-K868 were not formed spontaneously during MD simulations (Fig. 3E), although these side chains occasionally approached each other more closely than in the initial cryo-EM structure. This might be a reflection of different conformational states, because the template structure 2R9R represents an open state of the paddle chimera Kv1.2-2.1 channel, whereas 3J5P represents the TRPV1 channel in a closed state. However, we do not favor this interpretation, because the side chains of amino acids Q560 and R575 in TRPV1 (i.e. E854 and K868 in TRPA1) are also further than 10 Å apart in the structures of the two TRPV1 open conformations 3J5Q and 3J5R (Cao et al., 2013; Liao et al., 2013). The high conservation of the S4/S4–S5 domain throughout the mammalian members of the TRPV channel subfamily and TRPA1 (~50% amino acid identity) raises the question of to what extent the conformational states of TRPV1 could be generalized to TRPA1. Vanilloid ligands bind TRPV1 directly within a hydrophobic pocket comprising the S4–S5 linker, eliciting conformational changes that expand the lower gate (Cao

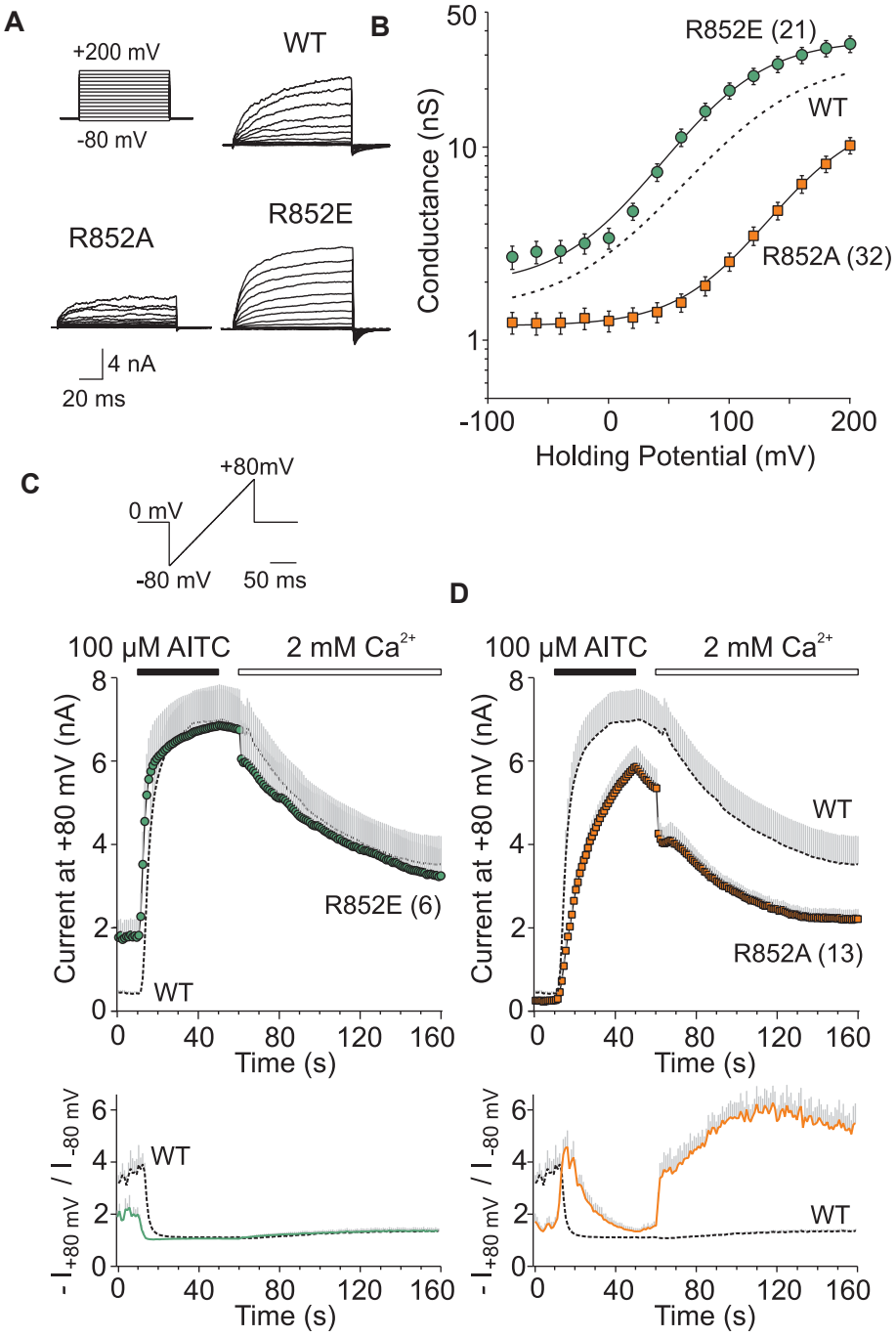

Fig. 6. Mutations of R852, located at turn between S4 and S4–S5 linker, likely to disrupt allosteric interactions involved in voltage-dependent gating and Ca^{2+}-dependent modulation. (A) Representative current traces in response to indicated voltage step protocol (holding potential −70 mV; 100 ms voltage steps from −80 mV to +200 mV; increment +20 mV) recorded in control extracellular solution ~1 min after whole-cell formation. (B) Average conductances obtained from voltage step protocols as in *A*. Solid lines are best fits to a Boltzmann function as described in Materials and Methods. The dashed line represents the fit obtained from data for wild-type TRPA1 shown in Fig. 4*B*. (C) Time course of average whole-cell currents induced by 100 μM allyl isothiocyanate (AITC) and by 2 mM Ca^{2+}, measured at +80 mV in R852E (green circles) and (D) in R852A (orange squares). The average current for the wild type is shown for comparison (dashed line with gray bars indicating S.E.M., $n = 20$). The application of AITC and subsequent addition of 2 mM Ca^{2+} are indicated above. In (C), note the increased basal R852E-mediated current at the beginning of the recording (0–10 s). Below, average rectification of currents shown above. Changes in rectification ratio plotted as a function of time, calculated as absolute value of current at +80 mV divided by current at −80 mV for each ramp from current–voltage relationships (similar to those shown in Fig. 4D), measured in R852E (C) and R852A (D) (colored line with gray bars indicating ± S.E.M.). The average rectification for the wild type is overlaid for comparison (dashed line ± S.E.M.; $n = 20$). Note the dramatically increased outward rectification upon Ca^{2+} application in R852A. (For interpretation of the references to color in this figure legend, the reader is referred to the web version of this article.)

et al., 2013). In contrast, electrophilic compounds activate TRPA1 through covalent binding at specific cysteine residues on the intracellularly located N-terminus (Hinman et al., 2006; Kang et al., 2010; Macpherson et al., 2007) and simulations using low-resolution electron density maps indicate that the chemical signal might be readily conveyed to the intracellular channel gate through cytoplasmic domains (Cvetkov et al., 2011; Takahashi et al., 2011). Compared to voltage-gated channels, the S1–S4 domain of TRPV1

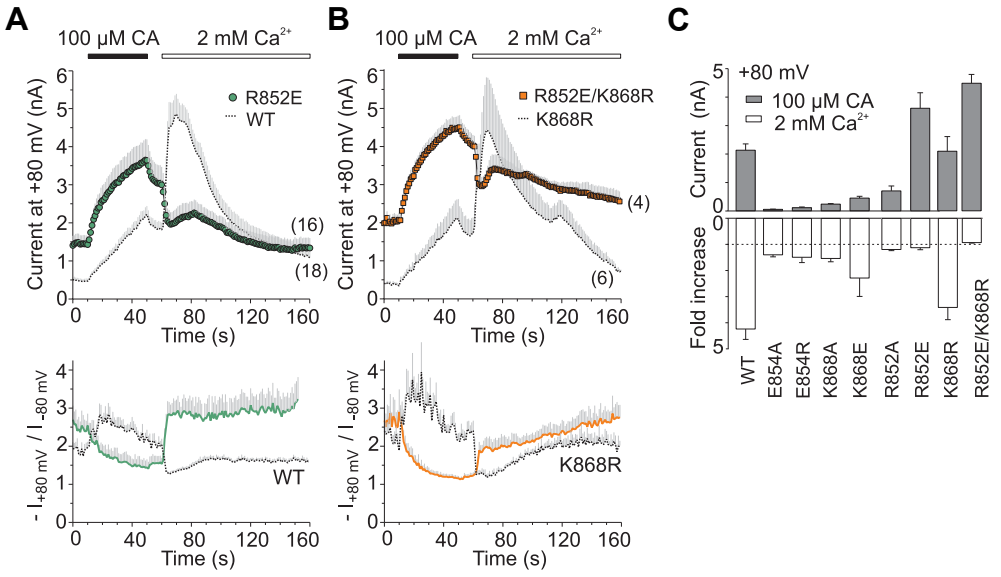

Fig. 7. Mutation R852E exhibits separation-of-function phenotype when exposed to cinnamaldehyde. (A) (B) Time course of average whole-cell currents induced by 100 μM cinnamaldehyde (CA) in Ca^{2+}-free solution and then exposed to 2 mM Ca^{2+}, measured at +80 mV in wild-type and indicated mutants. The application of CA and subsequent addition of 2 mM Ca^{2+} are indicated above. Each point represents the mean value ± S.E.M. (*n* indicated in brackets). The average currents for the wild type (A) and for R852E/K868R (B) are respectively shown for comparison (dotted lines with gray bars indicating S.E.M.; $n = 18$ and 6). Below, average rectification of currents shown above, calculated as absolute value of current at +80 mV divided by current at −80 mV, measured in R852E (A), and K868R and R852E/K868R (B) (colored lines with gray bars indicating ± S.E.M.). (C) Upper bars, average maximum CA-induced currents from experiments as in *A*, measured at +80 mV in absence of Ca^{2+} from wild-type and mutant TRPA1. Data represent mean ± S.E.M.; *n* from 4 to 25. Lower bars, degree of Ca^{2+}-induced potentiation quantified as fold-increase in amplitude with respect to preceding current level of CA-induced responses measured at +80 mV. Dotted line indicates no increase. For wild-type TRPA1, this value was 4.1 ± 0.4 at +80 mV ($n = 25$). Except for K868R, all mutants were significantly different from wild-type TRPA1 (*$P < 0.05$, unpaired *t*-test). (For interpretation of the references to color in this figure legend, the reader is referred to the web version of this article.)

has a surprisingly less active role in channel gating, functioning as a passive anchor upon which the S4–S5 linker moves in response to ligand binding (Cao et al., 2013). Opening the inner gate does not involve splaying the lower half of S6, which in Kv channels is enabled by a glycine (GX_3G) or proline (PVP) hinge in the middle of S6 (Fowler and Sansom, 2013; Jensen et al., 2012; Long et al., 2005). Within the S6 inner-pore region of TRPA1, however, there is a highly conserved glycine hinge motif GLAVG that is critically involved in the gating of the channel (Benedikt et al., 2009). Thus, the gating mechanisms in TRPV1 and TRPA1 may substantially differ. Also, we have previously demonstrated that structural determinants within the S4/S4–S5 region of TRPV1, although conserved in the primary sequence across the TRPV channel subfamily, do not necessarily play functionally conserved roles (Boukalova et al., 2010). We did not observe any significant changes between the structures obtained from MD simulations for the wild-type TRPA1 channel and the N855S, N855R, or N855V mutants (Fig. 2F and data not shown). This may suggest that the structural effects caused by these substitutions are too subtle to be captured by the models. However, we did observe an improved stability of inter-subunit salt bridges in the MD simulation of the charge-swap E854R/K868E double mutation model based on the 2R9R structure (Fig. 2E), which indicates that these two side chains may have an impact on the stability of the channel complex. Indeed, our electrophysiological data shows that the charge-swap mutation E854R/K868E, although capable of rescuing chemical responsiveness, still cannot recover the intrinsic voltage sensitivity of TRPA1 (Fig. 4B).

Our second key finding is that a single charge-reversing mutation at R852, which is located at the turn between S4 and the S4–S5 linker, three residues upstream of N855, generates channels with increased basal activity and close-to-saturated chemical responses. In this construct, Ca^{2+} did not substantially potentiate the CA-induced responses and immediately, and more strongly than in the wild-type channels, inactivated the currents induced by cinnamaldehyde (but not by AITC). The voltage-dependent gating in R852E was shifted toward less depolarizing voltages, indicating that the energy required to activate the putative voltage sensor and pore opening is reduced. In voltage-gated potassium and sodium channels, the voltage-sensing domain S1–S4 transforms membrane potential changes into channel gating through interactions between positively charged arginines in S4 and negatively charged residues in S1–S3. The opening of the channel then critically depends on the interaction of the residues from the S4–S5 linker with residues in the late S6 segment (Fowler and Sansom, 2013; Jensen et al., 2012; Long et al., 2005). Compared to voltage-gated channels, the voltage-dependency of TRPA1 is weak, with the estimated apparent number of gating charges being about 0.7 (Karashima et al., 2009; Samad et al., 2011). The S4 helix in TRPA1 does not contain any positively charged residues but we show here that the charge-neutralizing mutation R852A at the turn between S4 and S4–S5 decreases its voltage sensitivity (Fig. 6B). In TRPV1, the residue corresponding to R852, G558, is situated spatially close to the TRP domain, mutations in which result in changes in the efficient coupling of stimulus sensing and gate opening (Gregorio-Teruel et al., 2014), and generate gain-of-function phenotypes (Lin et al., 2012). To the best of our knowledge, it is not known whether TRPA1 possesses the TRP domain. There is a conserved sequence LWFLRK (992–997), showing a remarkable sequence similarity to the TRP box of TRPV1 (IWKLQR at positions 696–701), that follows S6. However, compared to TRPV1, there would be an insertion of approx. 25 amino acids (I964-K989) wedged between S6 and a potential TRP box. Thus determining whether R852 in TRPA1 could alternatively interact with K997 (because in TRPV1, R701 is directed to G558), or with some other residue near the inner pore helix, is an interesting subject for future study. Given the specific changes in voltage-dependent gating observed in the R852 mutants and the selective disruption of voltage-dependent gating in the charge-swap E854R/K868E channels, we do not want to

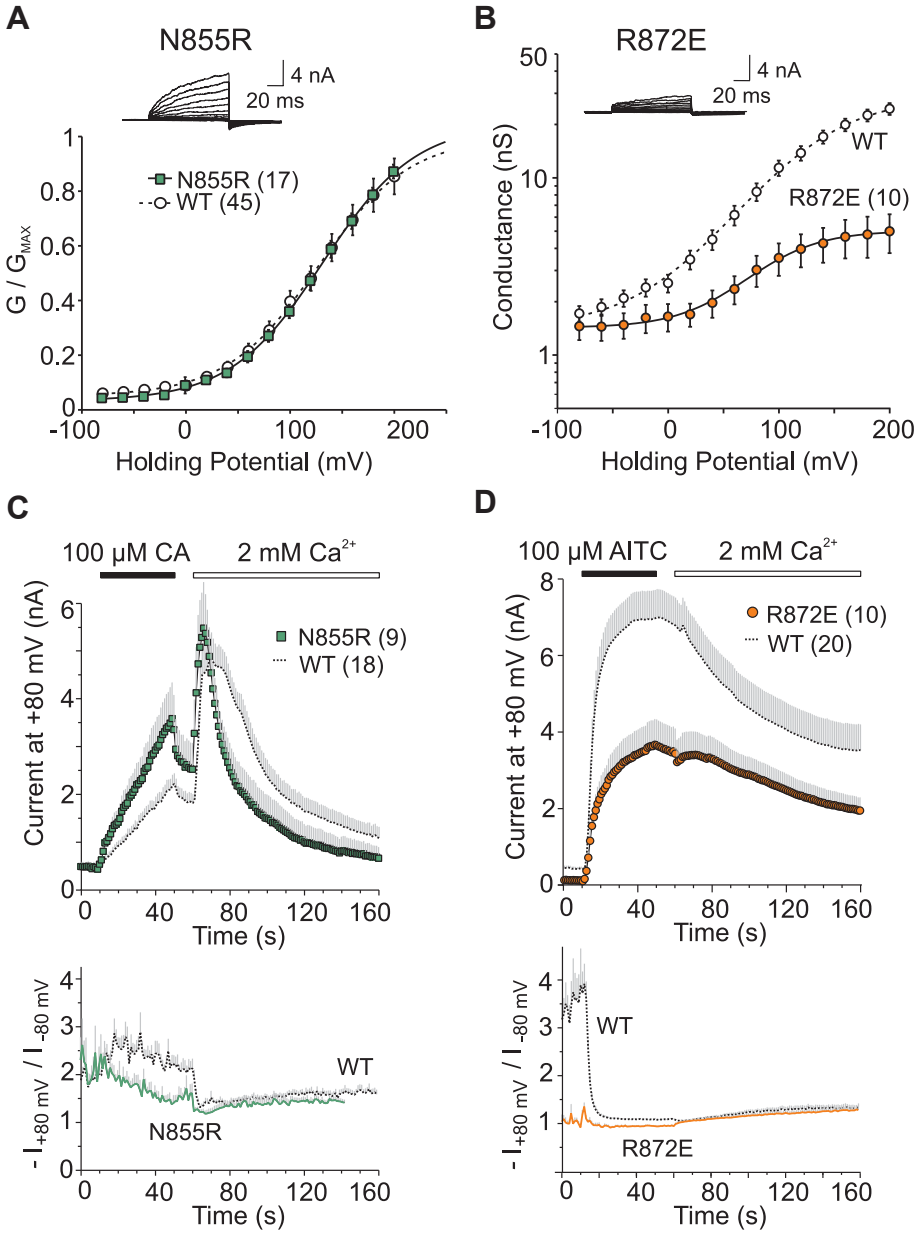

Fig. 8. N855 and R872 are not likely to play similar roles to their cognate residues from TRPV1. (A) Average conductances obtained from wild-type TRPA1 (solid circles) and N855R (green squares) using voltage step protocols as in Fig. 4A, normalized to show that N855R conductance is no different from wild-type. Solid and dashed lines are best fits to a Boltzmann function as described in Materials and Methods. For wild-type TRPA1, the fit gave a half-maximal activation voltage ($V_{1/2}$) of 127 ± 2 mV ($n = 45$). For N855R, $V_{1/2}$ was 131 ± 5 mV ($n = 17$). The conductance–voltage relationships were normalized to make the data better comparable and to demonstrate that there is no sign of any difference. (B) Mean steady-state activation curve obtained from R872E (orange circles). The dashed line with open symbols represents the best fit obtained from wild-type TRPA1. Note, logarithmic scale is used to compare the conductances at hyperpolarizing voltages. (C) Time course of average whole-cell currents induced by 100 µM cinnamaldehyde (CA) in Ca^{2+}-free solution and then in 2 mM Ca^{2+}, measured at +80 mV in N855R. Each point represents the mean value ± S.E.M. (n indicated in brackets). The application of CA and subsequent addition of 2 mM Ca^{2+} are indicated above. The average current for the wild type is shown for comparison (dotted line with gray bars indicating S.E.M.; $n = 18$). Below, average rectification of currents shown above, calculated as absolute value of current at +80 mV divided by current at −80 mV. The average rectification for the wild type is overlaid for comparison. (D) Average whole-cell currents measured at +80 mV from R872E, induced by 100 µM allyl isothiocyanate (AITC) recorded in Ca^{2+}-free solution and then in 2 mM Ca^{2+} (n indicated in brackets). Below, average rectification of responses shown above. Each point represents the mean value ± S.E.M. for n indicated above. (For interpretation of the references to color in this figure legend, the reader is referred to the web version of this article.)

exclude the possibility that these residues may comprise the voltage-sensing domain itself.

Consistent with the previously proposed involvement of N855 in the Ca^{2+}-dependent gating of TRPA1, our results imply that the S4–S5 linker contributes to agonist- and voltage-dependent activation and regulates the gating of the channel in a state-dependent manner, and via a Ca^{2+}-sensitive mechanism. In the original study by Kremeyer et al. (2010), the gain-of-function point mutation N855S has been shown to exhibit normal current–voltage plots in the absence of agonist but a 5-fold increase in inward currents on activation by chemical stimuli at normal resting membrane potentials. Consistent with this, our data shows that N855R also exhibits normal voltage-dependent gating (Fig. 8A), and increased, much less outwardly rectified CA-induced currents (Fig. 8C). We observed only a weak outward rectification of CA-induced responses in wild-type channels, which carried only about double the

current at +80 mV than at −80 mV under Ca^{2+}-free conditions with intracellular Ca^{2+} buffered to low levels (Fig. 8C). This is different from the results of the above study (Kremeyer et al., 2010), in which a substantially lower Ca^{2+}-buffering capacity of the pipette content was used in the whole-cell recordings. Taken together, these comparisons lead us to hypothesize that the main effect of the N855S mutation is an increased efficacy of CA and a reduced inactivation induced by permeating calcium ions at negative membrane potentials. It should also be considered that the neighboring residue is a reactive cysteine C856 (compare the relative side chain orientations in Fig. 3D and E), a target site of O_2 in hyperoxia, for which a cytoplasmic disposition has been recently proposed (Takahashi et al., 2011). Although the charged residues in the vicinity of N855 are apparently involved in the allosteric coupling of voltage sensor activation to channel opening, N855 itself does not seem to be involved in sensing changes in the membrane electric field under resting conditions. In this sense, N855S and N855R might be considered to be a rarer "separation-of-function" phenotype rather than a "gain-of-function" phenotype. During CA-induced activation, the S4–S5 linker apparently undergoes conformational changes, involving N855, that alter the voltage- and Ca^{2+}-dependency of TRPA1.

Acknowledgments

This work was supported by the Czech Science Foundation (15-15839S, 305/09/0081 and 304/12/G069), the Grant Agency of Charles University (GAUK 426311 and 888513), the Research Project Fund of the ASCR (RVO: 67985823), Ministry of Education, Youth and Sports of the Czech Republic (SVV 2012-265304). The work was supported within the project The Centre of Biomedical Research (CZ.1.07/2.3.00/30.0025). This project is co-funded by the European Social Fund and the State Budget of the Czech Republic.

Author contributions: VV and IB designed the study, VZ, KW, AH, LZ, IB and VV collected and analyzed data, VV and IB wrote the manuscript. All of the authors discussed the results and commented on the manuscript.

References

Andrade, E.L., Meotti, F.C., Calixto, J.B., 2012. TRPA1 antagonists as potential analgesic drugs. Pharmacol. Ther. 133, 189–204.
Beglov, D., Roux, B., 1994. Finite representation of an infinite bulk system – solvent boundary potential for computer-simulations. J. Chem. Phys. 100, 9050–9063.
Benedikt, J., Samad, A., Ettrich, R., Teisinger, J., Vlachova, V., 2009. Essential role for the putative S6 inner pore region in the activation gating of the human TRPA1 channel. Biochim. Biophys. Acta 1793, 1279–1288.
Bernsel, A., Viklund, H., Hennerdal, A., Elofsson, A., 2009. TOPCONS: consensus prediction of membrane protein topology. Nucleic Acids Res. 37, W465–W468.
Boukalova, S., Marsakova, L., Teisinger, J., Vlachova, V., 2010. Conserved residues within the putative S4-S5 region serve distinct functions among thermosensitive vanilloid transient receptor potential (TRPV) channels. J. Biol. Chem. 285, 41455–41462.
Cao, E., Liao, M., Cheng, Y., Julius, D., 2013. TRPV1 structures in distinct conformations reveal activation mechanisms. Nature 504, 113–118.
Cheatham, T.E., Miller, J.L., Fox, T., Darden, T.A., Kollman, P.A., 1995. Molecular-dynamics simulations on solvated biomolecular systems – the particle mesh Ewald method leads to stable trajectories of DNA, RNA, and proteins. J. Am. Chem. Soc. 117, 4193–4194.
Crooks, G.E., Hon, G., Chandonia, J.M., Brenner, S.E., 2004. WebLogo: a sequence logo generator. Genome Res. 14, 1188–1190.
Cvetkov, T.L., Huynh, K.W., Cohen, M.R., Moiseenkova-Bell, V.Y., 2011. Molecular architecture and subunit organization of TRPA1 ion channel revealed by electron microscopy. J. Biol. Chem. 286, 38168–38176.
Dittert, I., Benedikt, J., Vyklicky, L., Zimmermann, K., Reeh, P.W., Vlachova, V., 2006. Improved superfusion technique for rapid cooling or heating of cultured cells under patch-clamp conditions. J. Neurosci. Methods 151, 178–185.
Doerner, J.F., Gisselmann, G., Hatt, H., Wetzel, C.H., 2007. Transient receptor potential channel A1 is directly gated by calcium ions. J. Biol. Chem. 282, 13180–13189.
Eswar, N., Marti-Renom, M.A., Webb, B., Madhusudhan, M.S., Eramian, D., Shen, M.Y., Pieper, U., Sali, A., 2006. Comparative protein structure modeling with MODELLER. In: Coligan, J.E., Dunn, B.M., Speicher, D.W., Wingfield, P.T. (Eds.), Current Protocols in Bioinformatics. John Wiley & Sons, Inc., pp. 1–30. Unit 5.6.
Fowler, P.W., Sansom, M.S.P., 2013. The pore of voltage-gated potassium ion channels is strained when closed. Nat. Commun. 4.
Gregorio-Teruel, L., Valente, P., Gonzalez-Ros, J.M., Fernandez-Ballester, G., Ferrer-Montiel, A., 2014. Mutation of I696 and W697 in the TRP box of vanilloid receptor subtype I modulates allosteric channel activation. J. Gen. Physiol. 143, 361–375.
Hinman, A., Chuang, H.H., Bautista, D.M., Julius, D., 2006. TRP channel activation by reversible covalent modification. Proc. Natl. Acad. Sci. U. S. A. 103, 19564–19568.
Humphrey, W., Dalke, A., Schulten, K., 1996. VMD: visual molecular dynamics. J. Mol. Graph. 14, 33–38.
Jensen, M.O., Jogini, V., Borhani, D.W., Leffler, A.E., Dror, R.O., Shaw, D.E., 2012. Mechanism of voltage gating in potassium channels. Science 336, 229–233.
Jorgensen, W.L., Chandrasekhar, J., Madura, J.D., Impey, R.W., Klein, M.L., 1983. Comparison of simple potential functions for simulating liquid water. J. Chem. Phys. 79, 926–935.
Kabsch, W., Sander, C., 1983. Dictionary of protein secondary structure: pattern recognition of hydrogen-bonded and geometrical features. Biopolymers 22, 2577–2637.
Kang, K., Pulver, S.R., Panzano, V.C., Chang, E.C., Griffith, L.C., Theobald, D.L., Garrity, P.A., 2010. Analysis of Drosophila TRPA1 reveals an ancient origin for human chemical nociception. Nature 464, 597–600.
Karashima, Y., Talavera, K., Everaerts, W., Janssens, A., Kwan, K.Y., Vennekens, R., Nilius, B., Voets, T., 2009. TRPA1 acts as a cold sensor in vitro and in vivo. Proc. Natl. Acad. Sci. U. S. A. 106, 1273–1278.
Kremeyer, B., Lopera, F., Cox, J.J., Momin, A., Rugiero, F., Marsh, S., Woods, C.G., Jones, N.G., Paterson, K.J., Fricker, F.R., Villegas, A., Acosta, N., Pineda-Trujillo, N.G., Ramirez, J.D., Zea, J., Burley, M.W., Bedoya, G., Bennett, D.L., Wood, J.N., Ruiz-Linares, A., 2010. A gain-of-function mutation in TRPA1 causes familial episodic pain syndrome. Neuron 66, 671–680.
Larkin, M.A., Blackshields, G., Brown, N.P., Chenna, R., McGettigan, P.A., McWilliam, H., Valentin, F., Wallace, I.M., Wilm, A., Lopez, R., Thompson, J.D., Gibson, T.J., Higgins, D.G., 2007. Clustal W and Clustal X version 2.0. Bioinformatics 23, 2947–2948.
Liao, M., Cao, E., Julius, D., Cheng, Y., 2013. Structure of the TRPV1 ion channel determined by electron cryo-microscopy. Nature 504, 107–112.
Lin, Z., Chen, Q., Lee, M., Cao, X., Zhang, J., Ma, D., Chen, L., Hu, X., Wang, H., Wang, X., Zhang, P., Liu, X., Guan, L., Tang, Y., Yang, H., Tu, P., Bu, D., Zhu, X., Wang, K., Li, R., Yang, Y., 2012. Exome sequencing reveals mutations in TRPV3 as a cause of Olmsted syndrome. Am. J. Hum. Genet. 90, 558–564.
Long, S.B., Campbell, E.B., Mackinnon, R., 2005. Voltage sensor of Kv1.2: structural basis of electromechanical coupling. Science 309, 903–908.
Long, S.B., Tao, X., Campbell, E.B., MacKinnon, R., 2007. Atomic structure of a voltage-dependent K^+ channel in a lipid membrane-like environment. Nature 450, 376–382.
MacKerell, A.D., Bashford, D., Bellott, M., Dunbrack, R.L., Evanseck, J.D., Field, M.J., Fischer, S., Gao, J., Guo, H., Ha, S., Joseph-McCarthy, D., Kuchnir, L., Kuczera, K., Lau, F.T., Mattos, C., Michnick, S., Ngo, T., Nguyen, D.T., Prodhom, B., Reiher, W.E., Roux, B., Schlenkrich, M., Smith, J.C., Stote, R., Straub, J., Watanabe, M., Wiorkiewicz-Kuczera, J., Yin, D., Karplus, M., 1998. All-atom empirical potential for molecular modeling and dynamics studies of proteins. J. Phys. Chem. B 102, 3586–3616.
Macpherson, L.J., Dubin, A.E., Evans, M.J., Marr, F., Schultz, P.G., Cravatt, B.F., Patapoutian, A., 2007. Noxious compounds activate TRPA1 ion channels through covalent modification of cysteines. Nature 445, 541–545.
Marti-Renom, M.A., Stuart, A.C., Fiser, A., Sanchez, R., Melo, F., Sali, A., 2000. Comparative protein structure modeling of genes and genomes. Annu. Rev. Biophys. Biomol. Struct. 29, 291–325.
Moran, M.M., 2012. Transient receptor potential ankyrin 1 as a target for perioperative pain management. Anesthesiology 117, 8–9.
Myers, B.R., Bohlen, C.J., Julius, D., 2008. A yeast genetic screen reveals a critical role for the pore helix domain in TRP channel gating. Neuron 58, 362–373.
Nilius, B., Appendino, G., Owsianik, G., 2012. The transient receptor potential channel TRPA1: from gene to pathophysiology. Pflugers Archiv. Eur. J. Physiol. 464, 425–458.
Owsianik, G., Talavera, K., Voets, T., Nilius, B., 2006. Permeation and selectivity of TRP channels. Annu. Rev. Physiol. 68, 685–717.
Phillips, J.C., Braun, R., Wang, W., Gumbart, J., Tajkhorshid, E., Villa, E., Chipot, C., Skeel, R.D., Kale, L., Schulten, K., 2005. Scalable molecular dynamics with NAMD. J. Comput. Chem. 26, 1781–1802.
Picazo-Juarez, G., Romero-Suarez, S., Nieto-Posadas, A., Llorente, I., Jara-Oseguera, A., Briggs, M., McIntosh, T.J., Simon, S.A., Ladron-de-Guevara, E., Islas, L.D., Rosenbaum, T., 2011. Identification of a binding motif in the S5 helix that confers cholesterol sensitivity to the TRPV1 ion channel. J. Biol. Chem. 286, 24966–24976.
Roe, D.R., Cheatham, T.E., 2013. PTRAJ and CPPTRAJ: software for processing and analysis of molecular dynamics trajectory data. J. Chem. Theory Comput. 9, 3084–3095.
Ryckaert, J.P., Ciccotti, G., Berendsen, H.J.C., 1977. Numerical integration of the Cartesian equations of motion of a system with constraints: molecular dynamics of n-alkanes. J. Comp. Phys. 23, 327–341.
Samad, A., Sura, L., Benedikt, J., Ettrich, R., Minofar, B., Teisinger, J., Vlachova, V., 2011. The C-terminal basic residues contribute to the chemical- and voltage-dependent activation of TRPA1. Biochem. J. 433, 197–204.

Schlenkrich, M., Brickmann, J., MacKerell, J.A.D., Karplus, M., 1996. An empirical potential energy function for phospholipids: criteria for parameter optimization and applications. In: Roux, K.M.M.A.B. (Ed.), Biological Membranes: a Molecular Perspective from Computation and Experiment. Birkhauser Boston, pp. 31–81.

Susankova, K., Ettrich, R., Vyklicky, L., Teisinger, J., Vlachova, V., 2007. Contribution of the putative inner-pore region to the gating of the transient receptor potential vanilloid subtype 1 channel (TRPV1). J. Neurosci. 27, 7578–7585.

Takahashi, N., Kuwaki, T., Kiyonaka, S., Numata, T., Kozai, D., Mizuno, Y., Yamamoto, S., Naito, S., Knevels, E., Carmeliet, P., Oga, T., Kaneko, S., Suga, S., Nokami, T., Yoshida, J., Mori, Y., 2011. TRPA1 underlies a sensing mechanism for O_2. Nat. Chem. Biol. 7, 701–711.

Wang, Y.Y., Chang, R.B., Waters, H.N., McKemy, D.D., Liman, E.R., 2008. The nociceptor ion channel TRPA1 is potentiated and inactivated by permeating calcium ions. J. Biol. Chem. 283, 32691–32703.

Zayats, V., Samad, A., Minofar, B., Roelofs, K.E., Stockner, T., Ettrich, R., 2013. Regulation of the transient receptor potential channel TRPA1 by its N-terminal ankyrin repeat domain. J. Mol. Model. 19, 4689–4700.

Zurborg, S., Yurgionas, B., Jira, J.A., Caspani, O., Heppenstall, P.A., 2007. Direct activation of the ion channel TRPA1 by Ca^{2+}. Nat. Neurosci. 10, 277–279.

Publication 3

Sura L., Zima V., Marsakova L., **Hynkova A.**, Barvik I., Vlachova V.

C-terminal acidic cluster is involved in Ca^{2+}-induced regulation of human transient receptor potential ankyrin 1 channel.

The Journal of Biological Chemistry, 287(22):18067-77, 2012

The extent of participation: Control electrophysiological experiments, help with finalization of the manuscript.

THE JOURNAL OF BIOLOGICAL CHEMISTRY VOL. 287, NO. 22, pp. 18067–18077, May 25, 2012

C-terminal Acidic Cluster Is Involved in Ca^{2+}-induced Regulation of Human Transient Receptor Potential Ankyrin 1 Channel*[S]

Received for publication, January 12, 2012, and in revised form, March 20, 2012 Published, JBC Papers in Press, March 29, 2012, DOI 10.1074/jbc.M112.341859

Lucie Sura[‡], Vlastimil Zíma[§], Lenka Marsakova[‡], Anna Hynkova[‡], Ivan Barvík[§], and Viktorie Vlachova[‡1]

From the [‡]Department of Cellular Neurophysiology, Institute of Physiology, Academy of Sciences of the Czech Republic, Videnska 1083, 142 20 Prague 4, Czech Republic and the [§]Division of Biomolecular Physics, Institute of Physics, Faculty of Mathematics and Physics, Charles University, Ke Karlovu 5, 121 16 Prague 2, Czech Republic

Background: TRPA1 channel is modulated by Ca^{2+}, but the molecular mechanisms are unclear.
Results: Mutations in the distal C-terminal acidic domain altered Ca^{2+} dependence of TRPA1.
Conclusion: The C-terminal acidic cluster is involved in the Ca^{2+}-induced potentiation and inactivation of TRPA1.
Significance: Identification of the Ca^{2+}-dependent domain is important for understanding the role of TRPA1 in chemical nociception.

The transient receptor potential ankyrin 1 (TRPA1) channel is a Ca^{2+}-permeable cation channel whose activation results from a complex synergy between distinct activation sites, one of which is especially important for determining its sensitivity to chemical, voltage and cold stimuli. From the cytoplasmic side, TRPA1 is critically regulated by Ca^{2+} ions, and this mechanism represents a self-modulating feedback loop that first augments and then inhibits the initial activation. We investigated the contribution of the cluster of acidic residues in the distal C terminus of TRPA1 in these processes using mutagenesis, whole cell electrophysiology, and molecular dynamics simulations and found that the neutralization of four conserved residues, namely Glu^{1077} and Asp^{1080}–Asp^{1082} in human TRPA1, had strong effects on the Ca^{2+}- and voltage-dependent potentiation and/or inactivation of agonist-induced responses. The surprising finding was that truncation of the C terminus by only 20 residues selectively slowed down the Ca^{2+}-dependent inactivation 2.9-fold without affecting other functional parameters. Our findings identify the conserved acidic motif in the C terminus that is actively involved in TRPA1 regulation by Ca^{2+}.

The gating of transduction ion channels in response to various potential life-threatening events is a crucial mechanism underlying the function of sensory neurons. Among the channels that act as important signaling molecules involved in the perception of noxious chemical, mechanical, and cold stimuli in primary afferent neurons, there is one specific protein whose unique polymodal activation properties have drawn much attention over recent years for their potential therapeutic applications: the transient receptor potential ankyrin subtype 1 (TRPA1)[2] channel (1, 2). In addition to a host of pungent and other chemicals that either covalently interact with (isothiocyanates, cinnamaldehyde, acrolein, and allicin) or bind to TRPA1 (cannabinoids, icilin, eugenol, thymol, and nicotine), the channel can also be activated by deep cooling (<17 °C) or depolarizing (>+100 mV) voltages (3–10).

One of the ubiquitous and probably the most important physiological activators of TRPA1 are calcium ions (Ca^{2+}), which enter through the channel or are released from internal stores and, depending on the activation state of the channel, dynamically control its critical properties such as unitary conductance, ion selectivity, channel opening probability (8, 11–13), and surface expression levels (14). At micromolar concentrations, Ca^{2+} ions activate the channel from the intracellular side ($EC_{50} = 0.9 - 6\ \mu M$) (15, 16) and strongly potentiate its chemically and voltage-induced responses. This potentiation is followed by an almost complete and irreversible inactivation, and both processes are accelerated at higher intracellular concentrations of Ca^{2+} (17). Although physiologically extremely important, the molecular mechanisms of Ca^{2+}-dependent activation and inactivation are still a matter of controversy.

The obvious candidates for a domain through which Ca^{2+} could modulate TRPA1 are acidic residues on the intracellular side of TRPA1; unfortunately, information about the potential role of this portion of the receptor is still very scarce, and it is difficult to single out, in the human isoform, from the 112 cytoplasmic acidic residues. As for the cytoplasmic C terminus, evidence for the important functional roles of charged regions came from recent studies identifying a number of basic residues that confer both chemical and voltage sensitivity to the TRPA1 channel, several of them located within or near the two penultimate α-helices H4 and H5 (18). These two predicted helices flank a loop containing a highly conserved acidic stretch of amino acids, ^{1077}ETEDDD^{1082} (see Fig. 1*A*), and sharing sub-

* This work was supported by Czech Science Foundation Grant 305/09/0081, Research Project Fund of the Academy of Sciences of the Czech Republic Grant AV0Z50110509, and Ministry of Education, Youth and Sports of the Czech Republic Grants 1M0517, MSM0021620835, SVV-2010-261 304, and GAUK 426311.
[S] This article contains supplemental Fig. S1.
[1] To whom correspondence should be addressed: Inst. of Physiology AS CR, Videnska 1083, 142 20 Prague 4, Czech Republic. Tel.: 420-29644-2711; Fax: 420-29644-2488; E-mail: vlachova@biomed.cas.cz.

[2] The abbreviations used are: TRPA1, transient receptor potential ankyrin 1; Cin, cinnamaldehyde; RMSD, root mean square deviation.

stantial sequence similarity with the Ca^{2+}-binding domain found in the hBest1 channel (19) or the so-called Ca^{2+} bowl domain of the superfamily of BK channels (20). Here we examined the role of the above conserved acidic sequence motif and found that it is involved in the Ca^{2+}-mediated modulation of TRPA1.

MATERIALS AND METHODS

Expression and Constructs of hTRPA1 Channel—HEK293T cells were cultured in Opti-MEM I medium (Invitrogen) supplemented with 5% FBS as described previously (21, 22). The cells were transiently co-transfected with 300–400 ng of cDNA plasmid encoding wild-type or mutant human TRPA1 (wild type in the pCMV6-XL4 vector, OriGene) and with 300 ng of GFP plasmid (TaKaRa) per 1.6-mm dish using the magnet-assisted transfection (IBA GmbH) method. The cells were used 24–48 h after transfection. At least two independent transfections were used for each experimental group. The wild-type channel was regularly tested in the same batch as the mutants. For membrane-targeting experiments, we used the C-terminally GFP-tagged mutant D1080A of hTRPA1 (wild type in the pCMV6-AC-GFP vector; OriGene) and the cyan fluorescent protein-tagged pleckstrin homology domain of phospholipase C δ1 (kindly provided by Tamas Balla, NICHD, National Institutes of Health, Bethesda, MD). For fluorescence measurements, we used the Cell^R imaging system based on an Olympus IX-81 inverted microscope (Olympus) equipped with a dual emission setup (Dual-View Optical Insights), a Polychrome V polychromator (Till Photonics), and a Hamamatsu Orca ER camera (Hamamatsu Photonics). Intensity profiles were measured using the program ImageJ (National Institutes of Health). The mutants were generated by PCR using the QuikChange XL site-directed mutagenesis kit (Stratagene) and confirmed by DNA sequencing (ABI PRISM 3100; Applied Biosystems).

Electrophysiology—Whole cell membrane currents were recorded by employing an Axopatch 200B amplifier and pCLAMP 10 software (Molecular Devices). Patch electrodes were pulled from a glass tube with a 1.65-mm outer diameter. The tip of the pipette was heat-polished, and its resistance was 3–5 MΩ. Series resistance was compensated by at least 70% in all recordings. The experiments were performed at room temperature (23–25 °C). Only one recording was performed on any one coverslip of cells to ensure that recordings were made from cells not previously exposed to chemical stimuli. Conductance-voltage (*G-V*) relationships were obtained from steady-state whole cell currents measured at the end of voltage steps from −80 to +200 mV in increments of +20 mV. Voltage-dependent gating parameters were estimated by fitting the conductance $G = I/(V - V_{rev})$ as a function of the test potential V to the Boltzmann equation: $G = [(G_{max} - G_{min})/(1 + \exp(-zF(V - V_{½})/RT))] + G_{min}$, where z is the apparent number of gating charges, $V_{½}$ is the half-activation voltage, G_{min} and G_{max} are the minimum and maximum whole cell conductance, V_{rev} is the reversal potential, and F, R, and T have their usual thermodynamic meaning. A system for rapid superfusion of the cultured cells was used for drug application (23). The extracellular bath solutions contained: 150 mM NaCl and 10 mM HEPES, with an added 2 mM HEDTA for the Ca^{2+}-free solution, and 2 or 10 mM $CaCl_2$, for the Ca^{2+}-containing solutions, adjusted to pH 7.3 with NaOH, 300 mOsm. The *I-V* relationships were measured in the bath solution containing 160 mM NaCl, 2.5 mM KCl, 1 mM $CaCl_2$, 2 mM $MgCl_2$, 10 mM HEPES, 10 mM glucose, adjusted to pH 7.3 and 320 mOsm. The whole cell pipette solution contained the high buffer internal solution: 145 mM CsCl, 5 mM EGTA, 3 mM $CaCl_2$, 10 mM HEPES, 2 mM MgATP, pH 7.3, adjusted with CsOH, 320 mOsm. The pipette solution containing 100 μM free Ca^{2+} was obtained by adding 10.24 mM Ca^{2+} and 10 mM EGTA to the internal solution. Cinnamaldehyde solution was prepared prior to use from a 0.1 M stock solution in Me_2SO. All of the chemicals were purchased from Sigma-Aldrich.

Homology Modeling and Molecular Dynamics Simulations—The structure of the human BK channel was obtained from the Protein Data Bank (code 3MT5). The BK-TRPA1 chimera was constructed by replacing Ca^{2+} bowl residues (20) with homologous residues from human TRPA1. Sequences were aligned with ClustalW software (24) and then manually refined to ensure the alignment of conserved residues in the TRPA1 channel matches calcium-binding residues in the Ca^{2+} bowl of the BK channel. A model of the chimera was built using the software package MODELLER (25) resulting in 10 candidate models. The best structure was selected according to the MODELLER objective function, deviation of unmodified parts of the channel from the template and visual inspection. An all-atom structure was generated using the program LEaP from the AMBER suite (26) using the Amber99SB force field and TIP3P water model. One calcium ion and sulfate ion was added at a location corresponding to the template. Total net charge of the structure was neutralized using 17 sodium ions, and the structure was solvated with 21,109 water molecules. The initial equilibration of the system was performed using NAMD2.7 (27) with a time step of 1 fs, cutoff 10 Å, Particle Mesh Ewald grid size of 128 × 128 × 128, Langevin damping 5/ps. The system was first minimized for 10,000 steps and then thermalized to 310 K and equilibrated at 1 atm for 1 ns. Volume and potential energy was monitored and reached stable values. For production runs, we used the ACEMD software package (28) running on a local work station equipped with an Nvidia GPU. The simulations were run in the NVT ensemble with the same parameters as for equilibration, except a time step of 4 fs enabled by the hydrogen mass repartition scheme (29). Data were analyzed using the program PTRAJ from the AMBER suite (26) and visualized using VMD (30).

Statistical Analysis—All of the data were analyzed using pCLAMP 10 (Molecular Devices), and curve fitting and statistical analyses were done in SigmaPlot 10 (Systat Software). Statistical significance was determined by Student's *t* test or the analysis of variance; differences were considered significant at $p < 0.05$, where not stated otherwise. For statistical analysis of T_{50} data, a logarithmic transformation was used to achieve normal distribution. All of the data are presented as the means ± S.E.

RESULTS

Truncations in C Terminus Reveal Region Involved in Ca^{2+}-dependent Inactivation—We set out to investigate the Ca^{2+}-dependent potentiation and Ca^{2+}-dependent inactivation in human TRPA1 channels transiently expressed in HEK293T

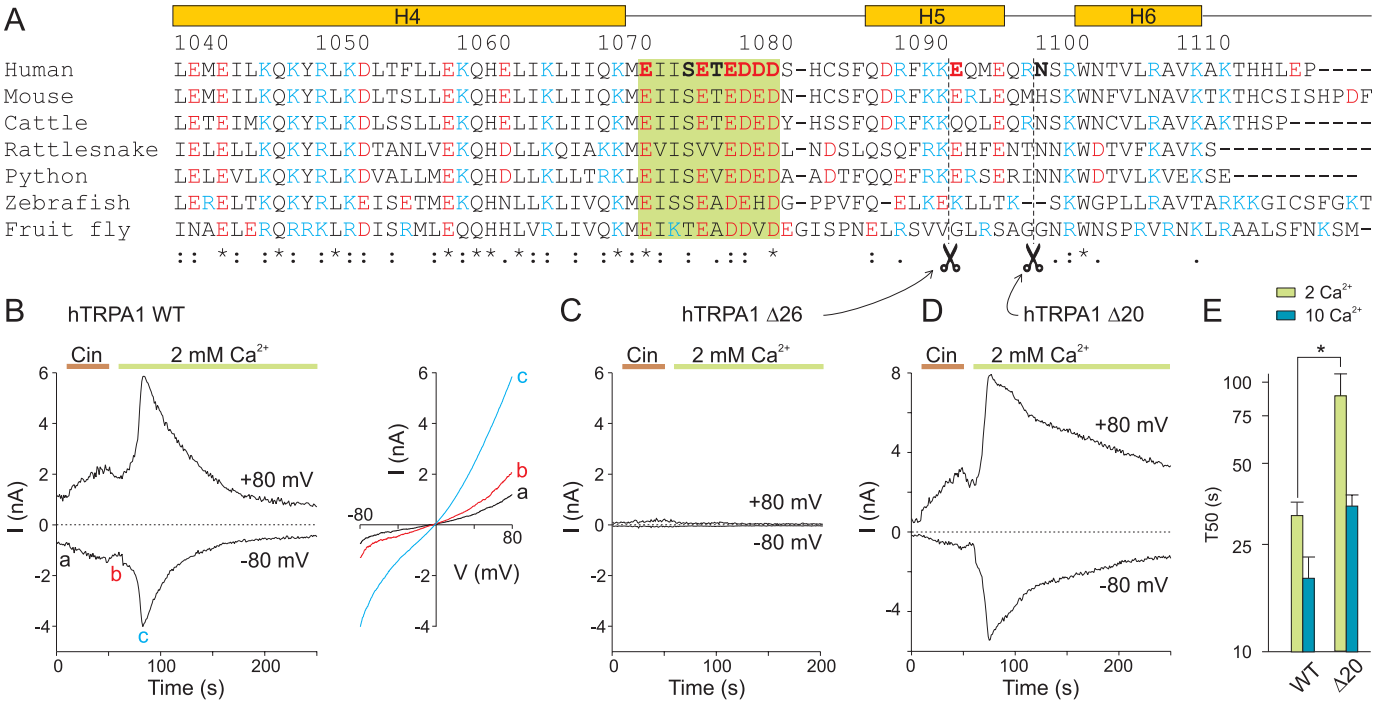

FIGURE 1. **Truncations in C terminus reveal region involved in Ca^{2+}-dependent inactivation.** *A*, alignment of distal C terminus of TRPA1 from various species. The predicted secondary structure for hTRPA1 is indicated above the alignment. The region of interest is *boxed*. The residues in human TRPA1 that were mutated in this study are indicated in *bold type*. *B*, time course of representative whole cell currents through human TRPA1 measured at +80 mV and −80 mV as marked. The application of 100 μM Cin and subsequent addition of 2 mM Ca^{2+} are indicated above. The *right panel* shows current-voltage relationships of traces measured at times indicated by *a*, *b*, and *c*. *C* and *D*, voltage-ramp protocol as in *B* used for truncation mutants. Note the obviously slower inactivation of the TRPA1-Δ20 truncation mutant upon the addition of 2 mM Ca^{2+} to the bath solution compared with WT in *B*. *E*, average rate of current decay represented as T_{50} for wild-type TRPA1 and truncation mutant TRPA1-Δ20. To obtain a similar rate of inactivation to the wild-type TRPA1, a 5-fold higher concentration of calcium needed to be introduced for the TRPA1-Δ20 mutant. *, $p = 0.006$, Student's *t* test. The data represent the means ± S.E.; $n \geq 6$ for wild type and $n \geq 3$ for mutant.

cells. Because some activation properties considerably differ between the mammalian TRPA1 orthologs, we first quantified the effects of Ca^{2+} by exploiting the same stimulation protocol as has been previously used by Wang *et al.* (17) for a detailed characterization of the rat TRPA1 variant (Fig. 1*B*). The membrane potential was ramped from −80 to +80 mV (1 V/s), and whole cell membrane currents were measured in the absence of extracellular Ca^{2+} and in the presence of agonist (cinnamaldehyde, Cin, 100 μM for 40 s). The agonist was then washed out for 10 s, and Ca^{2+} at a concentration of 2 mM or 10 mM was added to the extracellular solution. Intracellular Ca^{2+} was buffered with 5 mM EGTA in the patch pipette. In accordance with (17), Cin evoked slowly developing currents (2.4 ± 0.2 nA at +80 mV after 40 s, $n = 38$) that slightly relaxed (by 17 ± 1%) to a lower maintained level upon washout. The addition of Ca^{2+} to the bath solution induced a marked potentiation that was followed by an inactivation that was almost complete within 1 min (Fig. 1*B*). The degree of Ca^{2+}-induced potentiation was quantified as the fold increase in the amplitude after the addition of Ca^{2+} with respect to the preceding current level. For 2 mM Ca^{2+}, this value was 4.0 ± 0.4 at +80 mV and 6.0 ± 1.1 at −80 mV ($n = 24$), which is higher than that for the rat ortholog and is in good agreement with the value previously reported for human TRPA1 (17). The 10–90% rise time for potentiation was clearly dependent on external Ca^{2+}, being 7.8 ± 1.0 and 2.5 ± 0.5 s ($n = 22$ and 16) for 2 and 10 mM Ca^{2+}, respectively.

For Ca^{2+}-dependent inactivation, the decay was adequately described using a half-decay time, relative to the peak (T_{50}). After the introduction of 2 mM Ca^{2+}, the currents decayed to 50% of their peak value in 31.9 ± 4.0 s at +80 mV and in 18.9 ± 2.0 s at −80 mV ($n = 19$). At 10 mM Ca^{2+}, the inactivation was substantially faster (16.3 ± 3.0 s at +80 mV and 11.2 ± 2.0 s at −80 mV; $n = 15$), which was most likely the cause of a concomitant reduction in the degree of Ca^{2+}-induced potentiation (3.1 ± 0.4), compared with 2 mM Ca^{2+} ($p = 0.15$). We did not find any clear correlation between T_{50} and the degree of Ca^{2+}-dependent potentiation ($r = -0.35$, 2 mM Ca^{2+}, +80 mV; $n = 19$; Spearman's rank order correlation), which supports the previous suggestion that the inactivation of TRPA1 is not strictly coupled to potentiation (11, 17, 31).

Having established the main characteristics of the Ca^{2+}-dependent modulation for wild-type channels, we constructed a series of mutants in which the negative charges in the C-terminal subregion Glu^{1073}–Asp^{1082} were individually neutralized by alanine substitution. In addition, two charge-reversing mutations were created for the acidic cluster glutamates, E1077K and E1079K. Furthermore, to test the overall structural requirements of the distal C terminus for channel activation, we introduced stop codons at Glu^{1094} and Asn^{1100}, resulting in two C-terminal truncation mutants, TRPA1-Δ20 and TRPA1-Δ26. The conservation of the primary structure of this region and the residues chosen for mutagenesis are summarized and depicted in Fig. 1*A*.

Mutation TRPA1-Δ26 did not produce measurable currents in response to any of the stimuli tested, thus preventing further evaluation (Fig. 1*C*). In contrast, functional channels were

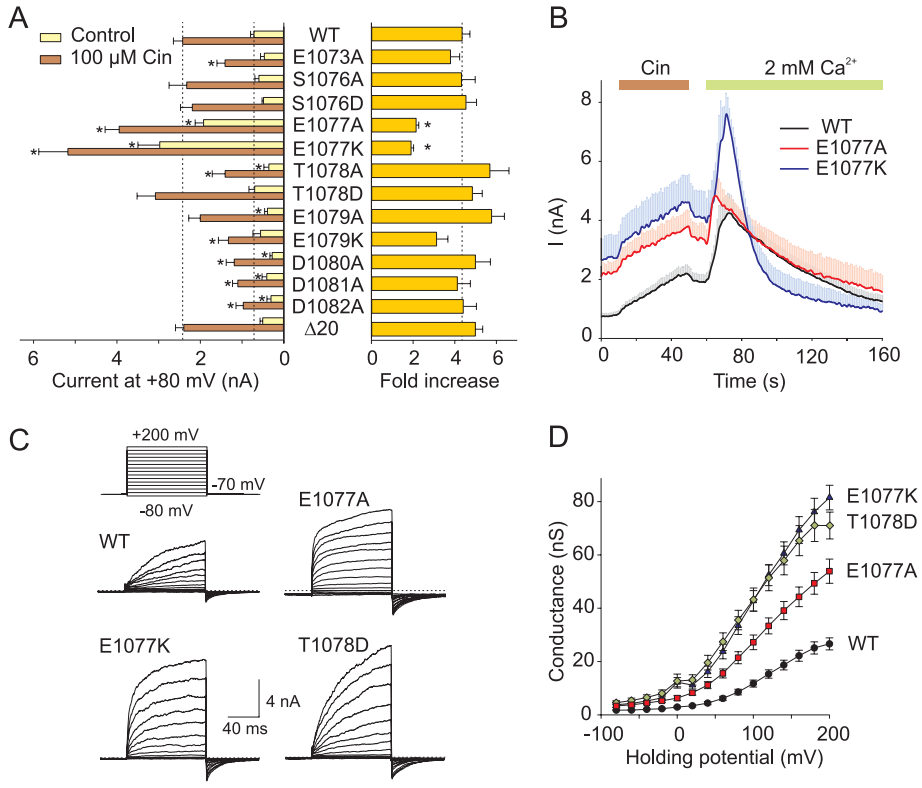

FIGURE 2. **Mutations in C-terminal acidic region alter voltage and cinnamaldehyde sensitivity of TRPA1.** *A*, *left bar graph* depicts average TRPA1 currents at +80 mV in Ca^{2+}-free extracellular solution before (control) and after 40 s of 100 μM Cin exposure. The *right bar graph* indicates relative activation by Cin for wild-type channel and individual mutants. The data represent the means ± S.E.; $n \geq 6$. The *asterisks* indicate significant differences between mutant and wild-type TRPA1. *, $p < 0.05$, unpaired *t* test. *Broken vertical lines* indicate the mean values obtained from wild-type TRPA1. *B*, average currents at +80 mV for wild-type TRPA1 and gain of function mutants E1077A and E1077K. The *horizontal bars* above the records indicate the duration of Cin and Ca^{2+} application. Note the difference in basal activation level at the very beginning of the record. The data represent the means ± S.E. for $n \geq 6$. *C*, representative current traces in response to indicated voltage step protocol (holding potential, −70 mV; voltage steps from −80 to +200 mV; increment +20 mV), recorded ~1 min after whole cell formation. The bath solution contained 160 mM NaCl, 2.5 mM KCl, 1 mM $CaCl_2$, 2 mM $MgCl_2$, 10 mM HEPES, 10 mM glucose. *D*, average conductances obtained from voltage step protocols as in *C*. The data represent the means ± S.E.; $n \geq 8$.

obtained with the TRPA1-Δ20 truncation mutant (Fig. 1*D*). Compared with wild-type TRPA1, this mutant exhibited strikingly slower inactivation upon the addition of Ca^{2+} (T_{50} of 89.0 ± 18.4 s for 2 mM Ca^{2+} and 34.7 ± 6.0 s for 10 mM Ca^{2+}; $p < 0.01$; $n = 6$ and 3; Fig. 1*E*). In other respects, this truncation mutant exhibited a normal degree of Ca^{2+}-induced potentiation (3.0 ± 0.1; $p = 0.63$; $n = 6$) and a normal responsiveness to voltage and Cin (Fig. 2*A*). The finding that truncation of the C terminus by a further six residues was deleterious indicates an important functional role for the distal part of the C terminus, particularly a likely structural role of the predicted α-helix H5. These initial screenings identified the distal C terminus as a critical modulatory domain of TRPA1 involved in its Ca^{2+}-dependent inactivation, and we therefore further examined whether the acidic region preceding this H5 helix could play its presumed role of a high affinity Ca^{2+} sensing site.

Mutations in C Terminus Reveal Strongly Sensitizing TRPA1 Phenotypes—The functionality of all constructed mutants was compared by measuring the maximum outward currents at +80 mV, in the absence and presence of 100 μM Cin. We detected a dramatic increase in the amplitude of the outward currents induced by voltage ramps in control Ca^{2+}-free bath solution through the E1077A and E1077K mutant channels at the 0.01 probability level (Fig. 2, *A* and *B*). Also, the conductance to voltage (*G-V*) relationships for these two mutants were significantly shifted toward less depolarizing potentials (the voltage for half-maximal activation, V_{50}, 110.8 ± 5.8 and 104.5 ± 6.0 mV; $n = 18$ and 12), compared with wild-type TRPA1 channels (128.0 ± 2.7 mV; $n = 57$; Fig. 2, *C* and *D*). In E1077K, but not in E1077A, the inactivation produced by the introduction of 2 mM Ca^{2+} was significantly faster compared with the wild type ($T_{50} = 14.4 \pm 5.5$ s; $n = 6$; $p < 0.05$), and the currents decayed to a steady value 66 ± 10% below their initial basal activity levels (Fig. 2*B*). In both mutants, E1077A and E1077K, the degree of potentiation of Cin responses by 2 mM Ca^{2+} was markedly reduced (2.5 ± 0.4; $n = 6$; $p = 0.087$ and 1.9 ± 0.3; $n = 7$; $p = 0.009$), obviously because of their initial close to saturation state at +80 mV.

We suspected that this sensitizing effect reflected either a gain of function (constitutively active) phenotype or tonic activation caused by an increased expression of the functional mutant channels on the cell surface. Indeed, within our region of interest, a sequence prediction analysis revealed two strong consensus phosphorylation motifs containing serine 1076 and threonine 1078, both predicted to be targeted by casein kinase CK2 (as determined from the prediction servers NetPhosK or NetPhorest). A similar phosphorylatable acidic cluster has been reported to constitute a cytosolic sorting motif that controls the trafficking and surface expression of some ion channels, including TRPA1-related TRPP2 and TRPV4 (32). To test this possi-

bility, we constructed additional four mutants in which either serine or threonine were replaced by either alanine or aspartate to mimic the nonphosphorylated and phosphorylated forms of the protein, respectively. To our surprise, mutation T1078D resulted in TRPA1 channels whose conductance to voltage (*G-V*) relationships were also strongly augmented (from 27 ± 2 to 71 ± 5 nS at +200 mV; $n = 59$ and $n = 8$) and shifted toward less depolarizing potentials (V_{50}, 98.1 ± 6.8 mV; Fig. 2*D*). This mutant responded relatively normally to Cin in Ca^{2+}-free bath solution (Fig. 2*A*) but had a faster 10–90% rise time of outward current potentiation of Cin responses upon the addition of 2 mM Ca^{2+} (2.7 ± 0.2 s; $n = 4$; $p < 0.05$) and slightly ($p = 0.094$) faster inactivation (16.1 ± 5.2 s; $n = 5$) compared with the T_{50} for wild-type channels.

Whereas T1078D was observed to have large effects on voltage-dependent activation when using the voltage-step protocol (Fig. 2, *C* and *D*), only modest effects on voltage- and cinnamaldehyde-dependent activation were seen when the standard voltage-ramp protocol was utilized (Fig. 2*A*). This apparent divergence seemed to be due to the alterations in the onset kinetics upon voltage changes ($\tau_{on} = 36 \pm 3$ ms *versus* 59 ± 5 ms for wild-type; measured at +160 mV; $n = 6$ and 17; Fig. 2*C*) and indicates that mutation T1078D affected the gating kinetics of TRPA1. This interpretation is further supported by our finding that mutation T1078A exhibited substantially reduced responses to voltage and Cin and was capable of strong potentiation by 2 mM Ca^{2+} (5.5 ± 0.8; $n = 6$; $p = 0.125$). The nonphosphorylatable mutant S1076A and the phosphorylation-mimicking S1076D mutant channels were otherwise normal in all general aspects of functionality.

This series of experiments indicates that a single mutation at Glu^{1077}, or the introduction of an additional negative residue at Thr^{1078} are both likely to destabilize the charge balance at the highly acidic C-terminal cluster of TRPA1. The findings that a neutralizing or charge-reversing mutation at Glu^{1077} had sensitizing effects support the notion that the functional changes caused by mutations are likely to be steric or local, rather than affected by increased membrane insertion of the channels because of disruption of a phosphorylation consensus. Moreover, single point mutations at the specific residues, located in the primary sequence far from the membrane proximal regions, are capable of increasing the sensitivity of TRPA1 to membrane voltage without affecting its responsiveness to Cin. In other words, a pathway distinct from voltage-dependent modulation and covalent modification effectively controls the activity of TRPA1 via conformational changes in the C-terminal acidic region.

Asp^{1080}, Asp^{1081}, and Asp^{1082} Are Residues Most Involved in Ca^{2+}-induced Potentiation of TRPA1—When the maximum Cin-induced outward currents were related to the control voltage-induced responses obtained at the same membrane potential of +80 mV, none of the single mutations, apart from E1077A and E1077K, exhibited a substantially decreased relative sensitivity to Cin compared with wild-type TRPA1, as depicted in Fig. 2*A*. What we found, however, was that the kinetics of the Ca^{2+}-dependent potentiation were dramatically changed in four out of the six charge-neutralized mutants: E1073A, D1080A, D1081A and D1082A. The former mutation strongly increased the degree of Ca^{2+}-dependent potentiation at both Ca^{2+} concentrations and caused a delay in the peak potentiation time in a significant number of cells (Fig. 3, *A* and *B*). Distinct phenotypes were generated by the latter three neutralizing mutations. Not only did these mutations lead to a marked slowing down of the rise time and delayed the peak potentiation time, they also led to a strongly reduced averaged degree of potentiation observed within an interval of ~120 s after the introduction of Ca^{2+}, which was readily apparent from the averaged current traces obtained from all cells tested (Fig. 3*A*). Ca^{2+}-dependent potentiation was most apparently blunted in the D1080A mutant. In five of ten D1080A-expressing cells that were treated with 2 mM Ca^{2+} and in three out of seven cells treated with 10 mM Ca^{2+}, no potentiation at all was observed within the time interval tested (3–4 min); instead, the Cin-induced currents decayed in the presence of Ca^{2+} to their initial value obtained before the agonist was applied to these cells (Fig. 3*A*). Weaker but similar effects were observed in D1081A and D1082A. The former mutation produced currents that also exhibited a "delayed phenotype", but when measured over a period longer than the median time to peak for the wild type (14 s), they frequently attained a similar degree of potentiation to wild-type TRPA1 (Fig. 3, *A* and *B*).

For wild-type channels, the peak potentiation time, measured from the time at which 2 mM Ca^{2+} was introduced, varied from 4 s to more than 30 s with a median of 14 s ($n = 22$) and this value became lower and normally distributed around the mean of 6.0 ± 1.1 s when the external Ca^{2+} concentration was increased to 10 mM ($n = 16$; Fig. 3*C*). The maximum potentiation time has been previously shown to depend on external Ca^{2+} concentration (17), and thus the observed changes in the kinetics of the Ca^{2+}-dependent modulation in the mutants shown in Fig. 3*A* could be due to a decreased sensitivity to external Ca^{2+}. Because the data for peak potentiation time in wild-type TRPA1 was not normally distributed, to achieve reliable statistical significance in the distribution for the mutants would require an unrealistically large number of cells to be tested for each group. However, it was still evident that the period of maximum potentiating effect was delayed in a considerable proportion of cells expressing D1080A, D1081A and D1082A (Fig. 3*A* and supplemental Fig. S1). The most affected mutant, D1080A, was functionally well expressed (Fig. 2*A*) and appeared to be correctly targeted to the cell membrane (Fig. 3*D*). In this mutant, the addition of a higher concentration of external Ca^{2+} (10 mM) reduced the 10–90% rise time (from 18.7 ± 7.2 s to 7.0 ± 2.4 s; measured from five and four responding cells; Fig. 4*A*), accelerated inactivation (Fig. 4*B*), and increased both the degree and probability of occurrence of the maximum Ca^{2+}-induced potentiating effect (Fig. 4*C*).

The high buffer internal solution used in our experiments was estimated to contain 150 nM free Ca^{2+}, which approximately corresponds to the basal intracellular concentration of Ca^{2+}. We therefore further tested whether allowing the internal concentration of Ca^{2+} to increase would change the activity, especially for the D1080A mutant, which exhibited the most significantly modified kinetics of Ca^{2+}-dependent potentiation. We compared the degree of potentiation and the rate of inactivation in cells dialyzed with an intracellular solution containing 100 μM free Ca^{2+} (Fig. 4, *C* and *D*). Under these condi-

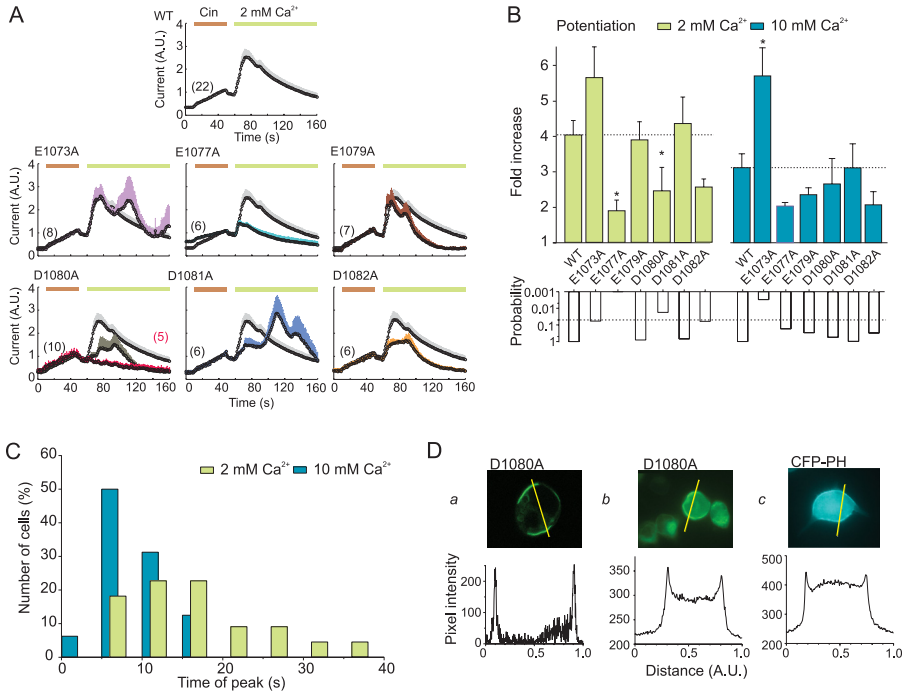

FIGURE 3. **Potentiation of TRPA1 mutants by extracellular Ca^{2+}.** *A*, average TRPA1 currents evoked in response to 40 s of exposure to 100 μM Cin and subsequent addition of 2 mM Ca^{2+} as indicated by *horizontal bars*. The average current for the wild type is shown for comparison in *gray* in each plot. The currents are normalized to their maximal cinnamaldehyde responses obtained prior to the addition of Ca^{2+} to the bath solution. The data represent the means ± S.E. for the number of cells indicated. For D1080A, the average current for nonpotentiated cells (in *red*) is overlaid onto the average current from all cells. *B*, average data from experiments as in *A*. Calcium-induced potentiation was measured as the fold increase in current, measured at +80 mV, following the addition of 2 mM (*left bar graph*) or 10 mM (*right bar graph*) extracellular Ca^{2+}. The *asterisks* indicate significant differences between mutant and wild-type TRPA1. *, $p < 0.05$, unpaired *t* test. The *lower bar graph* represents the probabilities obtained from the *t* tests that compared the individual mutants with the wild type. *C*, distribution of time to peak of Ca^{2+}-induced potentiation for wild-type TRPA1 channels. For 2 mM Ca^{2+}, four cells had time-to-peak outside the range of 60 s. *D*, D1080A mutant of hTRPA1 expresses on the surface of HEK293T cells to a similar level as a control molecule containing membrane-targeting motif. *Panel a*, typical confocal image from cell expressing D1080A mutant of the C-terminally GFP-tagged human TRPA1 and a fluorescence intensity profile plotted for the cross-section indicated above. *Panel b*, wide-field fluorescence image of HEK293T cell expressing D1080A mutant of the C-terminally GFP-tagged human TRPA1. The excitation wavelength was 470 nm, and emission was detected at 530 nm. *Below* is a fluorescence intensity profile plotted for the cell and a cross-section (marked by *line*) indicated above. *Panel c*, wide field fluorescence image of a fluorescent marker for the membrane surface, cyan fluorescent protein-tagged pleckstrin homology domain of phospholipase Cδ1 (*CFP-PH*), expressed in another HEK293T cell for comparison. *Below*, typical fluorescence intensity profile plotted for the cell and cross-section indicated above. The excitation wavelength was 430 nm, and emission was detected at 475 nm.

tions, the D1080A mutant channels produced robust currents in response to Cin in Ca^{2+}-free bath solution, and after the addition of external 10 mM Ca^{2+}, the currents were consistently potentiated (2.2 ± 0.4-fold; $n = 5$) without any delay. In contrast, Ca^{2+}-induced responses through wild-type channels dialyzed with the same internal solution were mostly inactivated immediately after the addition of external 10 mM Ca^{2+}, indicating a predominant effect on promoting inactivation over Ca^{2+}-induced potentiation (Fig. 4*C*). Despite differences between D1080A and wild-type channels in the degree of potentiation, we did not detect any difference in the rate of inactivation between D1080A-expressing cells dialyzed with an intracellular solution containing 100 μM free Ca^{2+} (T_{50} of 16.9 ± 4.6 s; $n = 5$) and the wild-type channels ($p = 0.919$) or the D1080A mutant channels (12.1 ± 2.0 s; $p = 0.374$; $n = 4$), measured with the high buffer internal solution. Because the identified mutation D1080A exhibits a normal responsiveness to Cin and approaches the wild-type phenotype when internal Ca^{2+} is allowed to increase to 100 μM, these results suggest that this mutation most likely has an effect on Ca^{2+} affinity.

Molecular Dynamics Simulations Indicate That C-terminal Acidic Cluster Is Capable of Playing Role of High Affinity Ca^{2+}-binding Site—The observations that Asp^{1080} indeed contributes to the Ca^{2+}-dependent modulation of TRPA1, together with the fact that substitutions at Glu^{1077} produced sensitized phenotypes, further supports the idea that the whole region containing the cluster of negative residues is structurally important and involved in the Ca^{2+}-dependent modulation of TRPA1. How could the C-terminal acidic domain in TRPA1 accomplish the role of a high affinity Ca^{2+} sensor?

To address this question, we utilized molecular dynamics simulations to probe the Ca^{2+}-binding capability of the acidic region from TRPA1, using the Ca^{2+} activation apparatus of the human BK channel (20) as the template protein (hSlo1; Protein Data Bank entry code 3MT5). Each of the four α subunits of the high conductance, Ca^{2+}- and voltage-activated potassium BK channel contain two tandem regulatory C-terminal domains (RCK) that form an intracellular gating ring (33). The second of these domains (RCK2) encompasses a primary binding site for Ca^{2+}, known as the Ca^{2+} bowl, which exhibits a considerable sequence similarity to the C-terminal acidic sequence of TRPA1 (Fig. 5*A*). We used homology modeling to replace the stretch of 10 consecutive residues Gln^{889}–Asp^{898} (QFLDQDDDD) in the structure of the Ca^{2+}-binding domain of BK with 10 residues Ile^{1074}–Ser^{1083} (IISETEDDDS) from human TRPA1 (Fig. 5*B*), and using molecular dynamics simulations, we explored whether this region is capable of binding Ca^{2+}. The system was simulated for a total of 200 ns after equilibra-

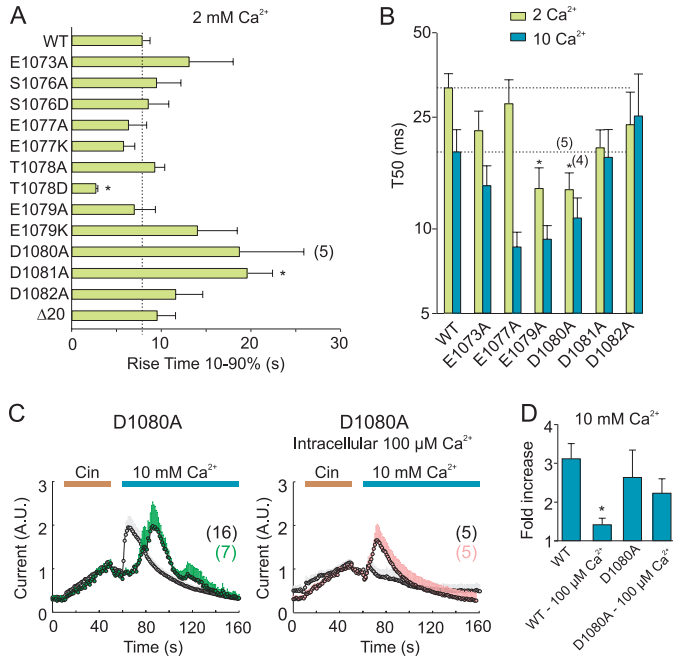

FIGURE 4. **Mutations in C-terminal acidic domain affect kinetics of Ca^{2+}-induced potentiation.** *A*, 10–90% rise time of Ca^{2+}-induced potentiation (2 mM) for wild-type and mutant TRPA1. The *broken vertical line* indicates the mean value obtained from wild-type TRPA1. *B*, average data from experiments as in Fig. 3*A*. Inactivation was measured at +80 mV and quantified as the time, relative to the peak, at which the currents had decayed to 50% of their maximum value. The *broken horizontal lines* indicate the mean values obtained from wild-type TRPA1 for 2 and 10 mM Ca^{2+}. In *A* and *B*, *asterisks* indicate significant differences between mutant and wild-type TRPA1. *, $p < 0.05$, unpaired *t* test. *C*, *left panel*, increasing the concentration of extracellular Ca^{2+} from 2 mM to 10 mM partially restored the Ca^{2+}-induced potentiation in D1080A. *Right panel*, increasing the intracellular Ca^{2+} concentration from 150 nM to 100 μM restored the potentiation of the cinnamaldehyde-induced currents in the D1080A mutant channels. The average current for the wild type is shown for comparison in *gray* in each plot. The currents are normalized to their maximal cinnamaldehyde responses obtained prior to the addition of Ca^{2+} to the bath solution. The data represent the means ± S.E. for the number of cells indicated. *D*, average data from experiments as in *C*, quantified as in Fig. 3*B*. The *asterisk* indicates a significant difference from wild-type TRPA1 measured with the high buffer internal solution containing 5 mM EGTA in the patch pipette. *, $p = 0.01$, unpaired *t* test.

tion. The time course of the root mean square deviation (RMSD) over the 200-ns period indicates that the system was sufficiently relaxed after 70 ns, and the calcium-binding motif was sufficiently relaxed after 110 ns (Fig. 5*C*). The displacement of the calcium ion inside the calcium-binding motif was under 1 Å for most of the simulation (Fig. 5*C*), indicating that the ion was quite stable. A significant increase in RMSD at the end of the simulation was identified to be caused by the loose ends of the polypeptides at residues 833–869. The structure between these residues is missing from the Protein Data Bank structure 3MT5 and is missing from the model structure as well. Therefore, we explored the influence of excluding these loose ends (residues 830–862) from the RMSD calculation (Fig. 5*C*). Because these residues do not interact with the residues of interest, except for weak interactions in the last 25 ns of the run, we do not expect this to have significant influence on the simulation results presented here.

The results of this computational experiment confirm that the calcium ion is bound in the structure and thus prove the ability of the acidic cluster from the TRPA1 C terminus to form a Ca^{2+}-binding domain. Fig. 5*D* depicts the time course of the number of calcium contacts with the protein and in total. The average number of contacts throughout the simulation period was 7.6, which is in good agreement with experimental measurements carried out on various other Ca^{2+}-binding proteins (34). Two residues, Ile^{889} (Ile^{1074} in TRPA1) and Glu^{892} ($Glu1077$), are in contact with the calcium ion via their main chain carbonyl oxygen atoms (Fig. 5*C*). Two residues, Asp^{895} (Asp^{1080}) and Asp^{897} (Asp^{1082}), use oxygen atoms from their side chains for direct contact with the calcium ion. These bonds are largely stable throughout the whole simulation period, which is again in good agreement with the binding mechanism of calcium ions in the Ca^{2+} bowl in the BK cytoplasmic domain (20).

To further test the model and to explore the effects of mutations on the stability of calcium ion binding, we performed additional molecular dynamics simulations using *in silico* alanine mutations: E894A, D895A, D896A, and D897A (E1079A, D1080A, D1081A, and D1082A in TRPA1). Disruptions of the calcium-binding pocket were observed in D895A (D1080A) and in D897A (D1082A) after, respectively, 11 and 4 ns of molecular dynamics simulation (Fig. 6*A*). Mutations E894A (E1079A) and D896A (D1081A) had no effect on the stability of calcium binding during a 20-ns simulation. These findings substantiate the importance of the residues D1080A and D1082A for Ca^{2+} binding.

Next, we examined whether the side chain volume at positions Asp^{1080} and Asp^{1082} is important for the functionality of the channel. Using site-directed mutagenesis, we individually replaced these two residues with isoleucine and measured whole cell responses to Cin in the absence and presence of 2 mM Ca^{2+} (Fig. 6*B*). Similar to what has been observed for D1080A, mutation D1080I produced channels that responded normally to cinnamaldehyde but exhibited strong changes in Ca^{2+}-dependent modulation. In three of seven D1080I-expressing cells that were treated with 2 mM Ca^{2+}, no potentiation at all was observed within the time interval tested (Fig. 6*B*, *left panel*). The D1082I mutant exhibited even more pronounced defects (compared with D1082A and the wild type), yielding channels that produced robust currents in response to Cin in Ca^{2+}-free bath solution, but the addition of external 2 mM Ca^{2+} did not exert any noticeable effect within the time interval tested (Fig. 6*B*, *right panel*). These results indicate that the side chain volume at Asp^{1082} is important for channel function and that isoleucine substitution at this position may create steric hindrance for Ca^{2+} access to the acidic region.

DISCUSSION

In this study, we identify the residues within the distal C-terminal domain of the human ankyrin receptor TRPA1 that when mutated affect the Ca^{2+}- and voltage-dependent gating of the channel. The first key finding of our study is that truncation of the C-terminal domain by 20 amino acids reduces the inactivation of the TRPA1 channel without altering its activation by the thiol-reactive compound cinnamaldehyde or the degree of Ca^{2+}-dependent potentiation. This result provides further support for the previous suggestion that the inactivation mechanism of TRPA1 is not coupled to activation/potentiation (17).

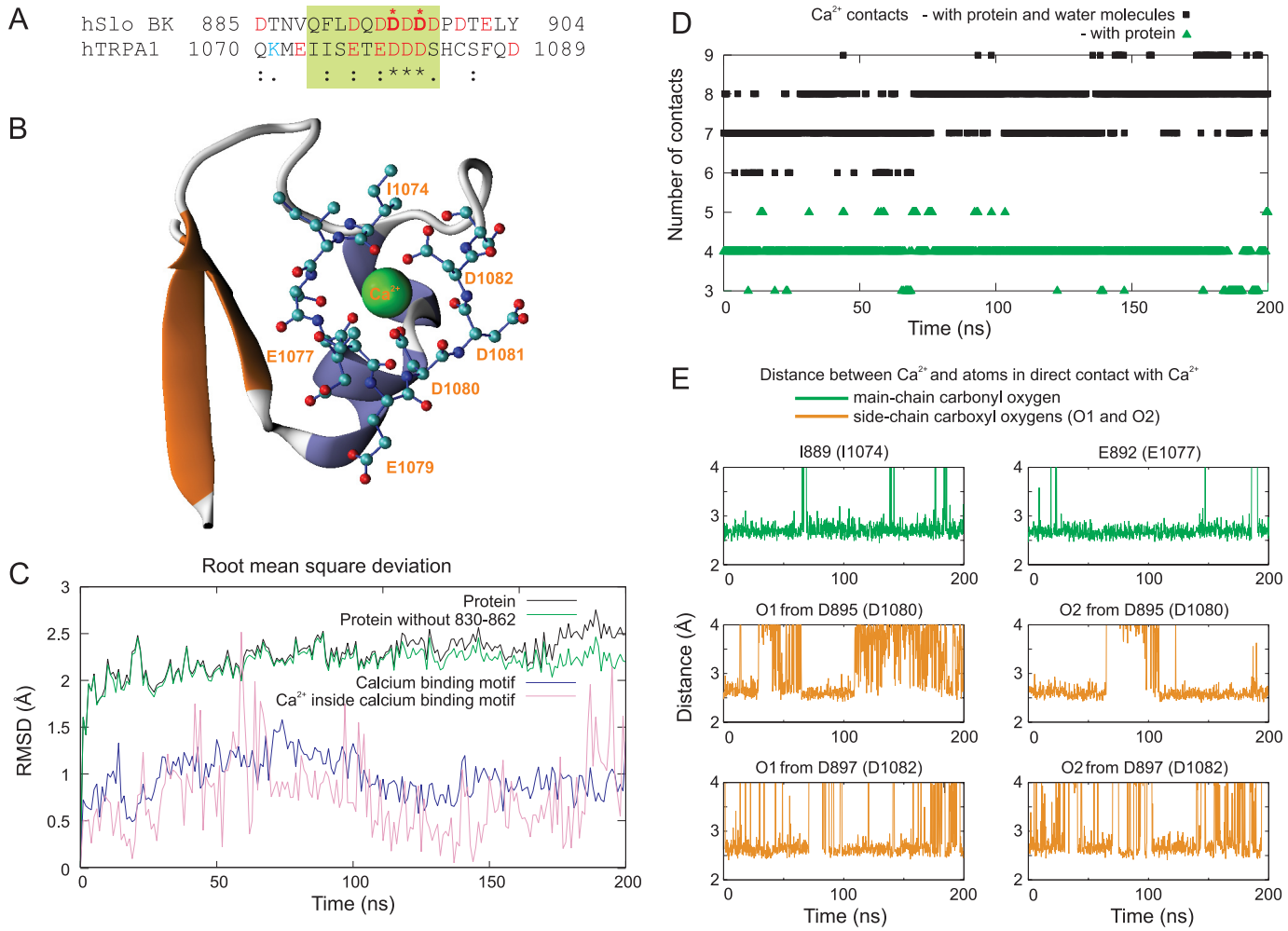

FIGURE 5. **Homology modeling and molecular dynamics simulations of acidic region from TRPA1 based on Ca^{2+} activation apparatus of human BK channel (hSlo1; Protein Data Bank entry code 3MT5) as template protein.** *A*, alignment of Ca^{2+}-binding domain of BK with C-terminal acidic region from human TRPA1. *B*, illustration of calcium-binding site in hSlo1-TRPA1 chimera with surrounding structures. Residues from the TRPA1 protein are shown in ball and stick representation. Snapshot is the frame at 200 ns of the simulation. *C*, RMSD of protein and calcium-binding site. *C* also indicates the displacement of the calcium ion inside of the calcium-binding domain. A significant increase in RMSD at the end of simulation was identified to be caused by loose ends of the polypeptides at residues 833–869, whose structure is not known and was missing from the model structure (see "Materials and Methods"). The system was simulated for a total of 200 ns after equilibration. The time course of RMSD indicated that the system was sufficiently relaxed after 70 ns, and the calcium-binding motif was sufficiently relaxed after 110 ns. The displacement of the calcium ion was less than 1 Å for most of the simulation, indicating that the ion was stable. *D*, number of contacts with Ca^{2+} ion throughout simulation. *E*, lengths of ionic bonds between calcium ion and atoms in calcium-binding site.

Moreover, the inactivation requires Ca^{2+} entry through the activated channel, and thus the structural regions close to the channel pore were proposed to undergo Ca^{2+}-induced conformational changes to regulate TRPA1 gating (11–13). The proximal C-terminal domain of TRPA1 is thought to contain functionally important juxtamembrane helix H1 (Ile^{964}–Lys^{989}) adjacent to the predicted inner vestibule of the channel. We have previously demonstrated that mutations in this domain have strong effects on several aspects of TRPA1 functioning, including changes in its voltage-dependent activation/deactivation kinetics and a significant increase in the current variance at depolarizing potentials (18). We then hypothesized that the pore-forming S6 helix of TRPA1 may extend to the cytoplasmic region so that the proximal helix H1 could directly participate in the regulation of gating or permeation properties of the channel. The new finding that a distal C-terminal structure provides the TRPA1 channel with its ability to respond to external calcium leads to the notion that the quarternary organization of the C-terminal domain includes an intracellular gating ring on the cytoplasmic surface, functionally reminiscent of the Ca^{2+}-dependent operation of the human BK channel gating ring apparatus (20, 35). This hypothesis is further supported by a recent report demonstrating a strong continuous density near the transmembrane region revealed by single-particle electron microscopy (36). Another line of evidence also supports this possibility.

Our second key finding that the two neighboring mutations within the acidic region, E1077K and T1078D, caused a shift in the conductance-voltage (*G/V*) curve to less depolarized membrane voltages indicates that the TRPA1 channel pore might be controlled by voltage via a connection between the distal portion of the C terminus and the putative voltage sensor or the S6-H1 module. Compared with voltage-gated potassium channels, the voltage dependence of TRPA1 is very weak, with the estimated apparent number of gating charges less than 1 (10, 18). It is anticipated that the putative voltage-sensing domain,

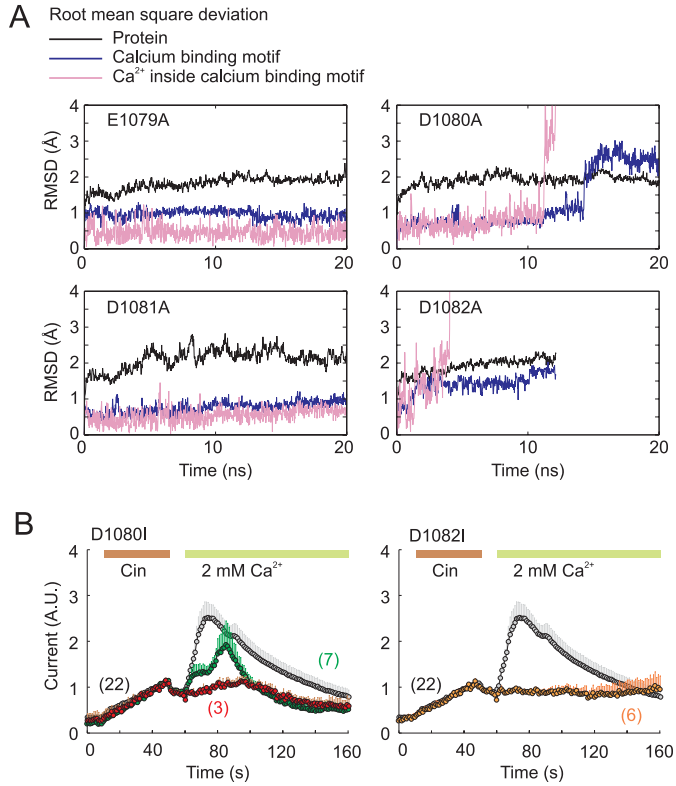

FIGURE 6. **Mutations in C-terminal acidic region.** *A*, molecular dynamics simulations of *in silico* alanine mutations of the BK/TRPA1 chimera. RMSDs of whole protein, calcium-binding site, and displacement of calcium ion in the predicted calcium-binding site for each mutant. Calcium ion was stable in E1079A and D1081A. Disruptions of the calcium-binding pocket were observed in D1080A and in D1082A after 11 and 4 ns of molecular dynamics simulation. The simulation of D1082A (D897A) mutation was particularly unstable, and the calcium ion left the binding site very soon after simulation entered production run. This simulation was interrupted after 10 ns of run. *B*, potentiation of the TRPA1 mutants D1080I and D1082I by extracellular Ca^{2+}. Average whole cell currents evoked in response to 40 s of exposure to 100 μM Cin and subsequent addition of 2 mM Ca^{2+} as is indicated by *horizontal bars*. The average current for the wild type is shown for comparison in *gray* in each plot. The currents are normalized to their maximal cinnamaldehyde responses obtained prior to the addition of Ca^{2+} to the bath solution. The data represent the means ± S.E. for the number of cells indicated. For D1080I, the average current for nonpotentiated cells (in *red*) is overlaid onto the average current from all cells (in *green*).

which has not been identified yet, most likely lies outside the conventionally considered fourth transmembrane segment (S4), because this region does not contain any charged residues at all. Within the S4-S5 linker of human TRPA1, a gain of function point mutation N855S has been identified to exhibit a 5-fold increase in inward currents on activation by cinnamaldehyde, menthol, or the endogenous aldehyde 4-hydroxynonenal at normal resting membrane potentials (37). Removing extracellular Ca^{2+} ions shifts the voltage-dependent activation by approximately +20 mV in both the wild type and the N855S mutant, compatible with the sensitizing effect of Ca^{2+}. This behavior can be explained well by the allosteric model of TRPA1 activation by two different stimuli (38). In addition, the decreased cooperativity of voltage-dependent gating under the Ca^{2+}-free conditions found in N855S indicates that this mutation destabilizes the closed conformation, which could account for a more general effect on channel gating (39) and is consistent with the proposed functional role for the S4-S5 linker in the gating of other thermosensitive TRP channels (40–42).

We do not have a strong structural explanation for the gain of function effects seen in the E1077A, E1077K, and T1078D mutants. The T1078D mutation in particular had large effects on voltage-dependent activation when using the voltage-step protocol, but only modest effects on voltage- and cinnamaldehyde-dependent activation when the standard voltage-ramp protocol was utilized (Fig. 2). We attribute this apparent discrepancy to the fast onset kinetics of the mutant channel upon voltage changes and suggest that Thr^{1078} is implicated in allosteric coupling between the activation site(s) (voltage sensor, Ca^{2+} sensor) and the movement of the gate. As for the proposed role of the whole acidic region in Ca^{2+} binding, one notion might be that the E1077K mutation mimics the Ca^{2+}-bound (*i.e.* sensitized) state of the channel. On the other hand, the addition of a negative charge at T1078 could help to attract and hold the positive calcium ions or transduce the Ca^{2+} signal further downstream. This interpretation would support the suggestion that this region is important both for TRPA1 inactivation and also for Ca^{2+}-dependent potentiation. Site-directed mutagenesis studies have previously shown that neutralizations at two basic residues predicted to be located in the distal helices H4 and H5, flanking the acidic C-terminal domain, Lys^{1071} and Lys^{1092}, are capable of significantly reducing the responsiveness of TRPA1 to allyl isothiocyanate at negative membrane potentials but also cause defects in its voltage-dependent gating (18). Mutations at the cysteine or histidine residues located in this region had no effect on TRPA1 activation (3). Therefore, together with our results, it appears that specific charged residues within the entire region between helices H4 and H5 may comprise an important functional unit which, depending on Ca^{2+} binding, transmits a chemical signal from the N terminus to the gate. The recent 16 Å resolution structure of TRPA1 indicates that covalent modifications within the N termini might bridge adjacent monomers and induce conformational changes in the cytoplasmic domains of TRPA1 that lead to channel gating (36). By looking at this structure, it is tempting to speculate that the C-terminal helices forming a symmetrical structure parallel to the membrane plane might be stabilized by interactions between the positively charged region Lys^{988}–Arg^{1011} and the acidic cluster of the adjacent subunit. Upon Ca^{2+} binding, this interaction is disrupted, which might result in the opening of the channel.

The third key finding of this study provides essential evidence that the cluster of acidic residues in the TRPA1 cytosolic C terminus plays an important role in Ca^{2+}-dependent modulation and may represent a candidate region for the site of Ca^{2+} binding. This portion of the TRPA1 protein does not possess a "classical" Ca^{2+}-binding motif; thus our homology model cannot lend any direct structural support for identifying the Ca^{2+}-binding site. However, this model does fit the requirements for the ^{1074}IISETEDDDS^{1083} motif being a Ca^{2+}-binding loop; it provides a basis for additional structural insights into the possible receptor-Ca^{2+} contacts and in general is consistent with our experimental results. According to our simulations, the two residues Asp^{1080} and Asp^{1082} are predicted to be crucial for binding calcium, whereas the side chains of Ile^{1074} and Glu^{1077} are in contact with the calcium ion using their main chain carbonyl oxygen atoms (Fig. 5*B*). Indeed, we identified residues

Glu^{1073}, Glu^{1077}, Asp^{1080}, Asp^{1081}, and Asp^{1082}, the specific properties of which are not involved in Cin activation, but all appear to be most important for the modulation of the TRPA1 channel by Ca^{2+}, thus supporting the homology model as a plausible structure. To gain additional information toward a possible structural explanation of our data, we conducted measurements in which we explored the effects of the charge-neutralizing double mutations E1077Q/E1079Q, E1079Q/D1081N, and D1080N/1082N. All of the double mutants did not produce measurable currents in response to any of the stimuli tested, supporting the structural importance of the acidic motif.

We can be reasonably certain that in most cases, the changes in the magnitudes of the responses to cinnamaldehyde or depolarizing voltage are not due to changes in expression levels or plasma membrane targeting, because (*a*) simultaneous application of voltage and Ca^{2+} revealed considerable differences in the relative cross-sensitization capacity between the mutants, (*b*) several mutants were more specifically responding to voltage, *i.e.* their current-voltage relationships were qualitatively different from that in the wild-type channel, and, moreover, (*c*) we found that the strong consensus phosphorylation motifs containing serine 1076 and threonine 1078 (^{1071}KMEI-I**S**ETEDD^{1081} and ^{1073}EIISE**T**EDDDS^{1083}), both predicted to be targeted by casein-kinase CK2 with similar probabilities to TRPP2 (NetPhorest Posterior probability of 0.6386 and 0.6261 *versus* 0.6453 (43)), unlike TRPP2 (32), do not constitute a cytosolic sorting motif involved in the trafficking and surface expression of TRPA1. The findings that the nonphosphorylatable mutations S1076A and T1078A and the phosphorylation-mimicking mutation S1076D generated near to wild-type phenotypes indicates that the functional changes caused by other substitutions in this region are likely to be steric or local, rather than related to changes in the membrane insertion of the channels. In any case, we cannot exclude the possible involvement of the identified residues in the recently proposed, but yet to be determined, mechanism by which localized Ca^{2+} influx upon TRPA1 activation controls channel functionality through its acute translocation to the membrane (14).

REFERENCES

1. Story, G. M., Peier, A. M., Reeve, A. J., Eid, S. R., Mosbacher, J., Hricik, T. R., Earley, T. J., Hergarden, A. C., Andersson, D. A., Hwang, S. W., McIntyre, P., Jegla, T., Bevan, S., and Patapoutian, A. (2003) ANKTM1, a TRP-like channel expressed in nociceptive neurons, is activated by cold temperatures. *Cell* **112,** 819–829
2. Jordt, S. E., Bautista, D. M., Chuang, H. H., McKemy, D. D., Zygmunt, P. M., Högestätt, E. D., Meng, I. D., and Julius, D. (2004) Mustard oils and cannabinoids excite sensory nerve fibres through the TRP channel ANKTM1. *Nature* **427,** 260–265
3. Hu, H., Bandell, M., Petrus, M. J., Zhu, M. X., and Patapoutian, A. (2009) Zinc activates damage-sensing TRPA1 ion channels. *Nat. Chem. Biol.* **5,** 183–190
4. Bandell, M., Story, G. M., Hwang, S. W., Viswanath, V., Eid, S. R., Petrus, M. J., Earley, T. J., and Patapoutian, A. (2004) Noxious cold ion channel TRPA1 is activated by pungent compounds and bradykinin. *Neuron* **41,** 849–857
5. Bautista, D. M., Movahed, P., Hinman, A., Axelsson, H. E., Sterner, O., Högestätt, E. D., Julius, D., Jordt, S. E., and Zygmunt, P. M. (2005) Pungent products from garlic activate the sensory ion channel TRPA1. *Proc. Natl. Acad. Sci. U.S.A.* **102,** 12248–12252
6. Macpherson, L. J., Geierstanger, B. H., Viswanath, V., Bandell, M., Eid, S. R., Hwang, S., and Patapoutian, A. (2005) The pungency of garlic. Activation of TRPA1 and TRPV1 in response to allicin. *Curr. Biol.* **15,** 929–934
7. Corey, D. P., García-Añoveros, J., Holt, J. R., Kwan, K. Y., Lin, S. Y., Vollrath, M. A., Amalfitano, A., Cheung, E. L., Derfler, B. H., Duggan, A., Géléoc, G. S., Gray, P. A., Hoffman, M. P., Rehm, H. L., Tamasauskas, D., and Zhang, D. S. (2004) TRPA1 is a candidate for the mechanosensitive transduction channel of vertebrate hair cells. *Nature* **432,** 723–730
8. Nagata, K., Duggan, A., Kumar, G., and García-Añoveros, J. (2005) Nociceptor and hair cell transducer properties of TRPA1, a channel for pain and hearing. *J. Neurosci.* **25,** 4052–4061
9. Sawada, Y., Hosokawa, H., Hori, A., Matsumura, K., and Kobayashi, S. (2007) Cold sensitivity of recombinant TRPA1 channels. *Brain Res.* **1160,** 39–46
10. Karashima, Y., Talavera, K., Everaerts, W., Janssens, A., Kwan, K. Y., Vennekens, R., Nilius, B., and Voets, T. (2009) TRPA1 acts as a cold sensor *in vitro* and *in vivo*. *Proc. Natl. Acad. Sci. U.S.A.* **106,** 1273–1278
11. Nilius, B., Prenen, J., and Owsianik, G. (2011) Irritating channels. The case of TRPA1. *J. Physiol.* **589,** 1543–1549
12. Cavanaugh, E. J., Simkin, D., and Kim, D. (2008) Activation of transient receptor potential A1 channels by mustard oil, tetrahydrocannabinol and Ca^{2+} reveals different functional channel states. *Neuroscience* **154,** 1467–1476
13. Patil, M. J., Jeske, N. A., and Akopian, A. N. (2010) Transient receptor potential V1 regulates activation and modulation of transient receptor potential A1 by Ca^{2+}. *Neuroscience* **171,** 1109–1119
14. Schmidt, M., Dubin, A. E., Petrus, M. J., Earley, T. J., and Patapoutian, A. (2009) Nociceptive signals induce trafficking of TRPA1 to the plasma membrane. *Neuron* **64,** 498–509
15. Doerner, J. F., Gisselmann, G., Hatt, H., and Wetzel, C. H. (2007) Transient receptor potential channel A1 is directly gated by calcium ions. *J. Biol. Chem.* **282,** 13180–13189
16. Zurborg, S., Yurgionas, B., Jira, J. A., Caspani, O., and Heppenstall, P. A. (2007) Direct activation of the ion channel TRPA1 by Ca^{2+}. *Nat. Neurosci.* **10,** 277–279
17. Wang, Y. Y., Chang, R. B., Waters, H. N., McKemy, D. D., and Liman, E. R. (2008) The nociceptor ion channel TRPA1 is potentiated and inactivated by permeating calcium ions. *J. Biol. Chem.* **283,** 32691–32703
18. Samad, A., Sura, L., Benedikt, J., Ettrich, R., Minofar, B., Teisinger, J., and Vlachova, V. (2011) The C-terminal basic residues contribute to the chemical- and voltage-dependent activation of TRPA1. *Biochem. J.* **433,** 197–204
19. Xiao, Q., Prussia, A., Yu, K., Cui, Y. Y., and Hartzell, H. C. (2008) Regulation of bestrophin Cl channels by calcium. Role of the C terminus. *J. Gen. Physiol.* **132,** 681–692
20. Yuan, P., Leonetti, M. D., Pico, A. R., Hsiung, Y., and MacKinnon, R. (2010) Structure of the human BK channel Ca^{2+}-activation apparatus at 3.0 A resolution. *Science* **329,** 182–186
21. Susankova, K., Ettrich, R., Vyklicky, L., Teisinger, J., and Vlachova, V. (2007) Contribution of the putative inner-pore region to the gating of the transient receptor potential vanilloid subtype 1 channel (TRPV1). *J. Neurosci.* **27,** 7578–7585
22. Vlachová, V., Teisinger, J., Susánková, K., Lyfenko, A., Ettrich, R., and Vyklický, L. (2003) Functional role of C-terminal cytoplasmic tail of rat vanilloid receptor 1. *J. Neurosci.* **23,** 1340–1350
23. Dittert, I., Benedikt, J., Vyklický, L., Zimmermann, K., Reeh, P. W., and Vlachová, V. (2006) Improved superfusion technique for rapid cooling or heating of cultured cells under patch-clamp conditions. *J. Neurosci. Methods* **151,** 178–185
24. Thompson, J. D., Higgins, D. G., and Gibson, T. J. (1994) CLUSTAL W. Improving the sensitivity of progressive multiple sequence alignment through sequence weighting, position-specific gap penalties and weight matrix choice. *Nucleic Acids Res.* **22,** 4673–4680
25. Sali, A., Potterton, L., Yuan, F., van Vlijmen, H., and Karplus, M. (1995) Evaluation of comparative protein modeling by MODELLER. *Proteins* **23,** 318–326
26. Case, D. A., Darden, T. A., Cheatham, T. E., III, Simmerling, C. L., Wang,

J., Duke, R. E., Luo, R., Walker, R. C., Zhang, W., Merz, K. M., Roberts, B., Wang, B., Hayik, S., Roitberg, A., Seabra, G., Kolossvai, I., Wong, K. F., Paesani, F., Vanicek, J., Liu, J., Wu, X., Brozell, S. R., Steinbrecher, T., Gohlke, H., Cai, Q., Ye, X., Wang, J., Hsieh, M. J., Cui, G., Roe, D. R., Mathews, D. H., Seetin, M. G., Sagui, C., Babin, V., Luchko, T., Gusarov, S., Kovalenko, A., and Kollman, P. A. (2010) *AMBER 11*, University of California, San Francisco

27. Phillips, J. C., Braun, R., Wang, W., Gumbart, J., Tajkhorshid, E., Villa, E., Chipot, C., Skeel, R. D., Kalé, L., and Schulten, K. (2005) Scalable molecular dynamics with NAMD. *J. Comput. Chem.* **26,** 1781–1802
28. Harvey, M., Giupponi, G., and De Fabritiis, G. (2009) ACEMD: Accelerated molecular dynamics simulations in the microseconds timescale. *J. Chem. Theory Comp.* **5,** 1632–1639
29. Feenstra, K. A., Hess, B., and Berendsen, H. J. C. (1999) Improving efficiency of large time-scale molecular dynamics simulations of hydrogen-rich systems. *J. Comp. Chem.* **20,** 786–798
30. Humphrey, W., Dalke, A., and Schulten, K. (1996) VMD. Visual molecular dynamics. *J. Mol. Graph.* **14,** 33–38
31. Cordero-Morales, J. F., Gracheva, E. O., and Julius, D. (2011) Cytoplasmic ankyrin repeats of transient receptor potential A1 (TRPA1) dictate sensitivity to thermal and chemical stimuli. *Proc. Natl. Acad. Sci. U.S.A.* **108,** E1184–E1191
32. Köttgen, M., Benzing, T., Simmen, T., Tauber, R., Buchholz, B., Feliciangeli, S., Huber, T. B., Schermer, B., Kramer-Zucker, A., Höpker, K., Simmen, K. C., Tschucke, C. C., Sandford, R., Kim, E., Thomas, G., and Walz, G. (2005) Trafficking of TRPP2 by PACS proteins represents a novel mechanism of ion channel regulation. *EMBO J.* **24,** 705–716
33. Latorre, R., Morera, F. J., and Zaelzer, C. (2010) Allosteric interactions and the modular nature of the voltage- and Ca^{2+}-activated (BK) channel. *J. Physiol.* **588,** 3141–3148
34. Lightstone, F. C., Schwegler, E., Allesch, M., Gygi, F., and Galli, G. (2005) A first-principles molecular dynamics study of calcium in water. *Chemphyschem* **6,** 1745–1749
35. Javaherian, A. D., Yusifov, T., Pantazis, A., Franklin, S., Gandhi, C. S., and Olcese, R. (2011) Metal-driven operation of the human large-conductance voltage- and Ca^{2+}-dependent potassium channel (BK) gating ring apparatus. *J. Biol. Chem.* **286,** 20701–20709
36. Cvetkov, T. L., Huynh, K. W., Cohen, M. R., and Moiseenkova-Bell, V. Y. (2011) Molecular architecture and subunit organization of TRPA1 ion channel revealed by electron microscopy. *J. Biol. Chem.* **286,** 38168–38176
37. Kremeyer, B., Lopera, F., Cox, J. J., Momin, A., Rugiero, F., Marsh, S., Woods, C. G., Jones, N. G., Paterson, K. J., Fricker, F. R., Villegas, A., Acosta, N., Pineda-Trujillo, N. G., Ramírez, J. D., Zea, J., Burley, M. W., Bedoya, G., Bennett, D. L., Wood, J. N., and Ruiz-Linares, A. (2010) A gain-of-function mutation in TRPA1 causes familial episodic pain syndrome. *Neuron* **66,** 671–680
38. Salazar, M., Moldenhauer, H., and Baez-Nieto, D. (2011) Could an allosteric gating model explain the role of TRPA1 in cold hypersensitivity? *J. Neurosci.* **31,** 5554–5556
39. Smith-Maxwell, C. J., Ledwell, J. L., and Aldrich, R. W. (1998) Role of the S4 in cooperativity of voltage-dependent potassium channel activation. *J. Gen. Physiol.* **111,** 399–420
40. Brauchi, S., Orta, G., Mascayano, C., Salazar, M., Raddatz, N., Urbina, H., Rosenmann, E., Gonzalez-Nilo, F., and Latorre, R. (2007) Dissection of the components for PIP2 activation and thermosensation in TRP channels. *Proc. Natl. Acad. Sci. U.S.A.* **104,** 10246–10251
41. Boukalova, S., Marsakova, L., Teisinger, J., and Vlachova, V. (2010) Conserved residues within the putative S4-S5 region serve distinct functions among thermosensitive vanilloid transient receptor potential (TRPV) channels. *J. Biol. Chem.* **285,** 41455–41462
42. Voets, T., Owsianik, G., Janssens, A., Talavera, K., and Nilius, B. (2007) TRPM8 voltage sensor mutants reveal a mechanism for integrating thermal and chemical stimuli. *Nat. Chem. Biol.* **3,** 174–182
43. Miller, M. L., Jensen, L. J., Diella, F., Jørgensen, C., Tinti, M., Li, L., Hsiung, M., Parker, S. A., Bordeaux, J., Sicheritz-Ponten, T., Olhovsky, M., Pasculescu, A., Alexander, J., Knapp, S., Blom, N., Bork, P., Li, S., Cesareni, G., Pawson, T., Turk, B. E., Yaffe, M. B., Brunak, S., and Linding, R. (2008) Linear motif atlas for phosphorylation-dependent signaling. *Sci. Signal.* **1,** ra2

Publication 4

Boukalova S., Touska F., Marsakova L., **Hynkova A.**, Sura L., Chvojka S., Dittert I., Vlachova V.

Gain-of-function mutations in the transient receptor potential channels TRPV1 and TRPA1: how painful?

Physiological Research, 63 Suppl 1:S205-13, 2014

The extent of participation: Help with writing of the part about the TRPA1 receptor and finalization of the manuscript.

Physiol. Res. 63 (Suppl. 1): S205-S213, 2014

REVIEW

Gain-of-Function Mutations in the Transient Receptor Potential Channels TRPV1 and TRPA1: How Painful?

S. BOUKALOVA[1], F. TOUSKA[1], L. MARSAKOVA[1], A. HYNKOVA[1], L. SURA[1], S. CHVOJKA[1], I. DITTERT[1], V. VLACHOVA[1]

[1]Department of Cellular Neurophysiology, Institute of Physiology Academy of Sciences of the Czech Republic, Prague, Czech Republic

Received August 30, 2013
Accepted September 12, 2013

Summary

Gain-of-function (GOF) mutations in ion channels are rare events, which lead to increased agonist sensitivity or altered gating properties, and may render the channel constitutively active. Uncovering and following characterization of such mutants contribute substantially to the understanding of the molecular basis of ion channel functioning. Here we give an overview of some GOF mutants in polymodal ion channels specifically involved in transduction of painful stimuli – TRPV1 and TRPA1, which are scrutinized by scientists due to their important role in development of some pathological pain states. Remarkably, a substitution of single amino acid in the S4-S5 region of TRPA1 (N855S) has been recently associated with familial episodic pain syndrome. This mutation increases chemical sensitivity of TRPA1, but leaves the voltage sensitivity unchanged. On the other hand, mutations in the analogous region of TRPV1 (R557K and G563S) severely affect all aspects of channel activation and lead to spontaneous activity. Comparison of the effects induced by mutations in homologous positions in different TRP receptors (or more generally in other distantly related ion channels) may elucidate the gating mechanisms conserved during evolution.

Key words

TRPV1 • TRPA1 • Gain-of-function mutation • Spontaneous activity • Gating • Nociception

Corresponding author

V. Vlachova, Institute of Physiology AS CR, Videnska 1083, 142 20 Prague 4, Czech Republic. Fax: 420-29644-2488. E-mail: vlachova@biomed.cas.cz

Introduction

The family of Transient Receptor Potential (TRP) ion channels mediates numerous sensory transduction processes, such as thermosensation, mechanosensation, sensation of irritative chemicals and different kinds of taste (for more information, see the TRP channel database: http://www.iuphar-db.org/DATABASE/FamilyMenuForward?familyId=78). As the voltage dependent potassium (K_v) channels, the TRP channels consist of four subunits, each with N- and C-terminal cytoplasmic domains, six transmembrane regions (S1-S6) and the central pore lined by S5 and S6 together with the loop between them (Fig. 1A) (Moiseenkova-Bell and Wensel 2011, Kalia and Swartz 2013). Among TRP channels, TRPV1 and TRPA1 are known to be specialized to transduce painful stimuli in mammals (Moran *et al.* 2011, Nilius and Owsianik 2011, Nilius *et al.* 2012). High temperature, low pH and some natural pungent compounds such as capsaicin act on TRPV1 to elicit nociception. TRPA1 is targeted by many environmental irritants including allyl isothiocyanate, responsible for the pungent taste of horseradish, and cinnamaldehyde from cinnamon. The activity of both channels is also modulated by voltage, but their sensitivity to depolarization is much lower than in K_v channels. Different parts of TRP channels are responsible for the sensitivity to different agonists (Nilius and Owsianik 2011, Winter *et al.* 2013). Due to the resulting allosteric gating, it is necessary to have in mind the complex character of TRP channels when evaluating the

mutational analysis data. Gain-of-function (GOF) mutation may enhance the responses of the channel to one type of stimuli, but sensitivity to other agonists may be unchanged or even diminished. Amino acid substitutions which affect gating can lead to altered phenotype regarding to all aspects of channel activation (Myers *et al.* 2008b, Minor 2009, Pertusa *et al.* 2012). Such GOF mutations are invaluable in elucidating the mechanisms of signal transduction from different domains of the protein complex to channel gating.

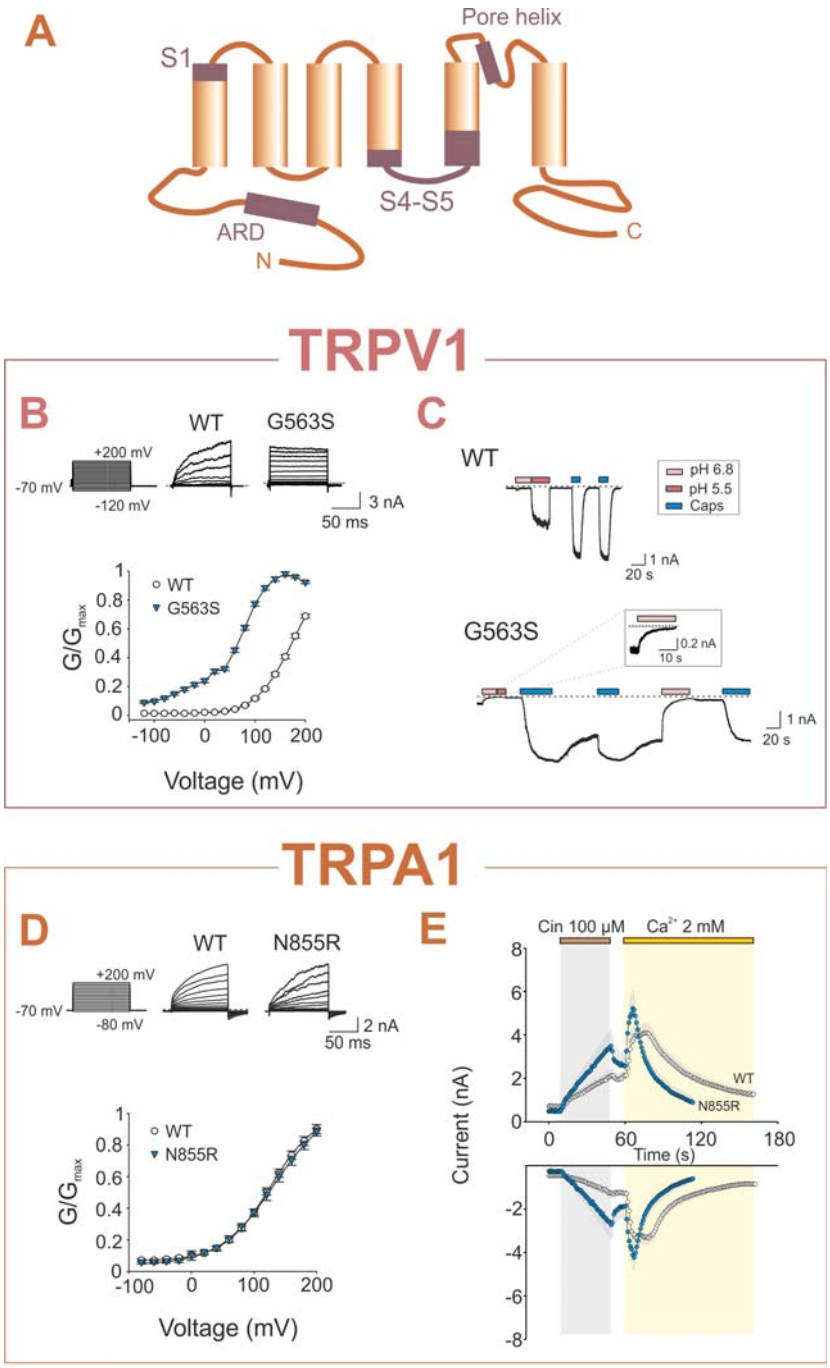

Fig. 1. (A) The topology of TRP channel subunit, that is formed by six transmembrane spanning domains (in orange), N- and C-cytoplasmatic ends. N-terminus contains ankyrin repeat domain (ARD), that is important in channel regulation. The regions containing gain-of-function mutation of TRP channels are depicted in darker color – extracellular part of the first transmembrane domain S1, loop between S4 and S5 helix (S4-S5) and the pore helix situated in the linker between S5 and S6. **(B)** Upper traces, representative whole cell patch clamp current recordings in response to voltage steps (from –120 mV to +200 mV) in HEK293T cells transfected with wild-type TRPV1 and G563S mutant. Lower trace, normalized conductance-voltage relationship obtained from steady state currents at the end of the pulse. The voltage depencence of G563S mutant is shifted towards less depolarizing voltages compared to wild-type TRPV1. **(C)** The sample recording of whole cell current responses of wild-type TRPV1 (upper trace) and G563S mutant (lower trace) to consecutive applications of low pH and 1 µM capsaicin. Holding potential –70 mV. Note the inhibitory effect of protons (pH 6.8) on TRPV1-G563S channel function, shown in inset. **(D)** Upper traces, representative current traces of wild-type TRPA1 and its N855R mutant in response to indicated voltage step protocol (voltage steps from –80 mV to +200 mV; increment +20 mV; holding potential –70 mV). Lower trace, normalized conductance-voltage relationship for wild-type TRPA1 (white symbols) and N855R mutant (blue symbols) fitted with Boltzmann equation. The data were obtained using the same voltage step protocol as shown in upper traces. **(E)** Time course of representative whole cell currents through human TRPA1 measured at +80 mV (upper trace) and –80 mV (lower trace). The horizontal bars above the records indicate the duration of 100 µM cinnamaldehyde and Ca^{2+} application. The chemical sensitivity of N855R mutant is increased and the inactivation kinetics is faster than in wild-type TRPA1. The voltage dependence of N855R mutant is unchanged. The data represent the means ± standard error.

GOF mutants in TRPV1 – proton sensitized or inhibited?

Several GOF mutants of the TRPV1 ion channel were revealed by unbiased genetic screening of a randomly generated population of TRPV1 mutants, which were tested for the ability to cause growth defects when expressed in yeast strains (Myers *et al.* 2008a). Two of the uncovered mutations, K160E and K155E, are located in the ankyrin repeat domain (ARD). These two

lysine residues were previously shown to modulate TRPV1 sensitivity and desensitization properties by binding ATP and calmodulin (Lishko *et al.* 2007). The study of Myers and colleagues (2008a) also revealed the important role of the outer pore region in TRPV1 gating. When mutated, the phenylalanine F640 and adjacent threonine T641 residues located in the putative flexion between pore helix and selectivity filter render the TRPV1 channel constitutively active with increased basal activity and enhanced chemical sensitivity. The authors hypothesised that F640L and T641S mutations mimic the proton-potentiated state, as they were insensitive to proton-mediated potentiation.

In our project aimed at mutational analysis of the transmembrane region of the TRPV1 ion channel, we depicted several overactive mutants with strikingly similar phenotypic properties comprising increased basal activity and voltage sensitivity, altered kinetics of capsaicin-induced responses and incomplete deactivation after capsaicin washout. In contrast to wild-type TRPV1, low pH neither activates nor potentiates these GOF mutants, but instead stabilize their resting conformation (Pertusa *et al.* 2012) (Fig. 1B,C). These findings were surprising to us, considering that the mutations are located in distant regions of the protein subunit, such as (i) extracellular portion of S1 (R455K mutation), (ii) lower part of S4 and S4-S5 linker (R557K and G563S) and (iii) pore helix (T633A) (Boukalova *et al.* 2013).

Uncovering the GOF mutations in the S4/S4-S5 region is consistent with its putative role in voltage sensing and signal transduction from peripheral domains (S1-S4) to the pore-forming domain subsequently leading to the opening or closing of the channel (Boukalova *et al.* 2010). On the other hand, finding of constitutively active mutant with single amino acid substitution in the peripheral region of TRPV1 protein complex was not expected. So far, R455K is the only overactive mutation found in the S1-upper S4 region of TRPV1 protein complex, which forms binding capsule for chemical agonists (Jordt and Julius 2002, Gavva *et al.* 2004), but which direct role in ion channel gating was not presumed. According to previously published homology model of TRPV1 tetramer (Brauchi *et al.* 2007), it seems that arginine R455 and threonine T633 in the pore helix of adjacent subunit could be in close proximity. We hypothesized that, in analogy to K_v channels, S1-pore interface between neighbouring subunits of TRPV1 might serve to stabilize conformations associated with channel gating (Lee *et al.* 2009). This presumption could explain the similarity of R455K and T633A mutant phenotypes and the crucial role of arginine in S1 in TRPV1 gating.

The most prominent feature of the GOF mutants described recently by us is the lack of low pH-induced activation. Conversely, relatively mild acidification of the extracellular solution inhibits the spontaneous activity and also the inward current remaining after capsaicin washout in R455K, R557K, G563S and T633A (Fig. 1C). Unlike in the outer pore region mutants F640L and T641S (Myers *et al.* 2008a), the phenotype of these mutants cannot be simply explained as mimicking the proton-potentiated state of TRPV1, as they failed to be activated by severe acidification of the extracellular solution (pH 5.5). In addition, in R455K, T633A and the S4-S5 overactive mutants we observed significantly slowed kinetics of the first capsaicin-induced response, which does not correspond to low pH-stimulated wild-type TRPV1 characterized by much faster onset rate of responses elicited by capsaicin.

In R455K, R557K, G563S and T633A, the washout phase of current responses after removal of capsaicin was markedly slowed down and the current did not deactivate to the basal level. The subsequent application of capsaicin led to rapid augmentation of the current amplitude, which in some cells was followed by again much slower onset phase (Fig. 1C). It appears that once exposed to capsaicin, the closed state of mutant ion channels is acutely destabilized. On the other hand, mild acidification of the extracellular space (pH 6.8) resulted in rapid and irreversible deactivation of the basal activity and also the current remaining after capsaicin washout. Overall, it seems that the overactive mutants can adopt at least two modes of activation and it is possible to switch between them using either capsaicin (to open the channel and leave it opened) or low pH (to close the channel and leave it closed). The question is whether this feature is unique for the GOF mutants, or whether it reflects innate phenotypic aspects of wild-type TRPV1 unmasked by the mutations. The later option is favoured by the fact that the same phenotype is found in several TRPV1 mutants with single amino acid substitution in different parts of the protein.

Gain-of-function: which function of the many?

High throughput unbiased functional screens and a combination of molecular evolution-selection

approaches helped to reveal a number of interesting mutants in TRPV1, TRPV3 and TRPM8 channels (Bandell *et al.* 2006, Grandl *et al.* 2008, 2010, Myers *et al.* 2008a). Pools of many thousands of mutants have been explored using random mutagenesis and calcium imaging in transfected HEK293 cells which led to the identification of some key regions of these channels that are likely to be important for channel activation or pore permeation (Pertusa *et al.* 2012). However, for the 250 residue transmembrane part of the TRPV1 channel subunit, for example, the theoretical number of possible sequences is 20^{250} which is a number exceeding our imagination and all our experimental capacities. Moreover, for the thermosensitive TRP channels, the prototypically polymodal ion channels, it is important to test as many aspects of function as possible for each mutant because the activation modes can be readily uncoupled. No doubt, the chance of discovering a mutation that changes the function of an ion channel has to be greatly increased by combining an appropriate analogy, reasoning and informed intuition.

In our recent project focused on the sixth transmembrane domain of the human transient receptor potential ankyrin receptor subtype 1 (TRPA1) channel (Story *et al.* 2003, Jordt *et al.* 2004), we aimed to identify residues that are likely to be core elements of the gating mechanism (Benedikt *et al.* 2009). This channel can be activated by a vast number of pungent and irritant chemicals that either covalently interact with (isothiocyanates, cinnamaldehyde, acrolein, allicin, oxidants and lipid peroxidation products) or bind to TRPA1 (cannabinoids, icilin, eugenol, thymol, nicotine), and can also be activated by deep cooling (<17 °C) or depolarizing (>+100 mV) voltages (Bandell *et al.* 2004, Corey *et al.* 2004, Bautista *et al.* 2005, Macpherson *et al.* 2005, Nagata *et al.* 2005, Sawada *et al.* 2007, Caceres *et al.* 2009, Hu *et al.* 2009, Karashima *et al.* 2009, Andrade *et al.* 2012, Nilius *et al.* 2012). Using mutagenesis, electrophysiology and sequence homology with certain potassium and sodium channels, we identified several residues within the S6 inner pore-forming region that contribute to allyl isothiocyanate (AITC) and voltage-dependent gating. We found that alanine substitution in the conserved mid-S6 proline (P949A) strongly affected the activation/deactivation and ion permeation. The P949A was functionally restored by substitution with a glycine but not by the introduction of a proline at positions –1, –2 or +1, which indicated that, just like in K_v channels, a flexible residue in the middle of S6 is structurally required for the normal functioning of the TRPA1 channel. Notably, we found a residue N954, at which alanine substitution generated a constitutively open (i.e. GOF) phenotype, suggesting a role in stabilizing the closed conformation. In a prospective unbiased functional screen, this mutant would probably remain unrecognized or misinterpreted as a loss-of-function, because AITC, at first, only slightly potentiates the currents through the N954A channels, but this is followed by a complete inactivation at negative membrane potentials (Benedikt *et al.* 2009). Our results also pointed to important functional roles for the two distal glycines G958 and G962, comprising the distal G*XXX*G-motif. The G958A "GOF" mutation strongly decreased the inactivation rate of AITC-induced whole-cell currents, whereas the G962A mutation led to a dramatically delayed onset of the secondary phase of AITC-induced activation, indicating that the distal G962 stabilizes the open conformation. G958, on the other hand, provides additional tuning leading to decreased channel activity. It seems likely that these two glycines play a role similar to that of the distal bi-glycine motif $G(X)_3G$ of the conserved IS6 domain of the $Ca_V1.2$ and $Ca_V2.3$ channels (Raybaud *et al.* 2006).

In fact, for the polymodal TRPA1 ion channel, it is not easy even only to define what is the "gain-of-function" because the channel has various activation modes and undergoes desensitization which depends on many factors, including its own activity (Story *et al.* 2003, Jordt *et al.* 2004, Nilius and Owsianik 2011, Nilius *et al.* 2012). For example, by performing the systemic neutralization of 27 positively charged residues within the C-terminal tail of human TRPA1, we identified eight residues that are important to the allosteric regulation of the channel by chemical and voltage stimuli (K969, R975, K989, K1009, K1046, K1071, K1092, and R1099). In addition, we revealed three charge-neutralizing "GOF" mutants (R975A, K988A, and K989A) which exhibited higher sensitivity to depolarizing voltages, indicating that these residues may be directly involved in the voltage-dependent regulation (Samad *et al.* 2011). However, the currents induced by AITC at negative membrane potentials were small or indistinguishable from wild-type in these mutants.

GOF mutants in the distal C-terminal acidic motif of TRPA1

An ubiquitous and physiologically important modulator of TRPA1 are calcium ions (Ca^{2+}), which enter

through the open channel, or are released from internal stores, and dynamically control channel opening probability, unitary conductance, ion selectivity (Nagata *et al.* 2005, Cavanaugh *et al.* 2008, Patil *et al.* 2010, Nilius and Owsianik 2011), but also surface expression levels (Schmidt *et al.* 2009). Intracellular Ca^{2+} ions activate the channel at micromolar concentrations (EC_{50}=0.9-6 µM) (Doerner *et al.* 2007, Zurborg *et al.* 2007) and strongly potentiate chemically and voltage-induced responses (Wang *et al.* 2008). This potentiation is followed by an almost complete and irreversible inactivation, and both processes are accelerated at higher intracellular concentrations of Ca^{2+}. In our recent study, we identified the residues within the distal C-terminal domain of TRPA1 that when mutated affected the Ca^{2+}- and voltage-dependent gating of the channel (Sura *et al.* 2012). This study revealed several acidic residues in the TRPA1 cytosolic C-terminus that play important roles in Ca^{2+}-dependent modulation and may represent a candidate region for the site of Ca^{2+} binding. According to our molecular dynamics simulations, the I^{1074}ISETEDDDS^{1083} motif has been shown to form a Ca^{2+} binding loop, in which the two residues D1080 and D1082 are predicted to be crucial for binding Ca^{2+}, whereas the side chains of I1074 and E1077 are in contact with the calcium ion using their main chain carbonyl oxygen atoms. We identified residues E1073, E1077, D1080, D1081, and D1082, the specific properties of which are not involved in cinnamaldehyde activation but all appear to be most important for the modulation of the TRPA1 channel by Ca^{2+}. Notably, we found two mutants in this region, E1077A and E1077K, in which the degree of potentiation of cinnamaldehyde responses by 2 mM Ca^{2+} was markedly reduced obviously due to their initial close-to-saturation state at +80 mV. We reasoned that this sensitizing effect might reflect either a gain-of-function (constitutively active) phenotype or tonic activation due to an increased expression of the mutant channels on the cell surface. In this region, we identified two strong consensus phosphorylation motifs containing S1076 and T1078, both predicted to be targeted by casein kinase CK2. Therefore, we tested additional mutants in which either serine or threonine were replaced by either alanine or aspartate to mimic the nonphosphorylated and phosphorylated forms of the TRPA1 protein, respectively. We found that the nonphosphorylatable mutant S1076A and the phosphorylation-mimicking S1076D mutant channels were normal in all general aspects of functionality. Mutation T1078A exhibited substantially reduced responses to voltage and cinnamaldehyde and was capable of strong potentiation by 2 mM Ca^{2+}, whereas mutation T1078D resulted in TRPA1 channels whose conductance to voltage relationships were also strongly augmented and shifted toward less depolarizing potentials. These findings indicate that the functional changes caused by other substitutions in this region are likely to be steric or local, rather than related to changes in the phosphorylation-dependent membrane insertion of the channels. We, however, did not exclude the possible involvement of these amino acid residues in the recently proposed mechanism by which localized Ca^{2+} influx upon channel activation controls TRPA1 functionality through its acute translocation to the membrane (Schmidt *et al.* 2009).

GOF mutant of TRPA1 – pain-related channelopathy

The TRPA1 channel has been recently linked to a heritable human pain disorder (Kremeyer *et al.* 2010). In the S4-S5 linker of TRPA1, the missense mutation N855S that leads to increased channel activity has been revealed as a cause of familial episodic pain syndrome manifested as paroxysmal pain induced by tiredness, fasting or cold (Kremeyer *et al.* 2010). In their study, the authors demonstrate that the N855S mutant exhibits a 4-fold increase in inward currents on activation by cinnamaldehyde, menthol, the endogenous aldehyde 4-hydroxynonenal, or cold at normal resting membrane potentials. Removing extracellular Ca^{2+} ions shifted the voltage-dependent activation by +20 mV in both the wild-type and the N855S mutant, but under the Ca^{2+}-free conditions, the cooperativity of voltage-dependent gating decreased only in N855S, but not in the wild-type TRPA1 channels. This finding was interpreted as indicating that this mutation might destabilize the closed conformation of the channel, which could account for a more general effect on channel gating (Smith-Maxwell *et al.* 1998) and is consistent with the proposed functional role for the S4-S5 linker in the gating of other thermosensitive TRP channels (Brauchi *et al.* 2007, Voets *et al.* 2007, Boukalova *et al.* 2010). It is generally accepted that the electrophilic compounds, such as allyl isothiocyanate activate TRPA1 through covalent binding at specific cysteine residues on the intracellularly located N-terminus (Hinman *et al.* 2006, Macpherson *et al.* 2007, Kang *et al.* 2010). It is, however, not known how

covalent cysteine modifications translate into TRPA1 activation. Simulations based on a low-resolution electron density map indicate that the chemical signal can be readily conveyed through cytoplasmic domains to the intracellular channel gate (Cvetkov *et al.* 2011). Although to discern the individual activation pathways in TRPA1 is very difficult even if we knew the actual structure of the channel (Cvetkov *et al.* 2011), it can be supposed that, analogous to K_v channels, the conformational changes within the S1-S4 "sensors" are converted by the inner S4-S5 linker helices directly into gate opening and closing through the motions of the S6 inner helices which dilate (open) and constrict (close) the pore entryway (Long *et al.* 2005a,b, 2007, Brauchi *et al.* 2007, Benedikt *et al.* 2009, Salazar *et al.* 2009). Interestingly, we found that the introduction of a positively charged residue at position N855 (N855R) increased the TRPA1-mediated current responses to cinnamaldehyde and speeded up the inactivation kinetics without affecting conductance to voltage relationships (Fig. 1D,E). This indicates that the mutation altered the chemical but not the voltage activation pathway of the TRPA1 channel.

Future perspectives

Chronic pain conditions, resulting from disease, injury or inherited, cause unimaginable suffering and constitute a huge burden for the individual and society. Both, TRPV1 and TRPA1 are implicated in acute and chronic pain states and are intensively studied as potential therapeutic targets (Brederson *et al.* 2013). Mutations in genes encoding ion channels associated with nociceptive pathways, e.g. voltage-gated sodium, potassium and calcium channels, TRP channels, ASIC channels or purinergic receptors, have been described to cause a variety of pathological states (Cregg *et al.* 2010, Lampert *et al.* 2010, Raouf *et al.* 2010, Nilius and Voets 2013, Waxman 2013). It is likely that with ongoing research further mutations will emerge and therefore future structural and functional studies will be necessary to enhance our understanding of the unique features of these channels and to elucidate how their pain-related functioning can be manipulated to therapeutic advantage.

Conflict of Interest

There is no conflict of interest.

Acknowledgements

This work was supported by the Grant Agency of the Czech Republic (305/09/0081 and 304/12/G069), GAUK 500512 and 888513, CZ.1.07/2.3./00/30.0025, and the Research Project Fund of the Academy of Sciences of the Czech Republic RVO:67985823.

References

ANDRADE EL, MEOTTI FC, CALIXTO JB: TRPA1 antagonists as potential analgesic drugs. *Pharmacol Ther* **133**: 189-204, 2012.

BANDELL M, STORY GM, HWANG SW, VISWANATH V, EID SR, PETRUS MJ, EARLEY TJ, PATAPOUTIAN A: Noxious cold ion channel TRPA1 is activated by pungent compounds and bradykinin. *Neuron* **41**: 849-857, 2004.

BANDELL M, DUBIN AE, PETRUS MJ, ORTH A, MATHUR J, HWANG SW, PATAPOUTIAN A: High-throughput random mutagenesis screen reveals TRPM8 residues specifically required for activation by menthol. *Nat Neurosci* **9**: 493-500, 2006.

BAUTISTA DM, MOVAHED P, HINMAN A, AXELSSON HE, STERNER O, HOGESTATT ED, JULIUS D, JORDT SE, ZYGMUNT PM: Pungent products from garlic activate the sensory ion channel TRPA1. *Proc Natl Acad Sci USA* **102**: 12248-12252, 2005.

BENEDIKT J, SAMAD A, ETTRICH R, TEISINGER J, VLACHOVA V: Essential role for the putative S6 inner pore region in the activation gating of the human TRPA1 channel. *Biochim Biophys Acta Mol Cell Research* **1793**: 1279-1288, 2009.

BOUKALOVA S, MARSAKOVA L, TEISINGER J, VLACHOVA V: Conserved residues within the putative S4-S5 region serve distinct functions among thermosensitive vanilloid transient receptor potential (TRPV) channels. *J Biol Chem* **285**: 41455-41462, 2010.

BOUKALOVA S, TEISINGER J, VLACHOVA V: Protons stabilize the closed conformation of gain-of-function mutants of the TRPV1 channel. *Biochim Biophys Acta* **1833**: 520-528, 2013.

BRAUCHI S, ORTA G, MASCAYANO C, SALAZAR M, RADDATZ N, URBINA H, ROSENMANN E, GONZALEZ-NILO F, LATORRE R: Dissection of the components for PIP2 activation and thermosensation in TRP channels. *Proc Natl Acad Sci USA* **104**: 10246-10251, 2007.

BREDERSON JD, KYM PR, SZALLASI A: Targeting TRP channels for pain relief. *Eur J Pharmacol* **716**: 61-76, 2013.

CACERES AI, BRACKMANN M, ELIA MD, BESSAC BF, DEL CAMINO D, D'AMOURS M, WITEK JS, FANGER CM, CHONG JA, HAYWARD NJ, HOMER RJ, COHN L, HUANG X, MORAN MM, JORDT SE: A sensory neuronal ion channel essential for airway inflammation and hyperreactivity in asthma. *Proc Natl Acad Sci USA* **106**: 9099-9104, 2009.

CAVANAUGH EJ, SIMKIN D, KIM D: Activation of transient receptor potential A1 channels by mustard oil, tetrahydrocannabinol and Ca(2+) reveals different functional channel states. *Neuroscience* **154**: 1467-1476, 2008.

COREY DP, GARCIA-ANOVEROS J, HOLT JR, KWAN KY, LIN SY, VOLLRATH MA, AMALFITANO A, CHEUNG EL, DERFLER BH, DUGGAN A, GELEOC GS, GRAY PA, HOFFMAN MP, REHM HL, TAMASAUSKAS D, ZHANG DS: TRPA1 is a candidate for the mechanosensitive transduction channel of vertebrate hair cells. *Nature* **432**: 723-730, 2004.

CREGG R, MOMIN A, RUGIERO F, WOOD JN, ZHAO J: Pain channelopathies. *J Physiol (Lond)* **588**: 1897-1904, 2010.

CVETKOV TL, HUYNH KW, COHEN MR, MOISEENKOVA-BELL VY: Molecular architecture and subunit organization of TRPA1 ion channel revealed by electron microscopy. *J Biol Chem* **286**: 38168-38176, 2011.

DOERNER JF, GISSELMANN G, HATT H, WETZEL CH: Transient receptor potential channel A1 is directly gated by calcium ions. *J Biol Chem* **282**: 13180-13189, 2007.

GAVVA NR, KLIONSKY L, QU Y, SHI L, TAMIR R, EDENSON S, ZHANG TJ, VISWANADHAN VN, TOTH A, PEARCE LV, VANDERAH TW, PORRECA F, BLUMBERG PM, LILE J, SUN Y, WILD K, LOUIS JC, TREANOR JJ: Molecular determinants of vanilloid sensitivity in TRPV1. *J Biol Chem* **279**: 20283-20295, 2004.

GRANDL J, HU H, BANDELL M, BURSULAYA B, SCHMIDT M, PETRUS M, PATAPOUTIAN A: Pore region of TRPV3 ion channel is specifically required for heat activation. *Nat Neurosci* **11**: 1007-1013, 2008.

GRANDL J, KIM SE, UZZELL V, BURSULAYA B, PETRUS M, BANDELL M, PATAPOUTIAN A: Temperature-induced opening of TRPV1 ion channel is stabilized by the pore domain. *Nat Neurosci* **13**: 708-714, 2010.

HINMAN A, CHUANG HH, BAUTISTA DM, JULIUS D: TRP channel activation by reversible covalent modification. *Proc Natl Acad Sci USA* **103**: 19564-19568, 2006.

HU H, BANDELL M, PETRUS MJ, ZHU MX, PATAPOUTIAN A: Zinc activates damage-sensing TRPA1 ion channels. *Nat Chem Biol* **5**: 183-190, 2009.

JORDT SE, JULIUS D: Molecular basis for species-specific sensitivity to "hot" chili peppers. *Cell* **108**: 421-430, 2002.

JORDT SE, BAUTISTA DM, CHUANG HH, MCKEMY DD, ZYGMUNT PM, HOGESTATT ED, MENG ID, JULIUS D: Mustard oils and cannabinoids excite sensory nerve fibres through the TRP channel ANKTM1. *Nature* **427**: 260-265, 2004.

KALIA J, SWARTZ KJ: Exploring structure-function relationships between TRP and Kv channels. *Sci Rep* **3**: 1523, 2013.

KANG K, PULVER SR, PANZANO VC, CHANG EC, GRIFFITH LC, THEOBALD DL, GARRITY PA: Analysis of Drosophila TRPA1 reveals an ancient origin for human chemical nociception. *Nature* **464**: 597-600, 2010.

KARASHIMA Y, TALAVERA K, EVERAERTS W, JANSSENS A, KWAN KY, VENNEKENS R, NILIUS B, VOETS T: TRPA1 acts as a cold sensor in vitro and in vivo. *Proc Natl Acad Sci USA* **106**: 1273-1278, 2009.

KREMEYER B, LOPERA F, COX JJ, MOMIN A, RUGIERO F, MARSH S, WOODS CG, JONES NG, PATERSON KJ, FRICKER FR, VILLEGAS A, ACOSTA N, PINEDA-TRUJILLO NG, RAMIREZ JD, ZEA J, BURLEY MW, BEDOYA G, BENNETT DL, WOOD JN, RUIZ-LINARES A: A gain-of-function mutation in TRPA1 causes familial episodic pain syndrome. *Neuron* **66**: 671-680, 2010.

LAMPERT A, O'REILLY AO, REEH P, LEFFLER A: Sodium channelopathies and pain. *Pflugers Arch* **460**: 249-263, 2010.

LEE SY, BANERJEE A, MACKINNON R: Two separate interfaces between the voltage sensor and pore are required for the function of voltage-dependent K(+) channels. *PLoS Biol* **7**: e47, 2009.

LISHKO PV, PROCKO E, JIN X, PHELPS CB, GAUDET R: The ankyrin repeats of TRPV1 bind multiple ligands and modulate channel sensitivity. *Neuron* **54**: 905-918, 2007.

LONG SB, CAMPBELL EB, MACKINNON R: Crystal structure of a mammalian voltage-dependent Shaker family K+ channel. *Science* **309**: 897-903, 2005a.

LONG SB, CAMPBELL EB, MACKINNON R: Voltage sensor of Kv1.2: structural basis of electromechanical coupling. *Science* **309**: 903-908, 2005b.

LONG SB, TAO X, CAMPBELL EB, MACKINNON R: Atomic structure of a voltage-dependent K+ channel in a lipid membrane-like environment. *Nature* **450**: 376-382, 2007.

MACPHERSON LJ, GEIERSTANGER BH, VISWANATH V, BANDELL M, EID SR, HWANG S, PATAPOUTIAN A: The pungency of garlic: activation of TRPA1 and TRPV1 in response to allicin. *Curr Biol* **15**: 929-934, 2005.

MACPHERSON LJ, DUBIN AE, EVANS MJ, MARR F, SCHULTZ PG, CRAVATT BF, PATAPOUTIAN A: Noxious compounds activate TRPA1 ion channels through covalent modification of cysteines. *Nature* **445**: 541-545, 2007.

MINOR DL JR: Searching for interesting channels: pairing selection and molecular evolution methods to study ion channel structure and function. *Mol Biosyst* **5**: 802-810, 2009.

MOISEENKOVA-BELL V, WENSEL TG: Functional and structural studies of TRP channels heterologously expressed in budding yeast. *Adv Exp Med Biol* **704**: 25-40, 2011.

MORAN MM, MCALEXANDER MA, BIRO T, SZALLASI A: Transient receptor potential channels as therapeutic targets. *Nat Rev Drug Discov* **10**: 601-620, 2011.

MYERS BR, BOHLEN CJ, JULIUS D: A yeast genetic screen reveals a critical role for the pore helix domain in TRP channel gating. *Neuron* **58**: 362-373, 2008a.

MYERS BR, SAIMI Y, JULIUS D, KUNG C: Multiple unbiased prospective screens identify TRP channels and their conserved gating elements. *J Gen Physiol* **132**: 481-486, 2008b.

NAGATA K, DUGGAN A, KUMAR G, GARCIA-ANOVEROS J: Nociceptor and hair cell transducer properties of TRPA1, a channel for pain and hearing. *J Neurosci* **25**: 4052-4061, 2005.

NILIUS B, OWSIANIK G: The transient receptor potential family of ion channels. *Genome Biol* **12**: 218, 2011.

NILIUS B, APPENDINO G, OWSIANIK G: The transient receptor potential channel TRPA1: from gene to pathophysiology. *Pflugers Arch* **464**: 425-458, 2012.

NILIUS B, VOETS T: The puzzle of TRPV4 channelopathies. *EMBO Rep* **14**: 152-163, 2013.

PATIL MJ, JESKE NA, AKOPIAN AN: Transient receptor potential V1 regulates activation and modulation of transient receptor potential A1 by Ca2+. *Neuroscience* **171**: 1109-1119, 2010.

PERTUSA M, MOLDENHAUER H, BRAUCHI S, LATORRE R, MADRID R, ORIO P: Mutagenesis and temperature-sensitive little machines. In: *Mutagenesis*. MISHRA R (ed), InTech Open Access publisher, Valparaíso, 2012, pp 221-246.

RAOUF R, QUICK K, WOOD JN: Pain as a channelopathy. *J Clin Invest* **120**: 3745-3752, 2010.

RAYBAUD A, DODIER Y, BISSONNETTE P, SIMOES M, BICHET DG, SAUVE R, PARENT L: The role of the GX9GX3G motif in the gating of high voltage-activated Ca2+ channels. *J Biol Chem* **281**: 39424-39436, 2006.

SALAZAR H, JARA-OSEGUERA A, HERNANDEZ-GARCIA E, LLORENTE I, ARIAS O, II, SORIANO-GARCIA M, ISLAS LD, ROSENBAUM T: Structural determinants of gating in the TRPV1 channel. *Nat Struct Mol Biol* **16**: 704-710, 2009.

SAMAD A, SURA L, BENEDIKT J, ETTRICH R, MINOFAR B, TEISINGER J, VLACHOVA V: The C-terminal basic residues contribute to the chemical- and voltage-dependent activation of TRPA1. *Biochem J* **433**: 197-204, 2011.

SAWADA Y, HOSOKAWA H, HORI A, MATSUMURA K, KOBAYASHI S: Cold sensitivity of recombinant TRPA1 channels. *Brain Res* **1160**: 39-46, 2007.

SCHMIDT M, DUBIN AE, PETRUS MJ, EARLEY TJ, PATAPOUTIAN A: Nociceptive signals induce trafficking of TRPA1 to the plasma membrane. *Neuron* **64**: 498-509, 2009.

SMITH-MAXWELL CJ, LEDWELL JL, ALDRICH RW: Uncharged S4 residues and cooperativity in voltage-dependent potassium channel activation. *J Gen Physiol* **111**: 421-439, 1998.

STORY GM, PEIER AM, REEVE AJ, EID SR, MOSBACHER J, HRICIK TR, EARLEY TJ, HERGARDEN AC, ANDERSSON DA, HWANG SW, MCINTYRE P, JEGLA T, BEVAN S, PATAPOUTIAN A: ANKTM1, a TRP-like channel expressed in nociceptive neurons, is activated by cold temperatures. *Cell* **112**: 819-829, 2003.

SURA L, ZIMA V, MARSAKOVA L, HYNKOVA A, BARVIK I, VLACHOVA V: C-terminal acidic cluster is involved in Ca2+-induced regulation of human transient receptor potential ankyrin 1 channel. *J Biol Chem* **287**: 18067-18077, 2012.

VOETS T, OWSIANIK G, JANSSENS A, TALAVERA K, NILIUS B: TRPM8 voltage sensor mutants reveal a mechanism for integrating thermal and chemical stimuli. *Nat Chem Biol* **3**: 174-182, 2007.

WANG YY, CHANG RB, WATERS HN, MCKEMY DD, LIMAN ER: The nociceptor ion channel TRPA1 is potentiated and inactivated by permeating calcium ions. *J Biol Chem* **283**: 32691-32703, 2008.

WAXMAN SG: Painful Na-channelopathies: an expanding universe. *Trends Mol Med* **19**: 406-409, 2013.

WINTER Z, BUHALA A, OTVOS F, JOSVAY K, VIZLER C, DOMBI G, SZAKONYI G, OLAH Z: Functionally important amino acid residues in the transient receptor potential vanilloid 1 (TRPV1) ion channel - an overview of the current mutational data. *Mol Pain* **9**: 30, 2013.

ZURBORG S, YURGIONAS B, JIRA JA, CASPANI O, HEPPENSTALL PA: Direct activation of the ion channel TRPA1 by Ca2+. *Nat Neurosci* **10**: 277-279, 2007.